Elucidating the Role of Chaperones in Prion Biosynthesis and Replication by siRNA Mediated Screening

---

Dissertation

zur

Erlangung der naturwissenschaftlichen Doktorwürde
(Dr. sc. nat.)

vorgelegt der

Mathematisch-naturwissenschaftlichen Fakultät

der

Universität Zürich

von

Valeria Eckhardt

von

Ermatingen TG

Promotionskommission

Prof. Dr. Adriano Aguzzi (Vorsitz und Leitung der Dissertation)

Prof. Dr. Stephan Neuhauss

Prof. Dr. Walter Schaffner

Zürich, 2018

Contents

1 Summary

Prion diseases are transmissible neurodegenerative disorders, fatally affecting humans and animals. The prion protein (PrP) is indispensable for prion disease, as mice devoid of PrP do not succumb to disease. Prion disease relies on the seeded nucleation of the “scrapie” conformer PrP^{Sc} onto the cellular prion protein PrP^{C}. The molecular mechanisms underlying the conformational alterations from PrP^{C} to PrP^{Sc} are still unknown. Chaperones are involved in the correct folding of proteins and can specifically unfold misfolded proteins, actively disaggreggate aggregated proteins, and convert them into harmless native proteins or fragmented peptides. The role of chaperones as potent suppressors of neurodegeneration is well-established. However, no comprehensive study including all mammalian chaperones has been achieved in prion research. I hence propose to shed light on the factors involved in the correct folding of PrP^{C} by identifying chaperones, that are involved in PrP^{C} biosynthesis by siRNA mediated screens. In addition I plan to identify chaperones involved in the misfolding from PrP^{C} to PrP^{Sc} or potential un-folding or disaggregation of PrP^{Sc}. This approach is plenary and unbiased because siRNAs targeting the entire mammalian repertoire of chaperones, e.g. the “chaperome”, are used in the screens. Because chaperones collaborate with one or two co-chaperones to compensate functional failure, I plan to simultaneously knock down two or three chaperones, after having evaluated single knockdown screens.

My first aim is to establish siRNA screens targeting chaperone genes in murine cells with PrP^{C} and PrP^{Sc} levels as readout. I completed two murine PrP^{C} single knock down screens with two different siRNA libraries targeting druggable and non-druggable chaperones in the neuronal CAD5 cell line. In total I screened 239 chaperones in ten 384-well plates. The screens passed quality control. Viability results were used to define thresholds for extreme low or high cell viability and implemented in the analysis of the PrP levels to select chaperones altering the PrP metabolism rather than cell viability. Of total 936 siRNAs, 26 siRNAs led to upregulation of PrP^{C}, whereas 82 siRNAs led to substantial downregulation of PrP^{C} levels. My screens validated the role of Hspa5 and Hsf1 in prion protein metabolism and furthermore discovered 21 novel chaperones involved in PrP metabolism. The majority of the genes leading to reduction of PrP^{C} were involved in protein processing in the endoplasmatic reticulum or were part of the 26S proteasome. I started to establish the murine PrP^{Sc} screen with a FRET assay and acute infection of CAD5 cells with RML6 prions. Because FRET was not sensitive enough to detect differences between uninfected and RML6 infected CAD5, I established PrP^{Sc}-ELISA. Acute infection of CAD5 and CAD5 *Prnp*-/-cells with RML6 resulted in high amounts of residual inoculum in CAD5 *Prnp*-/- cells, masking potential prion replication in CAD5 wild type cells.

By chronically infecting CAD5 cells, residual inoculum was completely removed in four consecutive splitting steps. PrP^{Sc}-ELISA with chronically infected scCAD5 resulted in very low ELISA signal. In order to get a higher signal, I had generated hyCAD5 cells overexpressing PrP. I chronically infected hyCAD5 cells with RML6 prions (scHyCAD) and transfected them with control siRNAs. PrP^{Sc}-ELISA showed good strictly standardized mean difference (SSMD) values for manually performed forward transfection, but insufficient knockdown efficiency and high inter-well variability with robotic reverse transfection. Therefore, I established the PrP^{Sc} screen on the robotic platform for forward transfection with chronically infected hyCAD5 cells. The test screen with control siRNAs resulted in good SSMD values. When I performed the PrP^{Sc} screen, the viability quality control showed six siRNAs reducing the viability of the cells significantly.

My second aim is to generate a murinized human cell line susceptible to murine prions to perform a human PrP^{Sc} screen with murine prions without elevated biosafety risk that would arise when working with human prions. Subsequently I plan to establish an siRNA screen targeting chaperone genes in human murinized cells with PrP^{C} and PrP^{Sc} levels as readout. I generated *PRNP* knock-out mutants in the human SH-SY5Y cell line by means of CRISPR-Cas9 and generated murinized SH-SY5Y cells by stable transfection of a *PRNP* knockout clone with murine *Prnp* and subsequent clonal isolation by limited dilution. To assess strain specific susceptibility to murine prions, I acutely infected a pool of seven murinized clones (mSY5Y), as well as single clone #M4 with eight different prion strains and according non-infectious brain homogenate. Western blots showed Proteinase K resistant PrP^{Sc} bands with the prion strains 79A, mNS and ME7. When I chronically infected mSY5Y and single clone #M4 with these three strains, no PrP^{Sc} band was visible. The screen would only have been feasible with chronically infected cells, because residual inoculum in SH-SY5Y cells acutely infected with 79A, mNS and ME7 prions masked potential PrP^{Sc} replication. In an alternative approach, I generated a human glioblastoma cell line U-251MG overexpressing murine PrP. I acutely infected mixed clones of U-251MG overexpressing murine PrP and un-transfected cells as negative control with murine RML6 prions. Western blots showed that U-251MG did neither replicate RML6 prions, nor human prions.

My third aim is to compare and validate hits from murine and human screens. I extracted the same genes that were screened in the two murine PrP^{C} screens from a human genome wide PrP^{C} screen and performed a side-by-side comparison. The comparison showed six genes, that led to downregulation of PrP in murine and human PrP^{C} screens. I established hit validation by Western blotting and qRT-PCR on the LabCyte acoustic dispensing robot for 384-

well plate format. To test alternative murine cell lines for hit validation, I successfully acutely and chronically infected N2A PK1 cells with RML6 prions. The murine myoblastoma cell line CH3H/10T1/2 of which I had generated *Prnp*-/- clones by CRISPR-Cas9 seemed not to be susceptible to RML6 and thus not suitable for hit validation.

Screening the entire chaperome allowed me to detect unexpected hits involved in the metabolism of PrP. A detailed understanding of the molecular basis of chaperone interactions with PrP, could contribute to the general understanding of other protein misfolding diseases such as Alzheimer's, Parkinson's or ALS.

2 Zusammenfassung

Prionenerkrankungen sind übertragbare, neurodegenerative Krankheiten, die im Menschen und in Tieren vorkommen. Da Mäuse ohne das Prionenprotein (PrP) gegen die Krankheit resistent sind, geht man davon aus, dass das Prionenprotein für die Krankheit unabdingbar ist. Das falsch gefaltete Prionenprotein (PrP^{Sc}) überträgt seine Konformation auf das richtig gefaltete zelluläre Prionenprotein (PrP^{C}) mittels Nukleation, die durch Zugabe von PrP^{Sc} beschleunigt wird. Die molekularen Mechanismen, welche an der Konformationsänderung vom zellulären PrP^{C} zum falsch gefaltetem PrP^{Sc} beteiligt sind, sind noch nicht bekannt. Chaperone sind in die korrekten Faltung von Proteinen involviert und können gezielt falsch gefaltete Proteine entfalten. Zudem zerteilen sie aggregierte Proteine und wandeln sie in ungefährliche, korrekt gefaltete Proteine oder fragmentierte Peptide um. Chaperone wirken protektiv gegen neurodegenerative Erkrankungen. In der Prionenforschung gibt es bis jetzt noch keine umfassenden Studien, die sämtliche Chaperone, die in Säugetieren vorkommen, untersucht haben. Deshalb habe ich mir zum Ziel gesetzt, Moleküle ausfindig zu machen, die an der korrekten Faltung von PrP^{C} sowie an der Fehlfaltung von PrP^{C} zu PrP^{Sc} beteiligt sind. Zudem wollte ich Moleküle identifizieren, welche PrP^{Sc} potentiell wieder in die richtige Konformation zurückfalten oder Aggregate auflösen können. Mittels siRNA screens wollte ich Chaperone identifizieren, die an der Biosynthese von PrP^{C} und der Replikation von PrP^{Sc} beteiligt sind. Dieser Ansatz ist vollständig und unvoreingenommen, da mittels siRNAs die Gesamtheit der Chaperone untersucht wird, die in Säugetieren vorkommen. Chaperone arbeiten mit Co-Chaperonen zusammen, welche bei Ausfall eines Chaperones dessen Funktion übernehmen können. Deshalb beabsichtigte ich zwei oder drei Chaperone gleichzeitig zu untersuchen.
Mein erstes Ziel bestand darin, einen siRNA screen mit Mauszellen zu etablieren, mit dem PrP^{C}- und PrP^{Sc}-Werte gemessen werden können. Mittels zweier verschiedener Sammlungen von siRNAs, welche die Expression von Chaperonen reduzieren, habe ich zwei Screens mit neuronalen Mauszellen durchgeführt. Insgesamt habe ich 293 Chaperone in zehn 384-Kavitätenplatten untersucht. Die Screens haben die Qualitätskontrollen bestanden. Zusätzlich zu den PrP-Werten wurde die Vitalität der Zellen gemessen und in die Analyse der PrP-Werte implementiert. Zellen mit enorm hoher oder tiefer Vitalität wurden ausgeschlossen, um Information über den Metabolismus des Prionenproteins und nicht über die Vitalität der Zellen zu erhalten. Von total 963 siRNAs erhöhten 26 siRNAs die Werte von PrP^{C}. 82 siRNAs führten zu tieferen PrP^{C} Werten. Meine Screens bestätigten die Beteiligung der Gene *Hspa5* und *Hsf1* im Metabolismus von PrP. Zudem entdeckte ich 21 neue Chaperone, die am Metabolismus von PrP beteiligt sind. Die Mehrheit dieser Gene war in die Prozessierung

von Proteinen im Endoplasmatischen Retikulum involviert, oder war Teil des 26S Proteasoms. Ich setzte den PrP^{Sc}-Mausscreen mit PrP^{Sc} als Readout mit der FRET Methode sowie mit akuter Infektion von neuronalen CAD5 Zellen mit RML6 Prionen auf. Da die FRET Methode nicht ausreichend empfindlich war, um infizierte von uninfizierten Zellen zu unterscheiden, etablierte ich die PrP^{Sc}-ELISA Methode. Akute Infektion von CAD5 Zellen und CAD5 *Prnp* knockout Zellen mit RML6 Prionen zeigte restliches RML6 in den CAD5 *Prnp* knockout Zellen. Deshalb infizierte ich die Zellen chronisch anstatt akut. Durch vierfaches Passagieren der Zellen wurde das restliche RML6 von den Zellen entfernt. Das Signal mit chronisch infizierten CAD5 Zellen, gemessen mit der PrP^{Sc}-ELISA Methode, war sehr schwach. Deshalb generierte ich hyCAD5 Zellen, die PrP überexprimieren. Ich infizierte die hyCAD5 Zellen chronisch mit RML6 Prionen (scHyCAD) und transfizierte sie mit Kontroll-siRNAs. Die SSMD Resultate des PrP^{Sc}-ELISAs mit händischer Vorwärts-Transfektion waren gut. Rückwärts-Transfektion mit dem Roboter reduzierte die Effizienz der Transfektion und erhöhte die Variabilität zwischen einzelnen Kavitäten. Deshalb setzte ich den PrP^{Sc} screen auf den Roboteranlagen für Vorwärts-Transfektion auf. Der Testscreen mit Kontroll-siRNAs zeigte gute SSMD Werte. Als ich den PrP^{Sc} Screen durchführte, zeigte die Qualitätskontrolle der Vitalität der Zellen sechs siRNAs, die die Vitalität der Zellen stark reduzierte.

Mein zweites Ziel war es, eine murinisierte menschliche Zelllinie zu generieren, die auf murine Prionen anfällig ist. Auf diese Weise konnte ich einen humanen Screen ohne das Risiko durchführen, das entsteht, wenn man Experimente mit humanen Prionen durchführt. Darüber hinaus beabsichtigte ich einen siRNA screen mit menschlichen murinisierten Zellen durchzuführen und humane Chaperone zu screenen. Ich generierte *PRNP* knockout Mutanten der humanen Zelllinie SH-SY5Y mittels CRISPR-Cas9. Ich transfizierte einen *PRNP* knockout Klon mit murinem *Prnp* und isolierte anschliessend murinisierte Klone. Um die Anfälligkeit der murinisierten Zellen auf murine Prionen zu testen, infizierte ich eine Mischung aus sieben murinisierten Klonen sowie den einzelnen Klon #M4 mit acht verschiedenen Prionenstämmen. Western Blots zeigten Proteinase K resistente PrP^{Sc} Banden nach Infektion mit den Prionenstämmen 79A, mNS und ME7. Als ich mSY5Y und den Klon #M4 chronisch mit diesen drei Prionenstämmen und RML6 infizierte, waren keine PrP^{Sc} Banden mehr sichtbar. Ein PrP^{Sc} Screen wäre nur mit chronisch infizierten Zellen realisierbar gewesen. Reste von Inokulum, die bei akuter Infektion entstehen, würden potentielle Prionenreplikation überdecken. Mit einem anderen Ansatz generierte ich die menschliche Glioblastoma Zelllinie tU-251-MG, die murines PrP überexprimiert. Ich infizierte PrP überexprimierende Zellen sowie untransfizierte Zellen akut mit RML6 Prionen. Western Blots zeigten, dass tU-251-MG weder humane noch

murine RML6 Prionen repliziert.

Mein drittes Ziel bestand aus dem Vergleich und der Validierung von Hits aus den murinen und humanen Screens. Ich extrahierte dieselben Gene, die ich auch in den zwei murinen Screens untersucht hatte, aus einem humanen genomweiten Screen. Anschliessend verglich ich die Resultate der murinen Screens mit dem humanen Screen. Der Vergleich resultierte in sechs Genen, die PrP in den murinen sowie im humanen Screen reduzierten. Ich etablierte die Validation von Hits mittels Western Blots und qRT-PCR auf der LabCyte Roboteranlage für 384-Kavitätenplatten. Um alternative murine Zelllinien zu finden, infizierte ich N2A PK1 Zellen erfolgreich akut und chronisch mit RML6 Prionen. Die murine Myoblastoma Zelllinie CH3H/10T1/2, von welcher ich mittels CRISPR-Cas9 knockout Klone generiert hatte, schien nicht anfällig auf RML6 Prionen zu sein und war deshalb nicht geeignet für die Validierung von Hits.

Durch das Screenen des ganzen Chaperomes habe ich unerwartete Hits entdeckt, die am Metabolismus von PrP beteiligt sind. Ein exaktes Verständnis der molekularen Grundlage von Interaktionen zwischen Chaperonen mit PrP könnte zum allgemeinen Verständnis von anderen Proteinfehlfaltungserkrankungen wie Alzheimer, Parkinson oder ALS beitragen.

3 Abbreviations

+/-	In the presence and in the absence of
aa	Amino acid
Aβ	Amyloid β
AD	Alzheimer's disease
ALS	Amyotrophic lateral sclerosis
BH	Brain homogenate
BSA	Bovine serum albumin
BSE	Bovine spongiform encephalopathy
CAD5	CAD-2A2D5 cell line responsive to RML, 22L, 79A, ME7, 301C prion strains
CJD	Creutzfeldt-Jakob's disease (including sCJD, vCJD, iCJD, gCJD)
CNS	Central nervous system
CRISPR	Clustered Regularly Interspaced Short Palindromic Repeats
CWD	Chronic wasting disease
DNA	Deoxyribonucleic acid
dpe	Days post-exposure
dpi	Days post-infection
DPR	Dipeptide repeat proteins
EDTA	Ethylenediaminetetraacetic acid
eGFP	Enhanced GFP
ELISA	Enzyme-linked immunosorbent assay
ER	Endoplasmic reticulum
FACS	Fluorescence-activated cell sorting
FBS	Fetal bovine serum
fCJD	familial Creutzfeldt-Jakob's disease
FFI	Familial fatal insomnia
FTD	Frontotemporal Dementia
gCJD	genetic Creutzfeldt-Jakob's disease
GFP	Green fluorescent protein
GPI	Glycosylphosphatidylinositol
gCJD	Genetic Creutzfeldt-Jakob's disease
GPCR	G-protein coupled receptor
GSS	Gerstmann-Sträussler-Scheinker disease
HP FRET	Homogeneous phase fluorescence resonance energy transfer

HD	Huntington's disease
$hPrP^C$	Human cellular prion protein
HRP	Horseradish peroxidase
iCJD	iatrogenic Creutzfeldt-Jakob's disease
IgG	Immunoglobulin G
kDa	kilo Dalton
KO	Knockout
mRNA	Messenger RNA
NBH	Non-infectious brain homogenate
NMR	Nuclear magnetic resonance
ORF	Open reading frame
PCR	Polymerase chain reaction
PD	Parkinson's disease
PK	Proteinase K
PK-Western	Western blot with samples digested with PK
POM 1 – 19	Set of 19 anto-PrP monoclonal antibodies
Prnp	Prion protein gene (murine)
PRNP	Prion protein gene (human)
PrP	Prion protein
PrP^C	Cellular prion protein
PrP^{Sc}	Scrapie prion protein
[PSI+]	Yeast protein, misfolded, self-propagating form of Sup35, analog to mammalian PrP^{Sc}
qRT-PCR	quantitative Real Time PCR
recPrP	Recombinant PrP ($rhPrP_{23-231}$ + $rmPrP_{23-230}$)
$rhPrP_{23-231}$	Recombinant, full-length human PrP, aa 23-231
RML6	Passage 6 of the Rocky Mountain Laboratory strain mouse-adapted scrapie prions
$rmPrP_{23-230}$	Recombinant, full-length murine PrP, aa 23-230
RNA	Ribonucleic acid
RNAi	RNA interference
RISC	RNA-induced silencing complex
sCJD	sporadic Creutzfeldt-Jakob's disease
SD	Standard deviation

SDS-PAGE	Sodium dodecyl sulfate polyacrylamide gel electrophoresis
sgRNA	single guide RNA
SKD	Single knockdown
SRP	signal recognition particle
SSMD	Strictly standardized mean difference
Sup35	Yeast protein, important for translation termination, analog to mammalian PrP^C
TRAM	Translocating chain associating membrane protein
TRAP	Translocon associated protein
TSE	Transmissible spongiform encephalopthy
UPR	Unfolded protein response
UPS	Ubiquitin proteasome system
vCJD	variant Creutzfeldt-Jakob's disease

4 Introduction

4.1 History of prions

Prion disease was first described 1732 in Merino sheep manifested by abnormal behavior such as altered gait and intense itching that caused affected sheep to pathologically scrape against fences (Figure 1). The disease was called Scrapie and classified as the first member of transmissible spongiform encephalopathies (TSEs) (Zabel and Reid 2015). In 1920, a human neurological disorder of unknown etiology described by the neurologists Hans Gerhard Creutzfeldt and Alfons Maria Jakob was termed Creutzfeldt-Jakob's disease (CJD) (Creutzfeldt 1920, Jakob 1921, Kovacs, Trabattoni et al. 2002). Based on findings that viral nucleic acids encode genetic information and were infectious, Sigurdsson hypothesized that the scrapie disease was caused by a "slow virus" in 1954 (Sigurdsson 1954). In the same year scientists discovered the human neurological disorder Kuru in Papua New Guinea among the Fore tribe, transmitted by practice of cannibalism, with similar symptoms as CJD and scrapie (Gajdusek and Zigas 1959). Hadlow, Klatzo, Gajdusek and Zigas linked 1959 Kuru, scrapie and CJD by showing they were distinct forms of the same neuropathy (Hadlow 1959, Klatzo, Gajdusek et al. 1959). 1966 Alper discovered that the scrapie agent was resistant to high amounts of UV radiation and therefore could not consist of nucleic acids (Alper 1967). Contradicting the central dogma of biology, T. Alper, I.H. Pattison and J.S Griffith proposed that the scrapie agent could be of protein origin. Patricia Merz detected scrapie associated fibrils in murine CJD brain fractions in experimentally transmitted disease as well as in human cases of CJD (Merz, Somerville et al. 1983). Stanley Prusiner delivered evidence for the "protein only" hypothesis by inactivating the scrapie agent, that he had isolated from affected animals, by methods that destroyed proteins. In 1982 Prusiner designated the term 'prion', derived from proteinaceous infectious particle, to describe the infectious scrapie agent (Bolton, Mckinley et al. 1982, Prusiner, Bolton et al. 1982, Prusiner, Mckinley et al. 1983). Three years later Bruce Chesebro and Richard Race found an mRNA transcript from the protease-resistant prion agent isolated by Prusiner. Unexpectedly, they found this prion protein mRNA in both infected and uninfected brain tissue (Chesebro, Race et al. 1985, Locht, Chesebro et al. 1986). The same year Prusiner and Charles Weissman detected the host gene encoding the prion agent, and the locus named *Prnp* was isolated by George Carlson and Prusiner (Oesch, Westaway et al. 1985). Mice devoid of *Prnp* were resistant to scrapie, showing physiologically expressed PrP^{C} was necessary for prion infection (Bueler, Aguzzi et al. 1993). 1986 British pathologists identified a scrapie like disease which previously had been known to occur only in sheep and

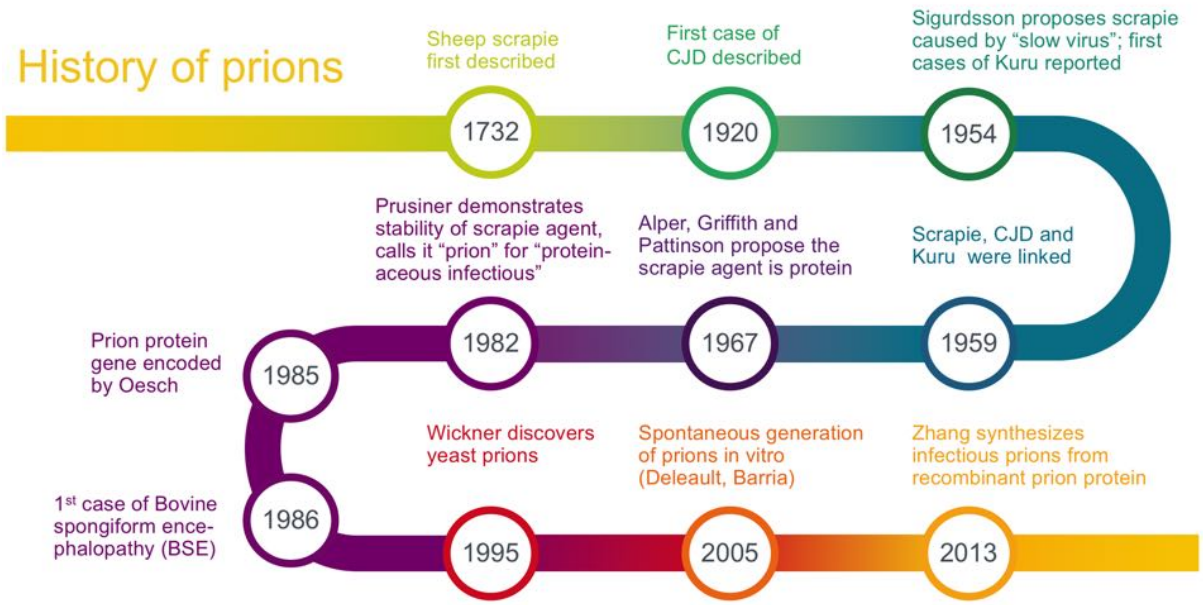

Figure 1: Milestones in the history of prion research. Adapted from (Zabel et al. 2015).

goats within food animals. They named the disease bovine spongiform encephalopathy (BSE). Detergent treated fibrils, extracted from BSE affected cattle shared morphological, chemical and immunological properties with scrapie-associated fibrils found in all other members of the disease group. The fibrils were transmissible from cattle brain to mice by intracerebral and intraperitoneal inoculation. These results provided conclusive evidence that BSE was a new member of TSEs (Bradley 1990). The principle of prion replication was confirmed in yeast. Analogous to mammalian prions, yeast prions were shown to convert their normal cellular isoforms into misfolded isoforms (Glover, Kowal et al. 1997). The normal protein isoforms Ure2p and Sup35 are indispensable to generate and maintain their prion forms [URE3] and [PSI+]. Both prion forms appear more frequently when Ure2p and Sup35 were overexpressed. Following generations inherit both elements as non-Mendelian dominant traits (Cox 1994). Skeptics dismissed the "protein only" hypothesis, because de novo prion generation experiments relied on extraction of PrP^C from living animals that might harbor a presumptive TSE virus. Spontaneous prion formation in vitro using a prion amplification technique and highly purified PrP^C from uninfected brain homogenate in combination with synthetic polyanions or using recombinant prion protein produced in bacteria, provided strong evidence that infectious prions lack nucleic acids differing in the sequence from PrP^C (Deleault, Geoghegan et al. 2005, Barria, Mukherjee et al. 2009, Zhang, Zhang et al. 2013). The prion hypothesis therefore affirmed a new paradigm of information storage and transfer in biological systems. Nowadays the "protein only" hypothesis is widely accepted.

4.2 Prion diseases

Prion diseases, also referred to as transmissible spongiform encephalopathies (TSEs), are neurodegenerative disorders affecting humans and animals (Mabbott and MacPherson 2006). TSEs are characterized by extensive neurodegeneration, manifested in neuronal loss, astrogliosis, microglial activation, spongiform change and aggregates of abnormally folded prion protein (Soto and Satani 2011). Prion diseases are fatal neurodegenerative diseases, which are currently incurable (Prusiner 1998). In animals, prion diseases include scrapie in sheep and goats, chronic wasting disease (CWD) in moose deer and elk, and bovine spongiform encephalopathy (BSE) in cattle (Brotherston, Renwick et al. 1968, Williams and Young 1980, Bradley 1990). BSE was identified 1986 by British pathologists. In the following years BSE epidemically spread from England to numerous countries affecting over 280,000 animals (Aguzzi and Calella 2009). BSE was transmitted by feeding cattle with meat and bone meal from animals that were partially infected, as a nutritional supplement (Wilesmith, Ryan et al. 1992). Since 1988, the use of dietary protein supplements derived from animals is forbidden for domestic animals in the United Kingdom. A second delayed wave of BSE cases occurred in countries where the feeding of animal derived proteins was prohibited at later time points(Aguzzi and Calella 2009). To date five prion diseases have been identified in humans: Creutzfeldt-Jakob disease (CJD), variant Creutzfeldt-Jakob disease (vCJD), Kuru, Gerstmann-Straäussler-Scheinker syndrome (GSS), and fatal familial insomnia (FFI) (Gibbs, Gajdusek et al. 1968, Medori, Tritschler et al. 1992, Brown, Preece et al. 2000). Human prion diseases are classified in iatrogenic, genetic or sporadic origin according to the transmitted, inherited or spontaneously misfolded source of PrP^{Sc} (Hasier Eraña 2016). 85% of human prion diseases show sporadic CJD (sCJD), 10 – 20% cases are familial (fCJD) and 1% of the cases are iatrogenically transmitted (iCJD) (Aguzzi and Calella 2009). Susceptibilty of patients to sCJD, fCJD and iCJD is influenced by an amino acid polymorphism at PrP codon 129, which can be homozygous or heterozygous for Methionine or Valine (Owen, Poulter et al. 1990, Kitamoto and Tateishi 1994). Clinical signs overlap considerably between the different forms of CJD and manifest in cognitive and motor dysfunction such as rapidly progressive dementia, myoclonus, visual or cerebellar impairment, pyramidal or extrapyramidal signs, and akinetic mutism (Mabbott and MacPherson 2006, Aguzzi, Baumann et al. 2008, Aguzzi and Calella 2009).

4.3 Structure of prion protein isoforms

Solution nuclear magnetic resonance (NMR) structural analyses and crystallographic studies revealed 40% of human and murine PrP^{C} consisted of α-helices and 3% β-sheets (Pan, Bald-

win et al. 1993, Riek, Hornemann et al. 1996, Ohhashi, Kihara et al. 2005). While the amino-proximal flexible tail is structurally less defined, the C-terminal globular domain is structured into three α-helixes (amino acids 144–154, 175–193 and 200–219) and a small antiparallel β-sheet (amino acids 128–131 and 161–164). Close to the small β-sheet, a disulfide bridge between Cys-179 and Cys-214 connects helix 2 and helix 3 (Prusiner and Scott 1997, Riesner 2003, Aguzzi and Calella 2009, Zabel and Reid 2015) (Figure 2). Depending on the glycosylation state at two Asparagine residues close to the C-terminus, mammalian PrP^C measures between 30 and 35 kDa (Riek, Hornemann et al. 1996). PrP^C is characterized by α-helical structure, proteinase K (PK) sensitivity, and solubility as a monomeric or dimeric molecule (Riesner 2003).

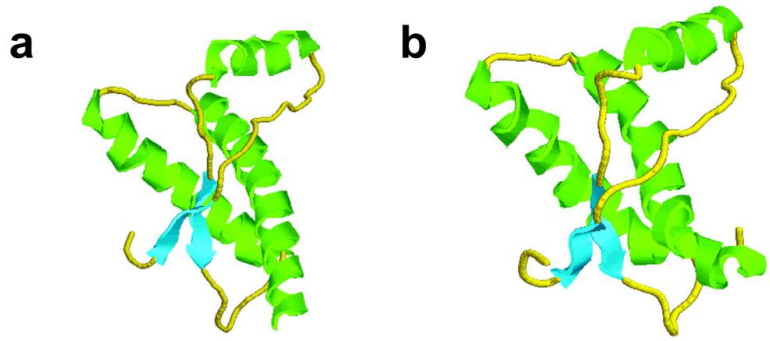

Figure 2: NMR structure of a) human and b) murine PrP^C. The ribbon diagram shows three α-helices (green) and the two antiparallel β-sheets (blue). The connecting loops are displayed in green yellow. Reprinted from (Riesner 2003). License number 4375851429736.

Fourier-transform infrared measurements of PrP^{Sc} and CD spectroscopy show a conformational transition to β–sheets (40%) with only 30% α-helices. In addition to a β-sheet-rich structure, the misfolded isoform PrP^{Sc} differs from PrP^C in physicochemical properties. PrP^{Sc} precipitates as an insoluble, detergent and protease-resistant aggregate of a core 27–30 kDa protein fragment that retains infectivity. No high-resolution structure is available for PrP^{Sc} (Pan, Baldwin et al. 1993, Safar, Roller et al. 1993, Riesner 2003).

4.4 Biosynthesis of PrP^c

In all mammals and birds, the entire open reading frame (ORF) of the prion protein gene is located within a single exon. The prion protein gene is found in the short arm of human chromosome 20 and in a homologous region in mouse chromosome 2 (Sparkes, Simon et al. 1986). The encoded prion protein is a widely expressed nonessential typical cell-surface

glycoprotein (Chakrabarti, Ashok et al. 2009). PrP synthesis begins at the endoplasmatic reticulum (ER) (Figure 3). As the N-terminal signal sequence is translated by the ribosome, it

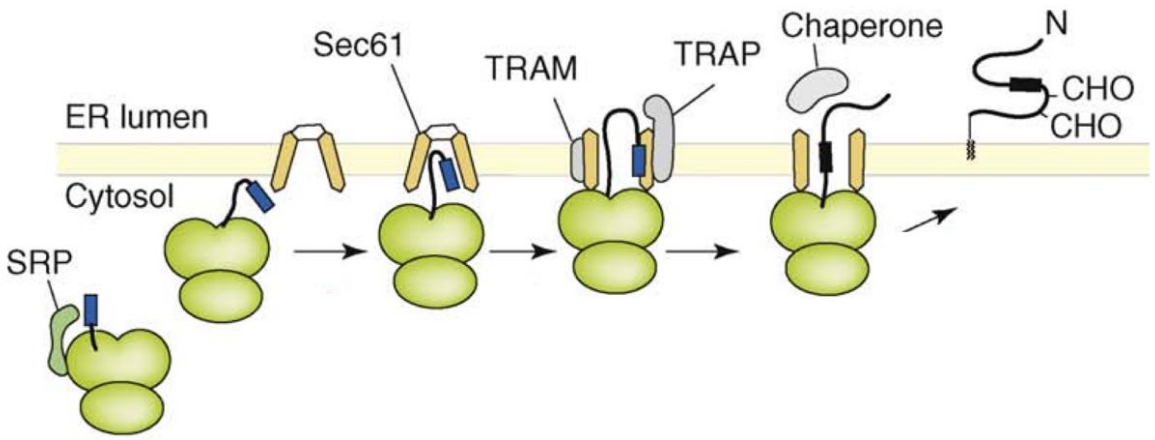

Figure 3: Nascent PrP (black line) is synthesized by the ribosome. As the N-terminal signal sequence (blue) emerges from the ribosome, it is recognized by the signal recognition particle (SRP, green) and interacts with the Sec61 translocon (yellow). Accessory factors such as TRAM and TRAP (grey), contribute in opening of the Sec61 channel to initiate translocation. Forward transport into the ER lumen or prevention of translocation back to the cytosol might be assisted by chaperones (grey). Fully translocated PrP attaches to the inner leaflet of the lipid bilayer via a GPI anchor. Reprinted from (Chakrabarti, Ashok et al. 2009). License number 4375850573324.

is recognized by the signal recognition particle (SRP) and interacts with the Sec61 translocon (Kim and Hegde 2002, Kim, Mitra et al. 2002). In combination with accessory factors such as translocon associated protein (TRAP) and translocating chain associating membrane protein (TRAM), the Sec61 channel opens and translocation into the ER lumen is initiated (Fons, Bogert et al. 2003). The entire ribosome–nascent chain complex is imported to the ER lumen. Chaperones might be involved in the forward transport into the lumen or in prevention of translocation back to the cytosol (Chakrabarti, Ashok et al. 2009). Freshly translated PrP undergoes several steps of posttranslational processing in the ER. PrP is glycosylated, a 22 amino acids long signal peptide is removed at the N-terminus, it is properly folded and a C-terminal glycosylphosphatidyl inositol (GPI) anchor is added. Fully translocated PrP attaches to the inner leaflet of the lipid bilayer via a GPI anchor (Stahl, Baldwin et al. 1993, Hebert and Molinari 2007, Rapoport 2007). Properly folded PrP is trafficked through the Golgi (Figure 4). As PrP passes the Golgi apparatus, it receives various additional modifications to its glycans and the GPI anchor. Most of mature PrP follows the common exocytic pathway to the cell surface and the endocytic pathway to internal endosomal compartments. From there it is either recycled to the cell surface or brought to lysosomes for degradation (Taylor and Hooper

2006). PrP biosynthesis and trafficking to the cell surface takes around 30 min in a standard cell, whereas degradation takes 6 to 12 hours (Caughey, Race et al. 1989, Borchelt, Scott et al. 1990).

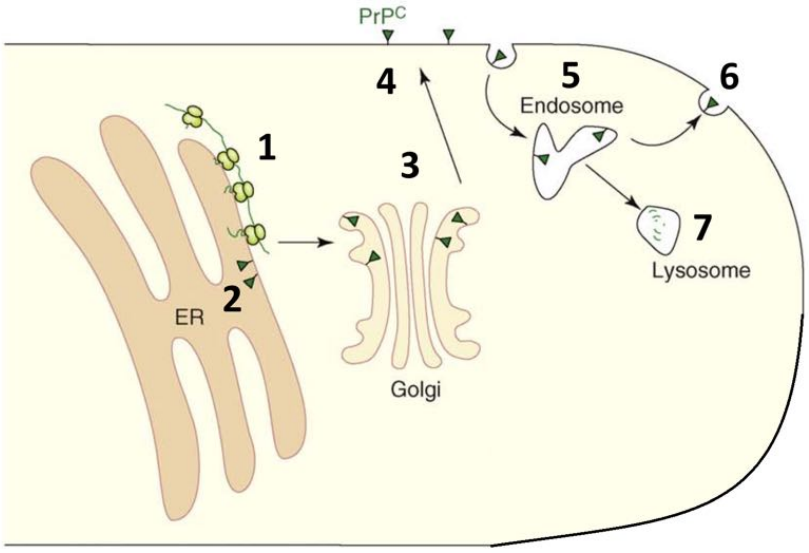

Figure 4: Overview of PrP^C metabolism. 1) Nascent PrP (green line) is translocated into the ER lumen. 2) in the ER PrP is posttranslationally processed and folded into its final conformation (green triangle). 3) Properly folded PrP is trafficked through the Golgi to the cell surface 4). 5) Mature PrP follows the endocytic pathway to internal endosomal compartments. From there it is either recycled to the cell surface 6) or brought to lysosomes for degradation 7). Reprinted from (Chakrabarti, Ashok et al. 2009). License number 4375850573324.

4.5 Prion strains and species barrier

Prion diseases have two particularly intriguing features. Different prion strains and the species barrier that limits the spread of infection between species (Liebman 2001). Prion strains are defined as infectious extracts that, when inoculated to identical hosts, show distinct phenotypes of prion disease. Based on clinical symptoms Pattison and Millson could show strain specific transmission of PrP^{Sc} over 10 passages resulting in the “drowsy” and “scratching” syndromes (Pattison IH 1960). Phenotypic traits can include as well specific locations of protein aggregate accumulation. Prion strains propagate in the CNS, secondary lymphoid organs, spleen or skeletal muscle (Glatzel, Abela et al. 2003, Aguzzi and Calella 2009). Another phenotypic trait is the incubation period, defined as the time interval between infection and onset of the clinical signs of the disease. The incubation period of different prion strains is determined after two or three serial passages in different mouse lines. Incubation periods of prion strains are not only

strain specific, but also species specific. (Beat Hörnlimann 2007). Further phenotypic traits include histopathological analyses, specific neuronal target areas and stability of biological properties. Most of the strains are relatively stable over many passages. Based on their stability, murine scrapie strains can be divided into three different classes. Class I strains are completely stable, even when passaged in mouse lines of different genotypes or in other species such as sheep or hamsters. ME7 strain is the prototype of a class I strain. Class II strains are stable in the mouse genotype they originate from but modify their characteristics during consecutive passages in other genotypes. As a typical class II strain 22A is stable when passaged in VM mice, the mouse line used for its isolation. When 22A is passaged in C57BL mice, the incubation periods and lesion profiles change. After four to five passages, the strain develops stable characteristics again and is then nominated 22F. This conversion from 22A to 22F might be due to a combination of adaptation and selection. Class III strains are unstable, even in their original mouse genotype and can change their biological characteristics during just a single mouse passage. Strain 87A is a classical class III strain. 87A was isolated from six different sheep from four different breeds showing characteristics of 87A. If 87A is passaged in C57BL mice in low concentrations, it is stable. However, when increasing the concentration of the prion strain used for inoculation within the same mouse genotype, the incubation period may be shortened. This newly developed strain was designated 7D. 7D differs in histopathology from 87A but seems to be identical with the ME7 scrapie strain (Bruce and Dickinson 1987). Therefore, ME7 might be a modified strain derived from 87A (Beat Hörnlimann 2007). These findings show, that distinct strains can be observed upon transfer of prions across a species barrier or into the same species differing in the genotype. This phenomenon is referred to as a “strain mutation” (Bruce 1993). Cellular cofactors such as chaperones, specific uptake receptors, RNAs, a certain lipid environment, or a specific prion replicating subcellular environment, might be involved in the conversion of distinct prion strains (Aguzzi, Heikenwalder et al. 2007). Since no genetic instructions transmit with the prion to new hosts, PrP^{Sc} must bear information about prion strain structure and propagation (Zabel and Reid 2015). A possible explanation is, that different conformations are responsible for different disease strains. Strains might be defined by the tertiary or the supramolecular structure of the PrP^{Sc} (Liebman 2001, Aguzzi 2008). Different prion conformation of distinct prion strains may vary their ability to cross species barriers (Liebman 2001). The strong species barrier between mice and hamsters could be due to the difference at 16 of 254 positions between hamster and mouse PrP, leading to a different protein structure. CWD has not been successfully transmitted by oral inoculation from infectious material of species other than the cervid family, indicating a

species barrier for heterologous PrP conversion (Sigurdson 2008, Aguzzi and Calella 2009).

4.6 Prion replication and prionoids

Some investigators claim that prion disease is caused by a virus containing a prion specific nucleic acid that encodes the information expressed by each infectious extract (Bruce and Dickinson 1987). But despite the use of a plethora of techniques, no such nucleotide has been identified to date. Based on the “prion only” hypothesis two models explain the transition from PrP^{C} into PrP^{Sc} and propagation of PrP^{Sc}. Historically, prion propagation was believed to occur through the “refolding” or template assistance model, where exogenously introduced PrP^{Sc} interacts with endogenous PrP^{C} and converts it into further PrP^{Sc}. Spontaneous conversion of PrP^{C} into PrP^{Sc} may be prevented by a high activation energy barrier. The activation energy might be lowered by the formation of PrP^{Sc}-PrP^{C} heteroduplexes, facilitating the formation of further PrP^{Sc} from PrP^{C} (Figure 5 a) (Aguzzi and Calella 2009) .The “seeding” or nucleation-polymerization model proposes that PrP^{C} and PrP^{Sc} are in a reversible thermodynamic equilibrium (Figure 5 b). The position of the equilibrium lies on the side of PrP^{C}, for what reason only few harmless PrP^{Sc} monomers are present. When several monomeric PrP^{Sc} molecules converge into oligomeric seeds, further monomeric PrP^{Sc} can be recruited and aggregate to amyloid. Fragmentation of PrP^{Sc} aggregates increases the number of seeds which can recruit further PrP^{Sc}. Continued rounds of replication concomitant with ongoing PrP^{C} production by the host leads to PrP^{Sc} accumulation, thereby generating additional transmissible agent (Aguzzi and Calella 2009, Chakrabarti, Ashok et al. 2009, Knowles, Waudby et al. 2009).

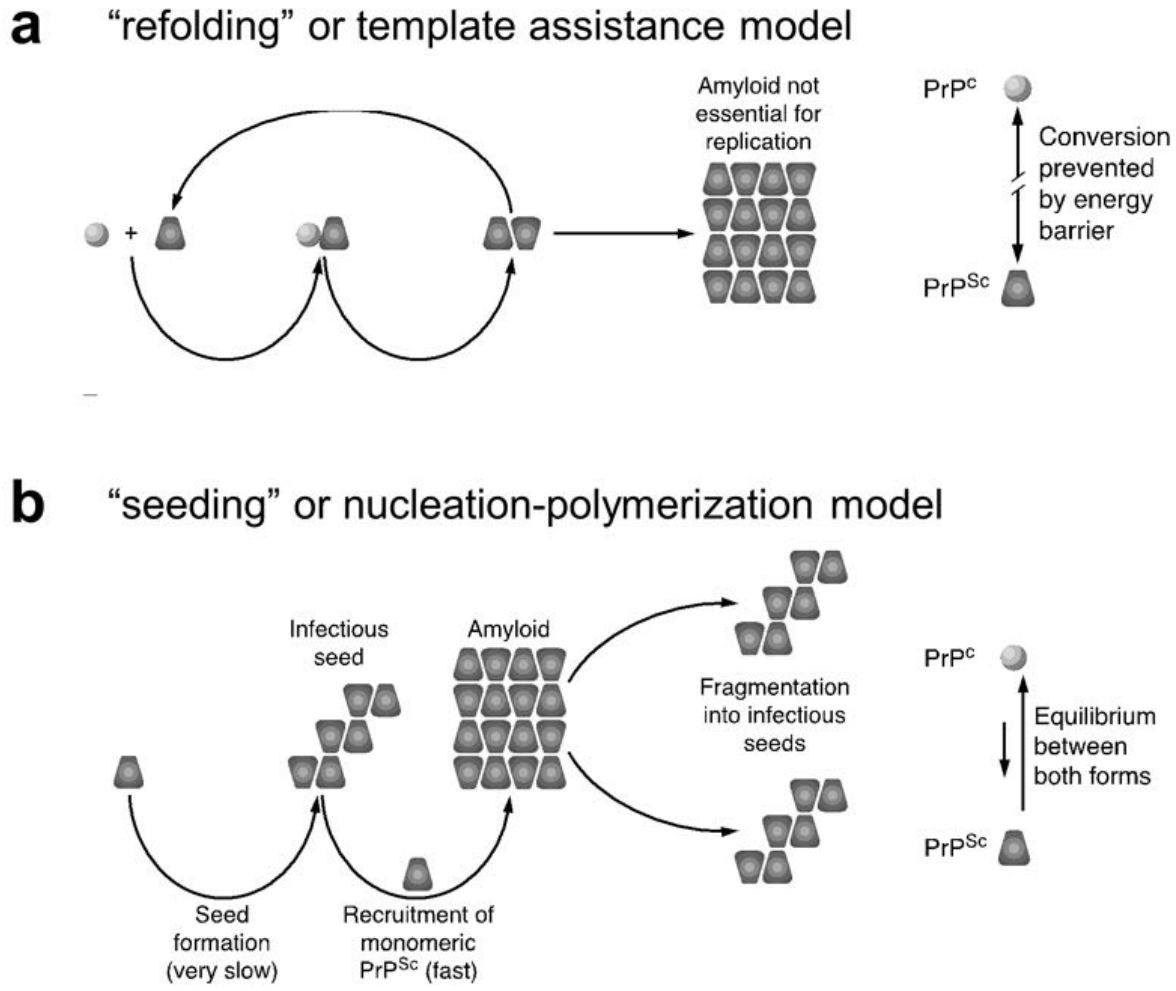

Figure 5: Models for the conformational conversion of PrP^C into PrP^{Sc}. a) in the “refolding” or template assistance model exogenously introduced PrP^{Sc} interacts with endogenous PrP^C, which is stimulated to transform itself into further PrP^{Sc}. A high energy barrier may prevent spontaneous conversion of PrP^C into PrP^{Sc}. b) in the “seeding” or nucleation-polymerization model PrP^C and PrP^{Sc} are in a reversible thermodynamic equilibrium. Solely if several monomeric PrP^{Sc} molecules converge into oligomeric seeds, further monomeric PrP^{Sc} can be recruited and aggregate to amyloid. By fragmentation of PrP^{Sc} the number of seeds is enhanced, which leads to the recruitment of further PrP^{Sc}, resulting in apparent replication of PrP^{Sc}. Reprinted from (Aguzzi and Calella 2009) under the Creative Commons Attributed License 4.0.

The “seeding” or nucleation-polymerization model, however, is not restricted to PrP^{Sc}. When mice were inoculated with aggregated Amyloidβ (Aβ) seeds, Aβ was generated de novo and disease was transmitted (Meyer-Luehmann, Coomaraswamy et al. 2006, Ruiz-Riquelme, Lau et al. 2018). Lewy pathology was induced when intracerebrally inoculating wild-type mice with synthetic α-synuclein (Luk, Kehm et al. 2012). Two subjects with Parkinson’s disease provided evidence, that the disease can propagate from host to graft cells. Patients that had been transplanted with dopaminergic neurons developed α-synuclein-positive Lewy bodies in

grafted neurons (Li, Englund et al. 2008). Experiments showed, that tau pathology resembled prion pathogenesis in cell-to-cell propagation. Inoculation of Tau aggregates into mice produced transmissible pathology and tau formed distinct strains (Kaufman, Thomas et al. 2017). Although the non-classical prions Aβ, α-synuclein and Tau show cell-to-cell propagation, one could certainly argue their transmissibility. Experimental evidence suggests that diseases like Alzheimer's and Parkinson's can be transmitted but are not naturally infectious. Conversely, several familial diseases caused by *PRNP* mutations are poorly or non-transmissible and cause little or no PrP^{Sc} accumulation (Tateishi and Kitamoto 1995, Kovacs, Trabattoni et al. 2002). Thus Aβ, α-synuclein and Tau were denominated "prionoids" to set them apart from "true" prions (Ashe and Aguzzi 2013).

4.7 Prion susceptible cell lines

In addition to animal models to investigate prion diseases, there is need for complementary experimental systems to model aspects of prion diseases (Krejciova, Alibhai et al. 2017). Cellular cultures supporting prion replication present numerous advantages amongst others shorter incubation time, the ability to analyze biological properties of PrP^{C} and PrP^{Sc} at the molecular and cellular levels, and screening of molecules with potential therapeutic values. To generate cells that propagate prions, cell cultures are inoculated with infectious brain homogenate and checked for replication of prions (Solassol, Crozet et al. 2003). In order to obtain cell lines producing sufficient amounts of PrP^{Sc}, mixed clones are subcloned and the subclones producing the most of PrP^{Sc} selected (Bosque and Prusiner 2000). Upon subpassaging, prion infected cells are able to promote stable and continuous replication of PrP^{Sc} as well as infectivity. To date, only a small amount of cell culture models capable of prion replication has been generated. In homologous cell culture models for prion propagation, PrP^{Sc} present in the inoculum and the cultured cells share the same species origin. This approach is thought to omit the species barrier phenomenon that would reduce the effectiveness of prion propagation, mostly due to mismatches in primary amino acid sequences of PrP (Solassol, Crozet et al. 2003). Chesebro and Prusiner generated the first prion infected cells in 1970, infecting mouse neuroblastoma N2a cell lines with the murine Rocky Mountain Laboratory (RML) strain (Race, Fadness et al. 1987, Butler, Scott et al. 1988). A N2a subclone N2a-PK1 (PK1), was later shown to be highly susceptible to the murine prion strains RML and 22L, but not to ME7, 22A, mouse-passaged 263K and the BSE-derived 301C (Mahal, Baker et al. 2007). The neuronal cell line called GT1 established from gonadotropin-releasing hormone neurons immortalized by genetically targeted tumorigenesis in transgenic mice, is infectable by Chandler, 22L, and 139A

strains (Schatzl, Laszlo et al. 1997, Nishida, Harris et al. 2000). Repeated subcloning procedure of Cath.a-differentiated (CAD) cells challenging with RML resulted in the CAD-2A2D5 line (CAD5), which are responsive to RML, 22L, 79A, ME7 and 301C prion strains (Qi, Wang et al. 1997, Klohn, Stoltze et al. 2003, Mahal, Baker et al. 2007, Mahal, Demczyk et al. 2008). Since PrP^{Sc} accumulates mainly in central nervous system cells, neuroblastoma cell lines were chosen for their neuronal phenotype. From various studies conducted with homologous cell culture models for prion propagation we know, that only some strains could replicate in one particular cell line. Further only some cells from a cell line can be infected and their susceptibility to prions is enhanced by subcloning (Bosque and Prusiner 2000, Solassol, Crozet et al. 2003). PrP expression levels were shown to be important for a successful infection. Transgenic *Prnp*-/- mice with extra copies of *Prnp* (*tga20/tga20*) show a tenfold increase in PrP^{C} expression compared to wild type mice such as CD1. *tga20/tga20* mice are very susceptible to scrapie and show much shorter incubation time upon prion infection than CD1 wild type mice (Fischer, Rulicke et al. 1996). Derived from the experience gained in transgenic animals, murine N2a#58 neuroblastoma cell line overexpressing murine PrP were more readily infected with three mouse PrP^{Sc} scrapie strains Chandler, 139A and 22L compared to N2A cells (Nishida, Harris et al. 2000). In contrast, another N2A cell line overexpressing PrP (N2a/2M11) was resistant to RML prions, whereas a very susceptible line, N2a/Bos2, was derived from cells that had been transformed with a control plasmid, and expressed PrP at about the same low level as the original N2a cells (Enari, Flechsig et al. 2001). Until 2017, there was only one, as yet unconfirmed, study of direct prion infection of a human immortalized SH-SY5Y neuroblastoma cell line with CJD prions from a sporadic CJD patient (Ladogana, Liu et al. 1995). In 2017 infection of terminally differentiated astrocytes derived from human induced pluripotent stem cells (iPSCs) with brain homogenate from human sporadic or variant CJD brain was reported. The infection was prion protein codon 129 genotype-dependent, meaning vCJD propagated readily in a line of 129MM astrocytes, but more slowly and less reliably in 129MV and not at all in 129VV astrocytes. Prions from a sCJD VV2 case replicated faster in 129VV astrocytes than in 129MM astrocytes. Infectivity could be demonstrated by subpassaging prions from infected to naive astrocyte cultures (Krejciova, Alibhai et al. 2017). Thus, prion propagation in heterologous cell culture models for prion propagation is slower than in homologous cell culture models. In heterologous models there are either differences between the expressed PrP, or between the cell line and species origin of the inoculum. A heterologous model for naturally occurring sheep scrapie was obtained by stable expression of ovine PrP gene and tetracycline in the rabbit epithelial cell line RK13 (Vilette, Andreoletti et al. 2001). Expression of heterolo-

gous PrP in the rabbit model show, that nonneuronal cells can replicate prions and the species barrier can be crossed by the expression of a suitable PrP gene. Heterologous experimental systems are important to investigate naturally occurring TSE agents. Considering that some strains can only replicate in one particular cell line, that just a fraction of all cells from a cell line become infected, most of the time subcloning is needed to enhance the cells susceptibility to prions, chronically infected cells show lower infectivity titers with increasing cell passages, and that successful propagation of human CJD in cell cultures has only been reported once, it is not surprising that many attempts to establish infected cell lines have been unsuccessful (Elleman 1984, Race 1991, Chesebro, Wehrly et al. 1993).

4.8 Chaperones

Chaperones are involved in the de novo folding of polypeptides, exhibit holding-function, unfold misfolded proteins, disaggregate aggregated proteins, and convert them into harmless native proteins or degraded peptides (Figure 6) (Hinault, Ben-Zvi et al. 2006, Finka, Mattoo et al. 2016).

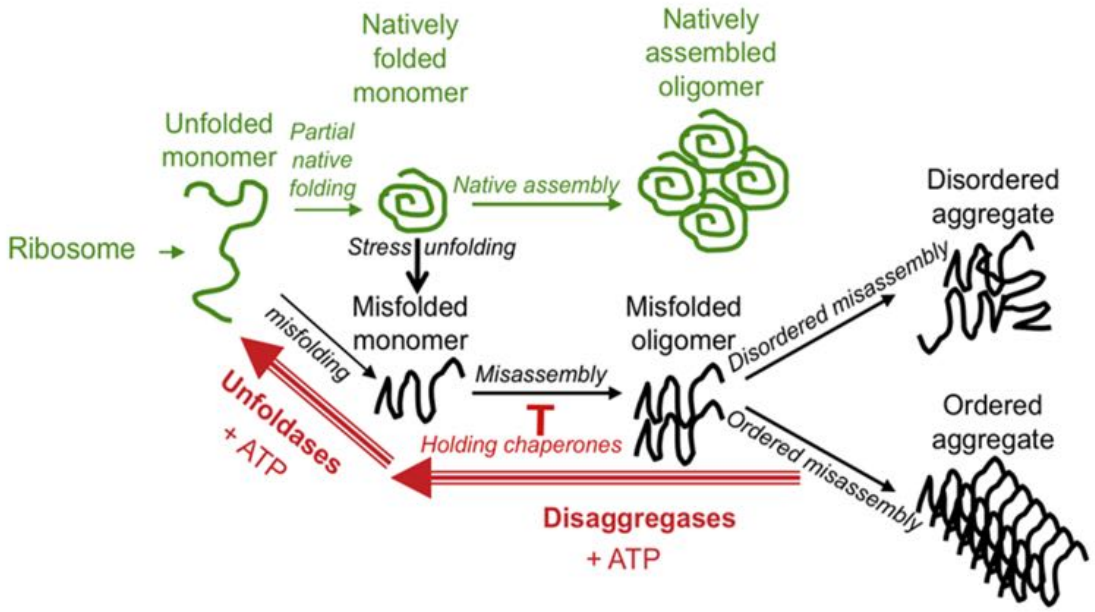

Figure 6: Green: the nontoxic native folding pathway. Black: the toxic non-native misfolding pathway. Red: Unfolding and disaggregating chaperones use ATP to break apart stable, potentially toxic aggregates and misfolded oligomers (Reprinted from (Priya, Sharma et al. 2013). License number 4375860575449.

Polypeptides synthesized at the ribosomes exhibit numerous hydrophobic residues, which are

exposed to the aqueous cytoplasm. Hydrophobic forces drive chain collapse and burial of non-polar amino acid residues within the interior of the protein. Upon this shaping process the polypeptide chain reaches a compact globular conformation, termed the native state (Goloubinoff 2016). However, hydrophobic collapse can lead to globular intermediates such as partially- or mis-folded states. Partially folded states can become transiently kinetically trapped. Such stages must cross substantial free energy barriers during folding to reach again the native state. Chaperones promote the proper folding of polypeptides and overcome energy barriers in an ATP-dependent mechanism (Langer, Lu et al. 1992, Frydman, Nimmesgern et al. 1994, Dunker, Silman et al. 2008). Stressors, such as hypoxia, toxins or heat-shock, may cause partial unfolding, which again leads to exposure of hydrophobic residues and a meta-stable state. To reach an energetically more stable state, hydrophobic residues can interact within a protein, leading to misfolded proteins. Interaction between proteins could lead to aggregation. Holding chaperones prevent in a non-catalytic passive way the aggregation of substrates, that may be aggregation-prone (Finka, Mattoo et al. 2016). Unfolding chaperones specifically bind exposed hydrophobic surfaces and unfold misfolded proteins. Following unfolding, some polypeptides are released to spontaneously refold into the native state (Goloubinoff 2016). Disaggregases obligatorily use ATP to break apart stable, potentially toxic aggregates by concerted ATP-fueled motions (Priya, Sharma et al. 2013, Goloubinoff 2016). In addition to molecular chaperones, cells have evolved the ubiquitin-proteasome system (UPS) and lysosome mediated autophagy for the degradation of misfolded proteins. Under certain conditions, when chaperones cannot repair misfolded proteins, overly sticky unfolded polypeptides are degraded via these two pathways into small peptides and subsequently by peptidases into amino acids to be reused in de novo protein synthesis (Muchowski and Wacker 2005, Goloubinoff 2016). Molecular chaperones are classified into six main families on the basis of their approximate molecular mass (in kDa): HSP100, HSP90, HSP70, HSP60, HSP40 and the small HSPs , which weight less than 40 kDa (Muchowski and Wacker 2005).

4.9 Protein-misfolding disorders and chaperones

Protein-misfolding disorders, such as Alzheimer's disease (AD), Parkinson's disease (PD), amyotrophic lateral sclerosis (ALS), and prion disease are characterized by the accumulation of intracellular or extracellular aggregates, consisting of misfolded proteins. The proteins that aggregate in these disorders are unrelated in size or primary amino acid sequence (Muchowski and Wacker 2005). Misfolded proteins are thought to accumulate in neurons and in other cells as a result of normal ageing, associated with a decrease in proteasome and lyso-

some activity and dysfunction of molecular chaperones (Muchowski 2002). This might account for the late onset of neurodegenerative diseases that are linked to protein aggregation (Soti and Csermely 2002). Recent evidence indicates that chaperones are potent suppressors of neurodegeneration. In AD, virally mediated overexpression of HSP70 successfully rescues neurons from the toxic effects of intracellular Aβ accumulation (Magrane, Smith et al. 2004). A possible mechanism how cytoplasmic HSP70 protects neurons in this system, might involve chaperone-stimulated degradation of Aβ in association with the endoplasmatic reticulum (ER). In this process misfolded proteins are recognized by a quality control mechanism in the ER, retro-translocated into the cytosol and degraded by the 26S proteasome (McCracken and Brodsky 2003). HSP70 overexpression in a PD model cell line caused a decrease in aggregated α-synuclein species and studies in Drosophila melanogaster indicate that HSP70 might have a protective role in PD (Auluck, Chan et al. 2002, Klucken, Shin et al. 2004). Overexpression of HSP70 and HSP40 in the presence of mutant SOD1, which aggregates in ALS, in an N2a (neuroblastoma-like) cell model resulted in reduction of aggregate formation (Takeuchi, Kobayashi et al. 2002). The yeast Sup35 protein, important for translation termination, is the analog to mammalian PrP^{C}. [PSI+], a misfolded, self-propagating form of Sup35, is the mammalian analog to PrP^{Sc} and leads to translational read-through. When performing a genetic screen in yeast, 1 out of 6'000 plasmids carrying Hsp104 inhibit nonsense suppression. Hsp104 is a member of Hsp100 family with ATP-dependent disaggregase function. Interestingly, overexpression or inactivation of Hsp104 causes the loss of [PSI+], whereas yeast prions under physiological Hsp104 conditions can replicate. Based on the nucleation-polymerization model, overexpression of Hsp104 enhances its disaggregase function, whereupon all [PSI+] is in a monomeric, soluble state. If Hsp104 is depleted, all [PSI+] is present in stable aggregates. Without [PSI+] oligomers functioning as seed, there is no [PSI+] replication (Chernoff, Lindquist et al. 1995). An Hsp104 analog in mammals is not known to date. In addition to Hsp104, Hsp70 and its Co-Chaperones, as well as Hsp110 interacts with yeast prions too (Sadlish, Rampelt et al. 2008). So far, interactions of prions and chaperones have mostly been studied in yeast (Sadlish, Rampelt et al. 2008). Although many studies have shown that chaperones are protective in models of neurodegenerative disease, the molecular basis of this protection is not known (Muchowski and Wacker 2005).

4.10 Small interfering RNAs and their application in prion disease

RNA interference (RNAi) protects the eukaryotic genome from invasive nucleic acids such as viruses, transposons, and transgenes. During the biological mechanism of RNAi a processed

non-coding RNA forms a single strand RNA-protein complex and induces gene silencing by targeting complementary mRNA for degradation (Dana, Chalbatani et al. 2017). Long non-coding double stranded RNA precursors are processed by an endonuclease called Dicer into short, active ($\sim 20 - 30$ nucleotide) fragments (Figure 7). A short siRNA duplex is loaded by Dicer and the RNA-binding protein TRBP, onto Argonaute (AGO2) forming an RNA-induced silencing complex (RISC). The Argonaute protein is the core component of the effector machinery (Carthew and Sontheimer 2009). AGO2 selects the siRNA guide strand, then cleaves and ejectes the passenger strand. The guide strand subsequently recognizes its complementary target mRNAs through Watson-Crick base pairing and cleaves it. The cleaved target mRNA is released and RISC is recycled, using the same loaded guide strand for another few rounds of cleavage (Jinek and Doudna 2009, Dana, Chalbatani et al. 2017).

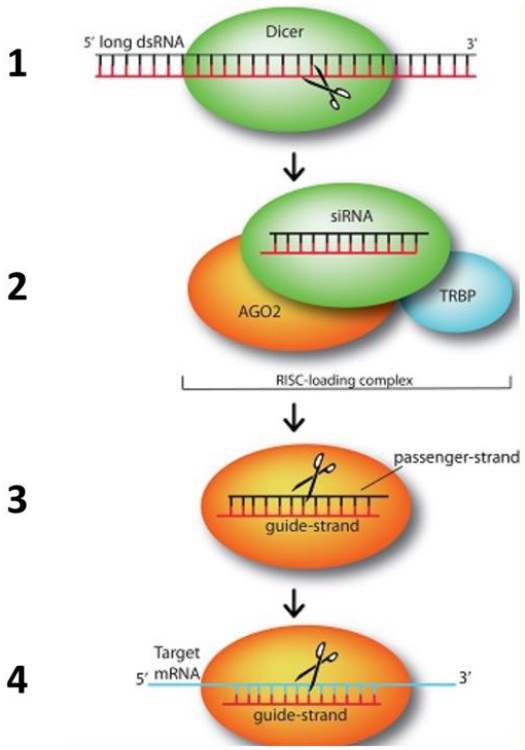

Figure 7: 1) Dicer processing of long dsRNA 2) RISC loading 3) Guide-strand selection, passenger strand cleavage and ejection 4) Target mRNA recognition and cleavage. Reprinted from (Dana, Chalbatani et al. 2017) under the Creative Commons Attributed License 4.0.

This mechanism has been revolutionizing the way researchers study gene function in the last decade. RNAi, first discovered in plants, was later demonstrated in the roundworm Caenorhabditis elegans, and can nowadays be easily applied to mammalian cells by directly transfecting siRNAs into cells (Dorsett and Tuschl 2004, Dana, Chalbatani et al. 2017). PrP^C levels in mice

correlate with the amount of PrP^{Sc} formation and the incubation period. *Prnp* overexpressing mice accumulate more PrP^{Sc} and show a shorter incubation time than wild type animals (Fischer, Rulicke et al. 1996). *Prnp*-/- mice are not replicating prions and thus resistant to prions (Bueler, Aguzzi et al. 1993). Hemizygous *Prnp*+/- mice show longer incubation periods when compared to wild type animals (Bueler, Raeber et al. 1994, Manson, Clarke et al. 1994). The same picture holds true when PrP levels are reduced by siRNAs targeting *Prnp* in infected cell cultures. Both the normal host prion protein and PrP^{Sc} are depleted in murine PrP overexpressing N2a#58 cells chronically infected with the Chandler strain as well as in GT1 cells infected with the 22L strain. The knock down efficiency of the *Prnp* targeting siRNAs was not influenced by different murine-adapted scrapie strains or different cell lines (Daude, Marella et al. 2003). An siRNA delivery system consisting of a small peptide binding siRNA and acetylcholine receptors, targets the siRNA specifically to acetylcholine receptor expressing cells and reduces PrP^{C} and PrP^{Sc} levels in N2a cells. Cationic liposomes injected intravenously into mice protected siRNA-peptide complexes from serum degradation (Pulford, Reim et al. 2010). RNAi targeting *Prnp* was applied to prion therapeutics in mice. Lentiviral delivery of a shRNA targeting *Prnp* reduced PrP levels and prolonged survival time (Pfeifer, Eigenbrod et al. 2006, White, Farmer et al. 2008). The robustness of the RNAi approach has motivated numerous groups to conduct genome-wide screens in mammalian cells to identify and validate potential drug targets. Thus, identifying genes involved in the modulation of PrP levels by RNAi screens represents a promising approach for prion therapeutics. However, one must be aware and test for the potential induction of non-specific and sequence-specific off-target effects of siRNAs (Fire, Xu et al. 1998, Dorsett and Tuschl 2004, Dana, Chalbatani et al. 2017).

5 Aims of the thesis

For my thesis I proposed to shed light on the factors involved in misfolding from physiological PrP^{C} to misfolded PrP^{Sc} or potential un-folding of PrP^{Sc} by identifying chaperones, that are involved in PrP^{C} biosynthesis and PrP^{Sc} replication by siRNA mediated screens. I planned to screen the entire mammalian repertoire of chaperones, e.g. the “chaperome” in a plenary and unbiased approach. Because chaperones collaborate with one or two co-chaperones to compensate functional failure, I planned to simultaneously knock down two or three chaperones, after having evaluated single knockdown screens. I opted for PrP^{C} and PrP^{Sc} levels as readouts, measured in two distinct screens on two fully automated robotic platforms. I proposed to analyze experimental data with a customized software and to validate hits with other siRNA or CRISPR-Cas9 in other cell types, such as primary neurons or iPSC-derived human neurons available in our lab. Upon thorough network analysis of validated hits, I aimed to formulate testable hypotheses on a potential involvement of chaperones in the machinery involved in PrP^{C} biosynthesis and PrP^{Sc} replication. To achieve these exciting goals, I structured my PhD project in four major objectives (Figure 8).

Objective 1: Establish siRNA screens targeting chaperone genes in murine cells with PrP^{C} and PrP^{Sc} levels as readout. I aim to detect chaperones, that are involved in the posttranslational folding processes of PrP^{C} by applying the murine cell-based homogeneous-phase bioassay established in our lab. I further plan to establish a PrP^{Sc} screen with RML6 infected neuronal cells on a LabCyte acoustic dispensing robot for 384-well plate format and Perkin-Elmer Janus liquid handling platform.

Objective 2: Generate a murinized human cell line susceptible to murine prions. Establish an siRNA screen targeting chaperone genes in human murinized cells with PrP^{C} and PrP^{Sc} levels as readout. By utilizing a human cell line as model system, I aim to identify human chaperones potentially involved in the cellular prion protein replication machinery. Cells suitable for the human PrP^{C} and PrP^{Sc} chaperone screens need to meet four requirements: 1) A *PRNP* knockout version of my cell line of interest as negative control, 2) for the human PrP^{C} screen, the cell line needs to express sufficient amounts of PrP^{C} for clear discrimination of controls transfected with scrambled siRNA and siRNA targeting PRNP, 3) to minimize the risks that arise when working with prion-infected human cells, a murinized version of the cell line is required for the human PrP^{Sc} screen, 4) finally, the murinized version should be susceptible to murine prions, ideally to RML6, which is prominently used in our lab.

After the generation of a suitable murinized cell line, I plan to run the human chaperone screen with siRNAs targeting the same chaperone transcripts as in the murine screen.

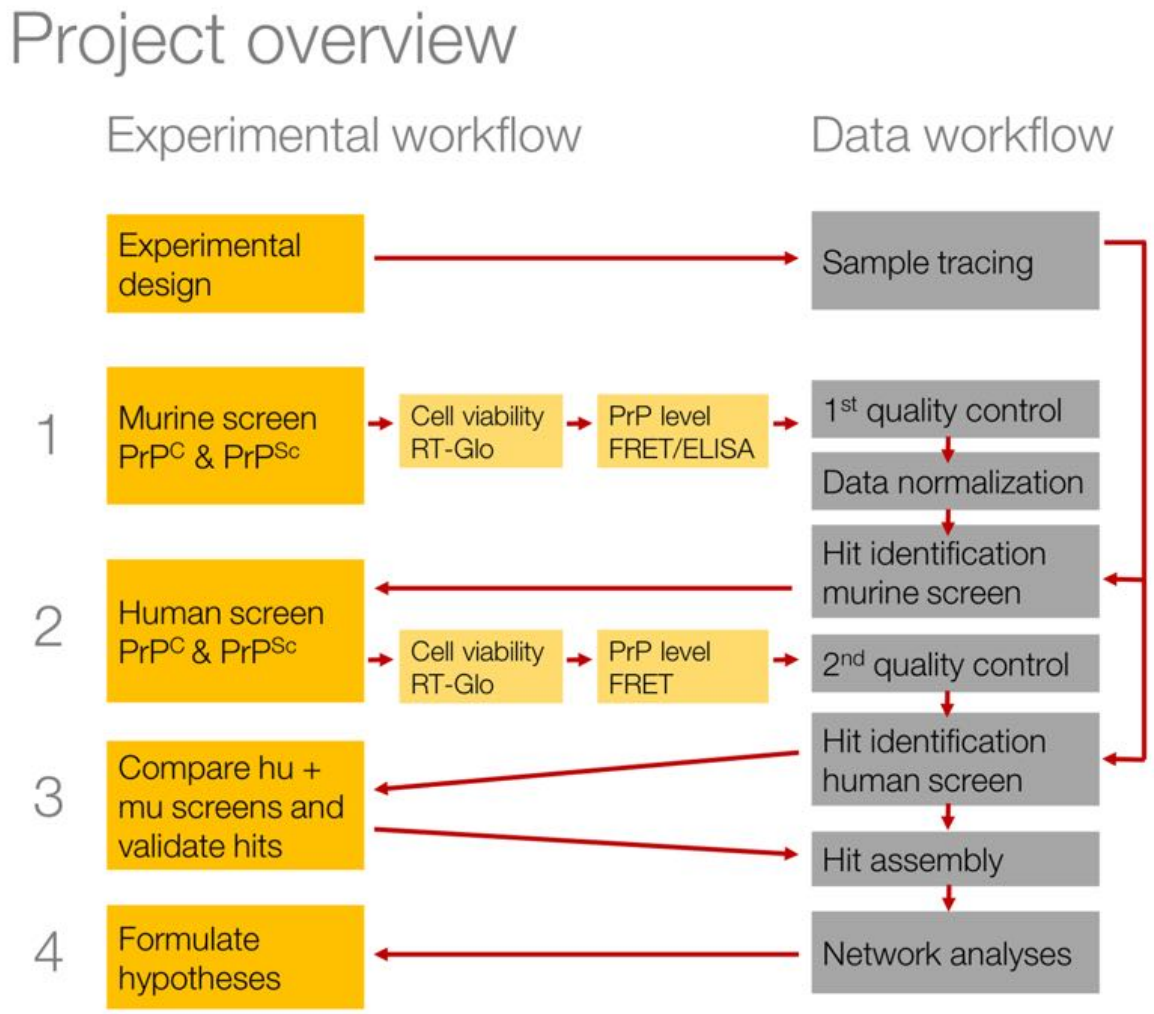

Figure 8: Project overview

Objective 3: After completing the murine and human PrP^C and PrP^{Sc} screens, I purpose to compare the hits to contrast the effect of chaperones on PrP levels in two different mammalian experimental systems. I subsequently plan to validate potentially therapeutic chaperones.

Objective 4: Upon network analysis of validated chaperone hits, I plan to formulate hypotheses on a potential involvement of chaperones in the biosynthesis of the prion protein and in the murine prion protein replication machinery.

6 Results

6.1 Chaperone siRNA screens in murine cells

6.1.1 siRNA preparation

Prof. Pierre Goloubinoff, (University of Lausanne, CH) provided me with a list of the entire mammalian repertoire of chaperones, e.g. the “chaperome” consisting of 240 chaperones. He selected 31 chaperone-pairs for double knockdown, based on the expression of co-chaperones in the same cellular compartments and known interactions. I performed the screens with two different siRNA libraries. The first arrayed druggable mouse siRNA library provided by Novartis contained 376 siRNAs against 99 transcripts of druggable chaperones, that were actually expressed in CAD5 cells based on a CAD5-RNASeq data set (13’752 expressed genes). Each gene was targeted by two up to four different siRNAs. The second library consisted of 560 siRNAs against 140 non-druggable chaperone transcripts, including transcripts that were not expressed in CAD5 cells. In this arrayed mouse siRNA library purchased at ThermoFisher, one gene was targeted by 4 different siRNAs. Because the DNA sequence of one chaperone was not available, no suitable siRNAs could be synthesized and totally 239 chaperones were screened. A scrambled non-target siRNA and an siRNA targeting the prion protein gene were used as negative and positive controls. The final concentration of siRNA per well was 30nM. For the double knockdown screen, I found the best cell viability and knockdown efficiency at a final concentration of 30nM for two pooled siRNAs per well (Figure 9).

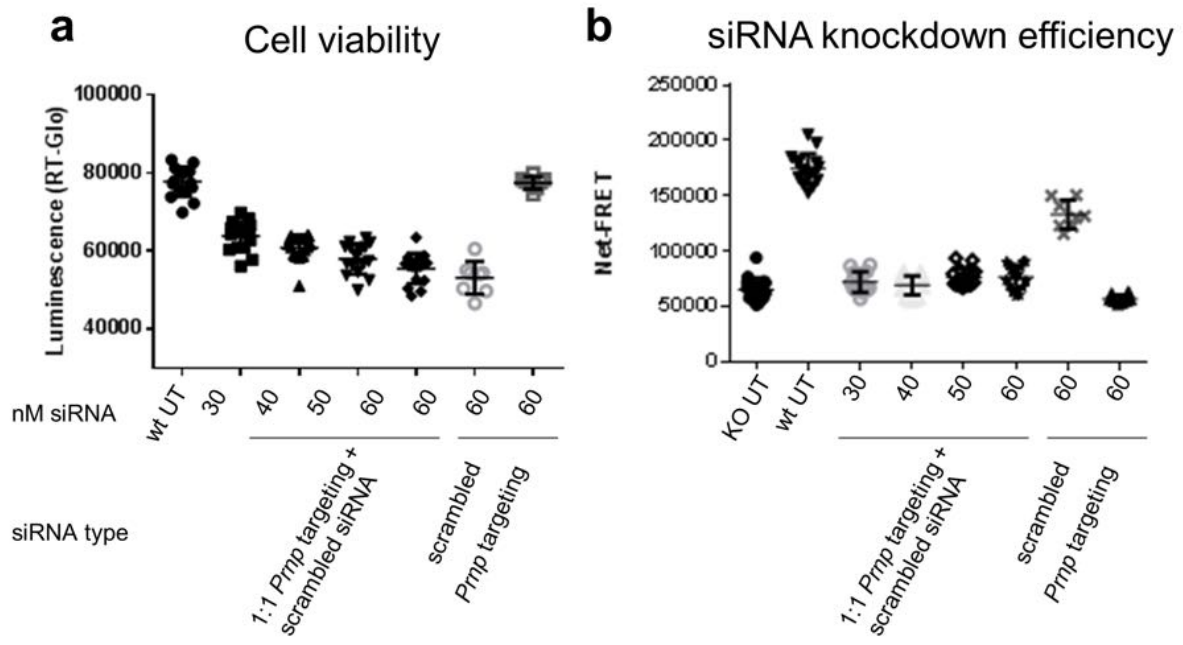

Figure 9: Cells transfected with individual Prnp targeting siRNA and scrambled siRNA or a 1:1 mixture of both siRNAs with concentrations from 30 nM – 60 nM. Untransfected cells (UT) served as control. a) the cell viability of CAD5 wild type (wt) cells decreased with increasing siRNA concentrations, except when transfecting Prnp targeting siRNA only. b) PrP levels depicted as Net-FRET levels showed no PrP in untransfected CAD5 Prnp-/- cells (KO UT) generated in our lab by CRISPR-Cas9 technology. PrP expression in untransfected CAD5 wt cells (wt UT) was high. All siRNA concentrations with pooled Prnp targeting siRNA and scrambled siRNAs led to the same reduction of PrP levels.

6.1.2 Murine PrP^C screen

I applied and advanced the murine cell-based homogeneous-phase bioassay established in our lab (Figure 10), to screen for chaperones that affect PrP^C levels (Li 2016).

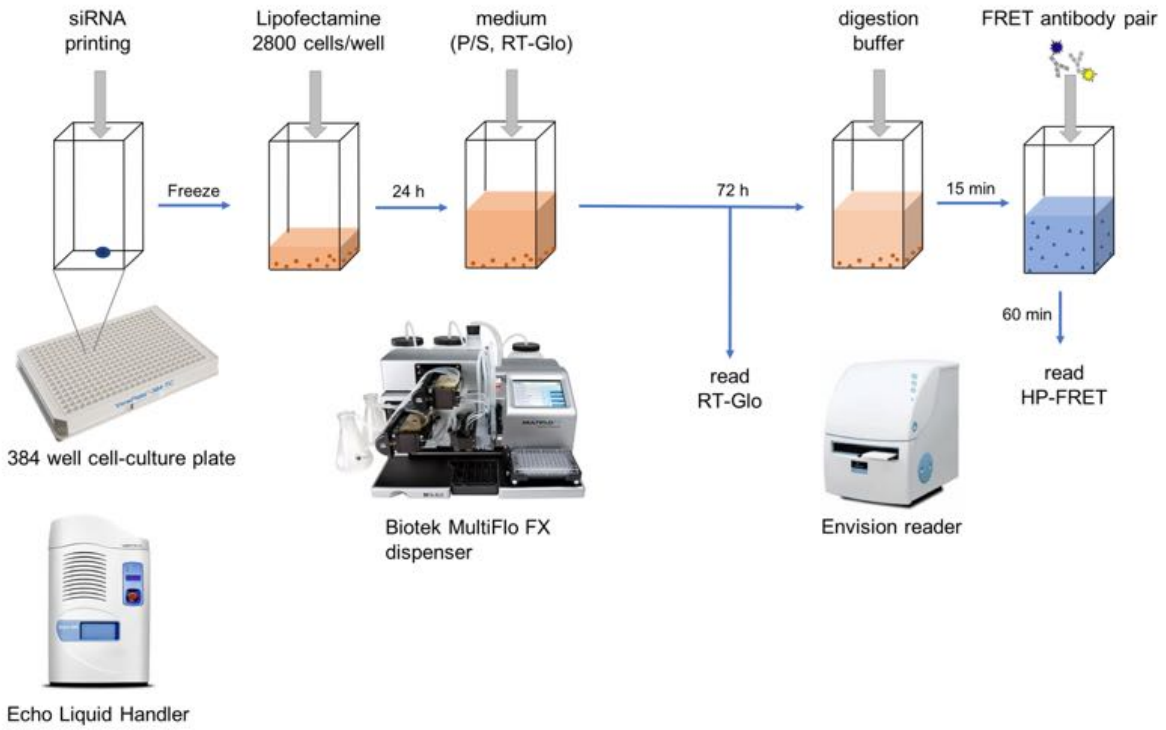

Figure 10: Workflow PrP^C screen.

Sample siRNAs targeting chaperone transcripts and control siRNAs were printed with an Echo Acoustic Liquid Handling technology in 384-well microtiter plates on the fully automated robotic LabCyte platform. The acoustic dispenser allowed contactless transfer of siRNAs according to a randomized plate layout (Appendix 79). The sophisticated plate layout was designed to compensate eventual plate gradients or biological variability within technical replicates in order to get real positive hits. The plates containing printed siRNAs were frozen until the assay day, when Lipofectamine RNAiMAX reagent and 2800 CAD5 cells per well are added for reverse transfection by Biotek MultiFlo FX dispenser within the Perkin-Elmer Janus liquid handling platform. CAD5 cells are prion-susceptible cells, derived from neuronal Cath.a-differentiated (CAD) cells (Qi, Wang et al. 1997). In addition to CAD5 treated with siRNA controls, CAD5 *Prnp*-/- cells generated in our lab by CRISPR-Cas9 technology, were used as negative control. After 24 hours, cell viability marker Real Time Glo (RT-Glo), measuring the reducing potential and metabolism of cells was added. After 72 hours of incubation, RT-Glo cell viability and PrP levels were assessed with the Envision reader. RT-Glo signals were used to define thresholds

for extreme low or high cell viability and could be used in the analysis of the PrP levels to select chaperones altering the PrP metabolism rather than cell viability. PrP levels were assessed by homogeneous-phase fluorescence resonance energy transfer (HP-FRET) assay. FRET was based on the energy transfer between two fluorophores, Europium (Eu^{3+}) and Allophycocyanin (APC), which were separately labelled to the anti-PrP antibodies POM1 and POM19 targeting alpha helices 1 and 3 in the globular domain of PrP less than 10 nm apart from each other (Figure 11 a) (Polymenidou, Moos et al. 2008). When Eu^{3+} and APC labelled anti-PrP antibodies bound to a single PrP molecule, the excited donor Eu^{3+} transferred energy to the acceptor APC by non-radiative dipole-dipole coupling, which emitted photons as fluorescence that could be measured at 665 nm (Figure 11 b).

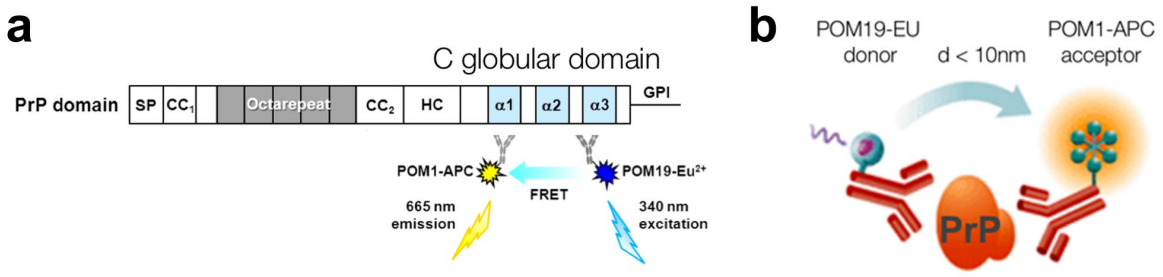

Figure 11: a) Europium (Eu^{3+}) and allophycocyanin (APC) separately labelled to the anti-PrP antibodies POM1 and POM19 targeting alpha helices 1 and 3 in the globular domain of PrP. Image courtesy Bei Li. b) Energy transfer from the donor Europium coupled to POM19, to the acceptor APC coupled to POM1 less than 10 nm apart from each other.

I performed a test screen with two plates containing CAD5 wild type (wt) and CAD5 *Prnp*-/- cells, transfected only with control, but no sample siRNAs. Since the test screen passed quality control, I did run the first murine single knockdown (SKD) PrP^C screen using an siRNA library targeting druggable chaperones in four 384-well plates. Raw data files from the Envision reader with data from cell viability (RT-Glo luminescence) and PrP levels (FRET Fluorescence) were exported and fed into a custom-written online software. Experimental data and quality controls (QC) were automatically pulled together in RMarkdown documents. Net-FRET data representing PrP levels were visualized in heatmaps for all four screen plates (Figure 12).

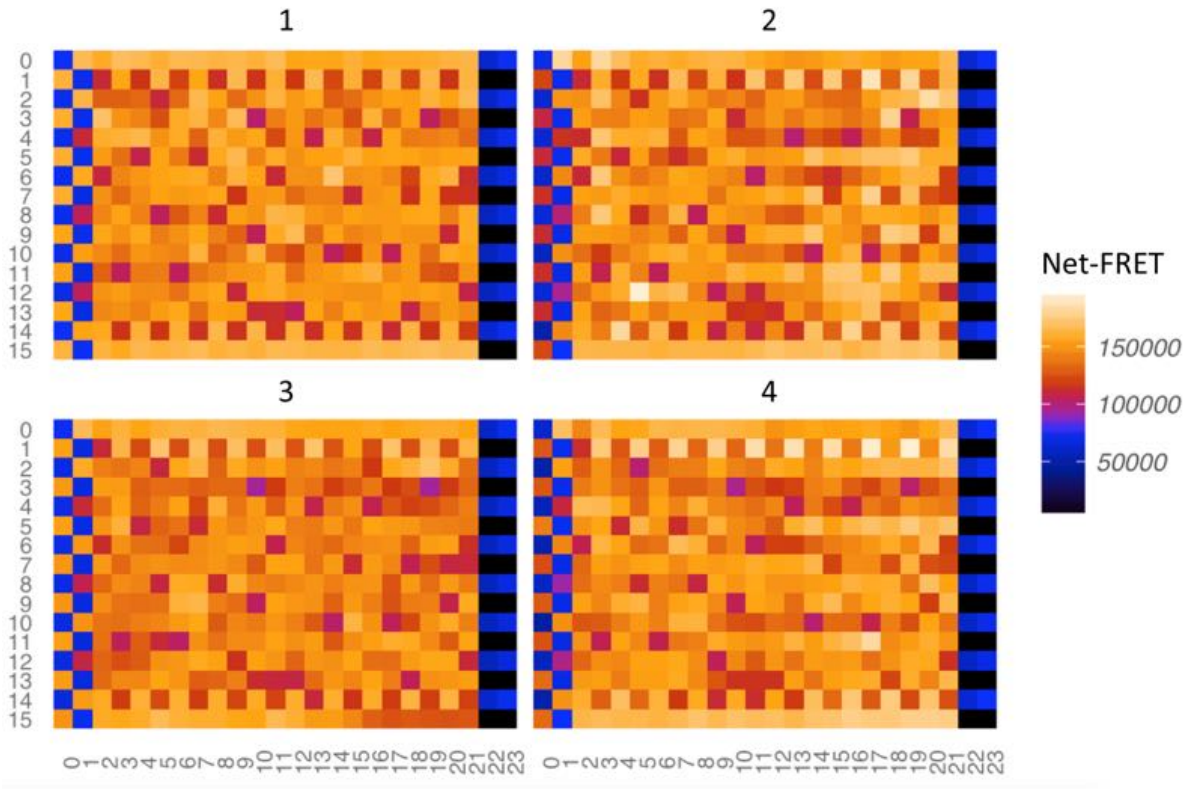

Figure 12: Net-FRET levels representing PrP^C levels were visualized for four plates as heatmaps. High PrP levels were depicted in orange, low PrP levels in blue. CAD5 Prnp-/- cells in every second well in columns one and two showed low Net-FRET levels around 75'000 depicted in dark blue. Cells transfected with Prnp siRNA controls showed Net-FRET levels around 125'000 depicted in dark orange. Non-target siRNA treated controls showed Net-FRET levels above 150'000 depicted in bright orange. Samples showed different Net-FRET levels.

To calculate Net-FRET, the APC background fluorescence and detection buffer were subtracted from the raw FRET signal of each sample in APC and Eu channels (equation 1). Spectral overlap compensation was measured by the proportionality factor P (equation 2) (Ballmer, Moos et al. 2017). The first QC of PrP^C levels in the form of Net-FRET signal showed distinct separation between the control groups (Figure 13).

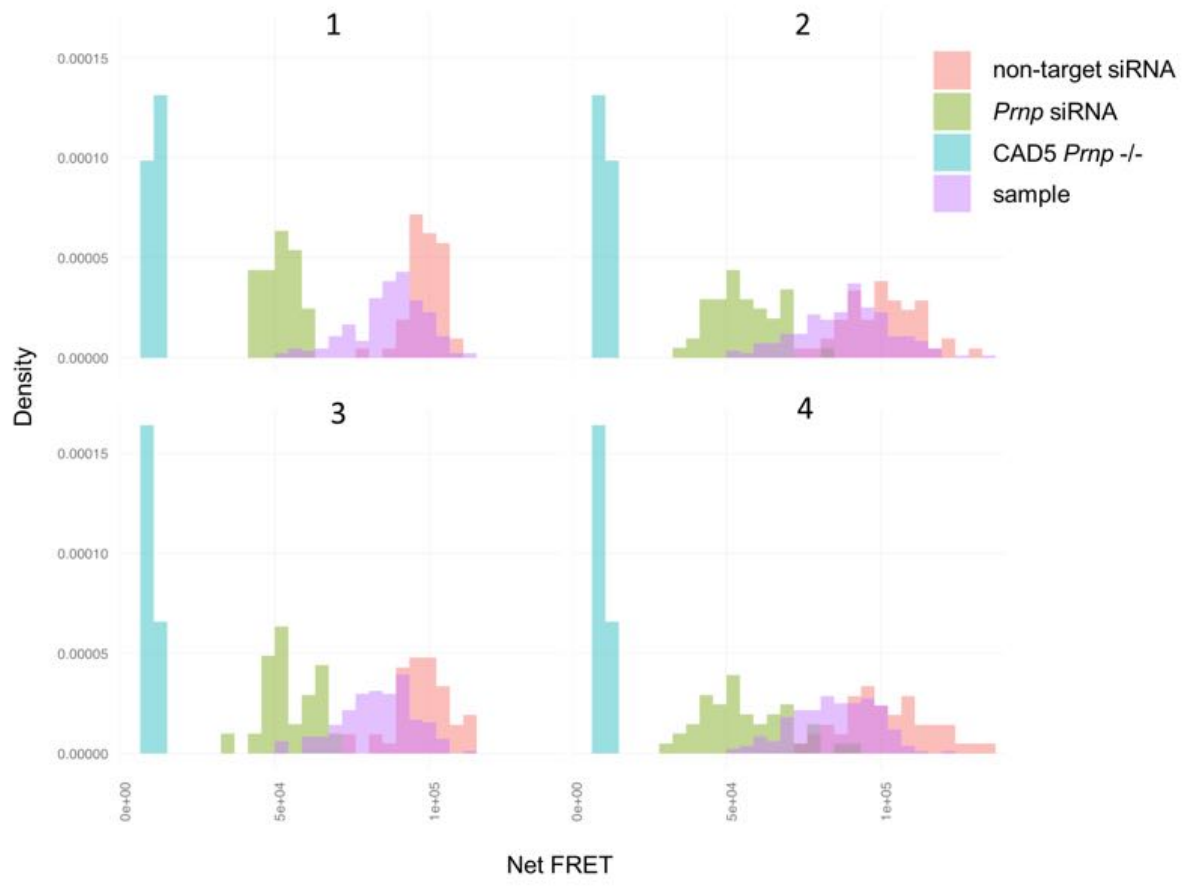

Figure 13: Net-FRET quality controls from the first PrP^C SKD screen. Each histogram represented one plate. CAD5 Prnp -/- control (blue), Prnp targeting siRNA control (green), and non-target siRNA control (orange) were clearly separated from each other. Samples (violet) were distributed between the Prnp targeting and scrambled siRNA controls.

Strictly standardized mean difference (SSMD), which is commonly used for QC in screening, was defined for a moderately strong control. SSMD calculated for Net-FRET values of non-target siRNA and *Prnp* targeting siRNA controls as well as for non-target siRNA and CAD5 *Prnp*-/- cells were in the excellent range and thus passed quality control (Figure 14) (Bosque and Prusiner 2000).

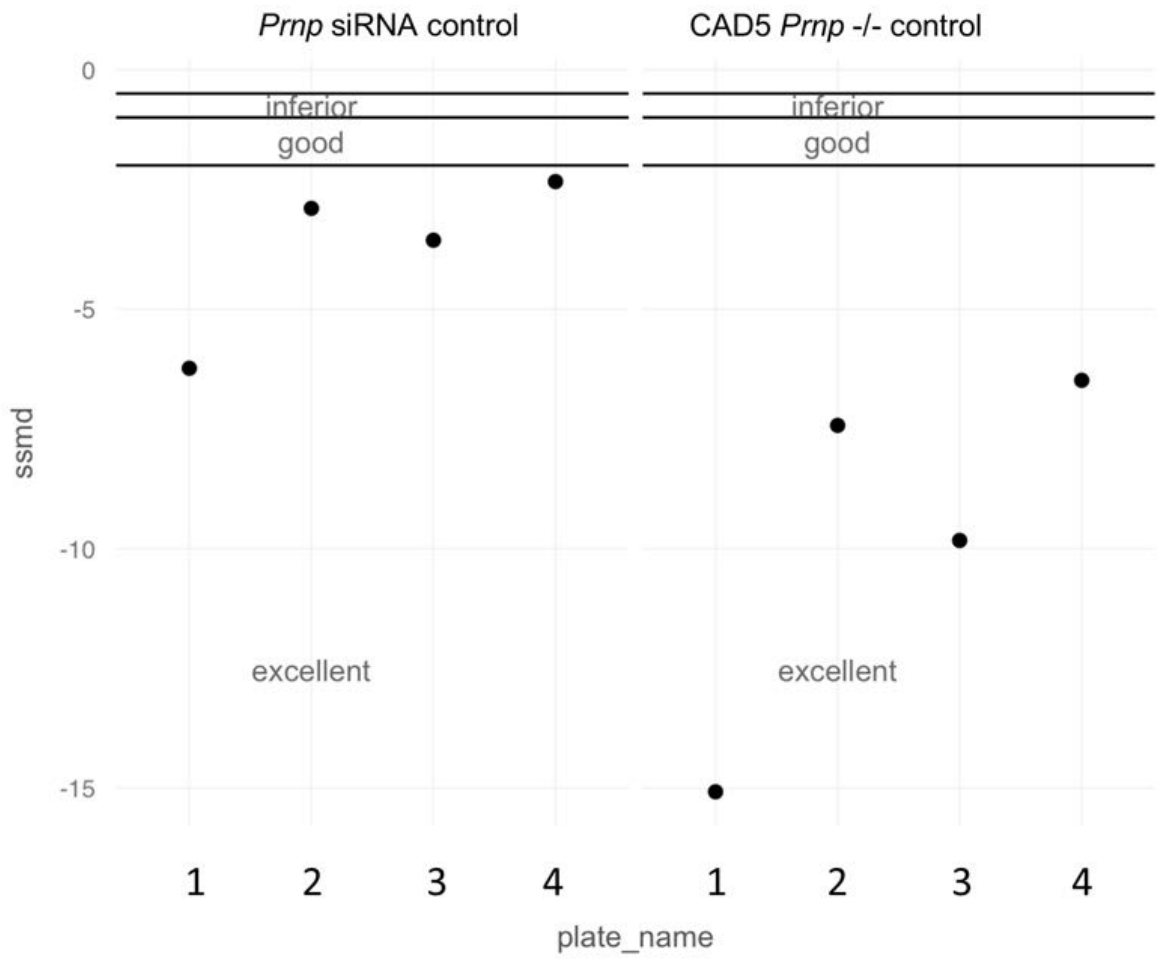

Figure 14: SSMD calculated for Net-FRET values of non-target siRNA and Prnp targeting siRNA controls were in the excellent range (left). SSMD calculated for Net-FRET values of non-target siRNA control and CAD5 Prnp-/- cells were in the excellent range too (right).

The QC of cell viability in the form of heatmaps representing the RT-Glo signal showed an overall gradient with decreasing signal from plate four to one (Figure 15).

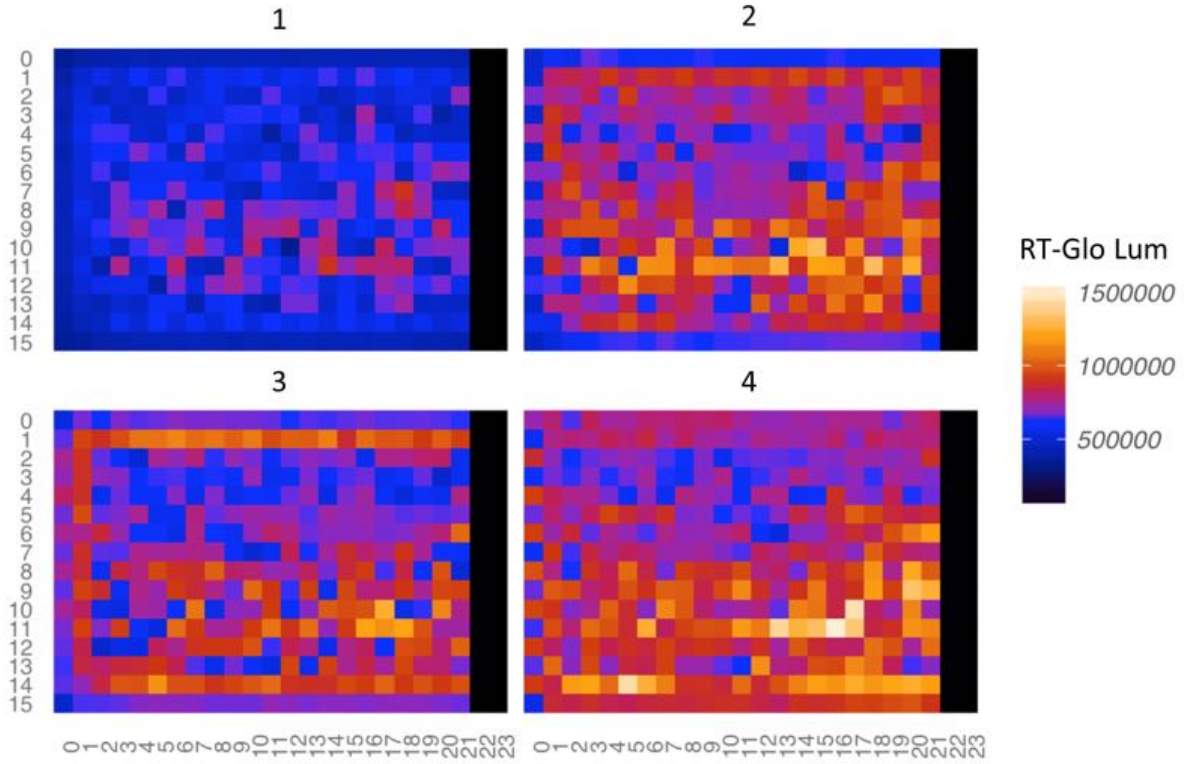

Figure 15: RT-Glo luminescence levels representing cell viability levels were visualized for four plates as heatmaps. High RT-Glo luminescence signal standing for high cell viability was depicted in orange, low RT-Glo levels in blue. QC of RT-Glo luminescence signal showed overall and inter-plate temperature gradients.

The overall gradient correlated with temperature, which could be explained by the order of plate measurement. Plate four which showed the highest RT-Glo signal was measured as first plate. Plate four was directly taken out of the incubator at 37°C and measured at room temperature. Meanwhile the other plates were cooling down at room temperature, which was reflected in progressively lower RT-Glo levels with lowest levels in plate one, which was measured as last plate. The outermost control wells showed low RT-Glo levels, which could be explained by cooling starting from the boarders, which resulted in an additional inter-plate temperature gradient. The outermost wells, which were prone to evaporation, were excluded from further data analysis. Consistent with the heat map, a swarm blot depicting the RT-Glo luminescence of the controls for each plate showed lower RT-Glo values in Plate 1 than in the other plates (Figure 16 a). The variability of the cell viability was high, however, the siRNA controls overlapped in the same range (Figure 16 b). CAD5 *Prnp*-/- cells, that were seeded only in the first two rows clustered closely in the middle of the swarm blot. The samples were within the the range of the controls with a slightly lower viability than the controls.

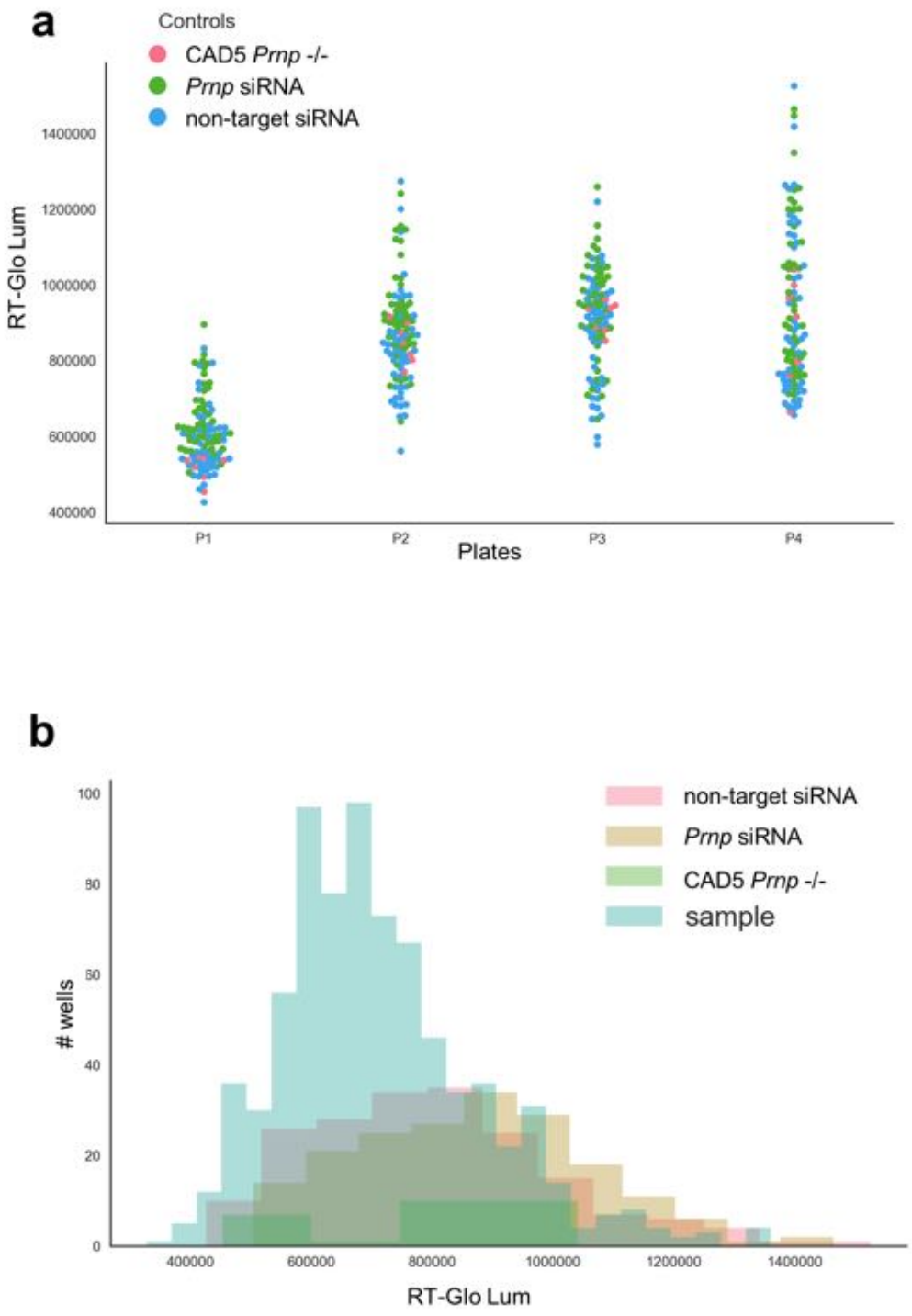

Figure 16: Cell viability QC. a) Swarm blot depicting the RT-Glo luminescence of the controls for each plate. One dot represented one well of CAD5 wt cells either transfected with non-target siRNA, Prnp targeting siRNA or CAD5 Prnp-/- cells. RT-Glo levels were reduced in plate 1. b) Histogram showing the overlap in cell viability of the controls and samples.

QC of Net-FRET further included checking for row or column effects on the plate that could

arise with unequal dispensing and cause inter-plate variability. The mean value of odd and even columns over plates one to four was more even than for odd and even rows, but both were in the acceptable range (Figure 17).

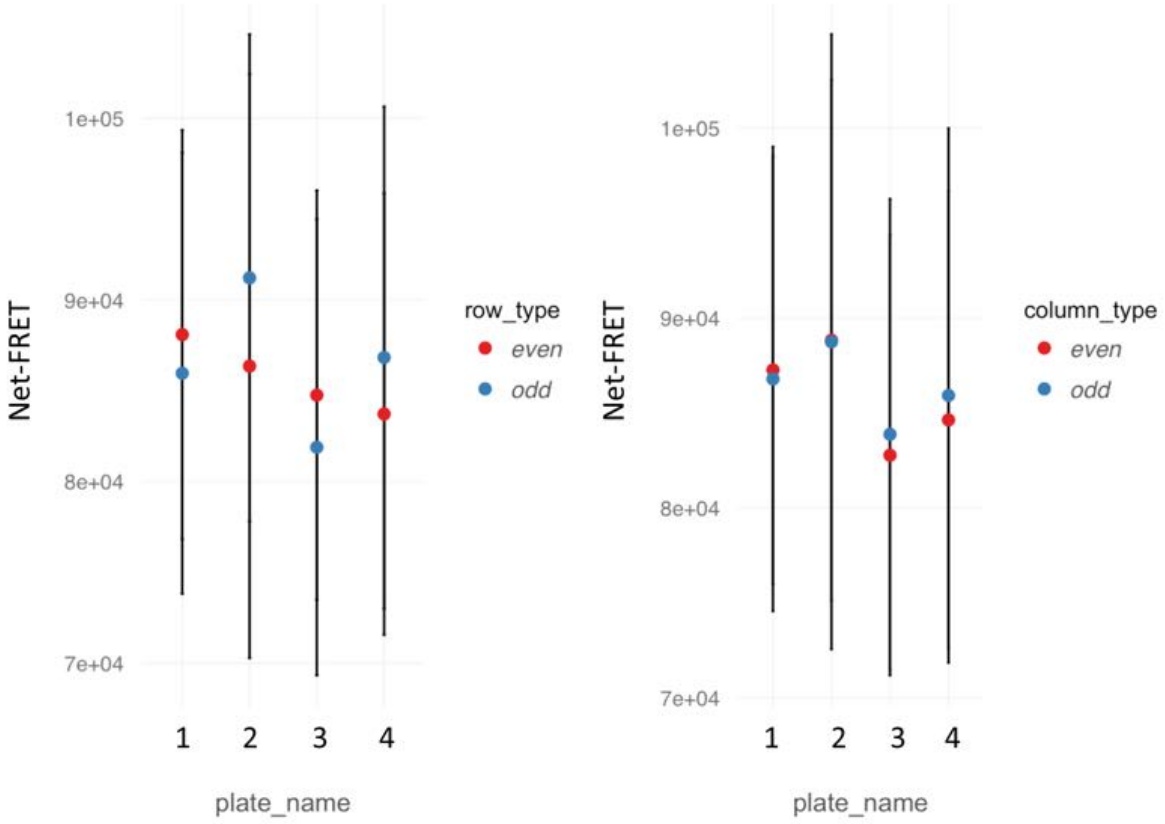

Figure 17: Quality controls of the first PrP^C SKD screen checking the mean value over plates 1 – 4 for odd and even rows and columns. The variability in rows was higher than within columns, but still in the acceptable range. Higher variability between rows could be explained by the dispensing pattern of the dispenser. Two subsequent rows were filled by the same tip of the cassette within the dispenser, whereas one column was filled by eight different tips. The differences within columns caused by eight tips are likely to neutralize each other, resulting in lower variability.

To allow comparison and combination of data from different plates in the screen, the Net-FRET values were normalized by Gaussian process prediction. For each plate, the Gaussian process with the best fit was chosen by lowest Bayesian information criterion to model the data (Figure 18) (Birmingham, Selfors et al. 2009, Wit, van den Heuvel et al. 2012).

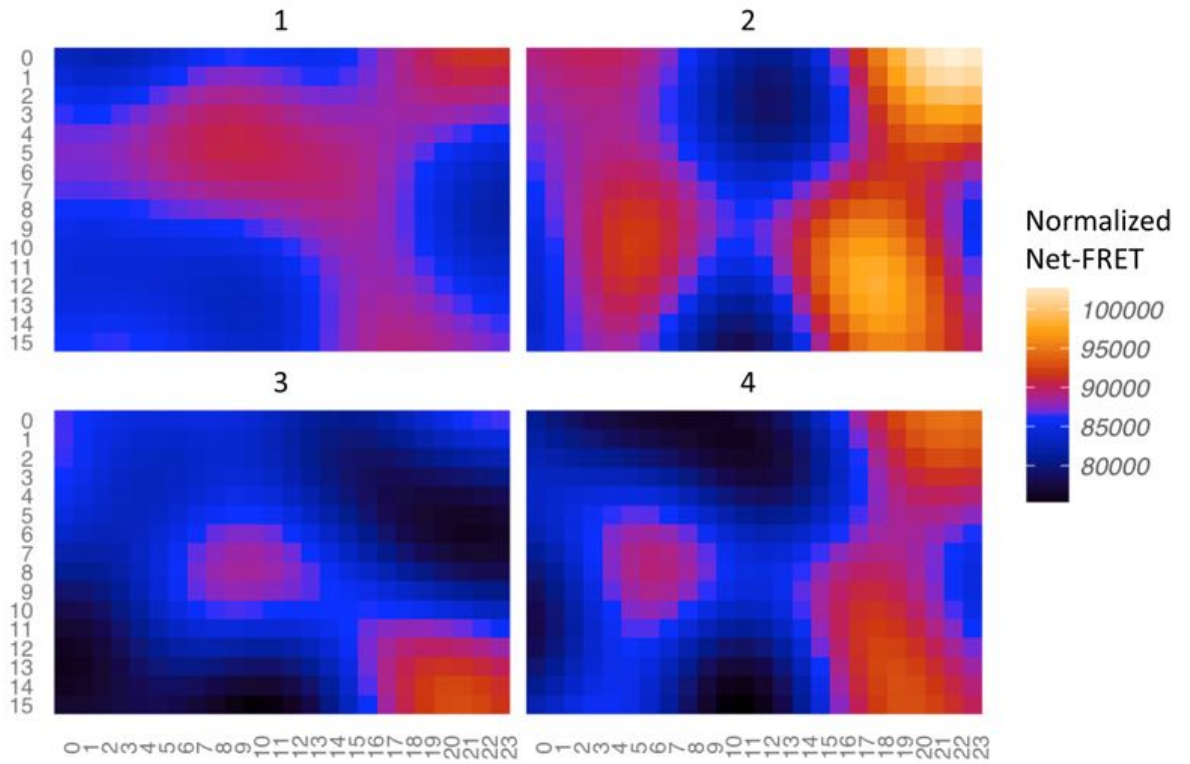

Figure 18: Best fit Gaussian process prediction based on Net-FRET values for plates 1 – 4 of the first PrP^C SKD screen.

Replicate correlation was calculated by robust linear regression applied to the raw Net-FRET signal of duplicates and to Gaussian process normalized net-FRET signal. The coefficient of determination for raw Net-FRET was r^2 = 0.424, r^2 for Gaussian process normalized Net-FRET signal was 0.467 (Figure 19).

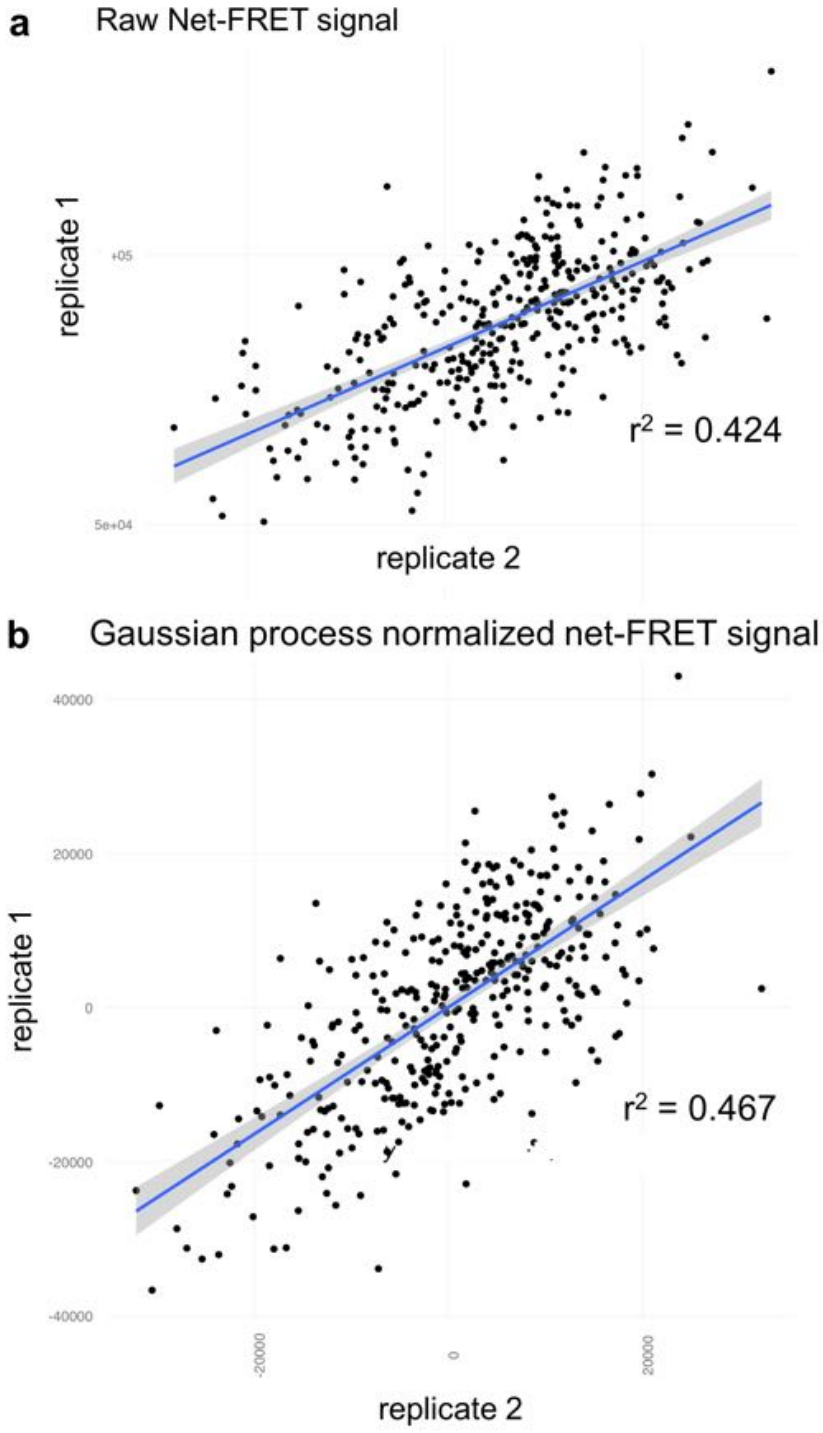

Figure 19: a) Robust linear regression of the raw net-FRET signal of duplicates with coefficient of determination r^2 = 0.424. b) Robust linear regression of the Gaussian process normalized net-FRET signal of duplicates with coefficient of determination r^2 = 0.467.

Due to the gradients in RT-Glo signals caused by differences in temperature, normalization of the Net-FRET signal with RT-Glo cell viability reduced the correlation between technical replicates in most of the cases. Therefore, I decided to implement the RT-Glo data manually. Hits

were selected based on the best gaussian processed normalized sample signal versus non-target comparison at a threshold p = 0.001. Of total 376 siRNAs, 82 siRNAs led to substantial downregulation of PrP levels. The library comprised multiple siRNAs against each target. The two top hits *Hspa5* and *Psmc5*, were both targeted by four siRNAs (Figure 20). Seven chaperones were targeted by three siRNAs, 12 chaperones by two siRNAs. 27 chaperones were targeted by one siRNA. The proteomic composition of the neuronal CAD5 cells was characterized, herein 4142 proteins, representing 96.8% of the total mass of polypeptides, were quantified significantly above the back-ground noise, out of 8403 protein identifications. The quantitative values as mass fractions and copy number per cubic micron were implemented into the chaperone hit characterization. Chaperone hits that were targeted by the RNAi screen but that were undetectable or not significantly quantified in the proteomics experiment, were high-lighted in red.

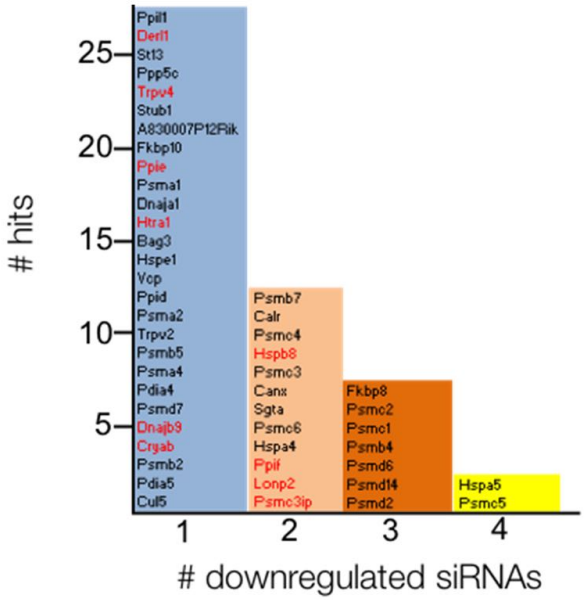

Figure 20: Druggable chaperone hits from the first PrP^C SKD screen reducing the PrP signal. The two top hits Hspa5 and Psmc5, were both targeted by four siRNAs (yellow). Seven chaperones were targeted by three siRNAs (dark orange), 12 chaperones by two siRNAs (bright orange). 27 chaperones were targeted by one siRNA (blue). Chaperone hits that were targeted by the RNAi screen but that were undetectable or not significantly quantified in the proteomics experiment, were high-lighted in red.

I performed the second murine SKD PrP^C screen with an arrayed siRNA library targeting non-druggable chaperones in six 384-well plates. Net-FRET data representing PrP levels were visualized in heatmaps for all six screen plates (Figure 21).

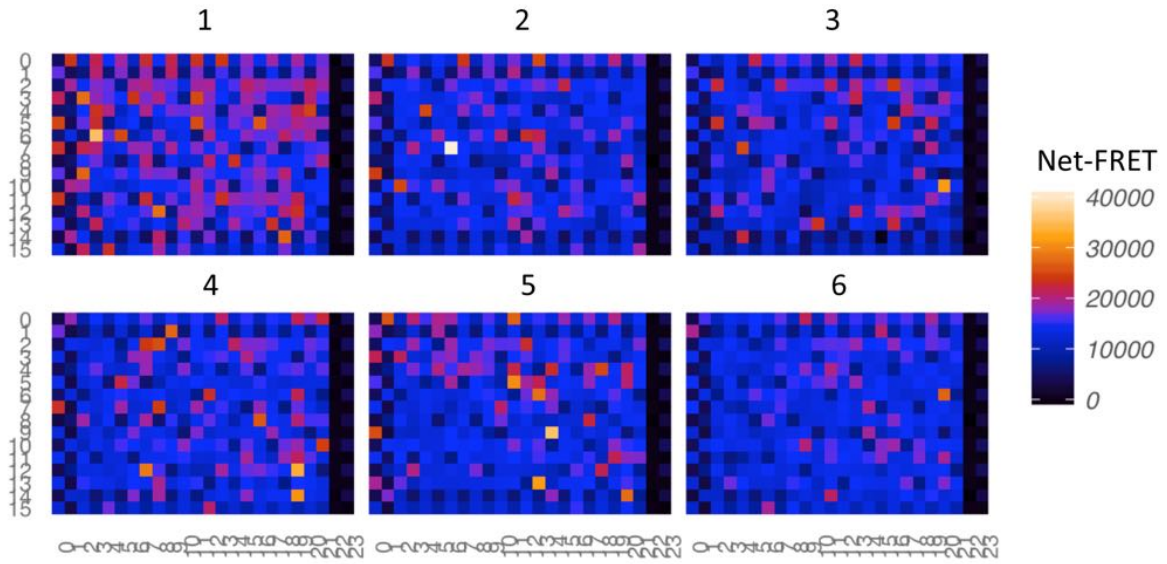

Figure 21: Net-FRET levels representing PrP^C levels were visualized for six plates as heatmaps. CAD5 Prnp-/- cells in every second well in columns one and two showed low Net-FRET levels below 5000 depicted in black. Cells transfected with Prnp siRNA controls showed Net-FRET levels between 5000 and 10'000 depicted in dark blue. Non-target siRNA treated controls showed Net-FRET levels between 10'000 and 20'000 depicted in violet and orange. Samples showed different Net-FRET levels.

QC of PrP^C Net-FRET signal showed distinct separation between the non-target and *Prnp* siRNA control groups (Figure 22).

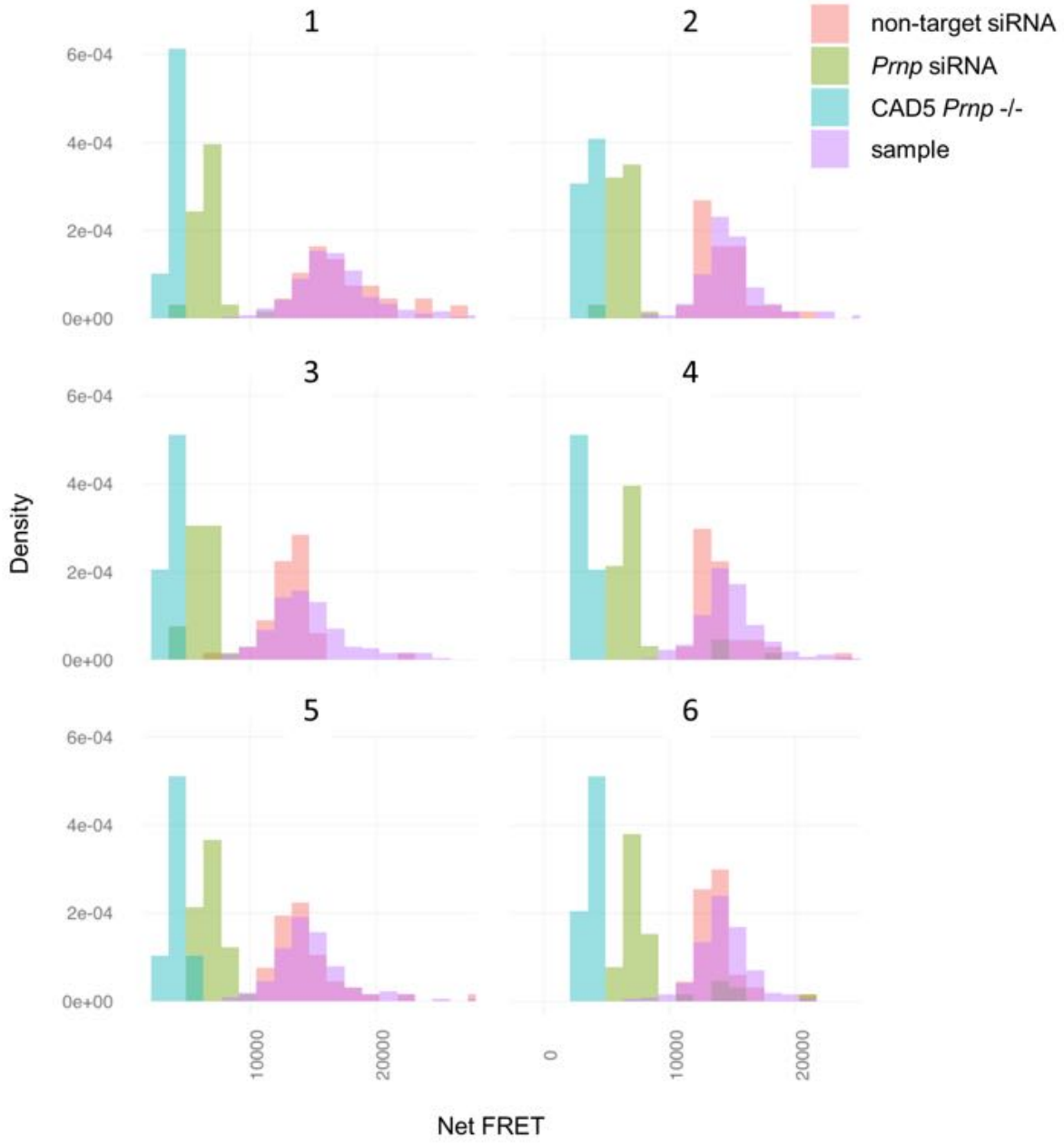

Figure 22: Net-FRET quality controls from the second PrP^C SKD screen. Each histogram represented one plate. CAD5 Prnp -/- control (blue), Prnp targeting siRNA control (green), and non-target siRNA control (orange) were clearly separated from each other. Samples (violet) were distributed around scrambled siRNA controls.

SSMD defined for a moderately strong control calculated for Net-FRET values of non-target siRNA and *Prnp* targeting siRNA controls were in the excellent and good range (Figure 23) (Bosque and Prusiner 2000). SSMD for non-target siRNA and CAD5 *Prnp* -/- controls were in the excellent range.

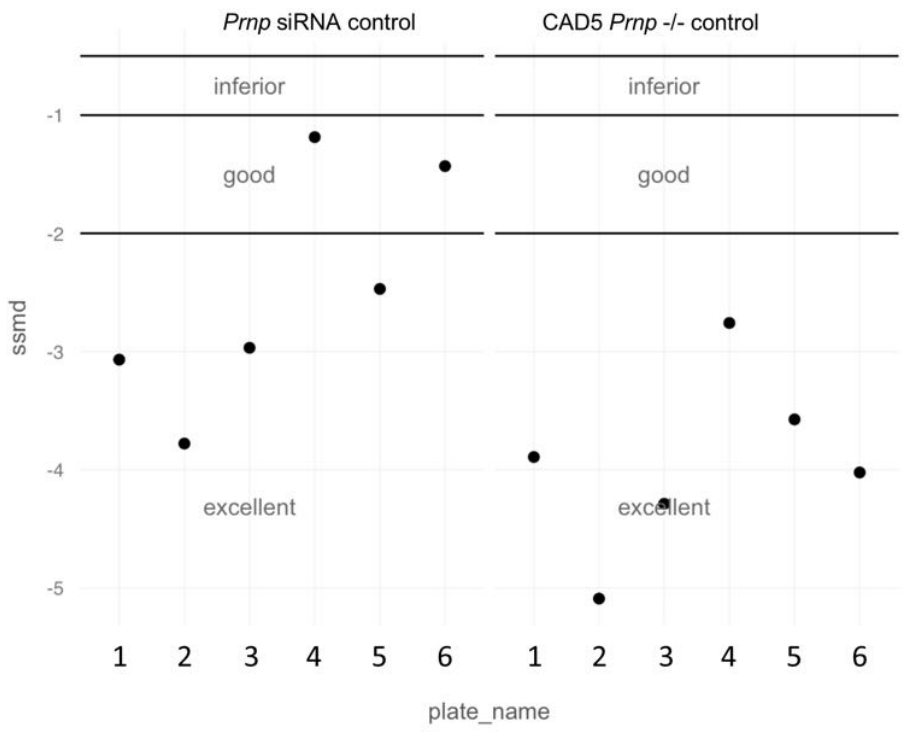

Figure 23: SSMD calculated for Net-FRET values of non-target siRNA and Prnp targeting siRNA controls of plates 1, 2, 3 and 5 were in the excellent range, plates 4 and 6 in the good range (left). SSMD calculated for Net-FRET values of non-target siRNA control and CAD5 Prnp-/- cells were in the excellent range for all plates (right).

In the second screen I acclimatized the plates for one hour to room temperature, before measuring the RT-Glo luminescence cell viability signal with the Envision reader. QC in the form of heatmaps representing the cell viability showed that the RT-Glo luminescence signal was much more homogeneous than in the first screen (Figure 24).

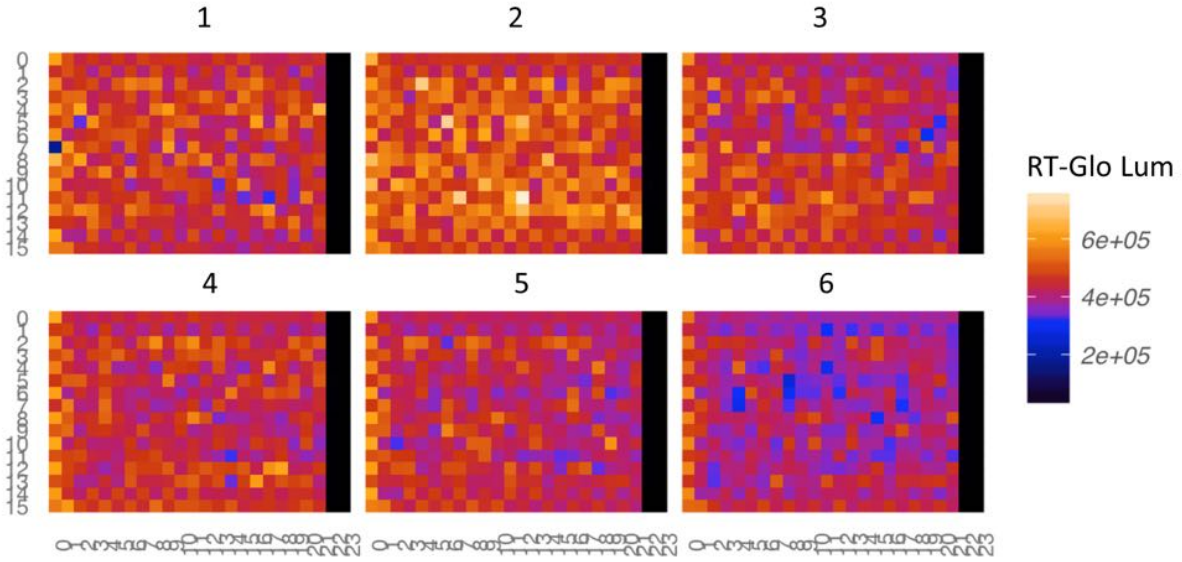

Figure 24: RT-Glo levels representing cell viability were visualized for four plates as heatmaps. Low RT-Glo levels around 200'000 were depicted in blue, medium RT-Glo levels around 400'000 were shown in dark orange, and high RT-Glo levels above 600'000 were shown in bright orange.

A swarm blot depicting the RT-Glo luminescence of the controls for each plate showed comparable viability between plates and separation between the different controls (Figure 25 a). CAD5 *Prnp*-/- cells showed the highest variability, followed by *Prnp* transfected cells. Non-target siRNA led to the lowest viability. The range of the cell viability was much smaller than in the first screen. The samples were within the range of the controls (Figure 25 b).

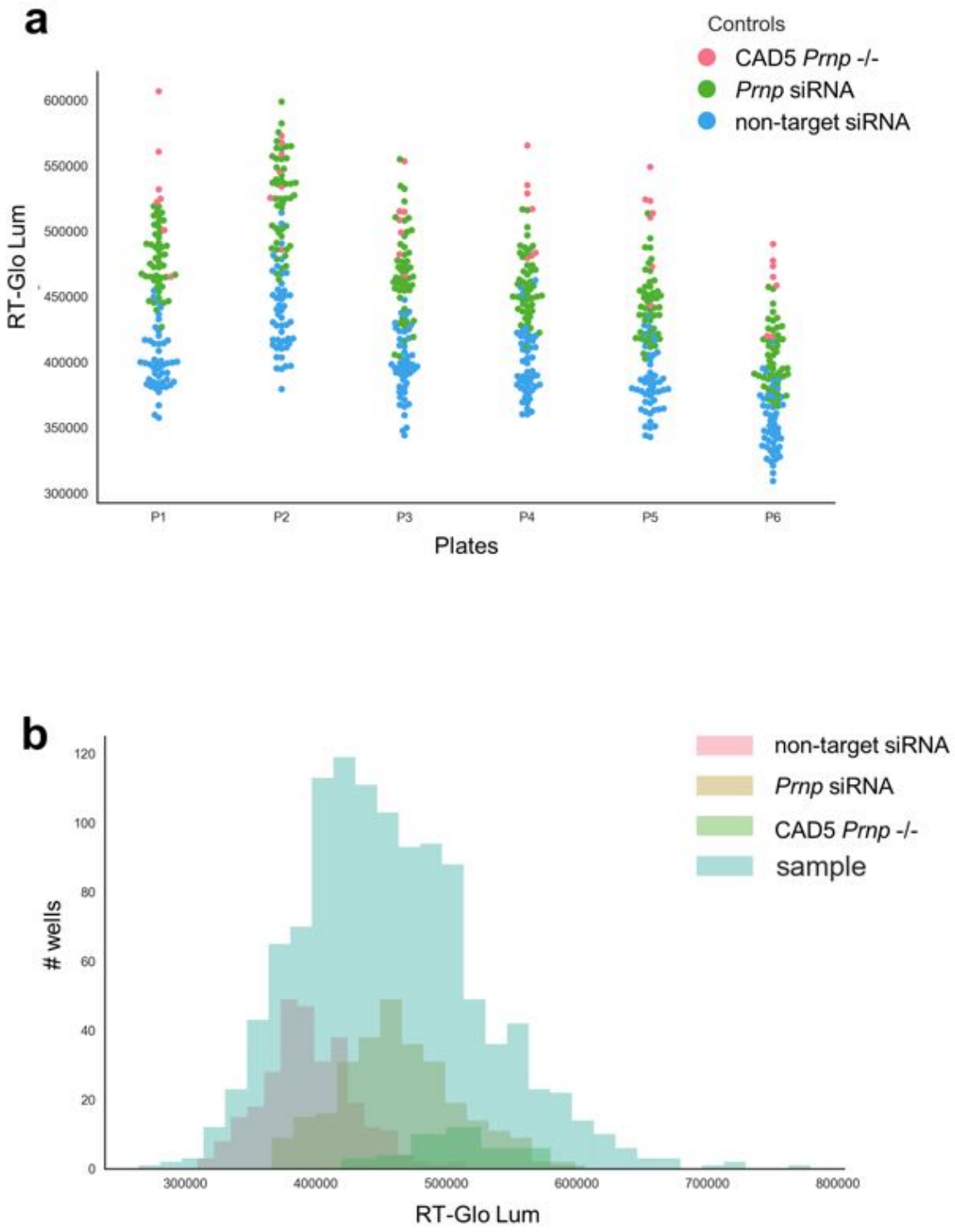

Figure 25: Cell viability QC. a) Swarm blot depicting the RT-Glo luminescence of the controls for each plate. One dot represented one well of CAD5 wt cells either transfected with non-target siRNA, Prnp targeting siRNA or CAD5 Prnp-/- cells. RT-Glo levels differed between the controls. b) Histogram showing the overlap in cell viability of the controls with slightly enhanced viability in some samples.

QC for row or column effects on the plate was comparable between rows and columns and

was in the acceptable range (Figure 26).

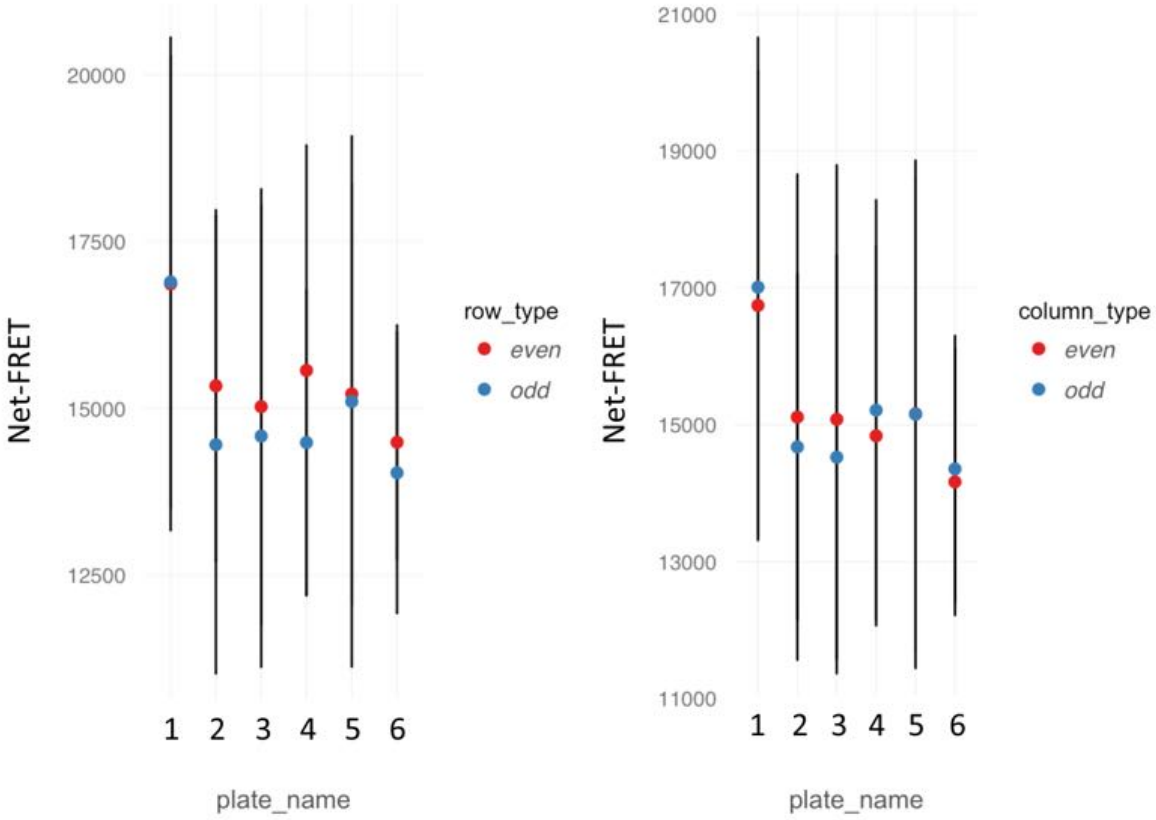

Figure 26: Quality controls of the second PrP^C SKD screen checking the mean value over plates for odd and even rows and columns. The variability in rows was comparable to columns and in the acceptable range for all six screen plates.

The Net-FRET values of each plate were normalized by Gaussian process prediction (Figure 27) (Birmingham, Selfors et al. 2009, Wit, van den Heuvel et al. 2012).

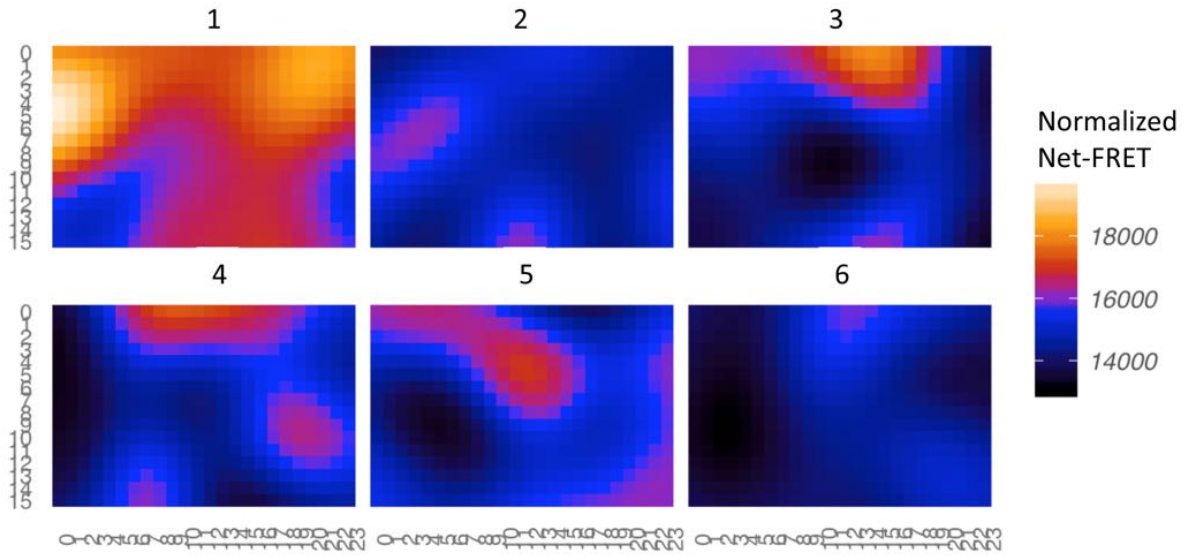

Figure 27: Best fit Gaussian process prediction based on Net-FRET values of the second PrP^C SKD screen.

Replicate correlation was calculated by robust linear regression applied to the raw Net-FRET signal of duplicates and to Gaussian process normalized net-FRET signal. The coefficient of determination for raw Net-FRET was r^2 = 0.125, r^2 for Gaussian process normalized Net-FRET signal was 0.16 (Figure 28).

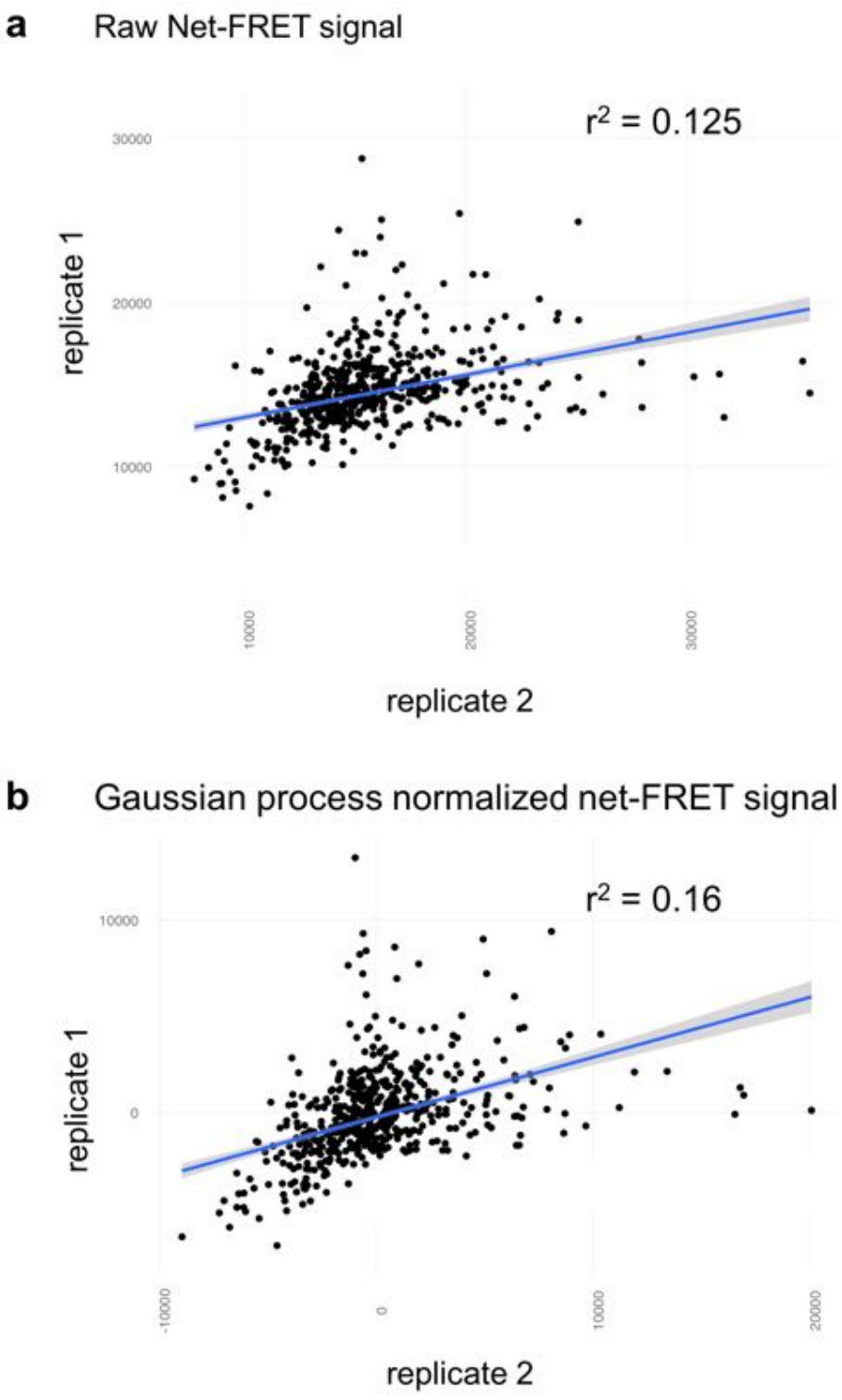

Figure 28: a) Robust linear regression of the raw net-FRET signal of duplicates with coefficient of determination r^2 = 0.125 b) Robust linear regression of the Gaussian process normalized net-FRET signal of duplicates with coefficient of determination r^2 = 0.16.

Hits were selected based on the best gaussian processed normalized sample signal versus non-target comparison at a threshold p = 0.001. Of total 560 siRNAs, one siRNA targeting

Psmd11 led to significant downregulation of PrP levels, 24 siRNAs to upregulation. 22 chaperones were targeted by one siRNA, chaperones *Hsf1* and *Chordc1* were targeted by two siRNAs, leading to elevated PrP levels (Figure 29). Chaperone hits that were targeted by the RNAi screen but that were undetectable or not significantly quantified in the proteomics experiment, were high-lighted in red.

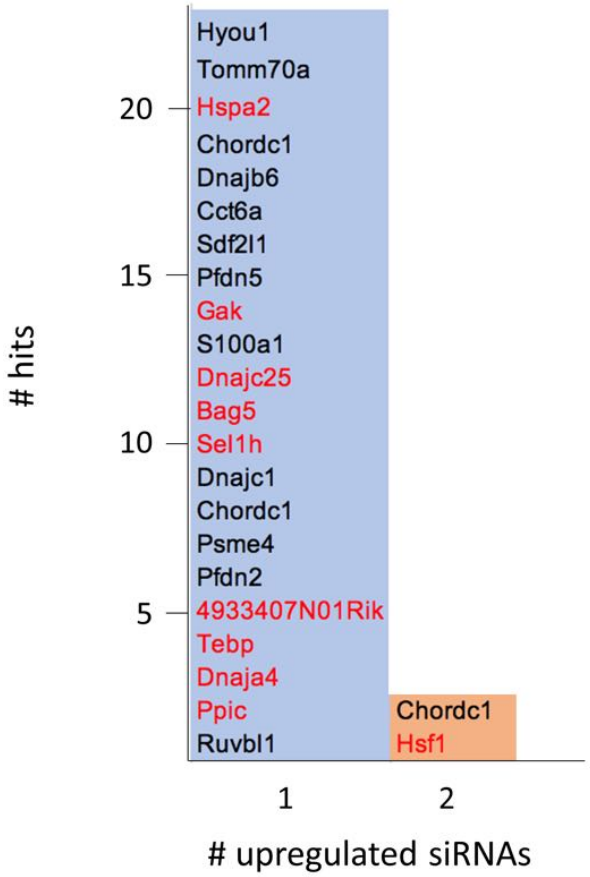

Figure 29: Non-Druggable chaperone hits from the second PrP^C SKD screen increasing the PrP signal. 2 chaperones were targeted by two siRNAs (bright orange), 22 chaperones were targeted by one siRNA (blue). Chaperone hits that were targeted by the RNAi screen but that were undetectable or not significantly quantified in the proteomics experiment, were high-lighted in red.

The libraries of the two PrP^C screens comprised multiple siRNAs against each target. Enrichment of these multiple siRNAs against a specific target facilitated the discrimination between true and false positives. I selected true positive chaperone hits according to the number of siRNAs present in siRNA hits, targeting the same chaperone. I considered chaperones targeted by more than one siRNA as true positive hits, if they were within the viability range (Figure 30). The viability range was defined by the mean of non-target controls +/- 2 SD. I analyzed the viability for each gene with all siRNAs in technical duplicates (Appendix 80 + 81). If more than

half of the siRNAs targeting the same gene were within the viability range, the gene passed viability QC. Gene and protein names of chaperone hits that were targeted by two, three and four siRNAs were summarized in a table with indication of up- or downregulating effect on PrP (Figure 30). All of these hits passed the viabilty QC.

Gene	Protein	up-/ down
Hspa5	Heat shock 70kDa protein 5	
Psmc5	26S protease regulatory subunit 8	
Fkbp8	Peptidyl-prolyl cis-trans isomerase FKBP8	
Psmc2	26S protease regulatory subunit 7	
Psmc1	26S protease regulatory subunit 4	
Psmb4	Proteasome subunit beta type-4	
Psmd6	26S proteasome non-ATPase regulatory subunit 6	
Psmd14	26S proteasome non-ATPase regulatory subunit 14	
Psmd2	26S proteasome non-ATPase regulatory subunit 2	
Psmb7	Proteasome subunit beta type-7	
Calr	Calreticulin	
Psmc4	26S protease regulatory subunit 6B	
Hspb8	Heat shock protein beta-8	
Psmc3	26S protease regulatory subunit 6A	
Canx	Calnexin	
Sgta	Small glutamine-rich tetratricopeptide repeat-containing protein alpha	
Psmc6	26S protease regulatory subunit 10B	
Hspa4	Heat shock 70 kDa protein 4	
Ppif	Cellular tumor antigen p53	
Lonp2	Lon protease homolog 2, peroxisomal	
Psmc3ip	Homologous-pairing protein 2 homolog	
Hsf1	Heat shock factor protein 1	
Chordc1	Cysteine and histidine-rich domain-containing protein 1	

4 siRNAs
3 siRNAs
2 siRNAs

downregulation
upregulation

Figure 30: Gene and protein names of all chaperone hits from the first and second PrP^C SKD screen of chaperone hits that were targeted by four (yellow), three (dark orange) and two siRNAs (bright orange). Chaperones leading to downregulation of PrP were marked in bright claret-red, hits leading to upregulation of PrP in dark claret-red. Chaperone hits that were targeted by the RNAi screen but that were undetectable or not significantly quantified in the proteomics experiment, were high-lighted in red.

6.1.3 Murine PrP^{Sc} screen

For the murine PrP^{Sc} screen I first established acute infection of cells with subsequent PK-Western blotting by optimizing existing protocols from the literature for CAD5 cells (Vorberg, Raines et al. 2004, Greil, Vorberg et al. 2008). I inoculated CAD5 wild type (wt) and *Prnp*-/- cells for 96 hours with infectious brain homogenate from mice inoculated with RML6 and non-infectious brain homogenate (NBH) (0.3 and 0.1 μg/mL). I washed the samples four times to remove residual inoculum. Subsequently, I lysed the samples, digested them with Proteinase K (PK) and performed Western blotting. PK-Western blots showed, that RML6 containing brain homogenate, which served as positive control, exhibited the typical diagnostic shift towards a smaller PK-resistant core with un-, mono- and di-glycosylated PrP^{Sc} (Figure 31). PrP^C from

uninfected and NBH treated CAD5 cells, which both served as negative controls, was completely digested. CAD5 cells infected with 0.3 μg RML6/mL did show a stronger PrP^{Sc} band than cells infected with 0.1 μg RML6/mL. Despite the four washing steps there was some residual RML6 inoculum in the CAD5 *Prnp*-/- cells. The PrP^{Sc} band of infected CAD5 wt cells was much stronger than in CAD5 *Prnp*-/- cells, indicating replication of PrP^{Sc}.

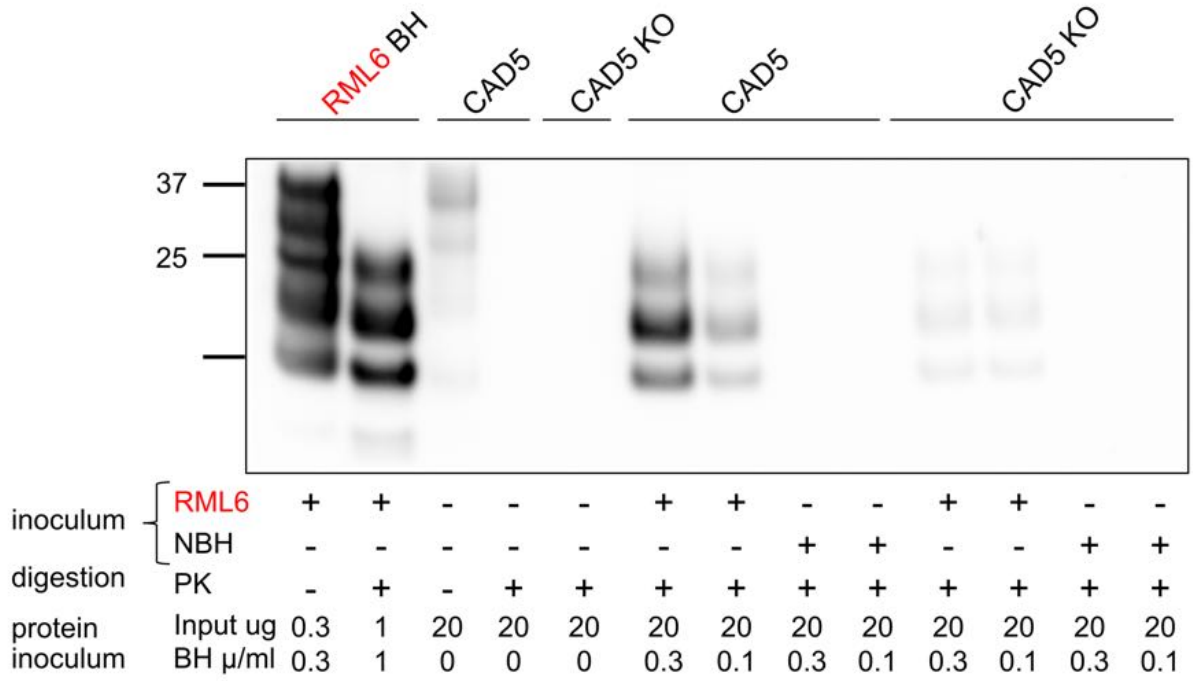

Figure 31: PK-Western with acutely infected CAD5 wt, and CAD5 Prnp-/- cells. CAD5 cells were successfully infected with RML6 by acute infection as shown by the typical shift of PK-digested RML6 with un-, mono- and di-glycosylated PrP^{Sc} bands. Chronically infected scCAD cells digested with PK showed reduced levels of PrP^{Sc} when inoculated with lower RML6 concentrations (0.1μg). RML6 brain homogenate served as a positive control (first and second band). Uninfected and NBH treated CAD5 cells, as well as CAD5 Prnp-/- cells digested with PK served as negative controls and did not show residual PrP^{C}.

Based on the PK-Western results and on a HP-FRET protocol that had been established previously in our lab, I performed the PrP^{Sc} screen with acute CAD5 cell infection in 384-well format (Li 2016). siRNAs were printed on a LabCyte acoustic dispensing robot into 384-well plates and frozen at -40°C (Figure 32). At the assay day the plates were thawed, Lipofectamine and 2800 CAD5 cells were added. After 24 hours infectious medium containing RML6 and RT-Glo cell viability marker were added. After 96 hours the cell viability was assessed with the Envision reader. In contrast to PrP^{C}, PrP^{Sc} is relatively Proteinase K (PK) resistant. PrP^{C} was completely digested by adding Protinase K (PK) to the lysis buffer. PK was inactivated by Phenylmethanesulfonyl (PMSF). Denaturation buffer (0.5M NaOH) disassembled PK-resistant

PrP^{Sc} aggregates into monomers and made epitopes available for the FRET-antibodies. Neutralizing buffer (0.5M NaH_2PO_4) was added to bring the pH to the physiological range, where the FRET antibodies were not degraded (Peretz, Scott et al. 2001). PrP^{Sc} levels were assessed by HP-FRET.

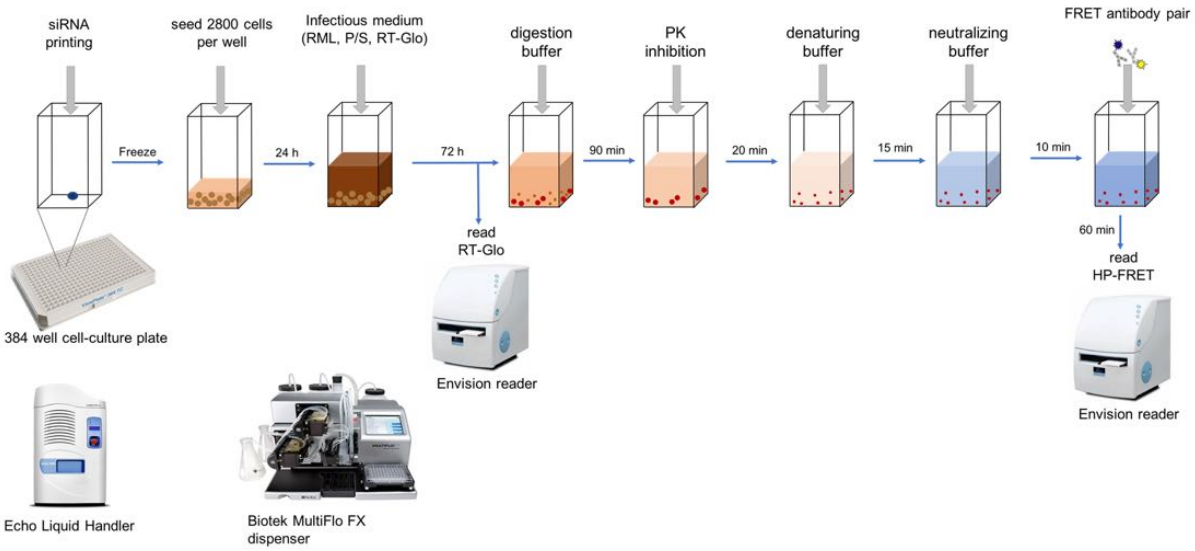

Figure 32: Workflow of PrP^{Sc} screen with reverse transfection and acute infection of CAD5 cells. After 96 hrs the cell viability was assessed with the Envision reader. Subsequently, the cells were lysed and digested with PK to remove PrP^{C}. PK was inactivated by Phenylmethanesulfonyl (PMSF). Denaturation buffer (0.5M NaOH) disassembled PK-resistant PrP^{Sc} aggregates into monomers and made epitopes available for the FRET-antibodies. Neutralizing buffer (0.5M NaH_2PO_4) was added to bring the pH to the physiological range, where the FRET antibodies were not degraded. PrP^{Sc} levels were assessed by HP-FRET.

To acutely infect CAD5 wt and CAD5 *Prnp*-/- cells, I used inoculum concentrations ranging from 1 μg/mL to 0.05 μg/mL of RML6 and NBH brain homogenate. The Net-FRET results did not show significant difference between the two infected cell types (Figure 33).

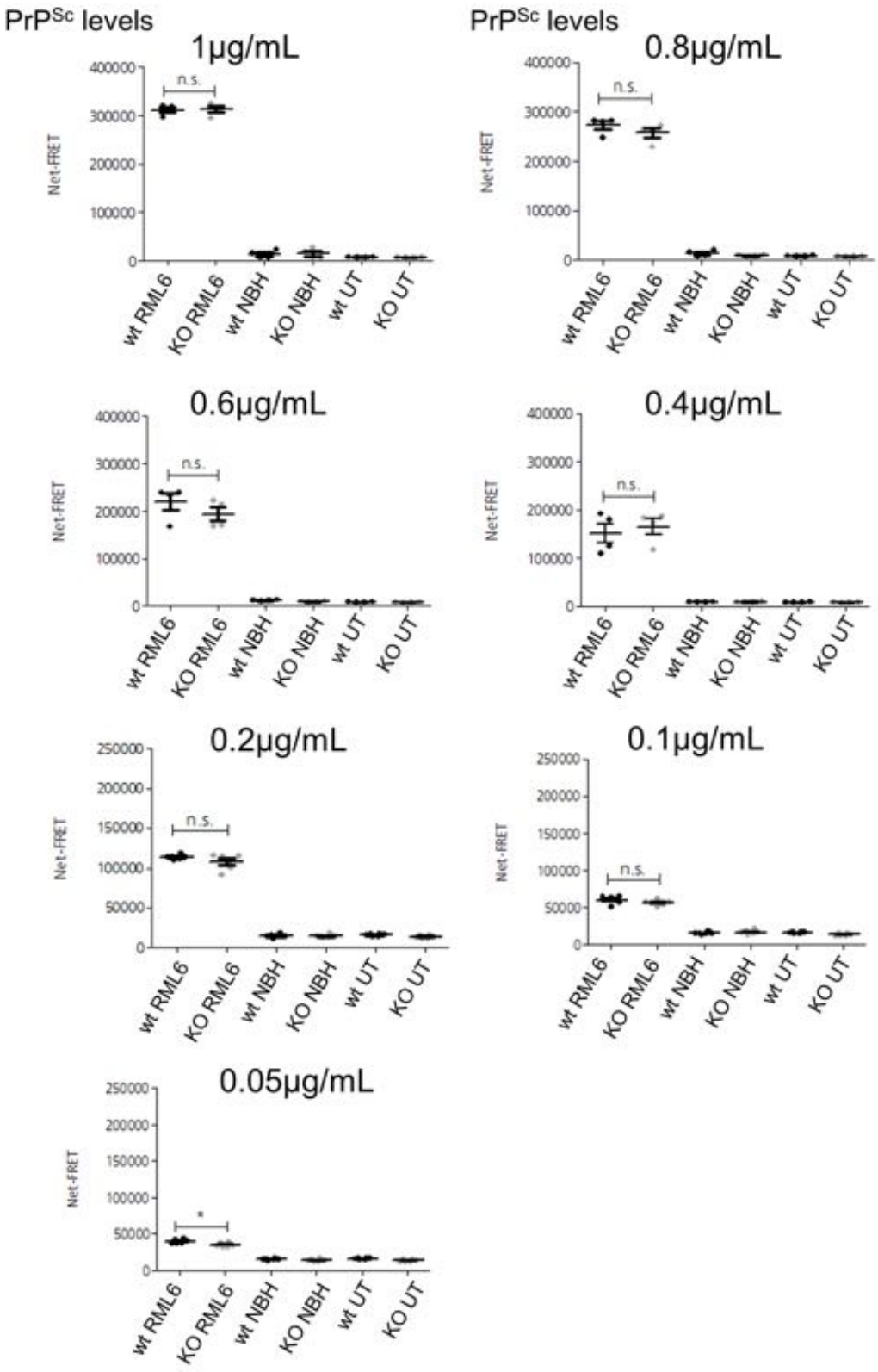

Figure 33: HP-FRET with CAD5 wt (wt) and CAD5 Prnp-/- cells (KO) acutely inoculated with different dilutions of RML6 and NBH ranging from 1 µg/mL to 0.05 µg/mL. Cells treated with NBH and untreated (UT) cells served as negative controls. Net-FRET signals standing for PrP^{Sc} levels showed no significant difference between CAD5 wt and CAD5 Prnp-/- cells.

Most probably residual inoculum masked endogenous prion replication. To reduce the concentration of the inoculum and still detect the PrP^{Sc} signal, I established an Enzyme-linked immunosorbent PrP^{Sc} assay (PrP^{Sc}-ELISA). After PK digestion, denaturation and neutralization, I transferred the PrP^{Sc} samples to ELISA plates that I had previously coated with PrP-binding POM1 antibody in PBS at 4°C overnight and blocked with 5% SuperBlock. I used Biotinylated POM19 anti PrP antibody and Streptavidin-HRP to detect PrP^{Sc}. PrP^{Sc}-ELISA was sensitive enough to distinguish the 10^{-5} dilution of RML6 from the blank (Figure 34 a). PrP^{Sc}-ELISA with PK undigested recombinant murine PrP ($rmPrP_{22\text{-}230}$) showed, that samples with concentration between 0.63 and 0ng/mL were in the linear range of the ELISA (Figure 34 b).

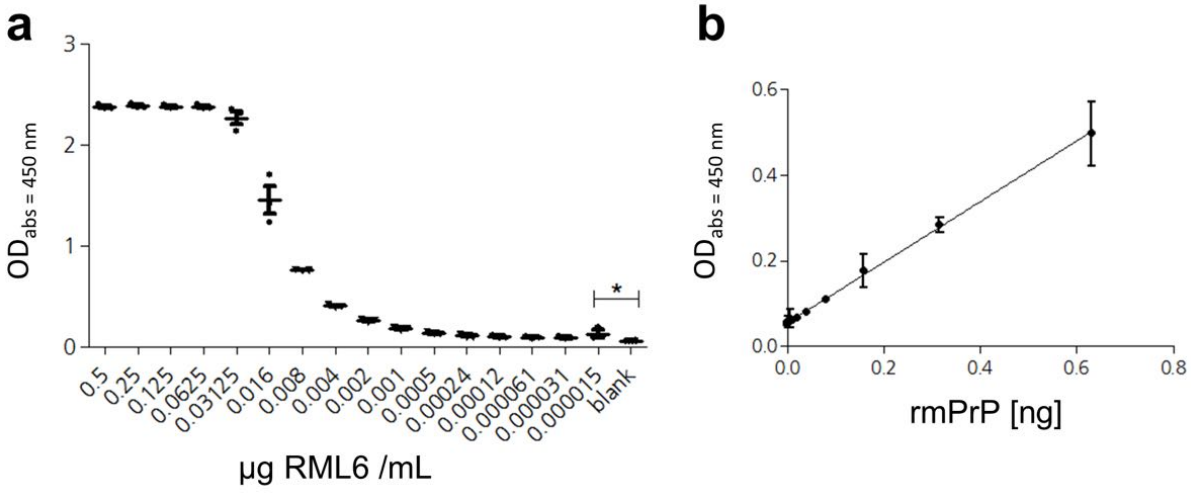

Figure 34: PrP^{Sc}-ELISA with 1:2 dilutions of infectious RML6 brain homogenate digested with PK. ELISA absorbance stands for PrP^{Sc} levels. PrP^{Sc}-ELISA was sensitive enough to distinguish the 10^{-5} dilution of RML6 from the blank. b) PrP^{Sc}-ELISA with 1:2 dilutions of recombinant murine PrP ($rmPrP_{22\text{-}230}$). ELISA absorbance stands for PrP^{C} levels. Samples were in the linear range of the ELISA when their concentration was between 0.63 and 0 ng/mL.

When I acutely infected CAD5 cells with very low concentrations of RML6 (0.03 – 0.008 μg/mL) PrP^{Sc}-ELISA showed that PrP^{Sc} levels were higher in inoculated cells than in the inoculum with 0.03 and 0.0016 μg RML6 per mL, but not anymore with 0.0008 μg RML6 per mL (Figure 35). The masking effect was still apparent and there was no clear distinction between infected CAD5 wild type (wt) and CAD5 *Prnp*-/- cells acutely infected with RML6.

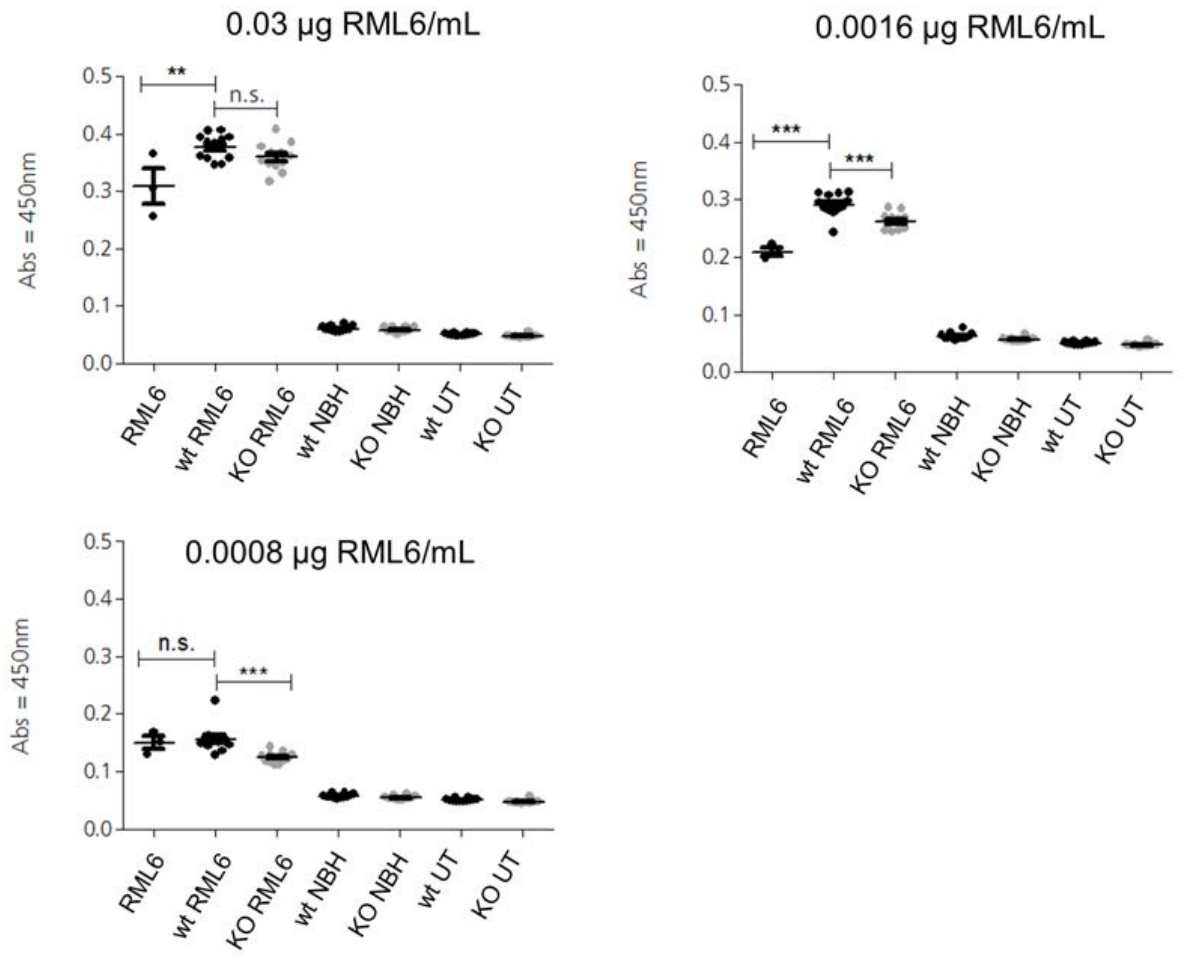

Figure 35: PrP^{Sc}-ELISA with CAD5 wt (wt) and CAD5 Prnp-/- cells (KO) acutely inoculated with different dilutions of RML6 and NBH. PrP^{Sc}-ELISA absorbance signals standing for PrP^{Sc} levels did not show clear distinction between CAD5 wt and CAD5 Prnp-/- cells. Cells treated with NBH and untreated (UT) cells served as negative controls and showed that PK digestion of PrP^{C} was complete.

In order to remove residual inoculum, I generated chronically infected scCAD cells by inoculating CAD5 cells with 0.1 μg/mL RML6 and non-infectious brain homogenate (NBH). I removed the medium containing the inoculum after 3 days and split the cells four times 1 : 5 every 3 – 4 days (Figure 36).

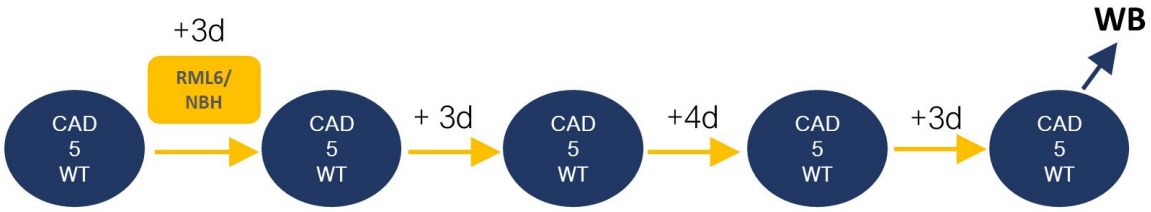

Figure 36: Scheme of chronical infection. I inoculated CAD5 cells with 0.1 μg/mL RML6 and NBH. After three days I removed the medium containing the inoculum and split the cells four times 1 : 5 every 3 – 4 days. After the fourth splitting, I lysed the cells and performed PK-Western blotting.

I generated CAD5 cells overexpressing PrP by stable transfection of CAD5 *Prnp*-/- clone #C12 with the coding region of murine *Prnp* and clonal selection through limited dilution. Sandwich ELISA of these cells showed that multiple, random integration of murine *Prnp* into the murine genome driven by the strong (Cytomegalovirus) CMV promoter led to significantly higher expression of murine PrP in three isolated clones (#6, #9 and #11), than in CAD5 wild type and CAD5 *Prnp* -/- clones (Figure 37 a). Immunohistochemistry of clone #9 (hyCAD) revealed physiological membranal expression of murine PrP (Figure 37 b).

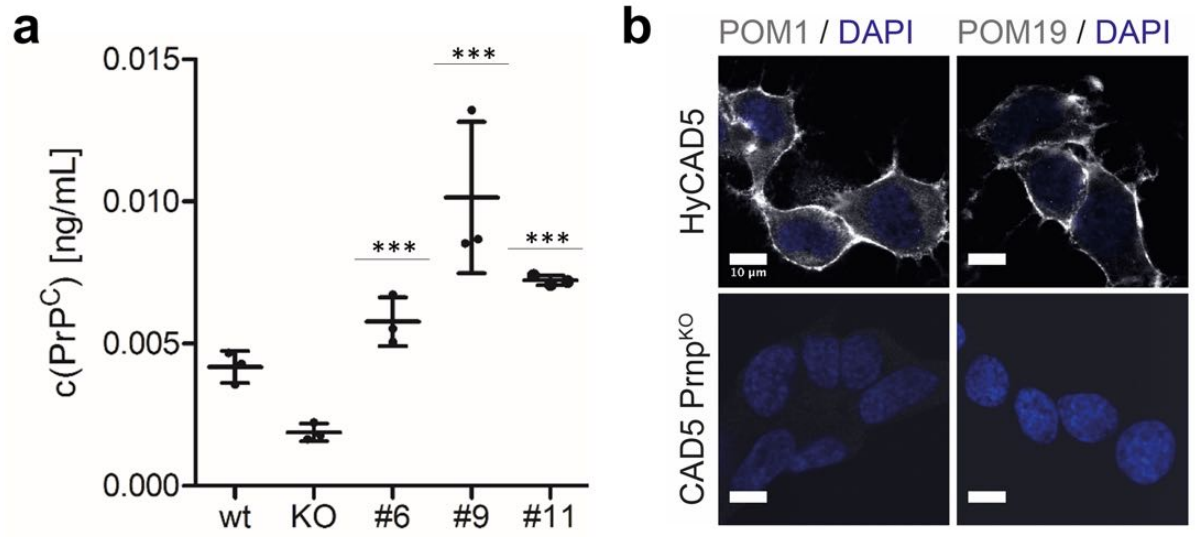

Figure 37: (Description on the next page)

*Figure 37: Characterization of CAD5 cells overexpressing PrP, which I generated by stably transfecting CAD5 Prnp-/- cells with the coding region of murine Prnp. Clonal selection through limited dilution resulted in three clones #6, #9 and #1. a) Sandwich ELISA with absolute PrP values showed significantly higher PrP levels in the three clones than in CAD5 wt. Clone #9 showed the highest PrP expression. Absolute PrP values were interpolated from the linear range of the calibration curve with rhPrP22-231. PrP overexpressing CAD5 clones were individually compared to CAD5 wild type. *** p ¡ 0.001, unpaired, two-tailed T-test. b) Confocal microscopy images of immunostaining of PrP with POM1 or POM19 antibody in #9 (hyCAD) showed physiological expression of PrP at the membrane. CAD5 Prnp-/- cells did not show any PrP. Scale bar 10 μm.*

I chronically infected as well PrP overexpressing CAD5 clone #9 (hyCAD) with RML6 prions (scHyCAD). I lysed the chronically infected scCAD and scHyCAD cells and digested them with Proteinase K (PK) before Western blotting. PK-Western showed complete digestion of PrP^C by PK in untreated and NBH treated CAD5 cells, which both served as negative controls (Figure 38). RML6 containing brain homogenate, which served as positive control, as well as RML6 infected CAD5 and hyCAD cells, exhibited the typical diagnostic shift towards a smaller PK-resistant core with un-, mono- and di-glycosylated PrP^{Sc}. hyCAD cells chronically infected with RML6 showed higher levels of PrP^{Sc} than CAD5 cells. No residual inoculum was detectable in CAD5 *Prnp*-/- cells.

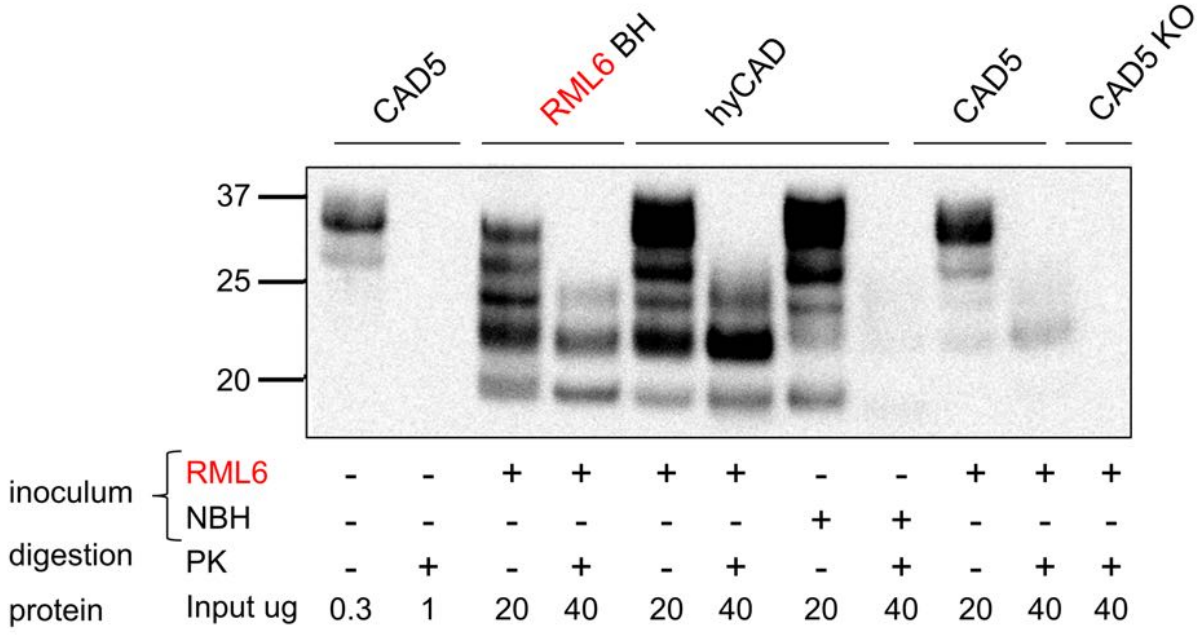

Figure 38: PK-Western with CAD5 wt and hyCAD chronically infected with RML6 show the typical diagnostic shift towards a smaller PK-resistant core with un-, mono- and di-glycosylated PrP^{Sc}. PK digestion of PrP^C in in untreated and NBH treated CAD5 cells was complete. There was no residual inoculum in RML6 infected CAD5 Prnp-/- cells.

I assessed cell growth of scCAD, CAD5 wt and CAD5 *Prnp*-/- with IncuCyte ZOOM live-cell

analysis system. I seeded cells in increasing concentrations into 384-well plates imaged the cells every 12 hrs for totally 160 hours. I quantified the confluence with the IncuCyte ZOOM software. CAD5 wt and *Prnp*-/- reached confluence at 72 or 80 hours respectively, with all cell seeding numbers (Figure 39). scCAD cells reached confluence at 72h, when seeding $\geq$ 2500 cells per well.

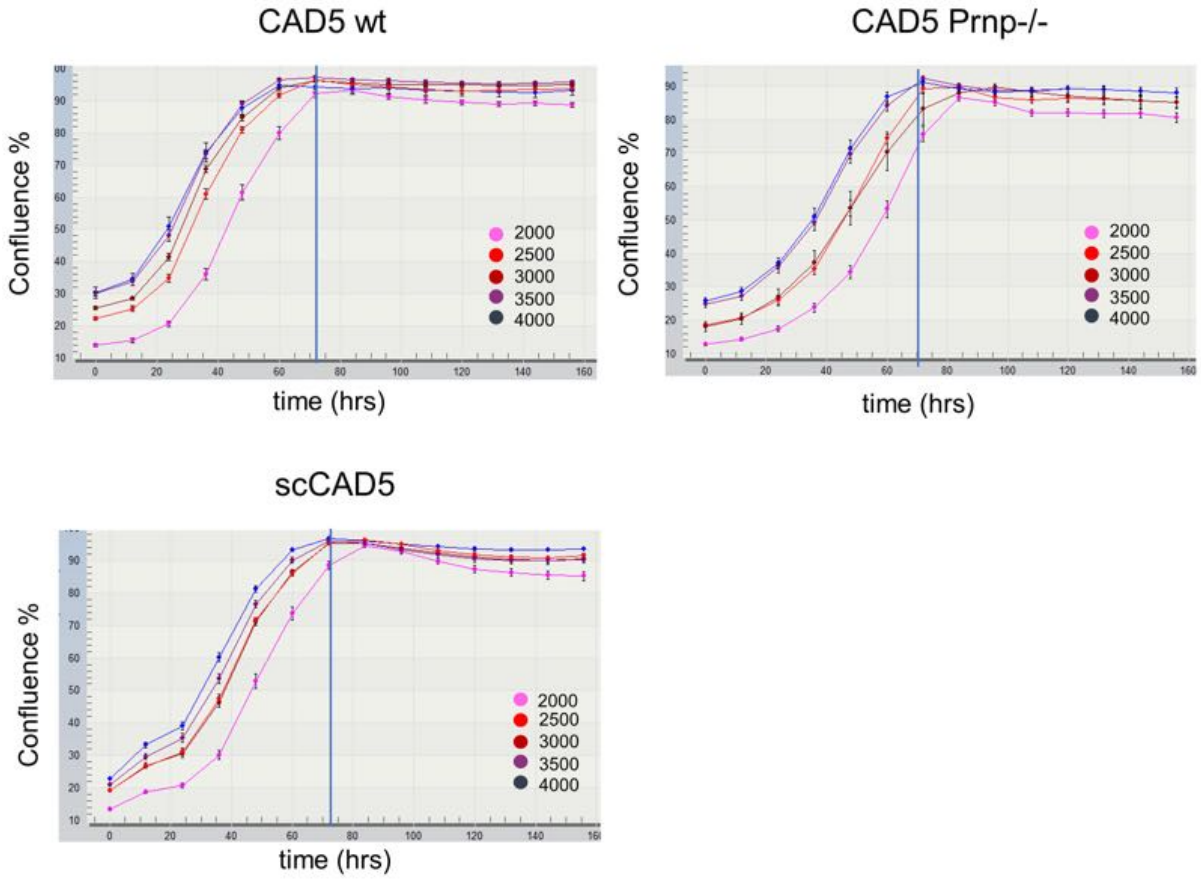

Figure 39: Quantification of the cell growth (confluence %) of different numbers (2000 – 4000 per well of 384-well plates) of CAD5 wt, CAD5 Prnp-/- and scCAD cells with IncuCyte ZOOM live-cell analysis system. CAD5 wt and Prnp-/- reached confluence at 72 or 80 hours respectively, with all cell seeding numbers. scCAD cells reached confluence at 72h, when seeding $\geq$ 2500 cells per well. The cells were imaged every 12 hours for totally 160 hours.

Since scCAD cells reached confluence at 72h, when seeding $\geq$ 2500 cells per well, I could perform the PrP^{Sc} assay within 72 hours, within the activity window of siRNAs. Compared to the PrP^{Sc} assay with acute infection, chronical infection shortened the incubation time by 24 hours and the cell population was more homogeneous. I performed PrP^{Sc}-FRET with cell lysate of scCAD inoculated with two different concentrations of RML6 (10-2 and 10-3) from two different passages (P12 and P18) (Figure 40). Net-FRET signals minus blank showed complete digestion of PrP^{C} in CAD5 wt and CAD5 *Prnp*-/- (KO), which served as negative

controls. PrP^{Sc} levels were reduced in scCAD cells inoculated with lower RML6 concentrations and with higher passages. Net-FRET signals minus blank of infected scCAD was sufficiently distinguishable from the negative controls with concentrations of 40 and 30 μg total protein. I found the actual total protein concentration per well with living cells was 3 to 5 μg per well.

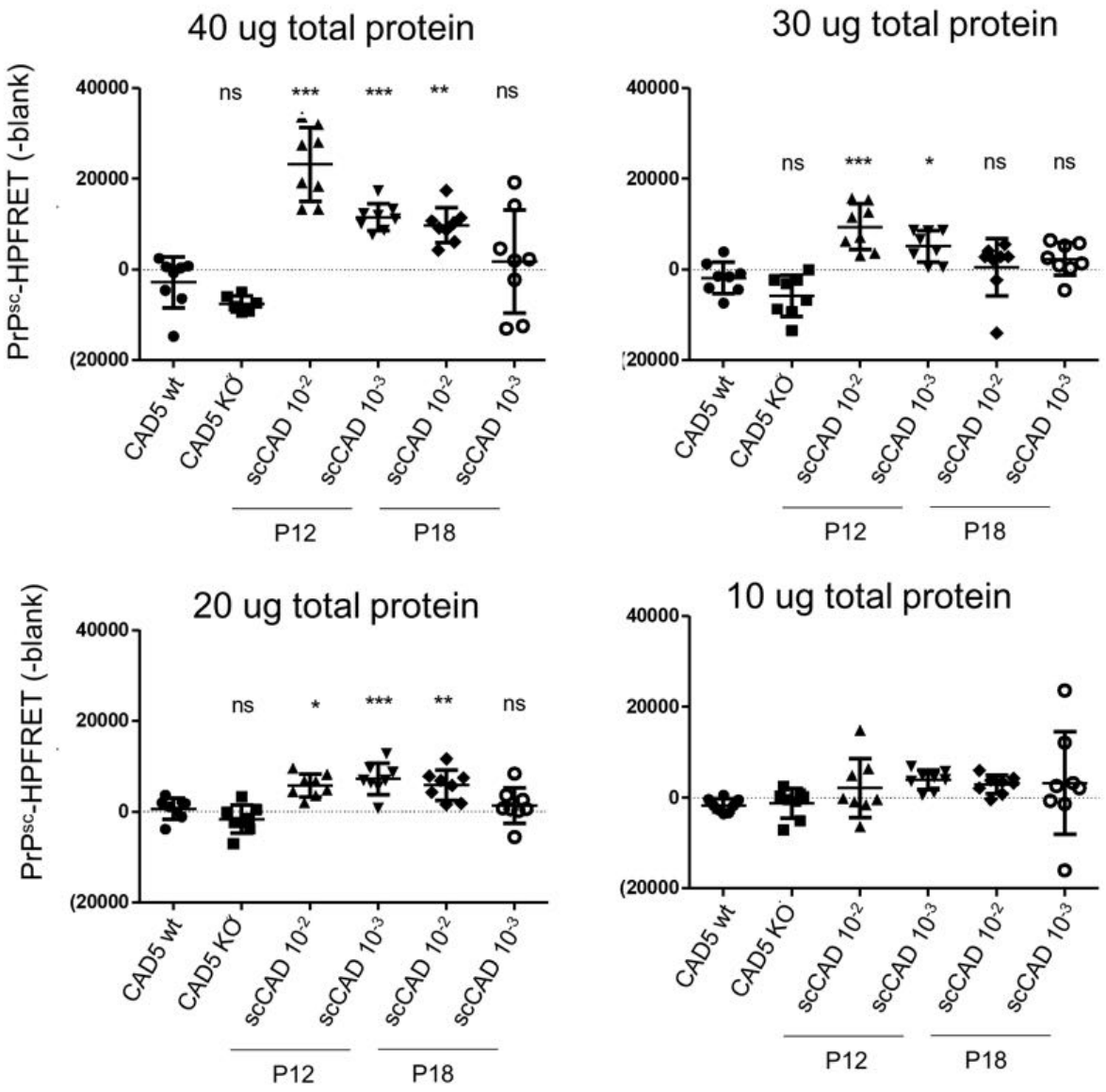

Figure 40: PrP^{Sc}-FRET with chronically infected scCAD5 lysate showed, that the PrP^{Sc} signal was significantly higher or clearly distinguishable from in CAD5 wt and CAD5 Prnp-/- (KO), which served as negative controls, with 40 and 30 μg total protein. These concentrations were one log higher than the actual protein concentration within one well with living cells.

The results with cell lysate of scCAD showed, that HP-FRET was not sensitive enough to detect the difference between living uninfected wild type CAD5 and chronically infected scCAD by one log. When I tested different PK concentrations lower than the established 5 μg per mL,

to increase the signal, PrP^C digestion was incomplete (Figure 41).

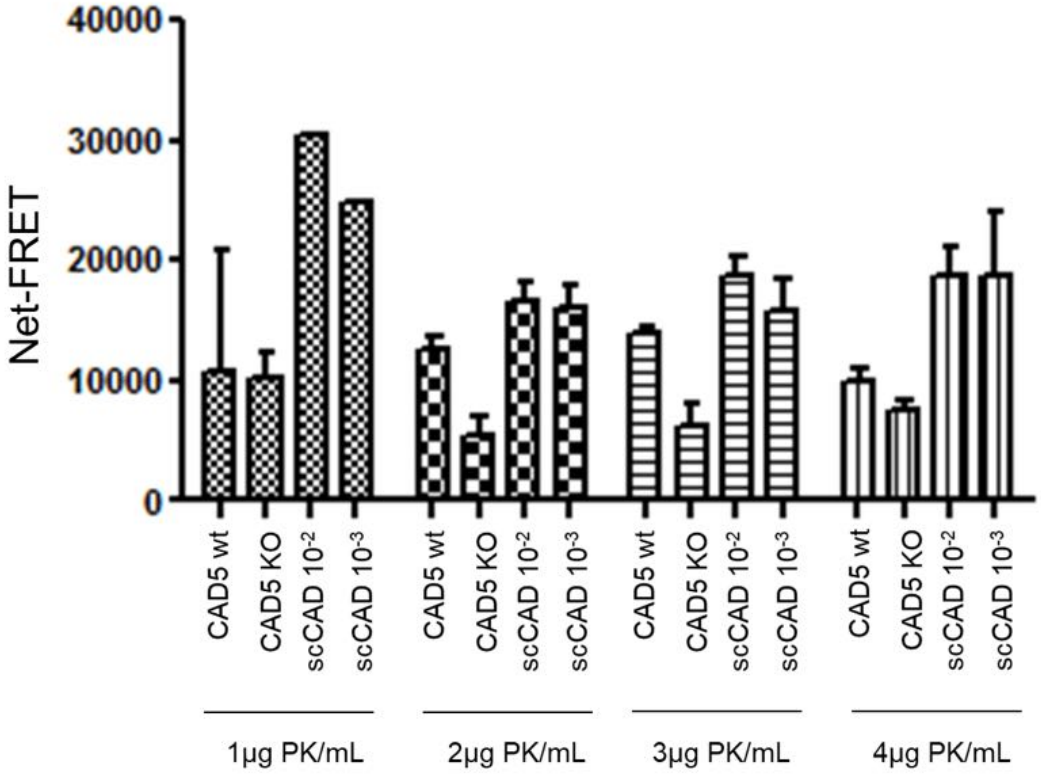

Figure 41: PrP^{Sc}-FRET with 40 µg chronically infected scCAD5 lysate digested with 1 to 4 µg of PK/mL showed incomplete digestion of PrP^C. Complete digestion of PrP^C would show equal Net-FRET levels of CAD5 wt and Prnp-/- (KO) cells.

The signal could be enhanced by reducing the PK concentration, however digestion of PrP^C was incomplete. To detect low PrP^{Sc} signals I performed PrP^{Sc}-ELISA with chronically infected scCAD cells, that I had forward transfected with 30nM of *Prnp* targeting and scrambled non-target siRNAs for 72 hours (Figure 42 a + b). Despite high inter-well variability, PrP^{Sc} levels were significantly reduced by *Prnp* siRNA compared to the scrambled siRNA control. When I performed the same assay with reverse transfection on the LabCyte acoustic dispensing robot, inter-well variability was higher and the difference between *Prnp* siRNA and scrambled siRNA treated cells was less distinct than with manual forward transfection (Figure 42 c + d). PrP^C digestion by PK was complete in both assays. The samples digested with PK were on the lower detection limit of the ELISA, whereas the ELISA absorbance of PK undigested samples was approximately one log higher. RML6 and $rmPrP_{22\text{-}230}$ standards were both in the linear range (Figure 42 e + f).

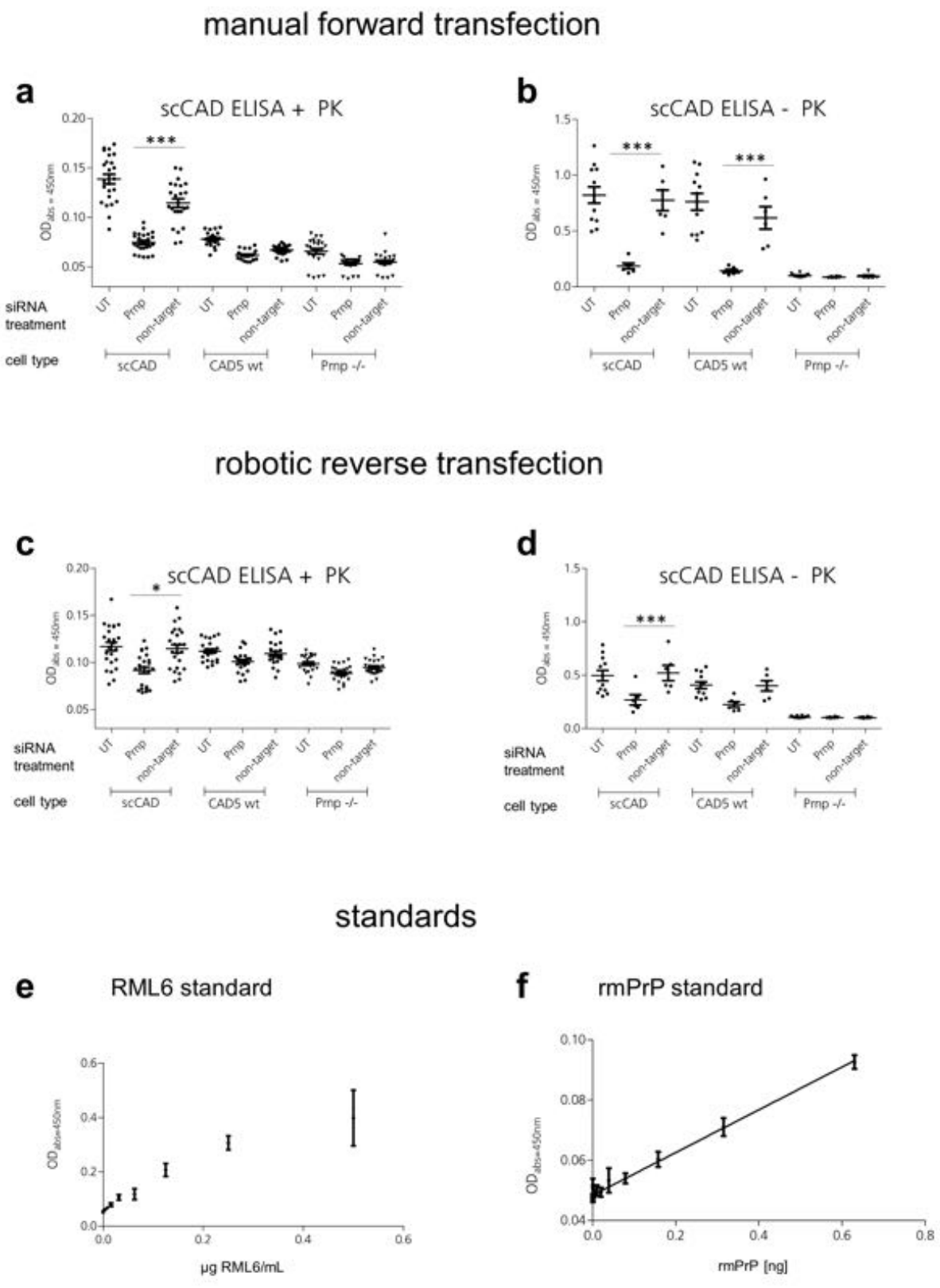

Figure 42: (Description on the next page)

Figure 42: PrP^{Sc}-ELISA with chronically infected scCAD cells transfected with 30nM Prnp targeting and scrambled non-target siRNAs incubated for 72 hours. Manual forward transfection a) with subsequent PK digestion and b) without PK digestion resulted in significantly reduced PrP^{Sc} and PrP^{C} levels by Prnp siRNA compared to the scrambled siRNA control. Robotic reverse transfection c) with subsequent PK digestion and d) without PK digestion resulted in higher inter-well variability and the difference between Prnp siRNA and scrambled siRNA treated cells was less distinct than with manual forward transfection. e) The Standard with RML6 brain homogenate was in the linear range with 0.5 – 0 μg RML6 per mL. f) The $rmPrP_{22\text{-}230}$ standard was in the linear range with 0.6 – 0 μg protein.

To enhance the transfection efficiency with reverse robotic transfection, I increased the siRNA concentrations stepwise from 30nM to 40nM (Figure 43). The difference between cells treated with *Prnp* siRNA and scrambled siRNA was significant with 37.5 nM siRNA.
I repeated the same experiment and reduced the incubation time from 72 hours to 48 hours in order to minimize the incubation time of the cells and biological variability. However, the siRNA efficiency was decreased (Figure 44).

Figure 43: PrP^{Sc}-ELISA with chronically infected scCAD cells reversely transfected with the robot with siRNA concentrations ranging from 30 – 40 nM. Prnp targeting and scrambled non-target siRNAs were incubated for 72 hours. All samples were digested with PK. ELISA absorbance represented PrP^{Sc} levels. Robotic reverse transfection showed significant distinction between Prnp siRNA and scrambled siRNA treated cells at 37.5 nM siRNA but not with other siRNA concentrations.

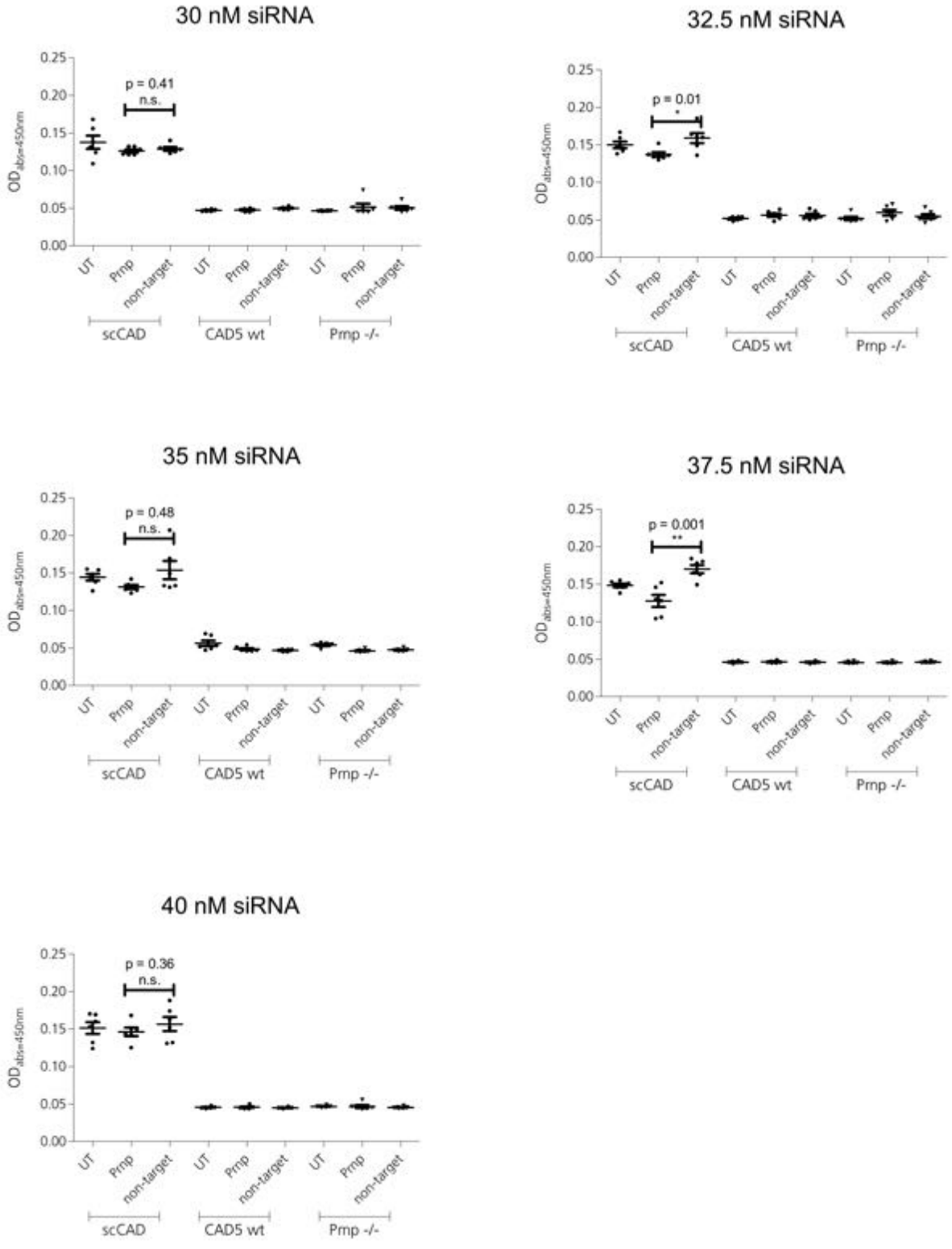

Figure 43: (Description on the previous page)

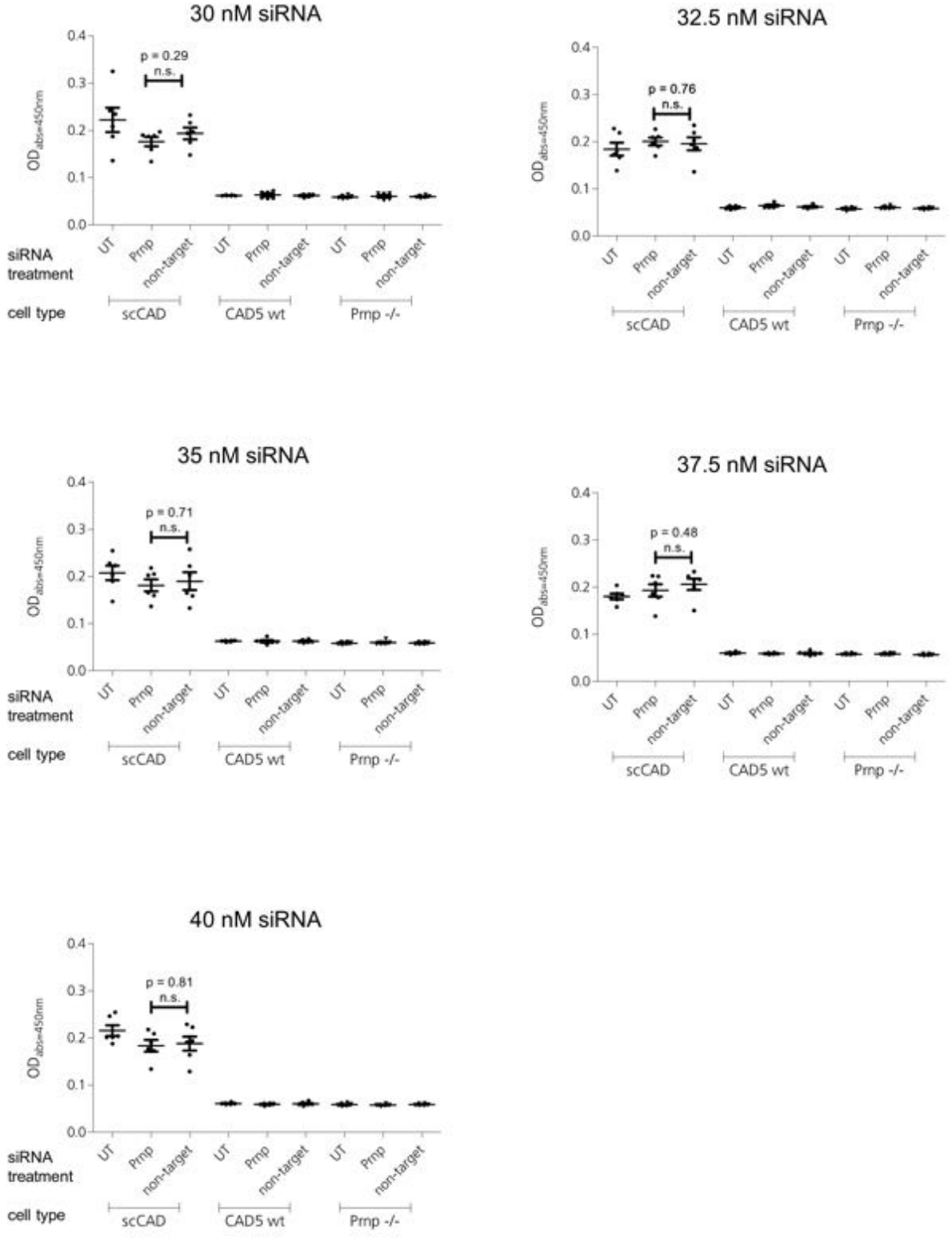

Figure 44: PrP^{Sc}-ELISA with chronically infected scCAD cells reversely transfected with the robot with siRNA concentrations ranging from 30 – 40 nM. Prnp targeting and scrambled non-target siRNAs were incubated for 48 hours. All samples were digested with PK. ELISA absorbance represented PrP^{Sc} levels. Robotic reverse transfection did not show significant distinction between Prnp siRNA and scrambled siRNA treated cells.

In order to get a higher PrP^{Sc} signal, I transfected PrP overexpressing HyCAD cells and chronically infected scHyCAD cells with control siRNAs and performed PrP^{Sc}-ELISA upon PK digestion (Figure 45 a + b). CAD5 *Prnp*-/- cells served as negative control. I transfected the cells with 37.5nM *Prnp* siRNA and scrambled siRNA, since this concentration had resulted in the best knockdown efficiency in previous experiments with scCAD cells. The PrP^{Sc} signal was significantly higher than in PrP^{Sc}-ELISA with CAD5 wild type and chronically infected scCAD cells. I compared manual forward to robotic reverse transfection. Knockdown efficiency was better and inter-well variability lower in manual forward than robotic reverse transfection. This led to better SSMD values defined for a strong control for hyCAD and scHyCAD in manual forward transfection (SSMD = -2.6 good screen quality) than in robotic reverse transfection (SSMD = -0,9 inferior screen quality). Z' prime factors, which were a more stringent quality control for screens were insufficient (Zhang 2007). PK digestion of PrP^{C} was complete. As well in samples that were not digested with PK the variability was higher and the knockdown efficiency lower in cells reversely transfected with the robot, which resulted in better SSMD values for manual forward transfection. (Figure 45 c + d).

To increase the transfection efficiency, I tested control siRNA concentrations from 5 nM to 70 nM and compared manual forward to reverse robotic transfection (Figure 46 + 47). Again, manual forward transfection of scHyCAD resulted in better knockdown efficiency and less variability than robotic reverse transfection. Manual forward transfection led to efficient knockdown from 5nM to 40nM. siRNA concentrations above 40 nM decreased the cell viability. With robotic reverse transfection, siRNA concentrations $\geq$ 30nM led to significant knockdown while cell viability was not affected by high siRNA concentrations. Samples without PK digestion served as additional control for knockdown efficiency and completeness of PK digestion.

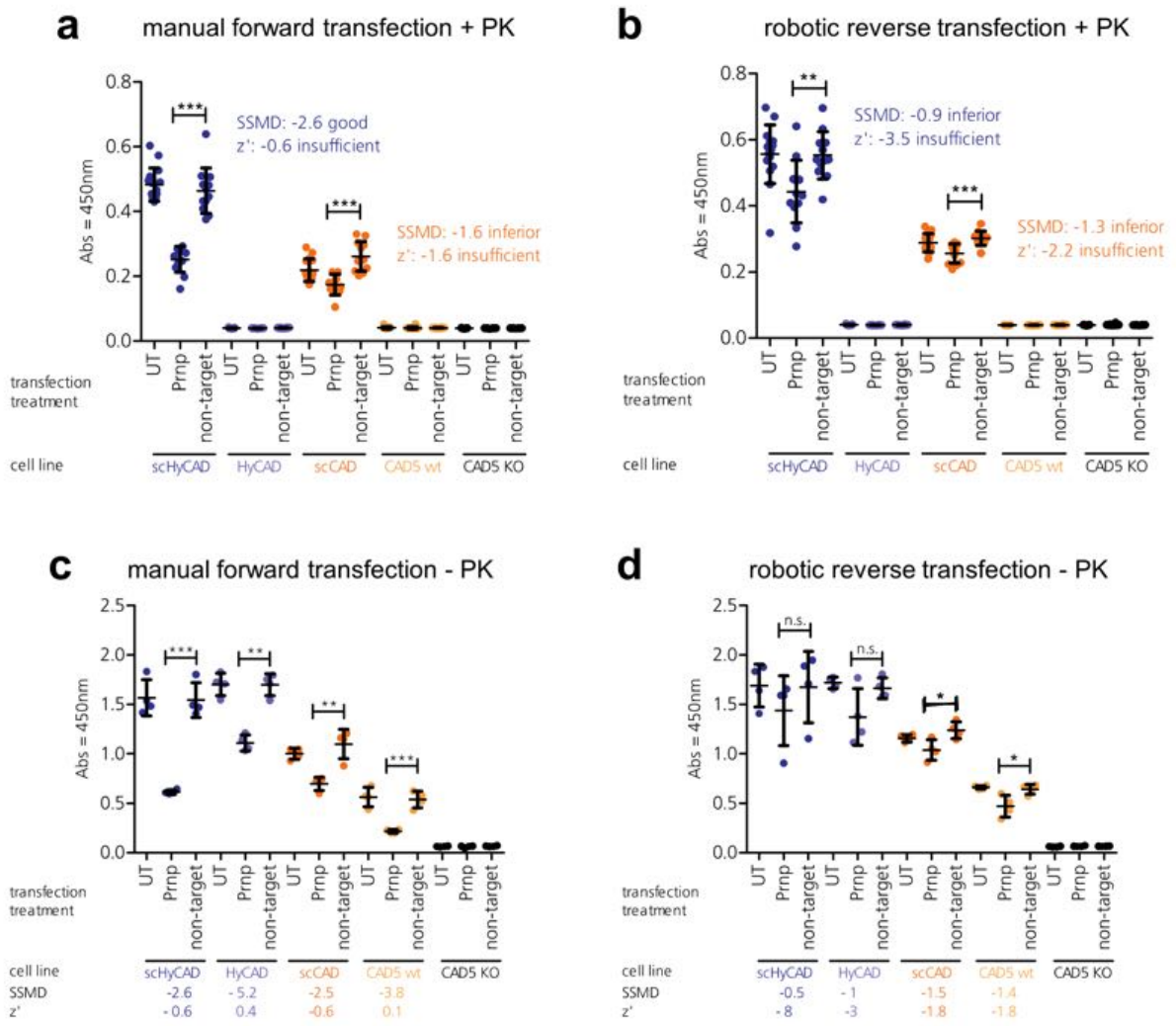

Figure 45: PrP^{Sc}-ELISA with PrP overexpressing HyCAD and chronically infected scHyCAD cells showed higher ELISA signal than CAD5 wt and scCAD. Cells were transfected with 37.5 nM Prnp targeting and scrambled non-target siRNAs for 72 hours. SSMD screen quality control defined for a strong control was better for hyCAD and scHyCAD in manual forward transfection (SSMD = -2.6 good screen quality) than robotic reverse transfection (SSMD = -0,9 inferior screen quality). PK digestion was complete in a) and b). SSMD for for hyCAD and scHyCAD without PK digestion showed the same picture as with PK digestion and better SSMD values with manual forward transfection.

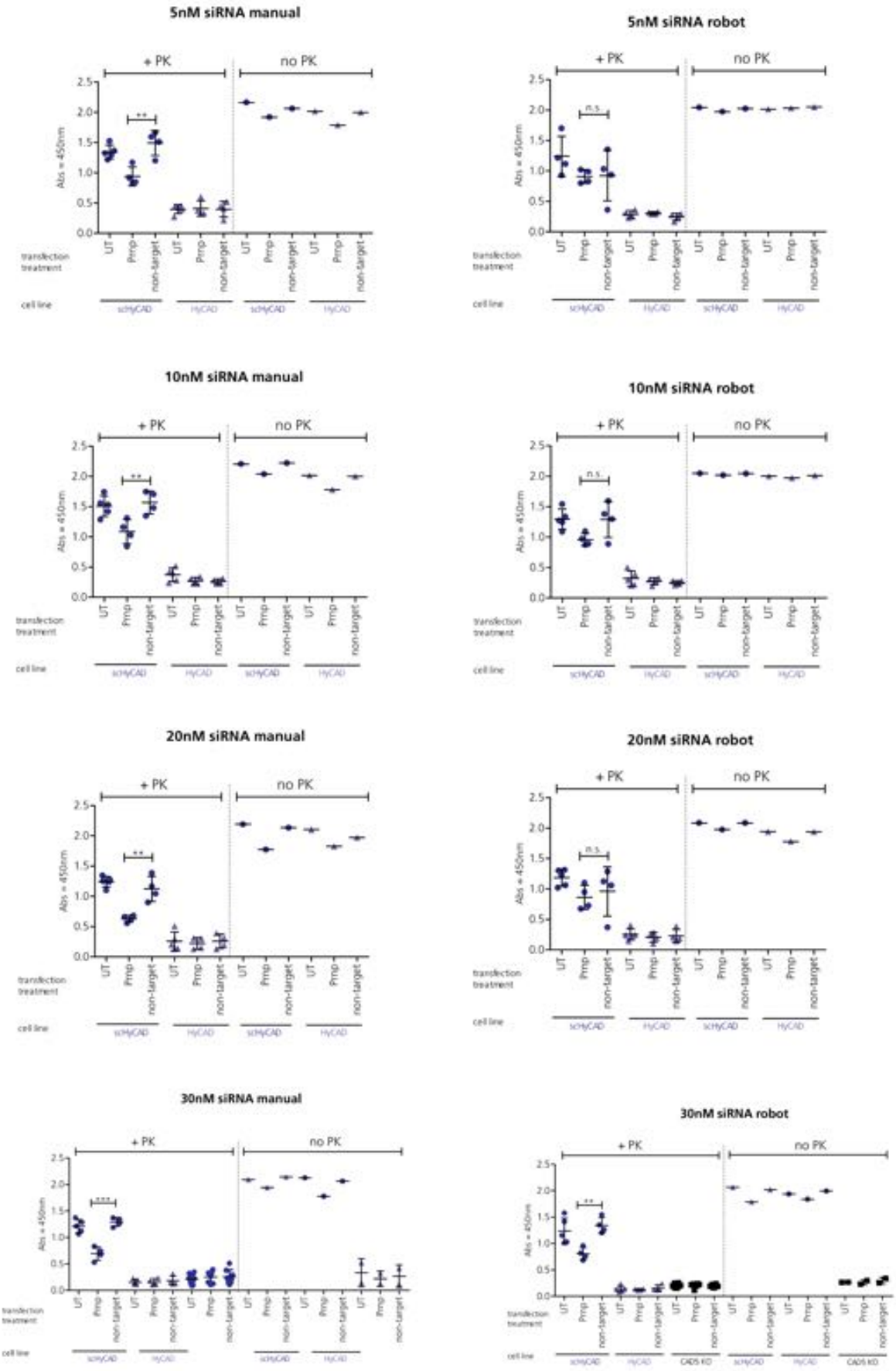

Figure 46: (Description on the next page)

Figure 46: PrP^{Sc} ELISAs with PrP overexpressing HyCAD and chronically infected scHyCAD transfected with siRNAs ranging from 5 to 30nM. I compared manual forward transfection to reverse robotic transfection with and without PK digestion. Manual forward transfection led to efficient knockdown from 5nM to 30n. With robotic reverse transfection, siRNA concentrations below 30nM did not lead to significant knockdown. Samples without PK digestion served as additional control for knockdown efficiency and completeness of PK digestion.

I attempted to reduce the variability between wells when reversely transfecting the cells with the robot, by printing siRNAs into Opti-MEM to avoid evaporation after printing and potential RNA degradation (Figure 48 c - f). However, transfection efficiency was more efficient without pre-filling Opti-MEM (Figure 48 a + b). Direct seeding of cells onto freshly printed siRNA plus Lipofectamine resulted in better knockdown than freezing of the siRNAs prior to cell seeding (Figure 48 c - f). Knockdown efficiency was better with 37.5 nM siRNA than with 30nM in robotic reverse transfection. After these optimizations the strictly standardized mean difference (SSMD) for robotic reverse transfection was still poor and z' factors insufficient.

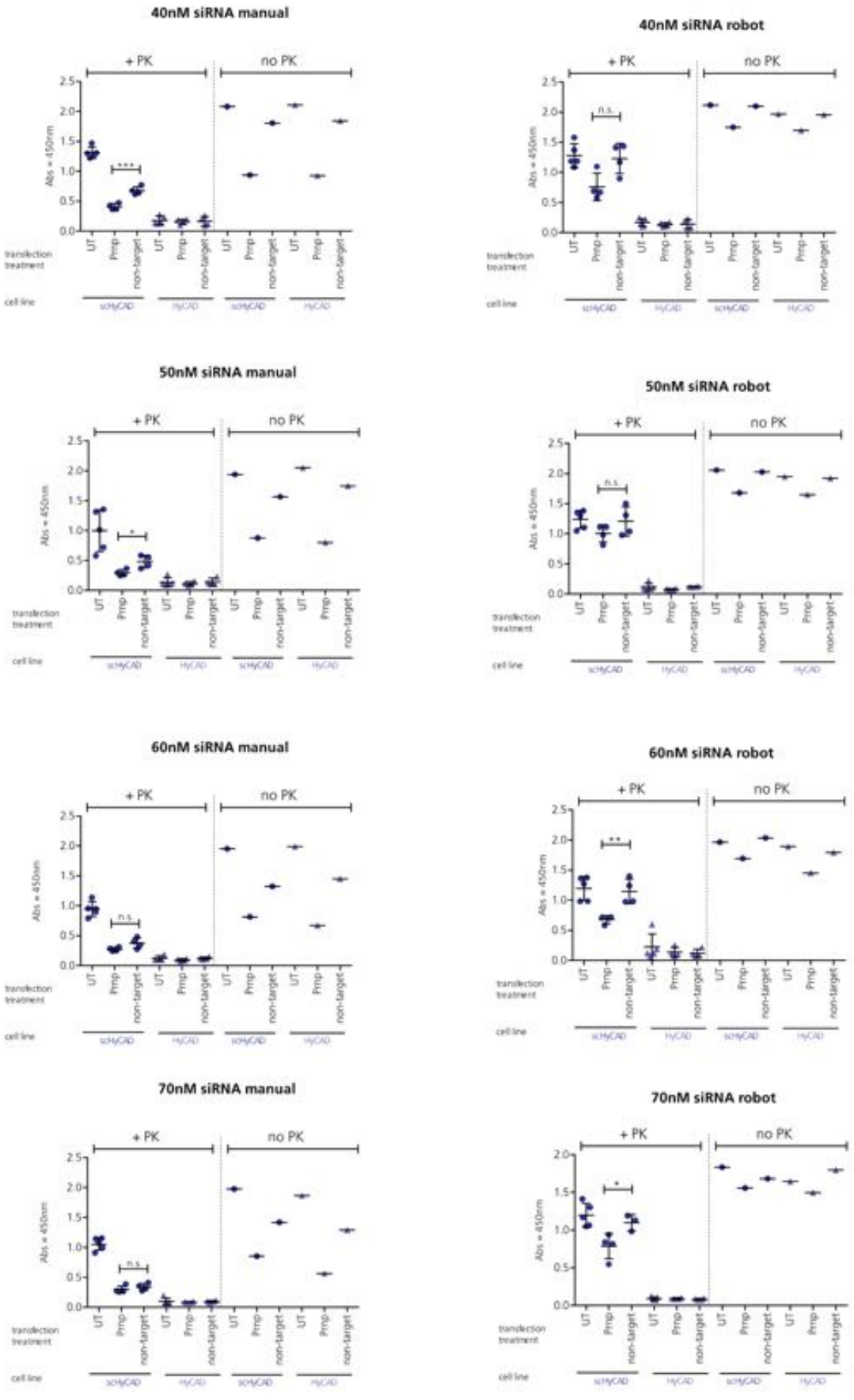

Figure 47: (Description on the next page)

Figure 47: PrP^{Sc} ELISAs with PrP overexpressing HyCAD and chronically infected scHyCAD transfected with siRNAs ranging from 40 to 70nM. I compared manual forward transfection to reverse robotic transfection with and without PK digestion. Manual forward transfection led to efficient knockdown from with 40nM. siRNA concentrations above 40 nM decreased the cell viability. With robotic reverse transfection, siRNA concentrations higher than 30nM led to significant knockdown while cell viability was not affected by high siRNA concentrations. Samples without PK digestion served as additional control for knockdown efficiency and completeness of PK digestion.

To investigate whether the transfection efficiency was reduced by robotic transfection, I compared manual reverse transfection with 30nM or 40nM siRNA to robotic reverse transfection (Figure 49). Robotic reverse transfection resulted in more efficient knockdown than manual reverse transfection, and manual forward transfection in the best knockdown efficiency and lowest variability.

Figure 48: PrP^{Sc} ELISA with PrP overexpressing HyCAD and chronically infected scHyCAD. a) manual forward transfection with 37.5 nM siRNA resulted in the same SSMD value as with b) 30nM siRNA and was in the excellent range. Robotic reverse transfection with pre-filling Opti-MEM to plates before siRNA printing and direct cell seeding upon siRNA printing resulted in better siRNA knockdown and SSMD values with c) 37.5 nM siRNA (SSMD = -2.3 good) than with d) 30nM siRNA (SSMD = -1.8 inferior). Robotic reverse transfection with pre-filling Opti-MEM to plates before siRNA printing and freezing before cell seeding resulted in high inter-well variability, low knockdown efficiency and insufficient SSMD levels with e) 37.5 nM siRNA and f) 30nM siRNA.

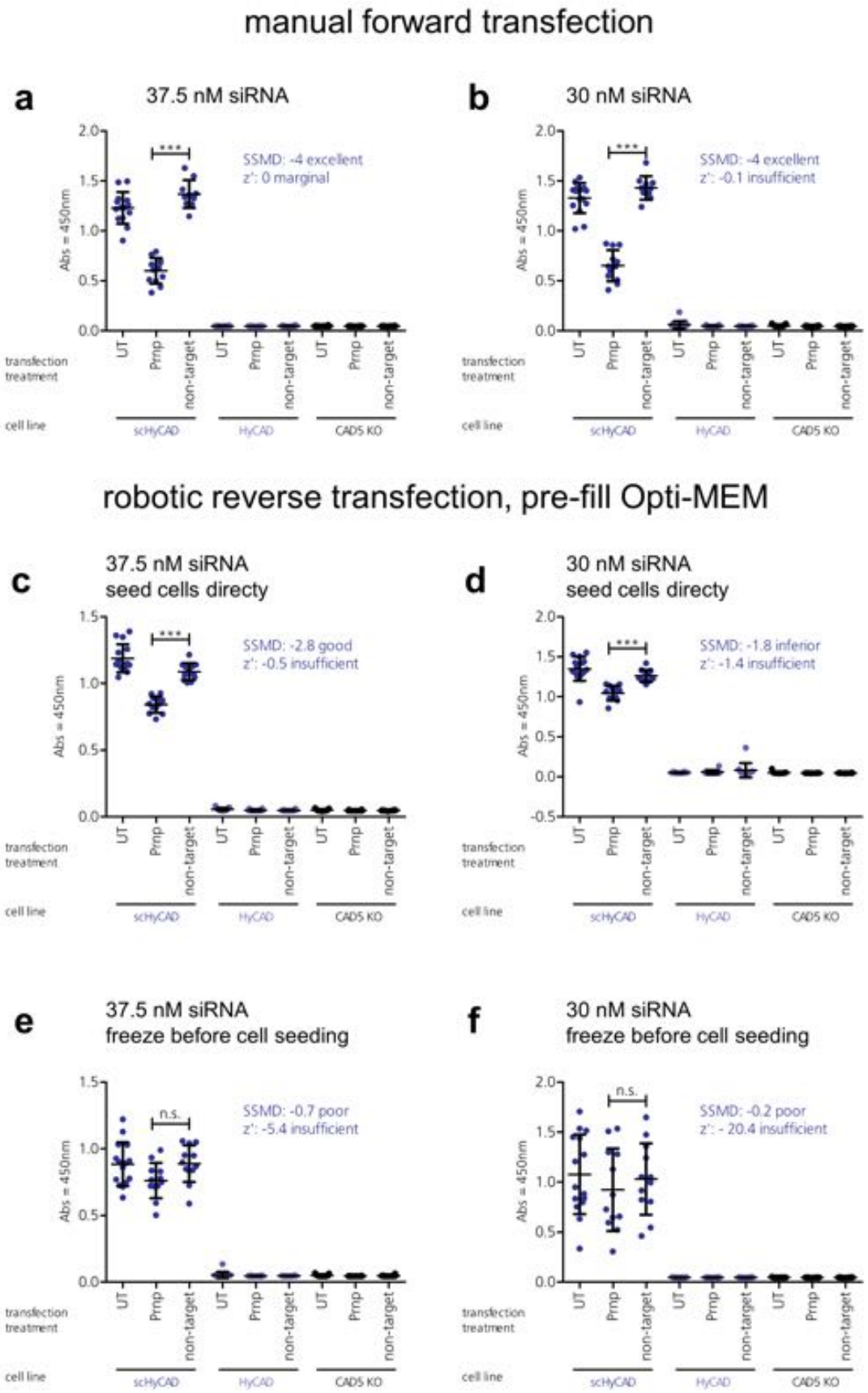

Figure 48: (Description on the previous page)

Thus, I established forward transfection for the PrP^{Sc}-ELISA screen on the robotic platform (Figure 50). I printed the siRNAs into an intermediate plate, added Lipofectamine® RNAiMAX Reagent and transferred the siRNA-Lipofectamine complexes to plates with previously seeded scHyCAD cells using the robotic Perkin Elmer platform.

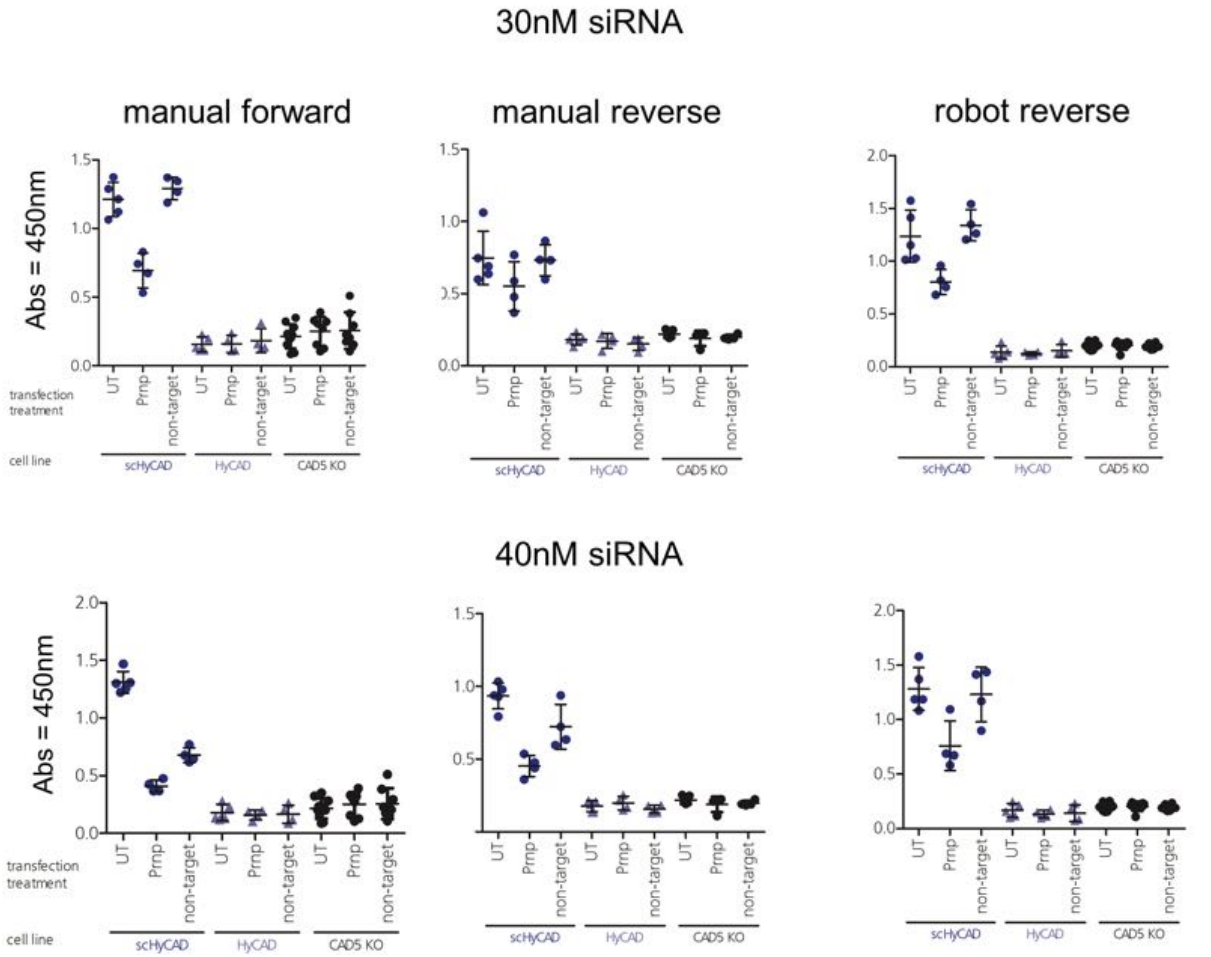

Figure 49: Comparison of manual vs. robotic reverse transfection to manual forward transfection with 30 and 40 nM siRNA. Manual reverse transfection with 30nM siRNA resulted in higher inter-well variability than robotic reverse transfection. The transfection efficiency was improved with 40nM in manual reverse transfection, but not in robotic reverse transfection. Manual forward transfection with 30nM siRNA resulted in the best knockdown efficiency and lowest variability. With 40nM the viability the cell viability was reduced, reflected by lower ELISA absorbance in non-target controls.

The test screen with control siRNAs resulted in a good SSMD value with distinct separation of non-target and *Prnp* siRNA treated controls (Figure 51).

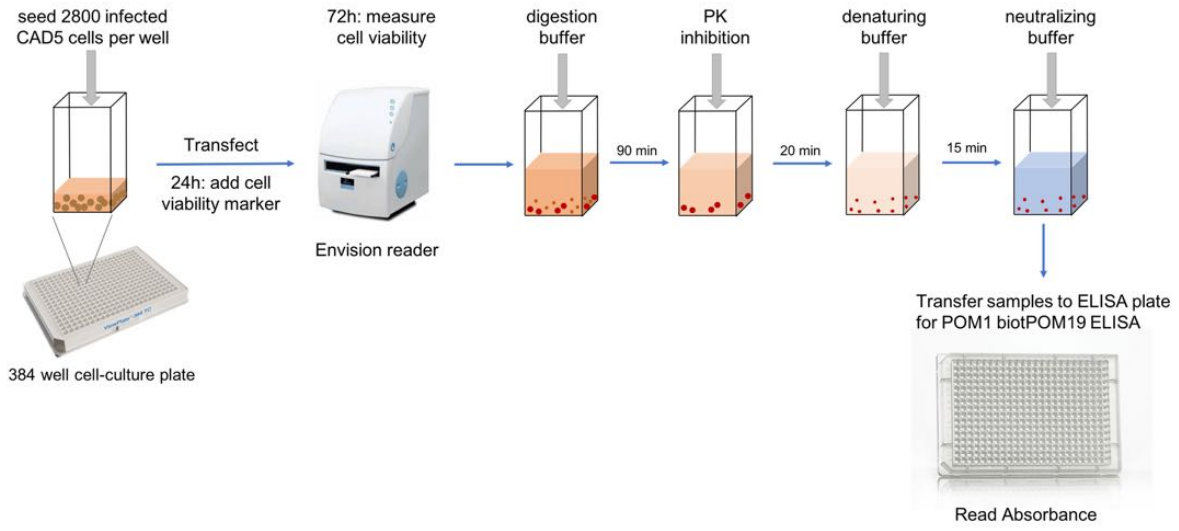

Figure 50: PrP^{Sc}-ELISA with forward transfection on the robotic platforms. 2800 chronically infected scHyCAD cells were seeded per well into 384-well plates. siRNAs were printed into an intermediate plate, Lipofectamine® RNAiMAX reagent was added and the siRNA-Lipofectamine complexes transferred to the cells. PK-digested, denatured and neutralized samples were transferred to ELISA plates and PrP^{Sc}-ELISA was performed.

I performed a PrP^{Sc}-ELISA screen with chronically infected scHyCAD transfected with robotic forward transfection with the murine non-druggable chaperone siRNA library. Before measuring the RT-Glo luminescence signal for cell viability with the Envision reader, I acclimatized the plates for one hour to room temperature. QC showed that the RT-Glo luminescence signal was homogeneous with some irregularities in plate four (Figure 52 a). Cell viability passed the QC, because non-target and *Prnp* siRNA treated controls were comparable (Figure 52 b). Viability was significantly decreased in cells transfected with six siRNAs (Figure 52 c).

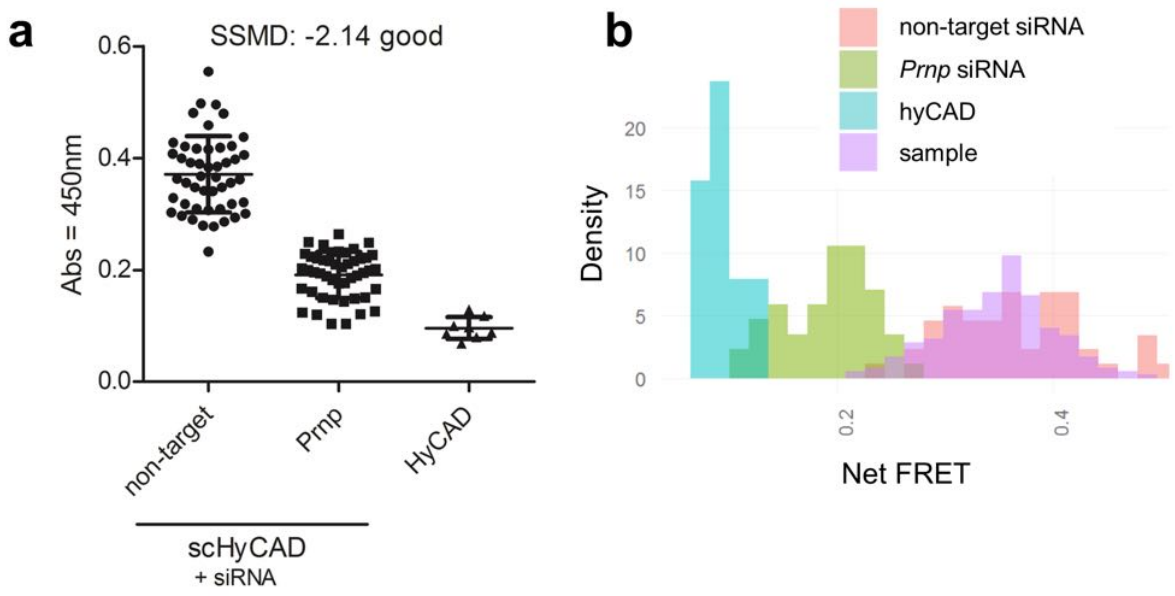

Figure 51: PrP^{Sc} test screen with robotic forward transfection of Prnp targeting and scrambled siRNAs resulted in good SSMD value (-2.14) defined for a strong control. a) In the scatter plot each dot represented one well of cells treated with control siRNAs. b) The same data depicted as histogram with the customized software including un-transfected cells (samples). Samples overlap with the non-target control.

The QC of the ELISA absorbance signal showed oversaturation (Figure 53 a). Thus, the signal of all controls and samples shared the same high values at the upper detection limit and no distinction between controls was possible (Figure 53 b). The SSMD values were in the unacceptable range.

Figure 52: RT-Glo levels representing cell viability were visualized for six plates as heatmaps. Low RT-Glo levels around 200'000 were depicted in blue, medium RT-Glo levels around 400'000 were shown in dark orange, and high RT-Glo levels above 600'000 were shown in bright orange. RT-Glo luminescence signal was homogeneous with some irregularities in plate four b) Cell viability of scHyCAD cells treated with scrambled siRNA and siRNA targeting Prnp was comparable. c) Six siRNAs significantly reduced the cell viability of scHyCAD, compared individually to the mean cell viability of all non-target controls (one dot = mean non-target control viability of one plate). For each siRNA technical duplicates were depicted.

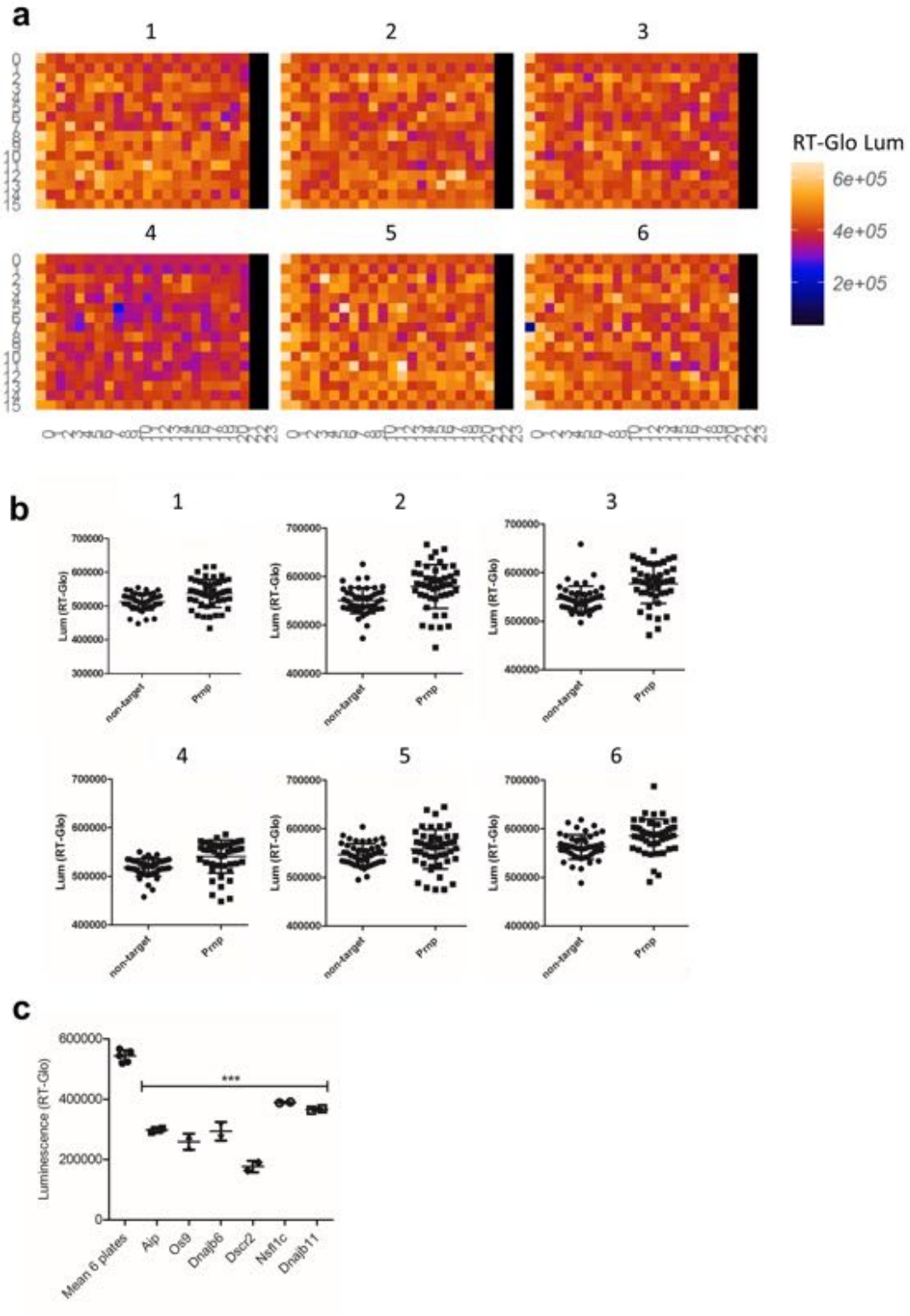

Figure 52: (Description on the previous page)

6.1.4 Hit validation murine PrP^C and PrP^{Sc} screens

I planned to validate chaperone hits with two siRNAs per chaperone, differing in the targeting locus from the siRNAs used in the screen (Figure 54). After assessing PrP levels upon treatment with hit targeting siRNAs by Western blotting, I purposed to test the knockdown efficiency of hit targeting siRNAs and their effect on PrP levels by quantitative real-time PCR (qRT-PCR). Subsequently I planned to confirm chaperone hits in a different cell line and to apply the hit validation strategy to following screens.

Figure 53: a) ELISA absorbance levels representing PrP^{Sc} levels were visualized for six plates as heatmaps. Because the signal was oversaturated, all samples high PrP^{Sc} levels around 2, depicted in bright orange. b) ELISA absorbance quality controls from the PrP^{Sc} screen showed no difference between hyCAD control (blue), Prnp targeting siRNA control (green), non-target siRNA control (orange) and samples (violet) because the signal was oversaturated.

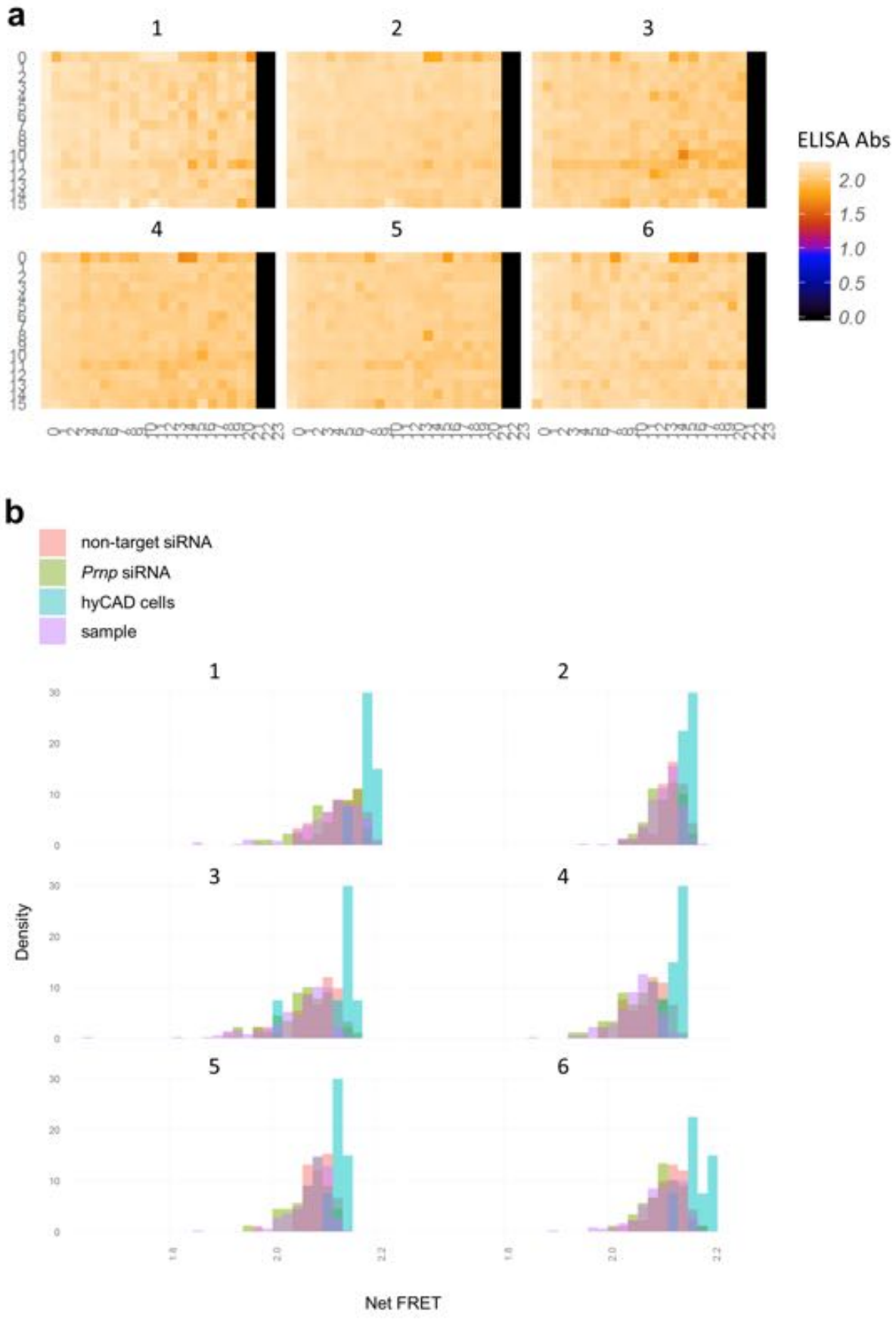

Figure 53: (Description on the previous page)

I selected five hits (Hspa5, Psmc5, Calr, Canx and Hspa4) from the first PrP^C SKD screen with druggable chaperones, to establish hit validation. For each hit I ordered two siRNAs, differing in the targeting locus from the siRNAs used in the screen. I transfected CAD5 wt cells with the hit targeting siRNAs and extracted protein and RNA. CAD5 wt cells transfected with scrambled and *Prnp* targeting siRNAs served as controls. I designed primers against the chaperone hits and tested their quality with amplification and standard curves by qRT-PCR (Figure 55). I designed new primer pairs for such that did not pass quality control.

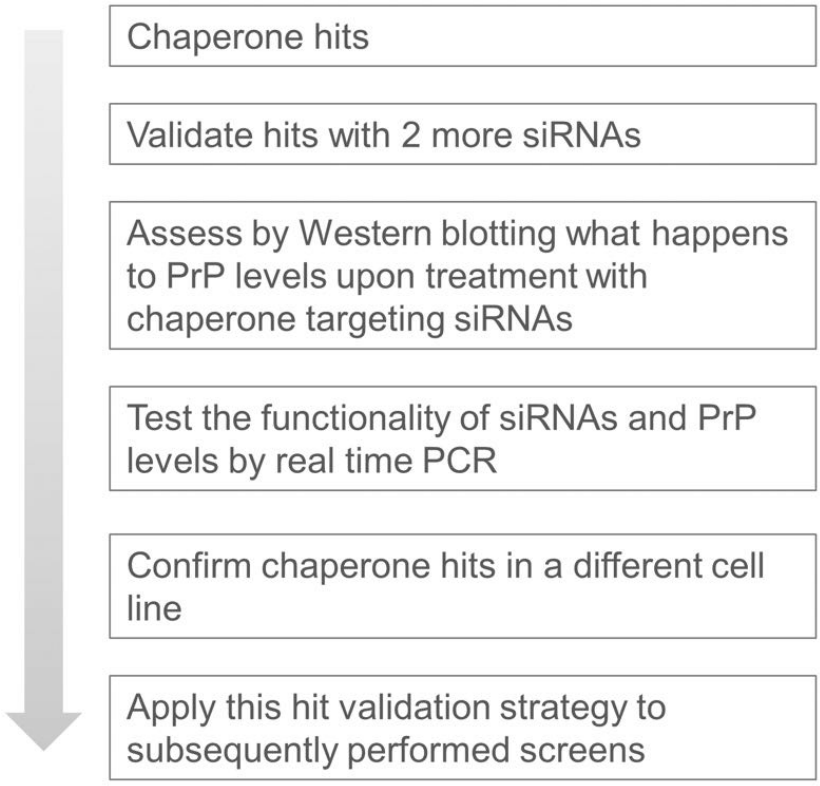

Figure 54: Hit validation strategy.

In order to cope with variability caused by different siRNA treatment of CAD5 wt cells, I tested 8 different housekeeping genes (B2m, Eif2a, Gapd, Hmbs, Hprt, Ppib, Tbp, Utp6c). I included B2m, Gapdh, Hprt and Ppib as stable housekeeping geenes, which I used in every experiment as controls. I normalized all samples to Hprt, the most robust housekeeping gene. I established the qRT-PCR protocol on a LabCyte acoustic dispensing robot for 384 well plate format and compared it to the results of manually pipetted RT-PCR in 96 well plates (Figure 56).

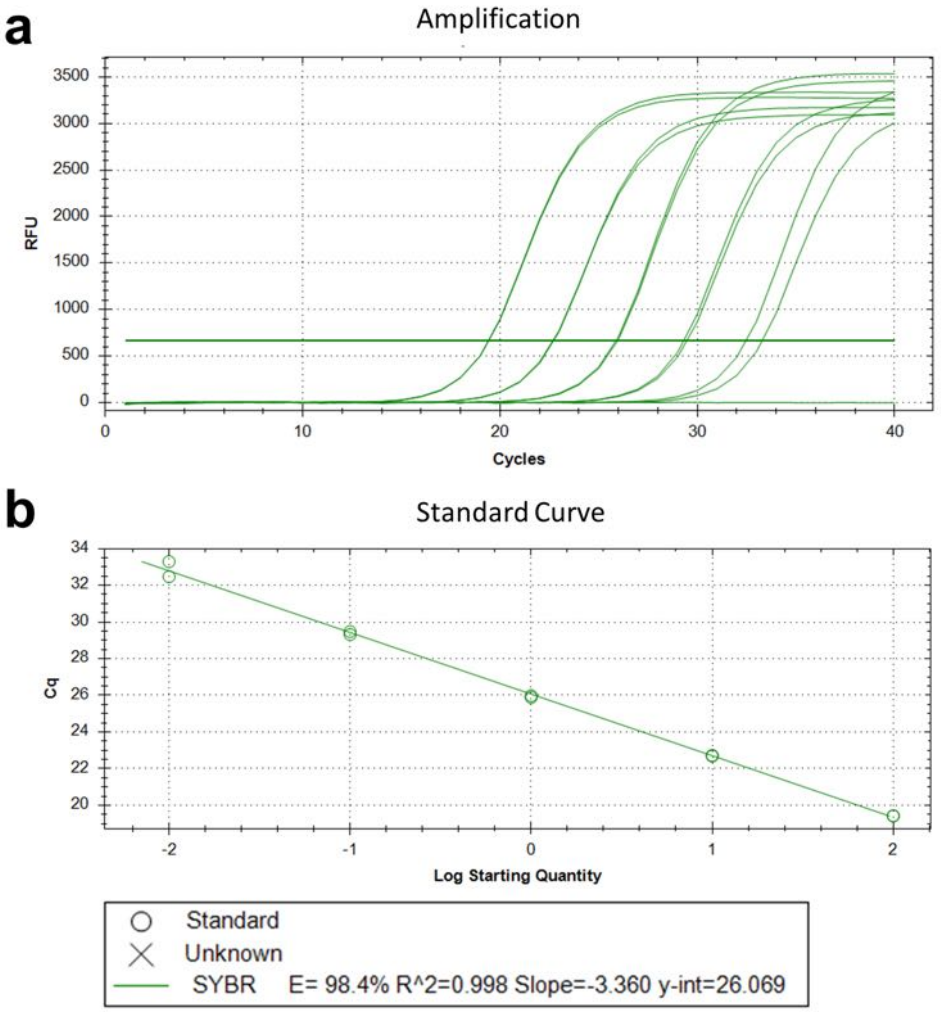

Figure 55: Testing primers against chaperone hit Hspa5. The same amount of primers was added to five 1:10 dilutions of cDNA from untreated CAD5 wt. Starting concentration was 100 ng cDNA. a) The amplification blot showed congruent amplification of technical duplicates in all cDNA concentrations despite 0.01 ng, indicating sample cDNA with concentrations until 0.1ng could be used. The negative control with cDNA from untreated CAD5 wt generated without reverse Transcriptase was not amplified during qRT-PCR. b) The standard curve with slope -3.36 showed that the cDNA amount actually increased 10-fold with each cDNA dilution. R^2 *was 0.998 (threshold 0.95), thus the primer pair passed quality control.*

Since the results were comparable, I continued with more efficient dispensing with the acoustic dispenser (Figure 57 a + b). I performed qRT-PCR with cDNA from CAD5 wt cells treated with 10 different siRNAs targeting chaperone hits. Untransfected CAD5 wt along with CAD5 wt transfected with *Prnp* targeting and scrambled siRNA served as controls. The average of three biological replicates and three technical replicates was depicted in each square of the heatmaps. All siRNAs despite first siRNA targeting Calreticulin and Hspa5 did lead to efficient reduction of mRNA. *Prnp* mRNA was reduced upon transfection with siRNAs targeting *Prnp*, Calnexin, Hspa4 and Hspa5.

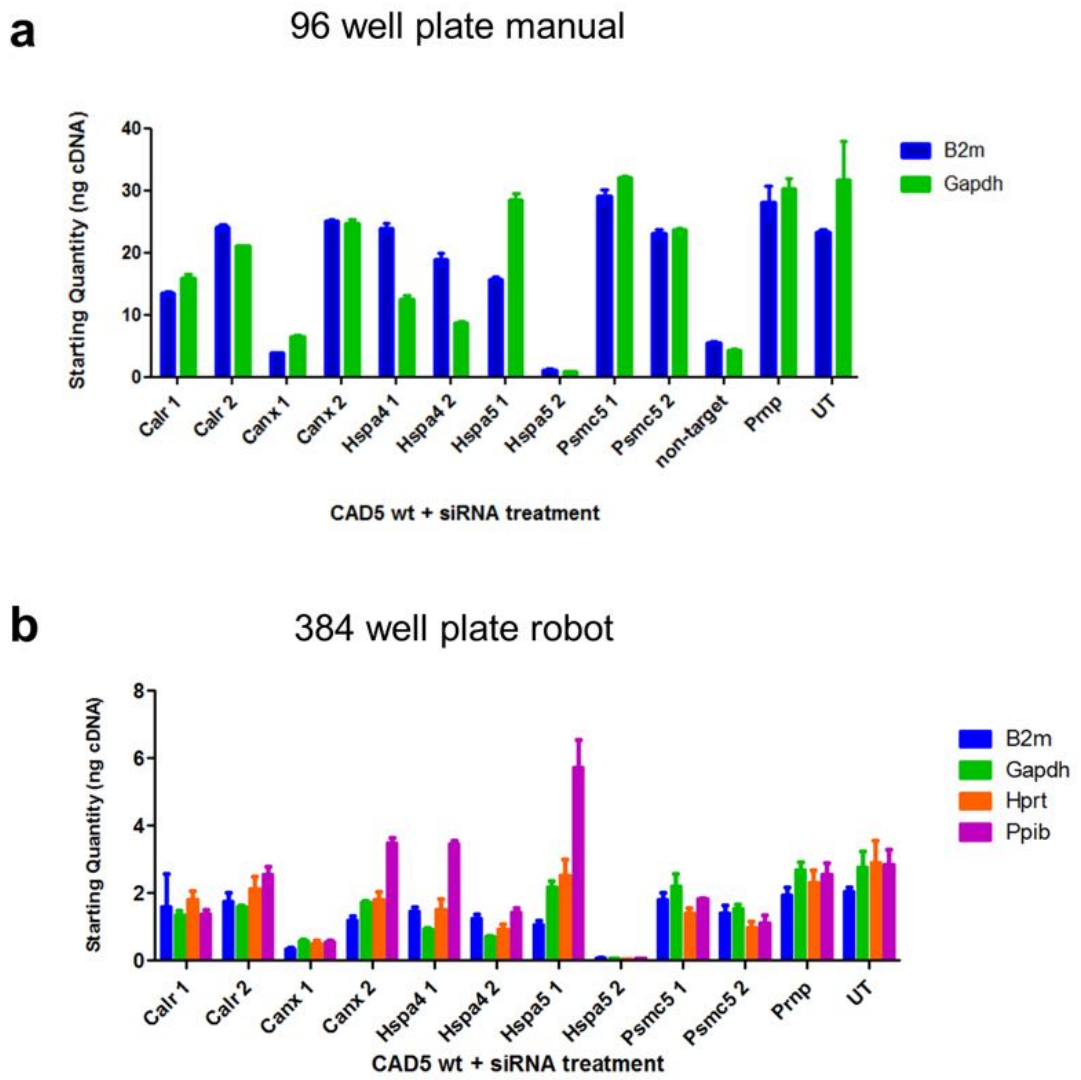

Figure 56: Comparison of a) manual pipetting in 96 well format to b) robotic dispensing in 384 well format with primers against the housekeeping genes B2m, Gapdh, Hprt, Ppib. B2m and Gapdh showed comparable absolute cDNA quantity as in 96 well format.

Figure 57: Absolute starting quantity (ng cDNA) of CAD5 wt samples transfected with control- and hit chaperone targeting siRNAs normalized to Hprt. The average of three biological replicates from different passages of CAD5 wt and three technical replicates was depicted in each square. High cDNA quantity was depicted in red, low quantity in dark blue. a) All primers were included in the figure. b) To render the figure more clearly, only primers against chaperone hits and Prnp were depicted. Squares highlighted in yellow showed knockdown efficiency siRNAs targeting hit chaperones. All siRNAs despite first siRNA targeting Calreticulin (Calr 1) and Hspa5 (Hspa5 1) did lead to efficient reduction of mRNA. Squares highlighted in orange showed significant downregulation of Prnp. Prnp mRNA was reduced upon transfection with siRNAs targeting Prnp, Calnexin, Hspa4 and Hspa5.

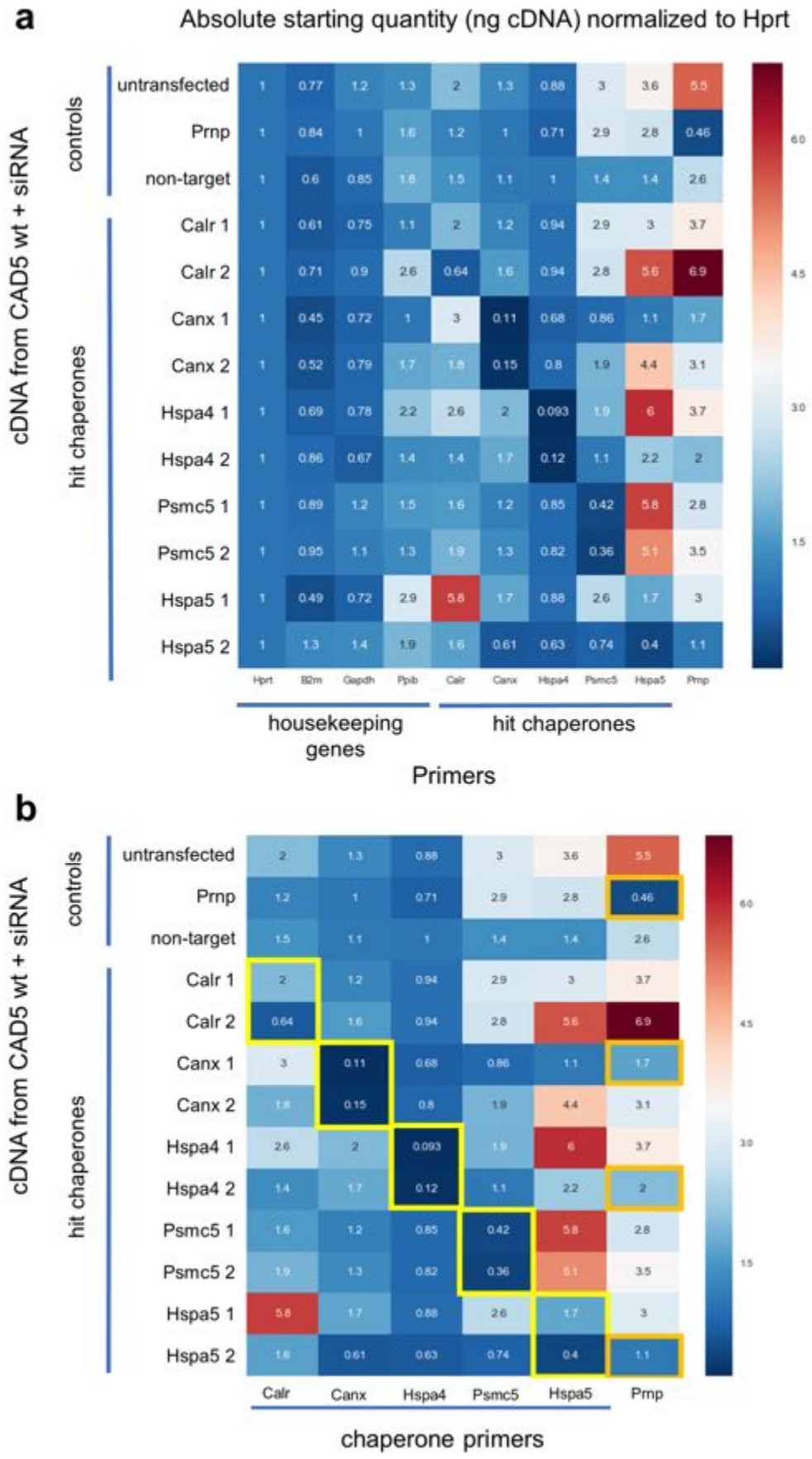

Figure 57: (Description on the previous page.)

When converting the same qRT-PCR results into a bar graph and comparing the mRNA level to the protein level in a Western blot, I could confirm reduction of PrP levels upon treatment with chaperone targeting siRNAs *Prnp*, *Calr_1*, *Canx_1* and *Hspa5_2*.

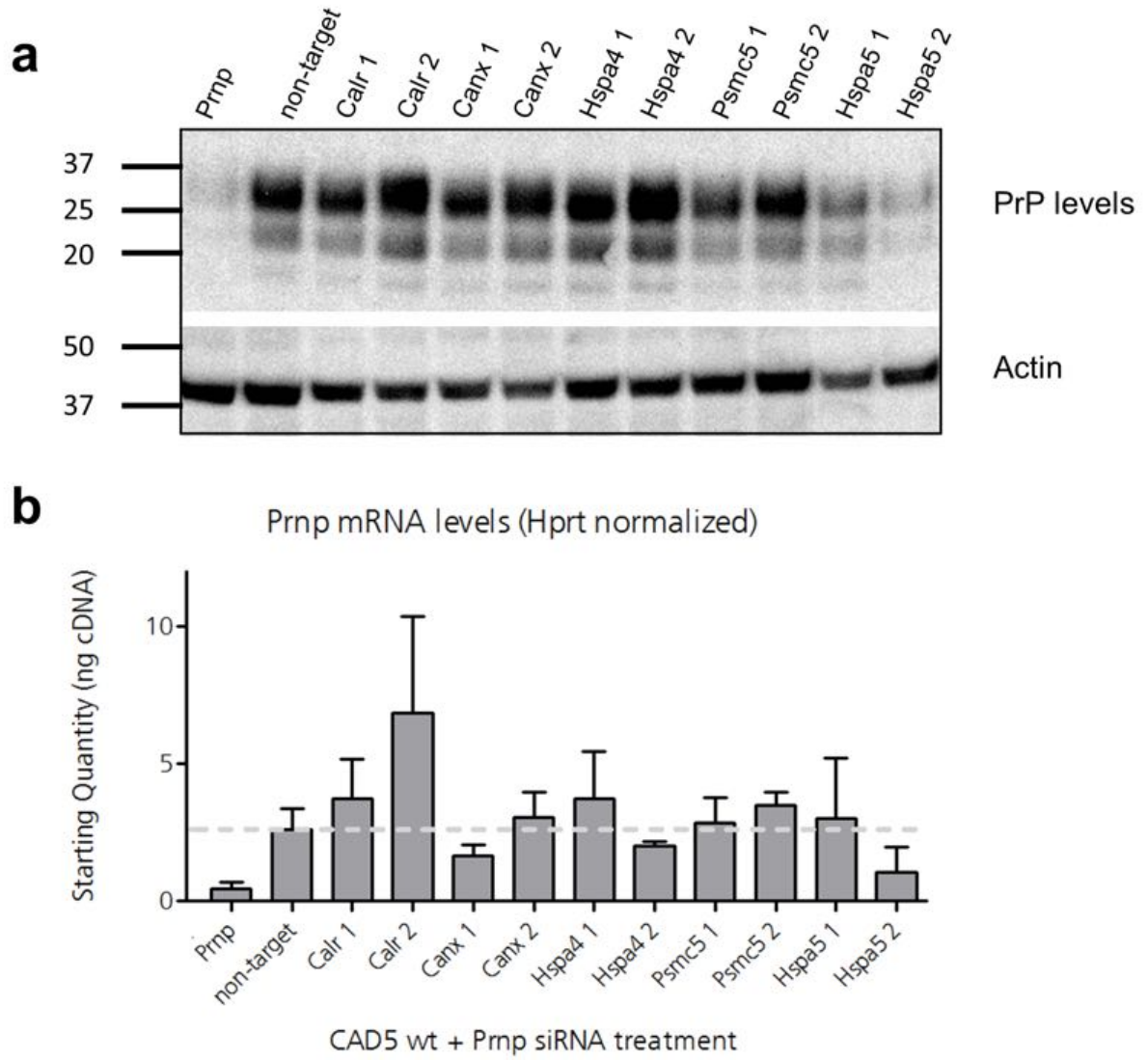

Figure 58: Comparison of the protein level in a Western blot to the mRNA level from qRT-PCR. I could confirm reduction of PrP levels upon treatment with chaperone targeting siRNAs Prnp, Calr-1, Canx-1 and Hspa5-2.

To establish hit validation for PrP^{Sc} screens, I transfected five different cell lines (CAD5 wt, chronically infected scCAD, PrP overexpressing hyCAD, chronically infected scHyCAD and CAD5 *Prnp*-/-), with *Prnp* targeting siRNA and performed PK-Westerns (Figure 59 a). In all five cell lines PrP^{C} or PrP^{Sc} levels respectively were clearly reduced upon transfection with *Prnp* targeting siRNA. To validate the chaperone hit Hspa5, I transfected the five cell lines with *Prnp* and Hspa5 targeting siRNAs. PK-Western showed, that both siRNAs led to reduction of PrP^{C} in CAD5 and hyCAD cells. PrP^{Sc} levels in scCAD and scHyCAD were clearly reduced

as well (Figure 59 b + c). To confirm chaperone hits in a different cell line than CAD5, I tested whether murine N2A PK1 cells were susceptible to murine RML6 prions by acute and chronical infection (Mahal, Baker et al. 2007). I chose N2A PK1 for their neuronal phenotype and for their high susceptibility to RML6 prions. PK-Western showed PrP^{Sc} bands in both, acutely and chronically infected N2A PK1 cells (Figure 60 a + b). Acute infection of N2A PK1 resulted in a less strong PrP^{Sc} band than acute infection of hyCAD cells, but much stronger than in CAD5 *Prnp*-/- cells. N2P PK1 cells chronically inoculated with RML6 showed a PrP^{Sc} band, whereas in untreated and NBH treated cells all PrP^{C} was completely digested. These results indicated that N2A PK1 cells were susceptible to RML6 prions. However, the knockdown efficiency in chronically infected N2A PK1 transfected with *Prnp* and non-target siRNA (5 – 70 nM siRNA) was very low and the cell viability decreased substantially with siRNA concentrations higher than 30nM (Figure 61).

Figure 59: PK-Western with five different cell lines transfected with Prnp targeting siRNA. RML6 containing brain homogenate, which served as positive control, exhibited the typical diagnostic shift towards a smaller PK-resistant core with un-, mono- and di-glycosylated PrP^{Sc} (first two lanes). PrP^{C} from uninfected CAD5 cells, was completely digested and the CAD5 Prnp-/- control showed no PrP. PrP^{C} and PrP^{Sc} levels respectively were reduced in all five cell lines upon transfection with Prnp targeting siRNA. b) PK-Western with CAD5 wt and scCAD transfected with Prnp and Hspa5 targeting siRNA. PrP^{C} from uninfected CAD5 cells, was completely digested. PrP^{C} and PrP^{Sc} levels in CAD5 wt and scCAD were reduced upon transfection with the two siRNAs. c)) PK-Western with hyCAD5 and scHyCAD transfected with Prnp and Hspa5 targeting siRNA. As well in hyCAD and scHyCAD cells the PrP^{C} and PrP^{Sc} levels were clearly reduced upon transfection with the Prnp and Hspa5 targeting siRNAs.

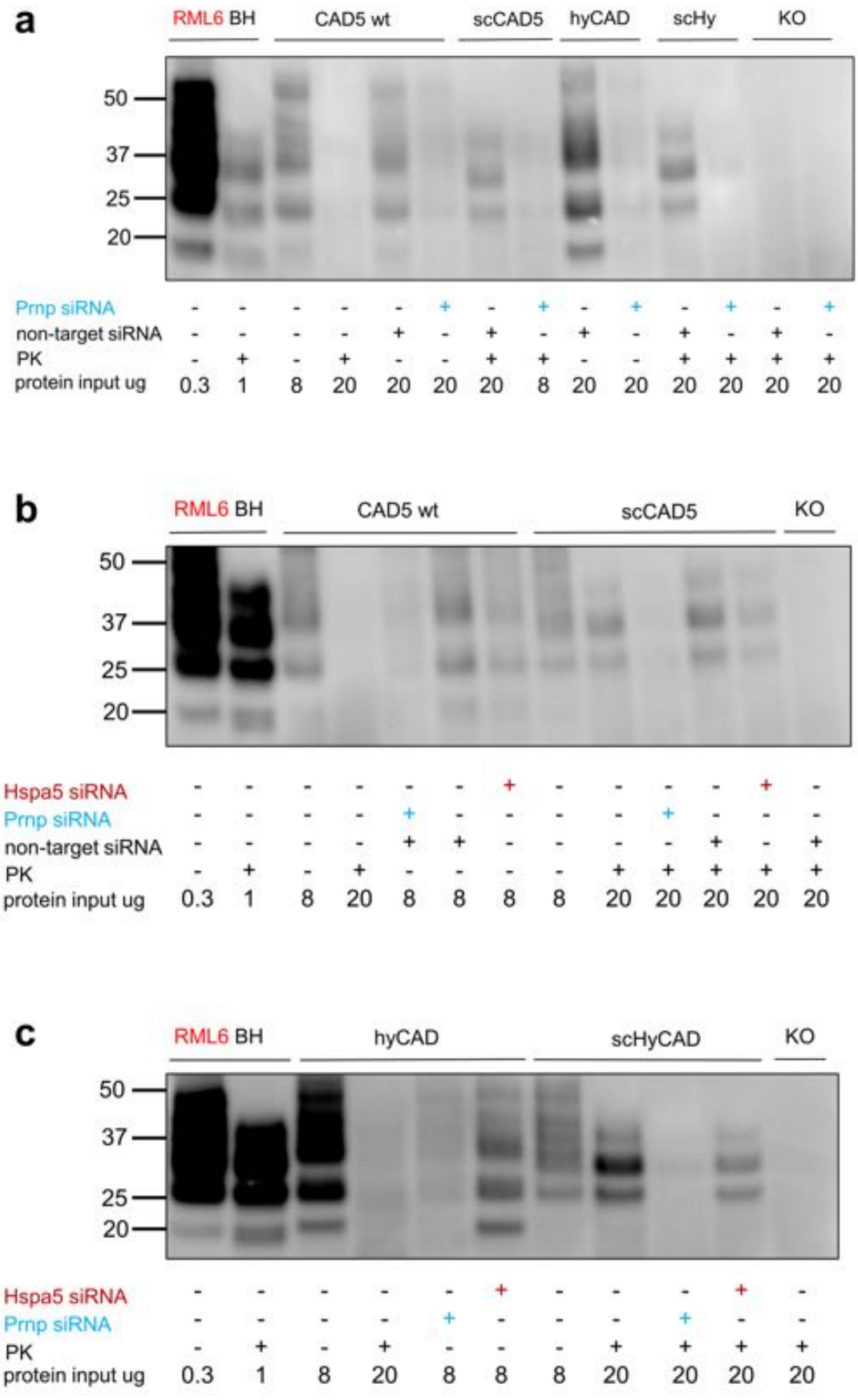

Figure 59: (Description on the previous page.)

I then tested whether murine myoblastoma CH3H/10T1/2 were susceptible to RML6. Myoblastoma cells were potentially interesting, because prion replication of murine Rocky Mountain Laboratory prion strain had been observed in muscle cells (Bosque and Prusiner 2000). I acutely and chronically infected CH3H/10T1/2 with RML6. *Prnp* knockout clone #C5, which I had generated by CRISPR-Cas9, served as negative control. Western blots of Proteinase K-digested samples showed a PrP^{Sc} band in acute infection, that was weaker than the one in the *Prnp*-/- control and no PrP^{Sc} band chronical infection (Figure 62 a + b).

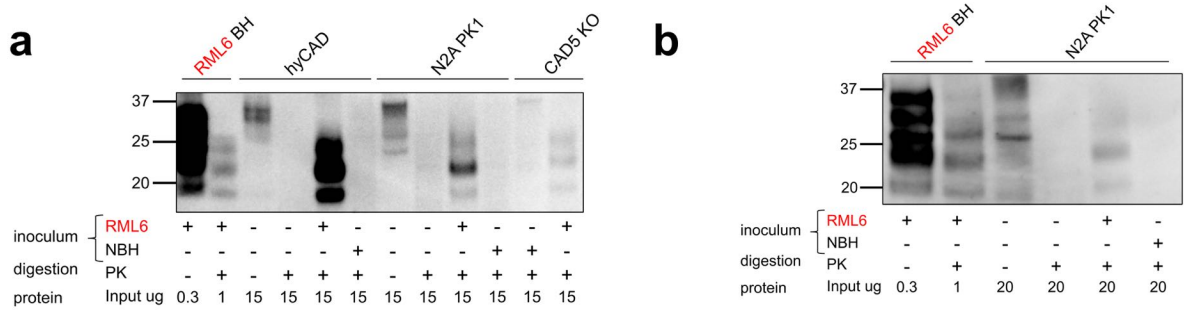

Figure 60: PK-Western of a) acute infection of N2A PK1, hyCAD and CAD5 Prnp-/- cells with 0.3 μg/mL RML6. RML6 containing brain homogenate exhibited the typical diagnostic shift (first two lanes). PrP^{Sc} band in RML6 infected hyCAD cells was stronger than in N2A-PK1 cells. Much less residual inoculum in CAD5 Prnp-/- than in RML6 infected N2A-PK1. b) Chronical infection of N2A PK1 showed a PrP^{Sc} band, whereas in untreated and NBH treated cells all PrP^{C} was completely digested.

Figure 61: PrP^{Sc} ELISA with N2A PK1 cells chronically infected with RML6 and manually transfected with Prnp targeting and scrambled siRNAs (5nM - 70nM) or untransfected (UT). In samples digested with PK, the ELISA absorbance signal was at the lower detection limit and no significant difference between cells transfected with Prnp targeting and scrambled siRNAs was evident. PK undigested samples exhibited an ELISA signal one log higher than PK digested samples. The transfection efficiency was too low to lead to a significant difference between cells transfected with Prnp targeting and scrambled siRNAs. With siRNA concentrations higher than 30 nM the cell viability was decreased, indicated by reduced PrP levels in the non-target control.

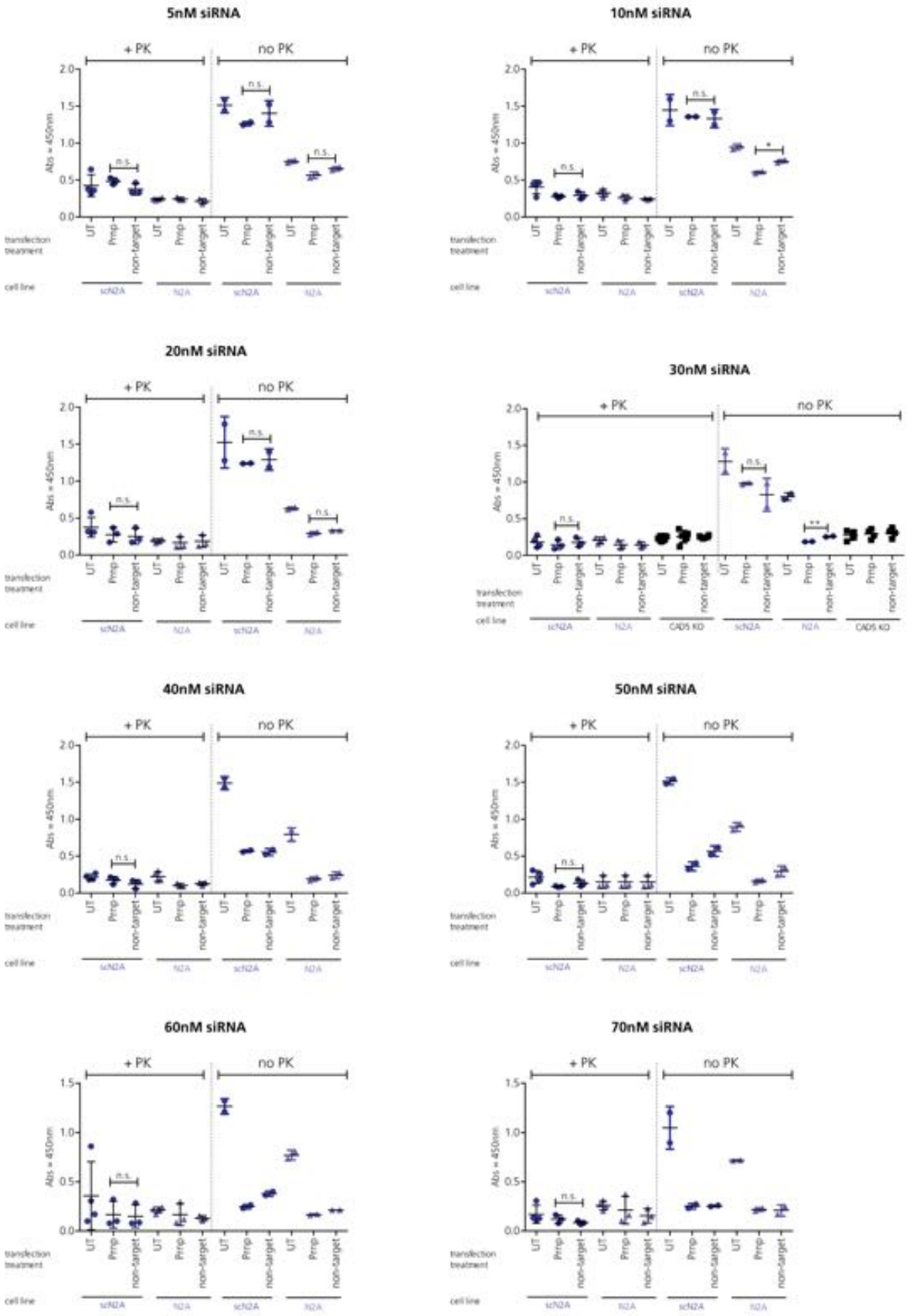

Figure 61: (Description on the previous page.)

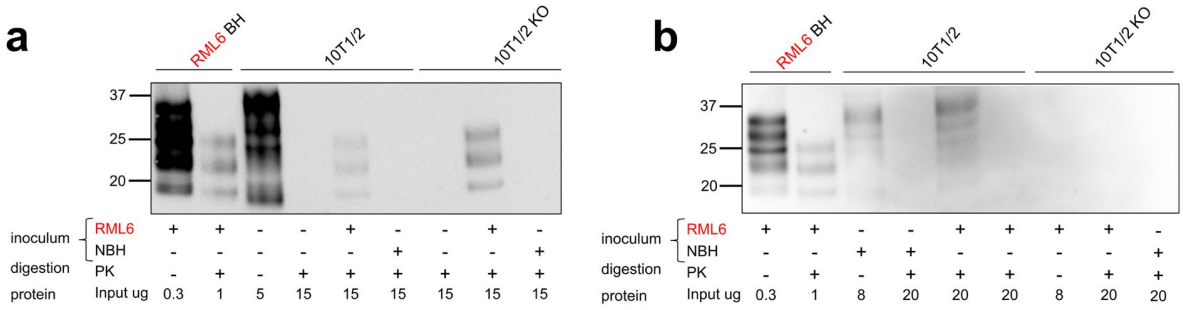

Figure 62: a) 10T1/2 acutely infected with 0.3 μg RML6 /mL for 96 hrs. The PrP^{Sc} band in acute infection was weaker than the one in the Prnp-/- control. b) PK-Western with chronically infected 10T1/2 and 10T1/2 Prnp-/- with 0.1 μg/mL RML6 did not show a PrP^{Sc} band in both cell lines.

6.2 Chaperone siRNA screens in human cells

6.2.1 Generating human murinized cells for siRNA screening

The human neuroblastoma SH-SY5Y cell line was well characterized and previously used for investigating neuronal death and alterations in gene expression profile upon prion infection and were permissive to prion replication when infected with brain homogenate from a sporadic CJD patient (Ladogana, Liu et al. 1995, Dupiereux, Zorzi et al. 2006, Martinez and Pascual 2007). Based on this, the SH-SY5Y cell line was chosen as model system for the human chaperone screen. To address prerequisite 1), I had generated PRNP-knockout mutants in the SH-SY5Y cell line by means of CRISPR-Cas9 during my masters. I had double-transfected the cells with an MLM3636-based sgRNA plasmid and an expression plasmid simultaneously expressing Cas9 and EGFP. After selection of clones by single cell fluorescence-activated cell sorting (FACS), I had expanded the clones in 96 well plates and screened total 350 clones for PrP levels, which finally resulted in five knockout (PRNP-/-) clones, which I had confirmed by sequence analysis, real time PCR and FACS binding experiments (V. 2015). I further characterized these five knockout clones by enzyme-linked immunosorbent assay (ELISA). All knockout clones showed clear ablation of PrP, when compared to CAD5 *Prnp*-/- cell lysate, whereas PrP in SH-SY5Y wild type was clearly present (Figure 63 a). In order to test the sensitivity of the ELISA, I spiked SH-SY5Y knockout clones #C75 and #C126 and CAD5 *Prnp*-/- with SH-SY5Y wt protein (Figure 63 b). At 1:64 dilution, the wild-type samples were diluted to the sensitivity limit of the ELISA (100 pg) and showed the same absolute PrP^{C} levels as un-spiked knock out clones. Absolute PrP^{C} levels of SH-SY5Y wild type were clearly discriminable from the knock-out clones. Absolute PrP values were interpolated from the linear range of the calibration curve with rhPrP22-231.

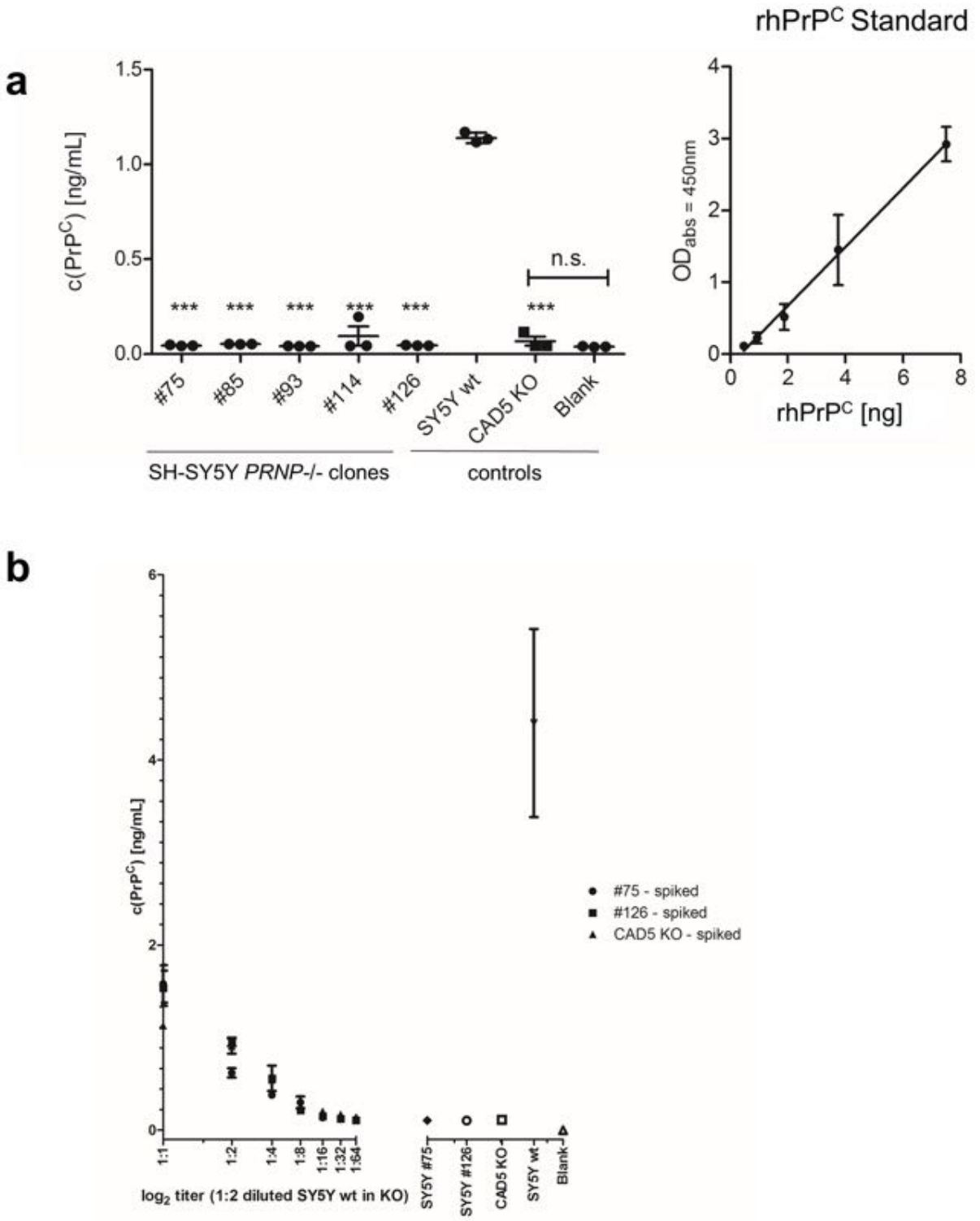

Figure 63: *(Description on the next page.)*

Figure 63: a) Using sandwich ELISA, I compared the absolute PrP^C levels of the five SH-SY5Y PRNP -/- clones to SH-SY5Y wild type and murine CAD5 Prnp -/- clones. All knockout clones showed clear ablation of PrP and were not distinguishable from the blank (what is the blank, "i.e. plain medium" etc.). Sample PrP^C concentrations were interpolated from the linear range of the calibration curve with rhPrP22-231. Each sample was compared to the positive control using an unpaired two tailed t test. b) Sandwich ELISA with SH-SY5Y knockout clones #C75 and #C126 and CAD5 Prnp-/- with SH-SY5Y wt protein. At 1:64 dilution, the wild-type sampC75 and #C75 and #C126 and CAD5 Prnp-/- with SH-SY5Y wt protein. At 1:64 dilution, the wild-type sampC126 and CAD5 Prnp-/- spiked with SH-SY5Y wt lysate in 1:2 dilutions. At 1:64 dilution, the wild type samples were diluted to the sensitivity limit of the ELISA (100 pg) and showed the same absolute PrP^C levels as the un-spiked knock out clones. PrP knockout clones were compared with one-way ANOVA and Bonferroni correction to SH-SY5Y wild type and showed very clear distinction from absolute PrP^C levels of SH-SY5Y wild type.

I confirmed depletion of PrP in the five SH-SY5Y PRNP-/- clones as well by immunoprecipitation (IP) with anti PrP antibody POM1 and subsequent western (Figure 64).

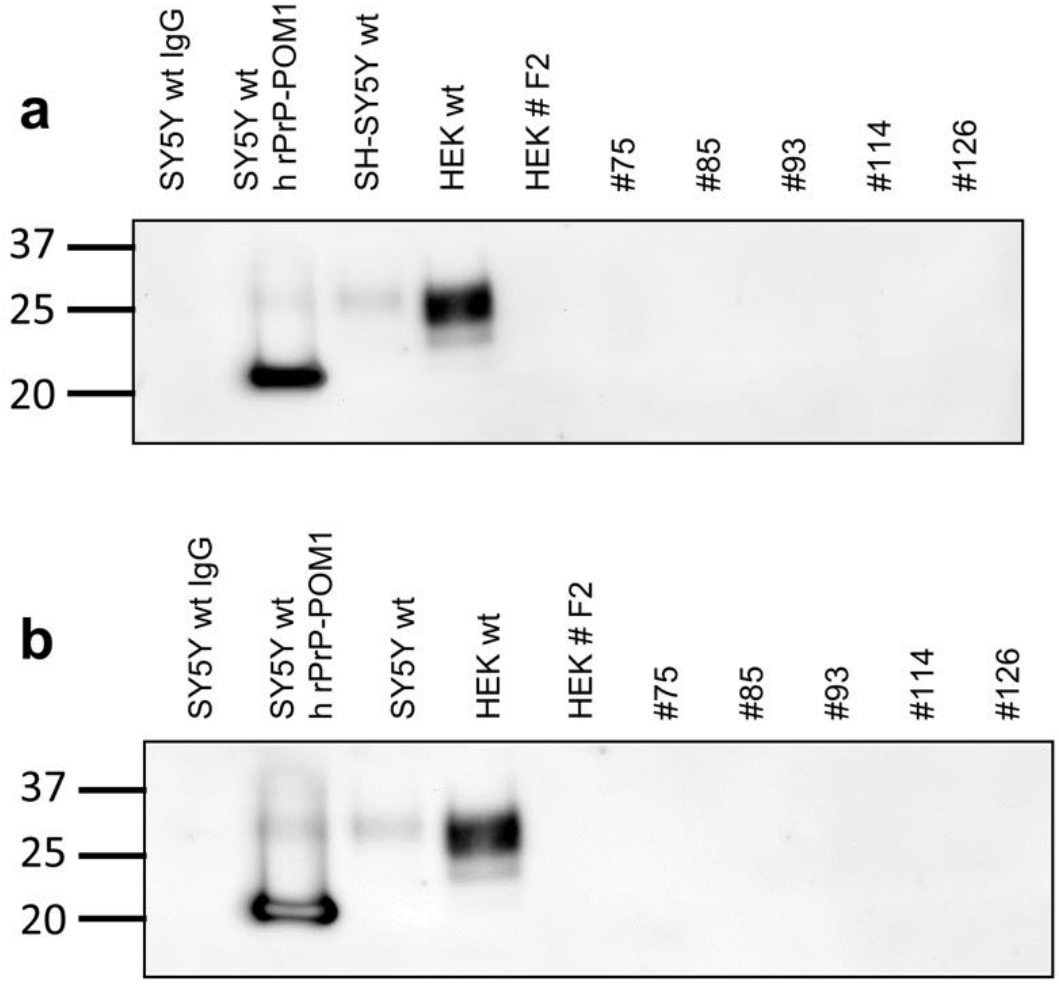

Figure 64:

Figure 64: Immunoprecipitation with 2000 μg of total protein and western blot with five SH-SY5Y PRNP-/- clones, SH-SY5Y wt, HEK293 cells and a HEK PRNP-/- clone. Immunoprecipitation of SH-SY5Y wt with IgG did not pull down any PrP, which showed that immunoprecipitation with POM1 was specific for PrP. Blocking POM1 with recombinant human PrP22-231, did work, the band at 23-25 kDa corresponded to the molecular weight of rhPrP22-231. PrP levels of SH-SY5Y wt were much lower than in HEK wt. No PrP was present in all knockout clones. a) IP-Western performed with biotinylated POM2 as 1° antibody and Avidin-HRP. b) IP-Western performed with XN as 1° antibody and Goat anti rabbit IgG as 2° antibody.

Even when performing immunoprecipitation with 2000 μg of total protein from SH-SY5Y lysate, the PrP signal in western was very weak. This could be explained by weak expression of PrP under the control of the *PRNP* promoter. If I would have murinized the cells by targeted knock-in of the open reading frame of murine *Prnp* with CRISPR-Cas9, murine PrP expression levels could have been low, as well. Therefore, I decided to generate murinized SH-SY5Y by stable transfection of *PRNP* -/- clone #C114 with a pcDNA3 plasmid harboring the coding sequence of murine *Prnp* and subsequent clonal isolation by limited dilution. Sandwich ELISA showed that multiple, random integration of murine *Prnp* into the human genome driven by the strong (Cytomegalovirus) CMV promoter led to significantly higher expression of murine PrP in six isolated clones (#M2, #M4, #M5, #M6, #M7, #M9, #M12), than in SH-SY5Y wild type and *PRNP* -/- #C114 clone (Figure 65).

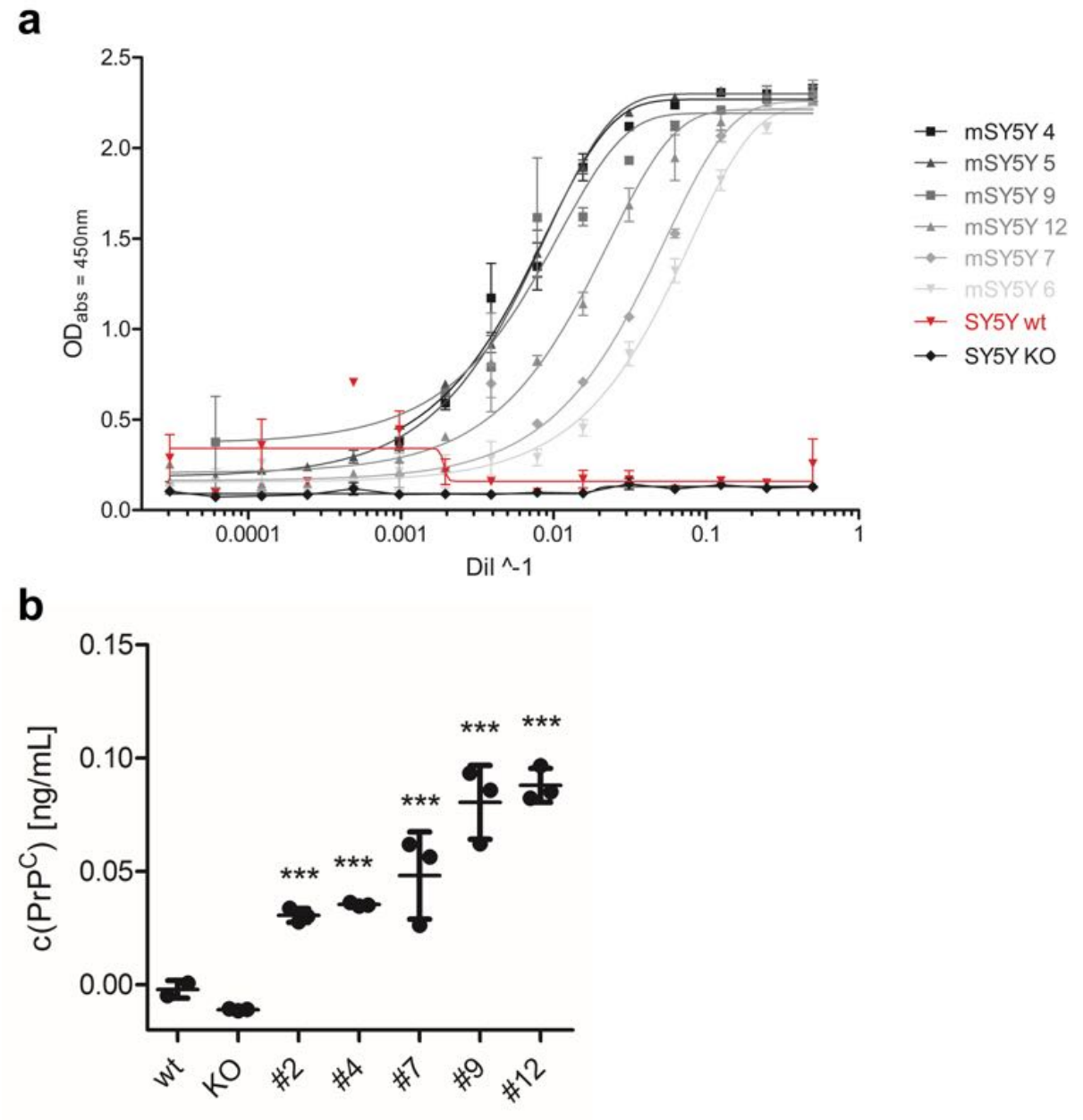

*Figure 65: Sandwich ELISA with samples diluted 1:2 from a starting concentration of 16 μg/mL. a) relative PrP values of murinized SH-SY5Y clones were significantly higher than in wild type (wt, red) and SH-SY5Y PRNP-/- (KO, black) cells. #M6 showed the highest PrP expression (brightest grey scale), #M4 the lowest (darkest grey scale). b) Absolute PrP values were interpolated from the linear range of the calibration curve with rhPrP$_{23\text{-}231}$. Murinized SH-SY5Y clones were, individually compared to SH-SY5Y wild type. *** $p < 0.001$, unpaired, two-tailed T-test.*

I tested the susceptibility of murinized SH-SY5Y cell lines to murine prions by acute infection. Since sibling clones of the same cell line can show very different relative susceptibilities to prion strains, I tested a pool of seven murinized SH-SY5Y clones (mSY5Y) in addition to single clone #M4 (Bosque and Prusiner 2000). To check strain specific susceptibility, I acutely infected

mSY5Y, as well as #M4 clone and SH-SY5Y PRNP-/- cells with eight different prion strains (RML6, 22F, 22L, 236K, 87A, 79A, ME7, mNS) and according non-infectious brain homogenate (Figure 66).

infectious BH	non-infections BH
RML6	CD1 NBH
22F	HsdC57BL
22L	HsdC57BL
87A	HsdC57BL
79A	HsdC57BL
mNS	JC57BL
ME7	HsdC57BL
263K	NBH (TgSHaPrP)

Figure 66: Overview of eight different prion strains and according non-infectious brain homogenate used for acute infection of murinized SH-SY5Y cells and PRNP-/- cells.

Western blots of proteinase K-digested cells acutely infected with 79A, ME7 and mNS strains showed PK resistant PrP bands stronger than the one in the SH-SY5Y PRNP-/- control, which served as negative control and does not replicate prions (Figure 67 g, h, i). The remained prion strains either showed no PK resistant bands in murinized cells or a strong band in SH-SY5Y PRNP-/- controls, pointing towards residual inoculum (Figure 67).

Figure 67: Acute infection of mSY5Y, single clone #M4 and SH-SY5Y PRNP-/- cells with eight different prion strains (RML6, 22F, 22L, 236K, 87A, 79A, ME7, mNS) and according non-infectious brain homogenate. The digested infectious brain homogenate shows the typical shift towards a smaller PK-resistant core. a) Acute infection of #M4 with RML6 showed a PrP^{Sc} band in infected #M4 and a stronger PrP^{Sc} band in SH-SY5Y PRNP-/- cells. b) Acute infection of mSY5Y with RML6 showed no PK resistant bands. c) Acute infection of #M4 and mSY5Y pool with 22F showed incomplete digestion of PrP^{C} in NBH treated M4 and no PK resistant bands. d) Acute infection of #M4 and mSY5Y pool with 22L showed, that PrP^{C} digestion of NBH treated #M4 was incomplete. The PrP^{Sc} band in SH-SY5Y PRNP-/- cells was stronger than in #M4 and mSY5Y. e) Acute infection of #M4 and mSY5Y pool with 263K hamster prions did not show any band in PK-Western despite in untreated, PK-undigested #M4 and mSY5Y. f) PK-Western with #M4 and mSY5Y pool acutely infected with 87A showed strong PrP^{Sc} bands in all infected cells. g) Acute infection of #M4 and mSY5Y pool with 79A showed stronger bands in infected #M4 and mSY5y than in PRNP-/- cells. PrP^{C} was not completely digested in NBH treated mSY5Y. h) Acute infection with ME7 showed a PrP^{Sc} band in #M4, no PrP^{Sc} in mSY5Y and very little residual inoculum in PRNP-/- cells. i) Acute infection with mNS showed a PrP^{Sc} band in infected #M4 weaker than the residual inoculum in PRNP-/- cells and an PrP^{Sc} band in infected mSY5Y cells stronger than the residual inoculum in PRNP-/- cells. PrP^{C} was not completely digested in NBH treated M4.

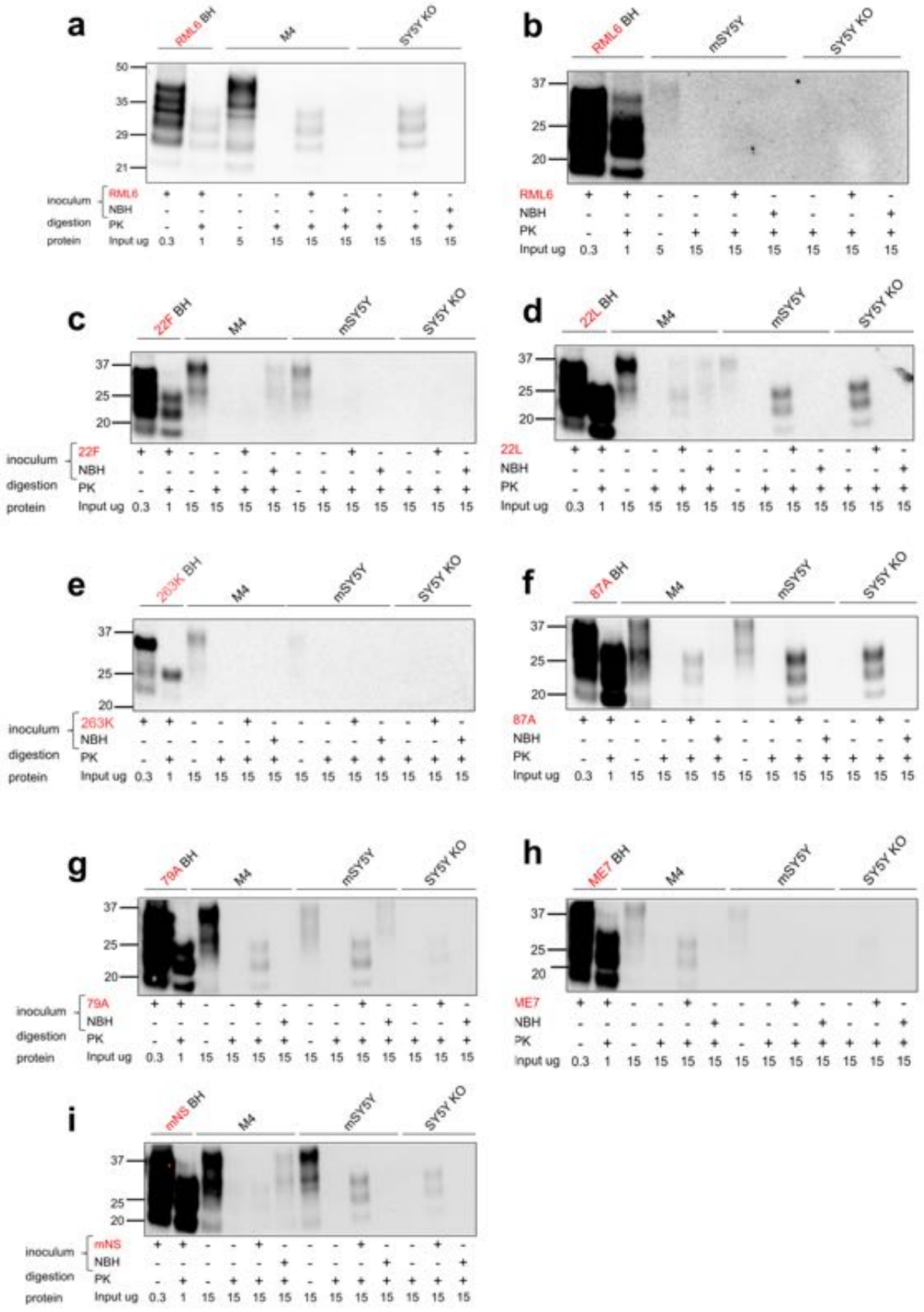

Figure 67: (Description on the previous page.)

Because RML6 was commonly used in our lab and my colleague Daniel Pease had performed a PrP^{C} screen with #M4 cells and was opting for a PrP^{Sc} screen too, I tested whether #M4 cells could be infected RML6 prions by chronical infection. The PK-Western blot did not show any PK-resistant murine PrP aggregates (Figure 68).

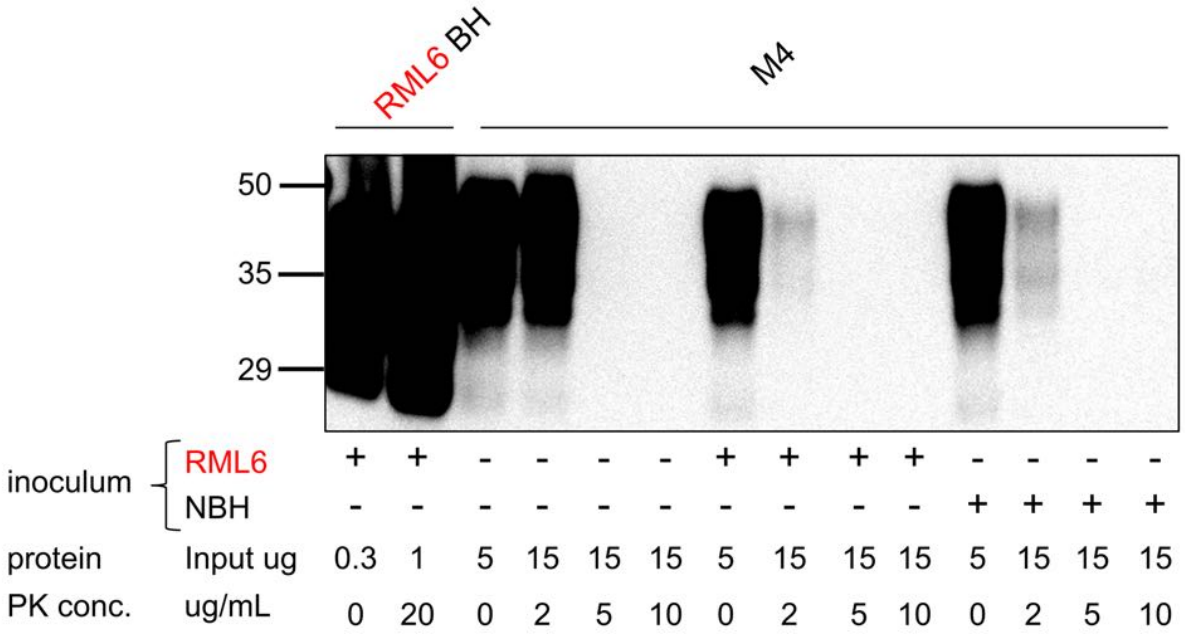

Figure 68: Chronical infection of #M4 with RML6. Samples were digested with 2, 5 and 10 μg PK /mL. The blot was highly overexposed, so the typical diagnostic shift in the molecular weight of PrP was not visible in the positive control with brain homogenate of terminally sick mice infected with RML6, digested with PK. PK digestion with 2 μg PK/mL resulted in residual PrP^{C}. 5 μg PK/mL were necessary to completely digest PrP^{C}. The Western blot did not show a PrP^{Sc} band in #M4 cells inoculated with RML6.

To test potential presence of PK-sensitive material in #M4, I ultracentrifuged the samples on a 10% - 60% sucrose gradient and collected fractions for Western blotting. On western blots, I did not find any PK-sensitive murine PrP aggregates in RML6 infected #M4 cells (Figure 69).

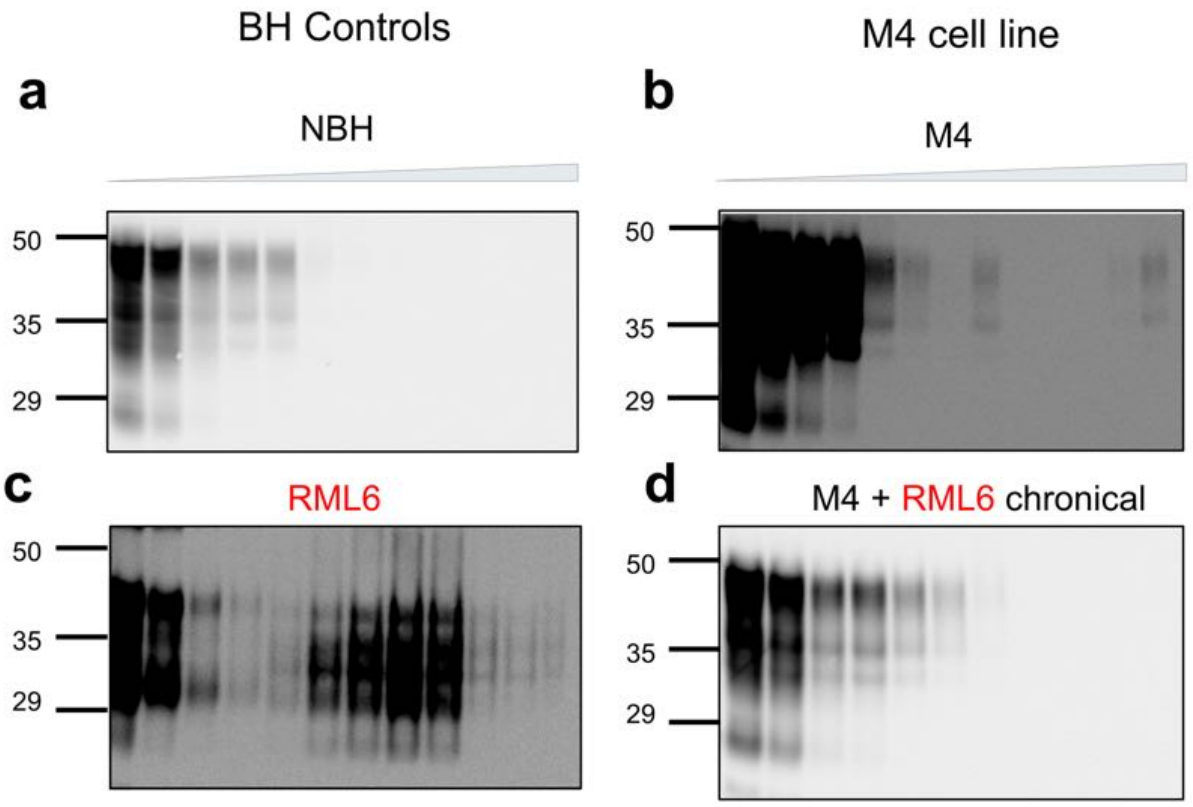

Figure 69: Western blots with fractions from gradient centrifugation. The density of the sucrose gradient was indicated by the scale with lowest density (10% sucrose) on the left, and highest density (60% sucrose) on the right side. a) The Western blot with non-infectious brain homogenate (NBH) fractions showed PrP in low density fractions and no PrP in high density fractions. b) The blot with RML6 brain homogenate did show PrP in low and high density fractions. c) The Western with untreated #M4 cell lysate showed PrP in low density fractions and in the highest density fraction. d) High density fractions of #M4 chronically infected with RML6 did not show any PK-sensitive PrP^C aggregates but clear bands in low density fractions.

Immunohistochemistry of #M4 revealed physiological membrane-bound expression of murine PrP and no stalling in the ER, which could have prevented prion replication (Figure 70) (Cardinale, Filesi et al. 2005).

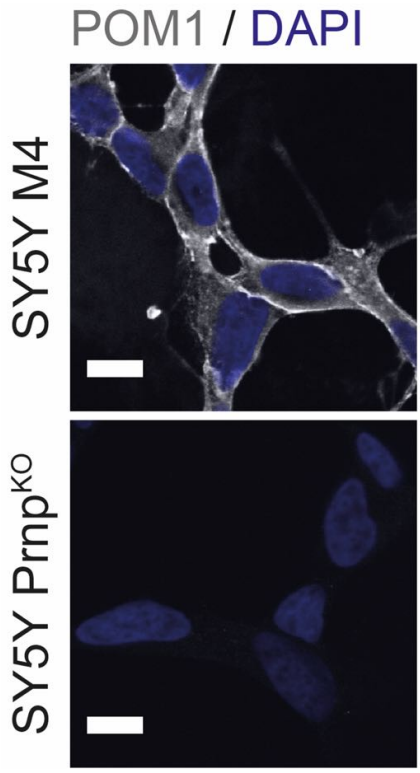

Figure 70: Confocal microscopy images of immunostaining of PrP with POM1 antibody in #M4 showed physiological expression of PrP at the membrane. SH-SY5Y PRNP-/- cells did not show any PrP. Scale bar 10 μm.

Sequencing of #M4 showed an unaltered wild-type *Prnp* sequence which led me to exclude any alterations of the murine PrP^{C} that would hinder RML6 replication. When I chronically infected the mSY5Y pool and single clone #M4 with the three strains (79A, ME7 and mNS), that had shown PK-resistant bands in PK-Western upon acute infection, no PrP^{Sc} band was visible in PK-Westerns siehe oben (Figure 71).

Figure 71: PK-Westerns with chronical infection of mSY5Y pool and #M4. There was no residual inoculum in al SH-SY5Y PRNP-/- controls treated with infectious brain homogenate and digested with PK. a) Chronical infection of #M4 with 79A did not show a PK resistant band, but some residual PrP^{C} in the NBH treated control. Chronical infection of mSY5Y with 79A b) and mNS d) did not show PK resistant bands. c) Neither did chronical infection of #M4 with ME7.

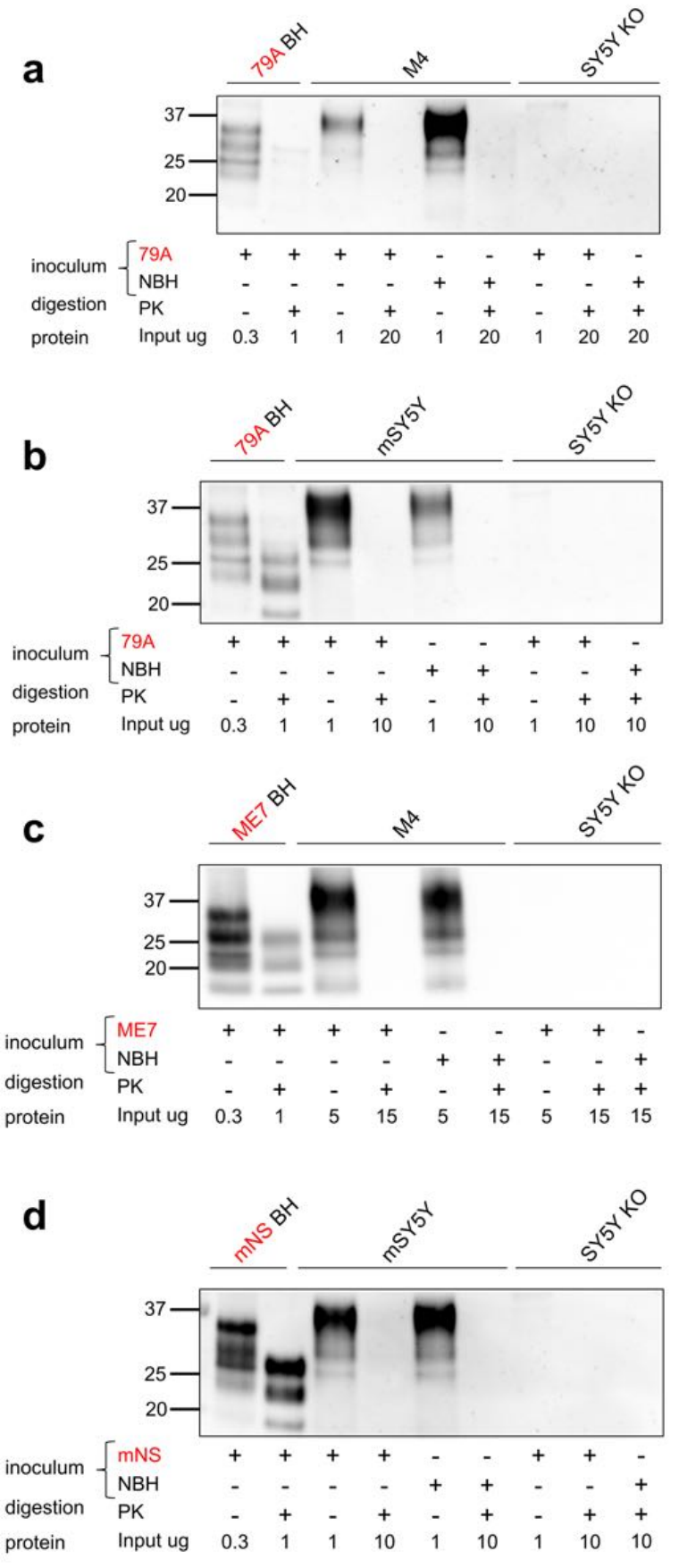

Figure 71: (Description on the previous page.)

In a different approach, I stably transfected the human glioblastoma cell line U-251MG with a pcDNA3 plasmid encoding the open reading frame of murine *Prnp*. I assumed that murine PrP^C overexpression outranged endogenous human PrP^C expression and might render the cells susceptible to murine prions, if they expressed the required cellular machineries for prion replication. I acutely infected mixed clones of U-251MG overexpressing murine PrP and untransfected cells as negative control with murine RML6 prions. PK-Western with mouse specific POM19 antibody showed that U-251MG transfected with *Prnp* actually expressed much more PrP^C in comparison to untransfected UMG cells (Figure 72 a). POM19 slightly bound human PrP. Untransfected U-251MG cells had a stronger PrP^{Sc} band, which could be explained by residual murine RML6 inoculum attached to the cells. PK-Western with human PrP specific 3F4 antibody showed weak bands in uninfected U-251MG cells, and no human PrP^{Sc} in infected cells (Figure 72 b). Thus, U-251MG did neither replicate RML6 prions, nor human prions.

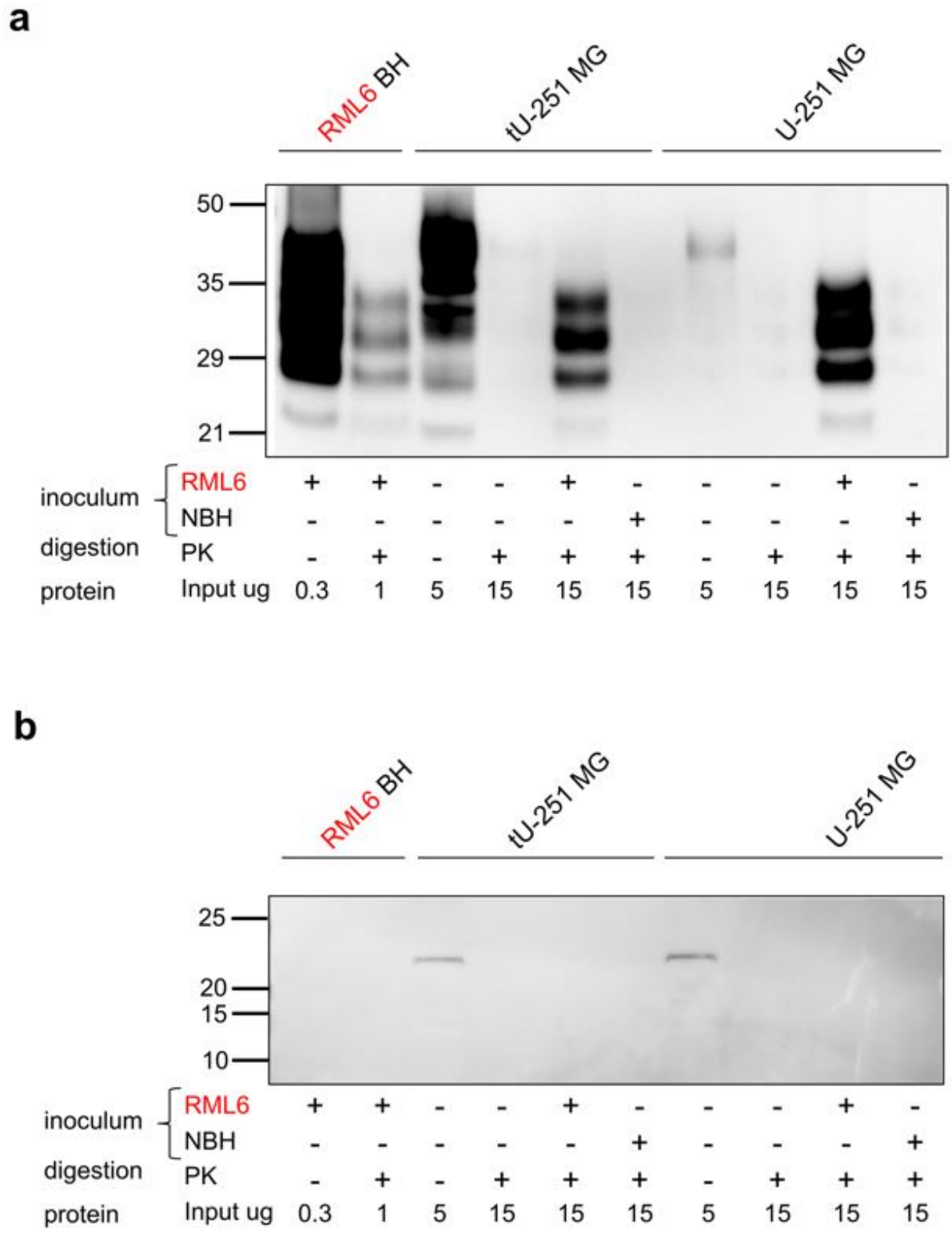

Figure 72: Acute infection of human U-251MG overexpressing murine PrP and untransfected cells as negative control with murine RML6 prions. a) PK-Western with mouse specific POM19 antibody showed higher PrP levels in U-251MG transfected with Prnp in comparison to un-transfected UMG cells. POM19 slightly bound human PrP. Untransfected U-251MG cells had a stronger PrP^{Sc} band than PrP overexpressing cells. b) PK-Western with human PrP specific 3F4 antibody showed weak bands in uninfected U-251MG cells, and no human PrP^{Sc} in infected cells.

6.2.2 Human PrP^C screen

Colleagues from the lab did perform a genome wide human PrP^C screen with U-251MG cells transfected with an arrayed druggable silencer select siRNA library purchased from ThermoFisher. The library consisted of 64752 siRNAs targeting 21584 transcripts. Each gene transcript was targeted by three siRNAs. siRNAs targeting the same transcript were pooled from 186 source plates to 62 low density volume plates (1536 wells). Three pooled *Prnp* siRNAs and the same scrambled non-target siRNAs as in the murine screen were used as controls. The total screen comprised n = 166 384-well plates. The final siRNA concentration was 5 nmol. Upon reverse transfection, the RT-Glo luminescence and FRET signal were measured, after adding Europium-POM2 and APC-POM1.

6.3 Comparison of murine and human siRNA screens

For the murine PrP^C screen I used CAD5 cells, which are prion-susceptible cells, derived from neuronal Cath.a-differentiated (CAD) cells (Qi, Wang et al. 1997). The human glioblastoma cell line U-251MG was used for the human PrP^C screen (Bigner, Bigner et al. 1981). In the two murine PrP^C screens, I screened two different libraries, targeting different chaperone genes. The same genes that were screened in the two murine PrP^C screens, where extracted from the human genome wide PrP^C screen (64752 distinct siRNAs targeting 21584 transcripts) and compared against one another separately.

6.3.1 Comparison 1. murine PrP^C screen vs. human PrP^C screen

The first arrayed druggable mouse siRNA library provided by Novartis consisted of 376 siRNAs against 99 transcripts of druggable chaperones, that were expressed in CAD5 cells based on a CAD5-RNASeq data set (13'752 expressed genes). Each murine gene was represented by one row in the heatmap (Figure 73 left).

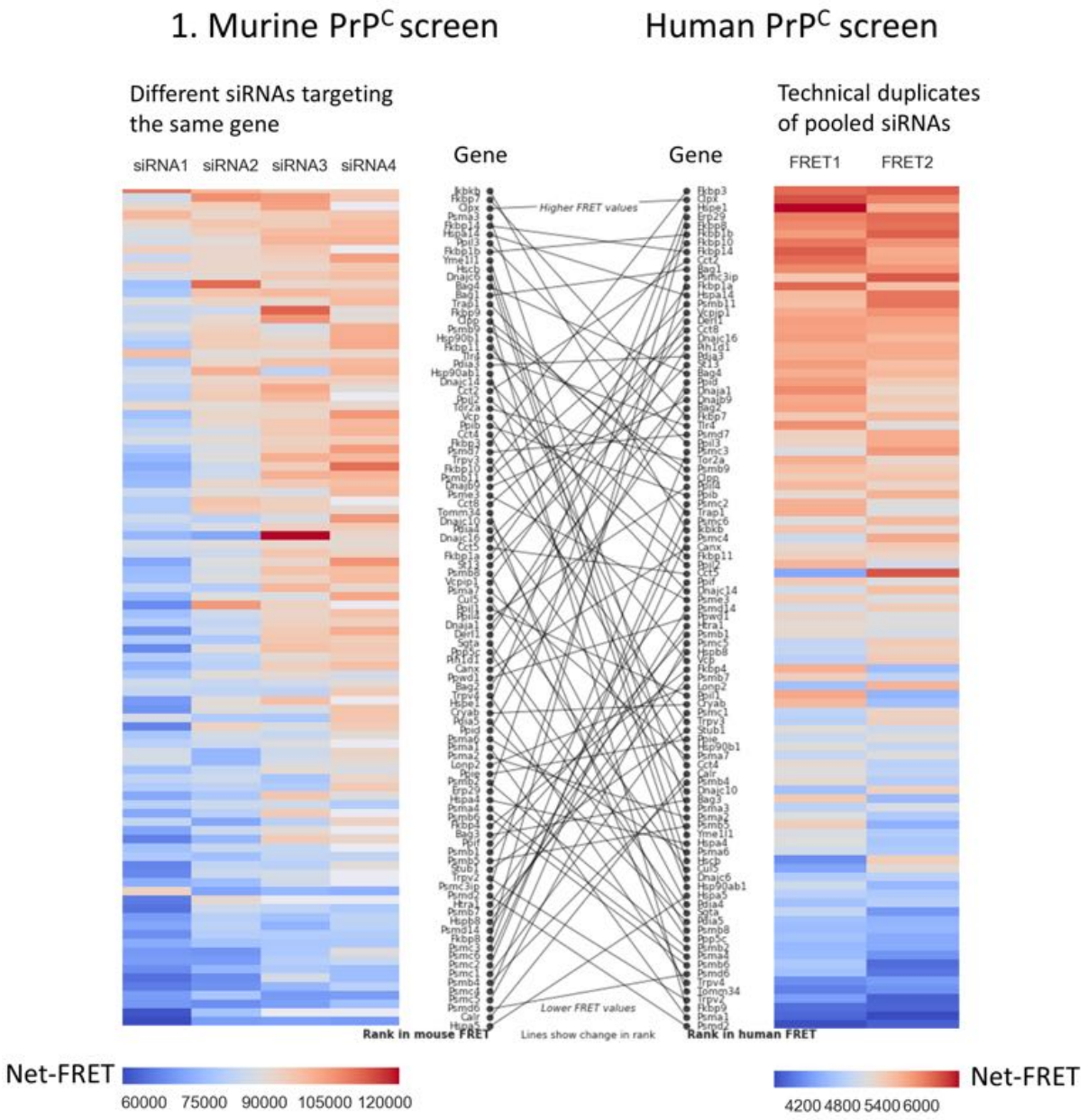

Figure 73: Comparison of 1. murine PrP^C screen vs. human PrP^C screen. Results from the first murine PrP^C screen are shown on the left side, results from the human PrP^C screen on the right side.

Each gene in the murine screen was separately targeted by up to four different siRNAs in four different wells, represented by four different columns (siRNA1 - 4). Each siRNA modulated the PrP^C levels of the transfected cells, which resulted in different PrP^C levels, represented by Net-FRET values. Each square in the heatmap showed the mean Net-FRET level of two technical replicates treated with the same siRNA. The Net-FRET signal of the murine samples ranged from 120'000 to 60'000 (Table 1). High Net-FRET levels were shown in red, low Net-FRET levels in blue. The murine genes were ranked according to the descending Net-FRET signal of the mean of four siRNAs targeting the same gene. The mean Net-FRET signal of all controls

transfected with *Prnp* siRNA was 54'510, whereas the mean Net-FRET signal of non-target siRNA treated controls was 99'833 (Table 1).

	Max Net-FRET	Min Net-FRET	Mean Pos.	Mean Neg.
Mouse	120'000	60'000	54'510	99'833
Human	6'000	4'200	957	5'401

Table 1: Comparison of 1. murine PrP^C screen vs. human PrP^C screen

The same genes that were screened in the first murine PrP^C screen, where extracted from the human genome wide PrP^C screen. Each gene was represented by one row in the heatmap (Figure 73 right). In the human PrP^C screen, three siRNAs targeting the same gene were pooled in one well. Technical duplicates of cells transfected with the same siRNA pool were presented in two different columns (FRET1 and FRET2). Each square in the heatmap represented the Net-FRET level of a single technical replicate treated with the same siRNA pool. The Net-FRET signal of the human samples ranged from 6'000 to 4'200 (Table 1). High Net-FRET levels were shown in red, low Net-FRET levels in blue. The human genes were ranked according to the descending mean Net-FRET signal of the technical duplicates targeted by the same pool of siRNAs against the same gene. The mean Net-FRET signal of all human controls transfected with *PRNP* siRNA was 957, whereas the mean Net-FRET signal of non-target siRNA treated controls was 5'401 (Table 1). Murine and human genes ranked according to descending Net-FRET levels as described above, were correlated by name (Figure 73 middle). The connecting lines showed the change in the rank of each gene. I compared the rank numbers of the first murine PrP^C screen and the human PrP^C screen and contrasted them to the chaperones obtained in the first murine PrP^C screen based on the best gaussian processed normalized sample signal versus non-target comparison at a threshold $p = 0.001$ (Figure 75 a). Genes leading to downregulation in the murine PrP^C screen were written in blue. Two chaperone genes leading to downregulation of PrP^C were targeted by four siRNAs (yellow), seven genes were targeted by three siRNAs (dark orange), and 12 genes by two siRNAs (bright orange). Six genes that differed maximally 15 ranks from each other in the murine and human PrP^C screens were marked in bright green and depicted in a Venn diagram (Figure 75 b). Five genes that differed maximally 30 ranks from each other in the murine and human PrP^C screens were marked in dark green.

6.3.2 Comparison 2. murine PrP^C screen vs. human PrP^C screen

The second library consisted of 560 siRNAs against 140 non-druggable chaperone transcripts, including transcripts that were not expressed in CAD5 cells. In this arrayed mouse siRNA library purchased from ThermoFisher, one gene was targeted by 4 different siRNAs. Each gene was represented by one row in the heatmap (Figure 74 left). The murine and human genes and their Net-FRET levels were depicted, ranked and correlated the same way as in the comparison of the 1. murine PrP^C screen vs. human PrP^C screen.

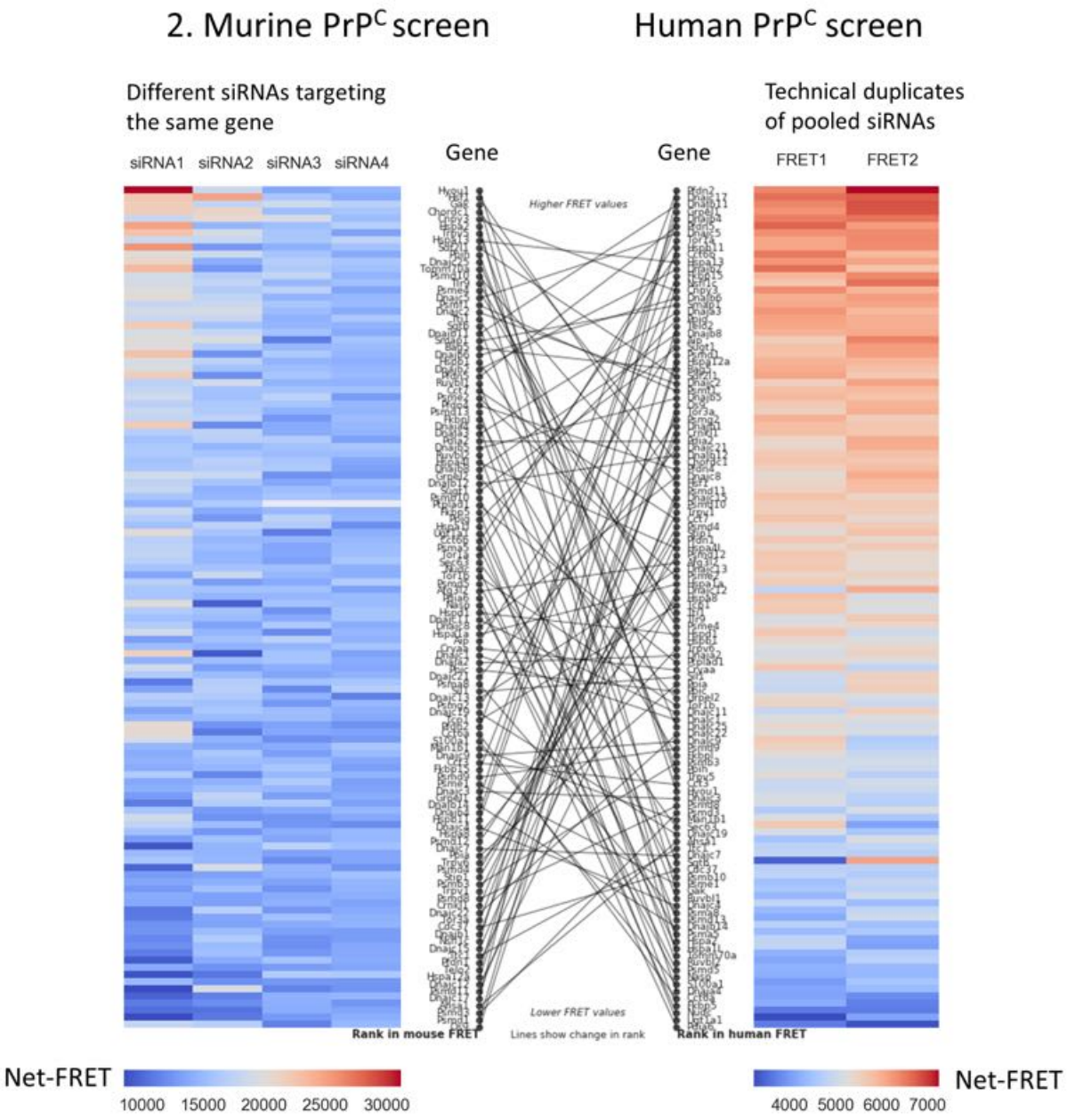

Figure 74: Comparison of 2. murine PrP^C screen vs. human PrP^C screen. Results from the second murine PrP^C screen are shown on the left side, results from the human PrP^C screen on the right side.

The Net-FRET signal of the murine samples ranged from 30'000 to 10'000 (Table 2). The mean Net-FRET signal of all controls transfected with *Prnp* siRNA was 6'862, whereas the mean Net-FRET signal of non-target siRNA treated controls was 14'550 (Table 2). In the second murine PrP^C screen one siRNA targeting *Hyou1* led to very high PrP- and Net-FRET levels. Because of the high signal, the entire heat map of the second murine PrP^C seemed to show reduced PrP^C levels in blue. However, most of the Net-FRET levels were around 15'000, which corresponded to the non-target controls (14'550). Thus, the high Net-FRET signal from *Hyou1* siRNA masked the gradient of PrP expression.

	Max Net-FRET	Min Net-FRET	Mean Pos.	Mean Neg.
Mouse	30'000	10'000	6'862	14'550
Human	7'000	4'000	957	5'401

Table 2: Comparison of 2. murine PrP^C screen vs. human PrP^C screen.

The Net-FRET signal of the human samples ranged from 7'000 to 4'000 (Table 2). The mean Net-FRET signal of all human controls transfected with *PRNP* siRNA was 957, whereas the mean Net-FRET signal of non-target siRNA treated controls was 5'401 (Table tab2). The connecting lines showed the change in the rank of each gene. I compared the rank numbers of the second murine PrP^C screen and the human PrP^C screen and contrasted them to the chaperones obtained in the second murine PrP^C screen based on the best gaussian processed normalized sample signal versus non-target comparison at a threshold p = 0.001 (Figure 75 c). Genes leading to upregulation in the murine PrP^C screen were written in black. Two genes were targeted by two siRNAs (bright orange) leading to upregulation of PrP. Both genes differed more than 30 ranks from each other in the murine and human PrP^C screens.

Figure 75: a) Comparison of rank numbers from the first murine PrP^C screen and the human PrP^C screen contrasted to the chaperones ranked as hits in the first murine PrP^C screen based on the best gaussian processed normalized sample signal versus non-target comparison at a threshold p = 0.001. Genes leading to downregulation in the murine PrP^C screen were written in blue. Two genes were targeted by four siRNAs (yellow), seven chaperones were targeted by three siRNAs (dark orange), 12 chaperones by two siRNAs (bright orange) leading to downregulation of PrP. b) Six genes that differed maximally 15 ranks from each other in the murine and human PrP^C screens were marked in bright green and depicted in a Venn diagram. Five genes that differed maximally 30 ranks from each other in the murine and human PrP^C screens were marked in dark green. c) I compared the rank numbers of the second murine PrP^C screen and the human PrP^C screen and contrasted them to the chaperones ranked as hits in the second murine PrP^C screen based on the best gaussian processed normalized sample signal versus non-target comparison at a threshold p = 0.001. Genes leading to upregulation in the murine PrP^C screen were written in black. Two genes were targeted by two siRNAs (bright orange) leading to upregulation of PrP. Both genes differed more than 30 ranks from each other in the murine and human PrP^C screens.

a Comparison 1. murine PrP^C screen vs. human PrP^C screen

Gene	rank human	rank mouse	difference	total ranks
Hspa5	16	1	15	97
Psmc5	45	4	41	97
Fkbp8	93	11	82	97
Psmc2	61	8	53	97
Psmc1	37	7	30	97
Psmb4	29	6	23	97
Psmd6	7	3	4	97
Psmd14	49	12	37	97
Psmd2	1	16	-15	97
Psmb7	41	14	27	97
Calr	30	2	28	97
Psmc4	57	5	52	97
Hspb8	44	13	31	97
Psmc3	67	10	57	97
Canx	56	42	14	97
Sgta	14	45	-31	97
Psmc6	59	9	50	97
Hspa4	22	27	-5	97
Ppif	52	22	30	97
Lonp2	40	31	9	97
Psmc3ip	87	17	70	97

difference
< 15
< 30
> 30

b

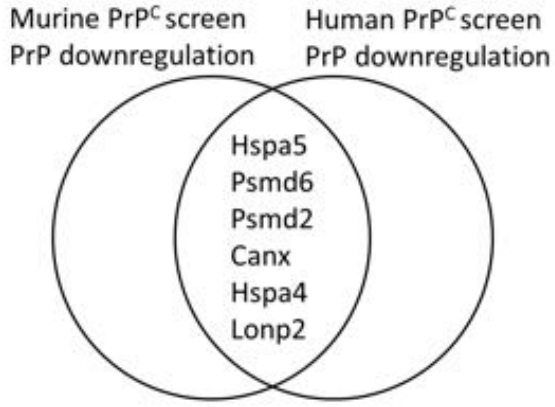

c Comparison 2. murine PrP^C screen vs. human PrP^C screen

Hsf1	77	117	-40	118
Chordc1	80	115	-35	118

Figure 75: (Description on the previous page.)

7 Discussion

7.1 Chaperone siRNA screens in murine cells

7.1.1 Murine PrP^C screens

Recent research has connected chaperones to prion disease (Allen, Wegrzyn et al. 2005, Rikhvanov, Romanova et al. 2007, Park, Eun Kim et al. 2017). However, no comprehensive study including all mammalian chaperones has been achieved in prion research. In this study I presented an unbiased and plenary approach to assess which chaperones are involved in the biosynthesis of PrP^C in the murine neuronal cell line CAD5 by siRNA mediated screens on two robotic platforms. The screens were comprised of two assays measuring cell viability and PrP^C levels. Viability results were used to define thresholds for extreme low or high cell viability and implemented in the analysis of the PrP levels to select chaperones altering the PrP metabolism rather than cell viability. My screens validated the role of *Hspa5* and *Hsf1* in prion protein metabolism and furthermore discovered 21 novel chaperones involved in PrP metabolism (Park, Eun Kim et al. 2017) (Steele, Hutter et al. 2008).

I completed two murine PrP^C screens with two different siRNA libraries targeting druggable and non-druggable chaperones. Both screens passed quality control and resulted in 26 siRNAs leading to upregulation of PrP levels and 82 siRNAs leading to substantial downregulation of PrP levels. I further tested acute and chronical infection of CAD5 cells with RML6 for the PrP^{Sc} screen. I generated the hyCAD cell line, which is highly susceptible to RML6 prions, tested numerous conditions for PrP^{Sc} assays and finally established a PrP^{Sc}-ELISA assay with chronically infected hyCAD cells on automated robotic screening platforms. I established hit validation by Western blotting and qRT-PCR on the LabCyte acoustic dispensing robot for 384-well plate format and tested alternative murine cell lines for hit validation. The quality of the screens was monitored by comprehensive quality control graphs, which allowed me to optimize the screen conditions and draw conclusions on the results. I could overcome temperature dependent variability in the cell viability signal apparent in the quality control of the first PrP^C screen by acclimatizing the plates to the temperature in the Envision reader.

The Net-FRET signal in the first murine PrP^C screen (Net-FRET range 54'528 - 123'602) was higher, than in the second murine PrP^C screen (Net-FRET range 8'503 - 31'168). A technical explanation could be that the labelling of POM1 or POM19 antibodies to APC and Europium was more efficient in the first screen than in the second screen, so that more labelled antibody bound PrP^C and elicited a signal. A possible biological explanation of the differences in PrP^C levels between the first and second murine screen could be that PrP is expressed in a

circadian rhythm, which is why the amount of prion protein messenger RNA can change over a relatively short period (Cagampang, Whatley et al. 1999). I harvested the cells in the morning and in the afternoon, which might have an effect on overall PrP^C expression levels as PrP^C expression underlies a circadian rhythm. My data confirmed the reported low reproducibility rates of siRNA data originating from different siRNAs targeting the same genes (Marine, Bahl et al. 2012). The first screen with r^2 = 0.424 for raw Net-FRET signal of duplicates was in a good range, the second screen with r^2 = 0.125 for raw Net-FRET signal of duplicates was comparable to published results where two different siRNA sets targeting the same genes showed a correlation coefficient R around 0.2 depending on the screens. Pooling siRNAs increased replicate correlation substantially (Ramo, Drewek et al. 2014). A genome wide siRNA screen with pooled siRNAs led to very good correlation coefficient r^2 of 0.6 (Papageorgiou, Rapley et al. 2015). It could be that the correlation between technical replicates in the second PrP^C screen was lower than in the first screen, because different libraries had been used.

I summarized the functions of al chaperone hits from the PrP^C screens in two tables (Appendix 82 + 83). Eleven of the chaperones that were downregulated by siRNAs leading to reduced PrP^C levels were parts of the 26S Proteasome. The 26S proteasome consists of a core 20S proteasome and one or two 19S regulatory particles (Glickman, Rubin et al. 1998). The 20S proteasome is a barrel-shaped structure composed of α- and β-subunits arranged in four rings (Figure 76).

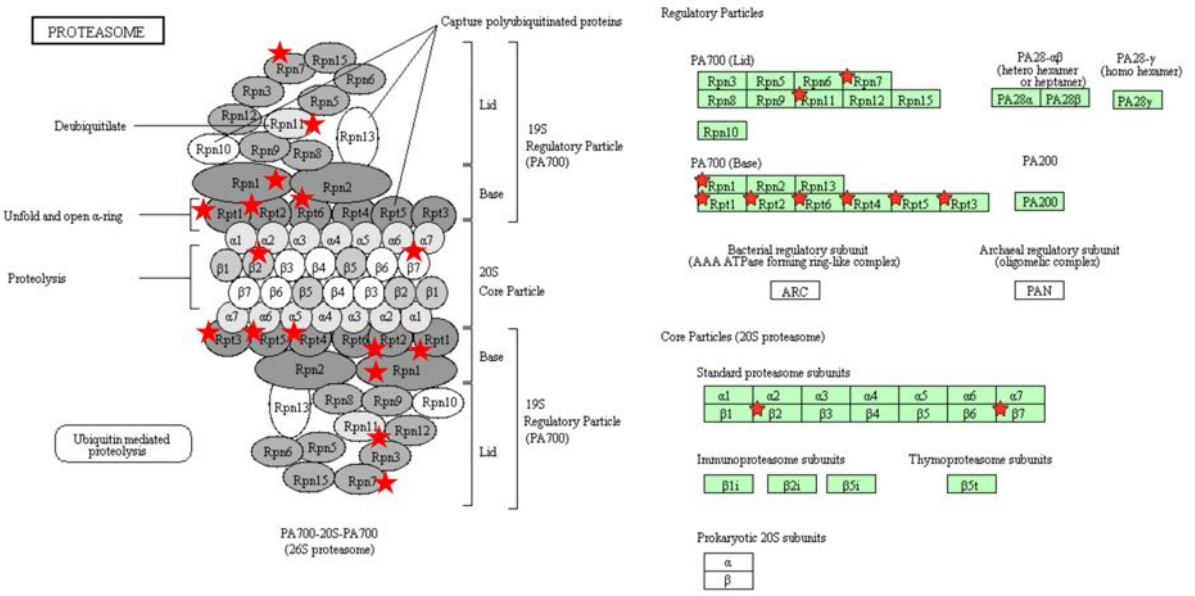

Figure 76: Structure of the 26S proteasome. Subunits that were classified as hits in the murine PrP^C screen were marked with stars. Figure was generated using the DAVID Functional Annotation Bioinformatics Microarray Analysis webtool (Huang et al. 2009)

The 19S regulatory particle consists of 19 canonical subunits which are divided into lid and base subcomplexes. The 19S subunits bind, deubiquitinate and unfold ubiquitinated proteins, and translocate them into the 20S proteasome for degradation (Liu and Jacobson 2013). The lid consists of 10 non-ATPase subunits (Rpn3, Rpn5–9, Rpn11, Rpn12, and Rpn15). Non-ATPase subunits Rpn7 and Rpn11 led to downregulation of PrP in the siRNA screen. Rpn11 deubiquitinates substrates prior to their degradation. Connection between lid and base are stabilized by Rpn10. The base contains six distinct ATPase subunits (Rpt1–6) and three non-ATPase subunits (Rpn1, Rpn2, Rpn13). Rpt1–6 and Rpn1 led to reduced PrP^C levels the siRNA screen (Figure 76). The six ATPase (Rpt1–6) subunits form the molecular motor for the proteasome (Lander, Estrin et al. 2012, Zhu, Hayat Khan et al. 2014). When 19S ATPase binds a nucleotide, HbYX motifs dock into the pockets of α-subunits of 20S, functioning as a 'key in a lock' to open the gate of the 20S proteasome (Figure 77) (Kim and Smith 2014). Rpn10 and Rpn13 are ubiquitin (Ub) receptors and can recognize polyubiquitinated substrates (Zhu, Hayat Khan et al. 2014).

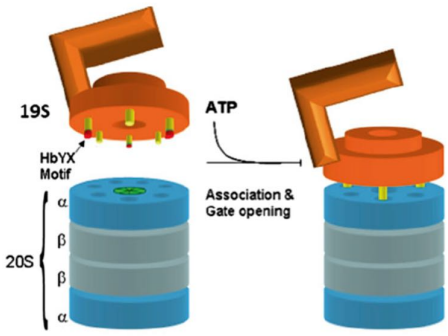

Figure 77: Mechanism of gate opening of 20S proteasome. When 19S ATPase binds a nucleotide, HbYX motifs dock into the pockets of α-subunits of 20S, functioning as a 'key in a lock'. Reprinted from (Kim and Smith 2014). License number 4376910427517.

The 26S proteasome is involved in the ubiquitin proteasome system (UPS) and acts in cellular quality control by degrading misfolded, unassembled, or damaged proteins potentially prone to aggregation (Hershko and Ciechanover 1998). Degradation of proteins via the UPS pathway involves two steps: conjugation of ubiquitin to a protein and degradation of the tagged protein by the 26S proteasome (Ciechanover, Orian et al. 2000). Accumulation of ubiquitin conjugates are found in the terminal stage of prion disease. Ubiquitination is a late event in prion disease and occurs after the formation of protease-resistant PrP^{Sc} (Kang, Brown et al. 2004). However, the results from the siRNA screen indicate that the 26S proteasome is already involved in the functioning of PrP^{C}.

The three chaperones Calnexin, Calreticulin and *Hspa5*, which are associated to the endoplasmatic reticulum (ER), reduced PrP^{C} levels in the siRNA screen. Calreticulin and Calnexin are members of a family of ER chaperones that fold newly synthesized polypeptides. They assist in the folding and subunit assembly of the majority of Asn-linked glycoproteins that pass through the endoplasmic reticulum (Leach 2000-2013). Human PrP is glycosylated at Asn181 and Asn197 on helices 2 and 3 and murine PrP has glycosylation sites as Asn180 and Asn196 (Haraguchi, Fisher et al. 1989). Thus, *Canx* and *Calr* might be involved in the proper folding of PrP. The ER chaperone *Hspa5* facilitates folding and assembly of nascent polypeptides, prevents their misfolding and aggregation, targets misfolded proteins for proteasome degradation, and controls the unfolded protein response (UPR). *Hspa5* regulates the UPR by reducing ER stress levels and apoptosis due to an enhancement of the cellular folding capacity. *Hspa5* and PrP interact in the cellular context. Prion replication in cell culture was shown to be related to the levels of expression of *Hspa5*. However, a reduction in the expression of this molecular chaperone accelerates prion pathogenesis in vivo (Park, Eun Kim et al. 2017). I could

show reduction of PrP^C and PrP^{Sc} in cell culture with four different cell lines upon reduction of *Hspa5* by RNAi (Figure 59 a+b), indicating that *Hspa5* might contribute to both, prion protein biosynthesis and prion replication.

Fkbp8 reduced PrP^C levels in the siRNA screen. *Fkbp8* encodes a Peptidyl prolyl cis/trans isomerase (PPIase), expressed in the cytosol, ER and mitochondria (Gaudet, Michel et al. 2017). PPIases assist the folding and restructuring of proteins (Schiene-Fischer 2015). *FKbp8* is activated by binding Calmodulin and calcium and seems to act as a chaperone for anti-apoptotic Bcl-2. Recombinantly expressed prion protein has been shown to be a target of anti-apoptotic Bcl-2 (Kurschner and Morgan 1995). In addition, BCL-2 binds and co-aggregates with misfolded PrP in the cytosol, but not in other cellular compartments of human neuronal SH-SY5Y cells (Rambold, Miesbauer et al. 2006). Overexpression of Bcl-2 in GT1 cells is neuroprotective and prevents apoptosis induced by amyloidogenic peptide PrP106-126 (Ferreiro, Eufrasio et al. 2007). The exact mechanism by which Bcl-2 counters apoptosis in cells with cytotoxic PrP is not fully understood, but binding to *Fkbp8* might play a role.

Hspb8 reduced PrP^C levels in the siRNA screen. *Hspb8* encodes heat shock protein 22 (Hsp22), a small heat shock protein (HSP20 family) localized in the cytosol, which translocates to nuclear foci during heat shock and shows temperature-dependent chaperone activity (Uhlen, Fagerberg et al. 2015, Pundir, Martin et al. 2017). *HSPB8* forms a stable complex with the *HSPA8* co-chaperone Bcl-2 associated anti-apoptotic BAG3 (Carra, Sivilotti et al. 2005). *Hspb8* plays a role in various neurodegenerative diseases such as AD, PD and Huntington (Vicario, Skaper et al. 2014). Mutations in *Hspb8* are related to Charcot-Marie-Tooth disease type 2 and distal hereditary motor neuropathy and myopathy (Nakhro, Park et al. 2013, Bouhy, Juneja et al. 2018). Overexpression of *HSPB8* in immortalized motoneuronal cell line NSC34 significantly decreased the accumulation of dipeptide repeat proteins (DPRs), which are the product of expansion of a repeated G4C2 hexanucleotide sequence present in the *C9ORF72* gene linked to in ALS and Frontotemporal Dementia (FTD). *HSPB8* overexpression might be an approach to decrease DPR-mediated toxicity and maintain motoneuron viability in ALS and FTD (Cristofani, Crippa et al. 2018). Misfolded and aggregate-prone TDP-43 species are targeted to autophagic degradation if they are bound to the *HSPB8–BAG3–HSP70* complex (Crippa et al. 2010a; Crippa et al. 2010b). *Hspb8* may be as well involved in the neuroprotective response of Prion disease.

Sgta reduced PrP^C levels in the siRNA screen. *Sgta* encodes a co-chaperone that binds newly synthesized and misfolded proteins as well as proteins containing hydrophobic patches in the cytosol and targets them to the ER (Pundir, Martin et al. 2017). *Sgta* has been shown

to reverse *BAG6*-dependent ubiquitination of mislocalized protein. *Bag6* and *Sgta* monitor certain newly synthesized proteins during protein maturation and quality control (Leznicki and High 2012).

Hspa4 reduced PrP^C levels in the siRNA screen. *Hspa4* encodes heat shock protein family A (Hsp70) member 4 expressed in the nucleoplasm and the cytosol (Uhlen, Fagerberg et al. 2015). It is involved in ATP binding, chaperone-mediated protein complex assembly, and protein import into the mitochondrial outer membrane (Pundir, Martin et al. 2017).

Hsf1 and *Chordc1* did lead to upregulation of PrP^C in the siRNA screen. *Chordc1* is proposed to act as co-chaperone for *HSP90* and involved in stress response (Pundir, Martin et al. 2017). The transcriptional regulator of the stress response *Hsf1* is known to be involved in prion disease. When *HSF1* knockout (KO) mice were inoculated with Rocky Mountain Laboratory (RML) prions they showed a dramatically shortened lifespan, succumbing to disease approximately 20% faster than controls (Steele, Hutter et al. 2008). I compared *Hsf1* and *Chordc1* to RNASeq data from C57BL76J mice inoculated with RML6 and non-infectious brain homogenate (NBH). mRNA levels were assessed at different timepoints. After 12 weeks post inoculation both *Hsf1* and *Chordc1* showed decreasing mRNA levels in cerebellum and hippocampus (Figure 78). Thus, I hypothesized that these genes might be involved in prion disease.

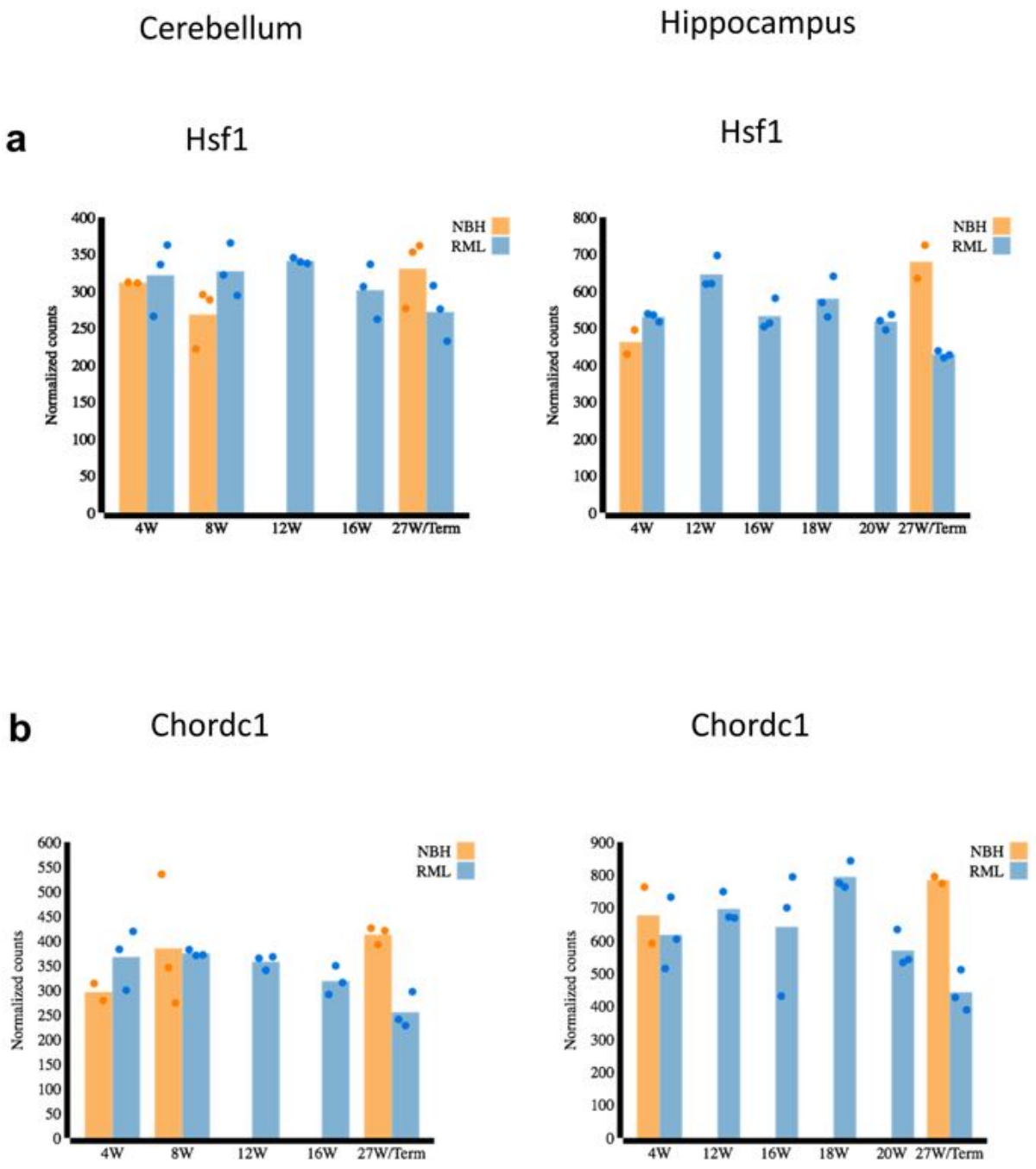

Figure 78: Hsf1 and Chordc1 showed decreasing mRNA levels in cerebellum and hippocampus in C57BL76J mice inoculated with RML6 after 12 weeks post inoculation. The images were generated with the Neurinox Bioinformatics Platform.

7.1.2 Murine PrP^{Sc} screen

I started to establish the murine PrP^{Sc} screen with a FRET assay and CAD5 cells. Because FRET was not sensitive enough to detect differences between uninfected and RML6 infected

CAD5 (Figure 33), I established PrP^{Sc}-ELISA, that is sensitive enough to distinguish RML6 brain homogenate at a 10^{-5} dilution from the blank (Figure 34). This dilution corresponded to the lowest RML6 dose injected into mice in *in vivo* assays. Acute infection of CAD5 cells with RML6 and CAD5 *Prnp*-/- resulted - even with very low inoculum concentrations - in high amounts of residual inoculum in CAD5 *Prnp*-/- cells, masking potential prion replication in CAD5 wild type cells (Figure 35). Thus, I proceeded in establishment of the PrP^{Sc} screen with chronical infection of cells, where residual inoculum was removed by four consecutive splitting steps (Figure 36). Western blots with chronically infected scCAD cells digested with PK showed reduced levels of PrP^{Sc} when inoculated with lower RML6 concentrations and with higher passages (Figure 31). It is generally difficult to keep immortalized continuously growing cells infected with prions. Loss of infectivity over time could be the result of prion replication that is slower than cell division (Aguzzi, Lakkaraju et al. 2018). In mice, the level of PrP^{C} expression correlates with the rate of PrP^{Sc} formation (Aguzzi and Calella 2009). Overexpression of PrP in N2A cells with subsequent chronical infection showed higher and more stable production of PrP^{Sc} that seen in scrapie-infected N2A cells (ScN2A) (Nishida, Harris et al. 2000). I could confirm this finding by chronical infection of PrP overexpressing hyCAD cells with RML6 prions, which showed more PrP^{Sc} than chronically infected CAD5 cells in PrP^{Sc} -ELISA and Western blots upon PK digestion (Figure 38). However, another N2A clone overexpressing PrP N2a/2M11 was shown to be resistant to RML prions, whereas a N2a/Bos2 clone transformed with the control plasmid, expressing PrP at about the same low level as the original N2A cells was most susceptible to prion infection (Enari, Flechsig et al. 2001). These results confirm that single clones derived from the same cell line vary in their susceptibility to prions. The PrP^{Sc} test screen with PrP^{Sc} -ELISA showed distinct separation between the control groups and a good SSMD value (Figure 51). However, the readout in the PrP^{Sc} -ELISA screen had been complicated through oversaturated absorbance due to a new batch of Streptavidin (Figure 53). The cell viability quality control showed six siRNAs, which led to starkly reduced cell viability (Figure 52 c). I compiled an overview of the functions of the genes (*Aip, Os9, Dnajb6, Nsfl1c, Dnajb11*) targeted by these siRNAs (Appendix 84). *Os9* is involved in the quality control of ER related degradation, which might play a role in prion disease. *Dnajb11* serves as a co-chaperone for *Hspa5* (Pundir et al. 2017). When *Hspa5* levels were reduced by RNAi in the first murine PrP^{C} screen, PrP^{C} levels were decreased too. The reduced cell viability may be caused by synthetic lethality but caution should be exercised to assess false positives caused by off-target effects. The established hit validation by Western blotting and qRT-PCR on the LabCyte acoustic dispensing robot for 384-well plate format provided proof-of-concept with

five genes how hit validation could be performed in a larger scale. Three of five genes led to downregulation of PrP^C with siRNAs differing in the sequence from the ones used in the PrP^C screen. Knockdown of two genes (*Calr, Psmc5*), which reduced PrP^C levels in the first murine PrP^C screen did not show the same effect in qRT-PCR and Western blots. This could be due to the different loci that were targeted by the siRNAs used in hit validation. In the majority of the genes that led to downregulation of PrP^C not all four siRNAs targeting this gene led to downregulation of PrP^C in the RNAi screens. When I tested alternative murine cell lines for hit validation, I could acutely and chronically infect N2A PK1 cells with RML6 prions (Figure 60). However, the signal in PrP^{Sc}-ELISA was very low and the transfection efficiency of *Prnp* targeting siRNA was low (Figure 61). The murine myoblastoma cell line CH3H/10T1/2 of which I had generated *Prnp*-/- clones by CRISPR-Cas9 seemed not to be susceptible to RML6 and thus not suitable for hit validation (Figure 62). Due to time reasons I had skipped the double knockdown and triple knockdown screens to assess compensation of functional failure by one or two co-chaperones.

7.2 Chaperone siRNA screens in human cells

I had murinized the human SH-SY5Y neuroblastoma cell line to perform a human PrP^{Sc} screen with murine prions without elevated biosafety risk that would arise when working with human prions. I generated this heterologous human cell culture model for prion propagation by knockout of *PRNP* by CRISPR-Cas9 and overexpression of murine *Prnp* in a *PRNP* knockout clone. Due to very low endogenous PrP^C levels of SH-SY5Y wild type cells, which was as well reported in literature, conventional western blotting was not sensitive enough to detect a difference between SH-SY5Y wild type and *PRNP*-/- clones (Rambold, Miesbauer et al. 2006). Thus, I had to perform immunoprecipitation with very high amounts of total protein (2000 μg) and sandwich ELISA to confirm *PRNP* knockout in SH-SY5Y (Figures 63 and 64). To assess strain specific susceptibility to murine prions, I acutely infected a pool of seven murinized clones (mSY5Y), as well as single clone #M4 with eight different prion strains and according non-infectious brain homogenate and performed Western blotting upon PK digestion (Figure 67). SH-SY5Y *PRNP*-/- cells served as negative control. PK-Western blots showed that acute infection with 79A, mNS and ME7 strains resulted in prion replication. When I chronically infected the mSY5Y pool and #M4 with these three strains and RML6, no prion replication was evident (Figures 68 and 71). To detect potential PK-sensitive PrP aggregates I performed gradient centrifugation with #M4 clone chronically infected with RML6 prions and treated with non-infectious brain homogenate as controls (Figure 69). The brain homogenate controls

showed the expected aggregation pattern after gradient centrifugation. The uninfected #M4 control showed PK sensitive aggregates in the highest density fraction. A possible explanation is overexpression of PrP in this clone, which favors aggregation due to higher local PrP^{C} concentrations. Confocal microscopy images upon immunostaining of PrP in the #M4 clone showed PrP expression at the membrane (Figure 70). Thus, I could exclude trapping of PrP in the endoplasmatic reticulum, which impairs PrP^{C} maturation and prevents PrP^{Sc} accumulation (Cardinale, 2005). It is known, that not all cells are infected by chronical infection. The first data obtained by dilution and subcloning of infected N2A cells revealed that only 1% of the cells were actually infected (Race 1991). This could be due to inhomogeneously infected cultures and might be a reason why mSY5Y and #M4 did not show prion replication upon chronical infection with prion strains, that showed prion replication upon acute infection. Maybe SDS-PAGE analysis of cell lysates treated with proteinase K, followed by PK-Western blot analysis was not sensitive enough to detect a small number of infected cells. In fact, Bosque et al. have shown that Western blotting could detect PrP^{Sc} when 10% of the cells were infected with prions, whereas cell blotting was positive with only 1% of the cells infected (Bosque and Prusiner 2000). Maybe prions replicated to some degree, but at such low levels, that again a more sensitive detection method would have been advantageous. Possibly, prion replication was not as fast as cell division and thus infectivity was lost during the splitting steps of chronical infection (Aguzzi, Lakkaraju et al. 2018). Hence it could be, that PrP^{Sc} was lost during chronical infection as I had observed in the chronically scCAD cells, but much faster. Another hypothesis why chronical infection did not show prion replication with strains that previously showed replication in acute infection is that prion replication entailed a disadvantage in fitness, which led to some prion resistant cells that overgrew the system (Aguzzi, Lakkaraju et al. 2018). Sequencing of #M4 did not show any difference from the wild type sequence, which could have caused misfolding and aggregation. However, sequencing revealed a Methionine at murine amino acid polymorphism at PrP codon 128. Maybe the polymorphism of the *Prnp* sequence encoded by SH-SY5Y was not compatible with the murine strains. In a different approach to generate murinized human cells, I stably transfected the human glioblastoma cell line U-251MG with a pcDNA3 plasmid encoding the open reading frame of murine *Prnp*. I acutely infected mixed clones of U-251MG overexpressing murine PrP and untransfected cells as negative control with murine RML6 prions (Figure 72). U-251MG did neither replicate RML6 prions, nor human prions. Various factors might influence the susceptibility of a cell line to different prion strains: the level and the type of PrP molecules expressed in cells, different co-factors necessary for the replication of the agent such as chaperones, specific RNA species, a particular lipid envi-

ronment, or a particular prion replicating subcellular environment (Aguzzi, Heikenwalder et al. 2007). In addition, general trafficking of PrP in the different lines can play a role in susceptibility. The endogenous cleavage and degradation pathways of PrP may also be involved. Finally, post-translational modifications of PrP (e.g. glycosylation) could modulate the conversion (Solassol, Crozet et al. 2003, Aguzzi, Heikenwalder et al. 2007, Aguzzi and Calella 2009). The screen would have only been feasible with chronically infected cells, because residual inoculum in SH-SY5Y cells acutely infected with 79A, mNS and ME7 prions masked potential PrP^{Sc} replication.

7.3 Comparison murine and human siRNA screens

I compared the rank numbers of the first murine PrP^{C} screen and the human PrP^{C} screen and contrasted them to the chaperones obtained in the first murine PrP^{C} screen based on the best gaussian processed normalized sample signal versus non-target comparison at a threshold p = 0.001. With a stringent selection (maximally 15 ranks difference between murine and human PrP^{C} screens) six genes showed downregulation of PrP. With a less stringent selection (maximally 30 ranks difference between murine and human PrP^{C} screens) eleven genes showed downregulation of PrP^{C}. The two chaperones *Hsf1* and *Chordc1*, which led to upregulation of PrP^{C} differed in more than 30 ranks between the murine and human PrP^{C} screens and did thus not correlate. The genes that differ in their impact on PrP modulation might be specific for mice and humans. Differences in the ranking can be explained by the different cell types that were used. For the murine PrP^{C} screen I used CAD5 cells, which are prion-susceptible cells, derived from neuronal Cath.a-differentiated (CAD) cells (Qi, Wang et al. 1997). The human cell line U-251MG was used for the human PrP^{C} screen (Bigner, Bigner et al. 1981). CAD5 cells are neuroblastoma cells, whereas U-251MG are glioblastoma cells. The two cell lines differ in the degree of ploidy. Human U-251MG are diploid, CAD5 are polyploid. Thus, the cells might differ in their gene expression pattern. The overall PrP signal could vary between the murine and human PrP^{C} screens due to different amounts of PrP expressed by the cells, time of harvesting the cells because PrP expression is circadian or efficiency of APC and EU coupling. Technically, the screens were performed slightly different. The murine screen was performed with single siRNAs targeting the same gene in different wells, which bears the advantage of directly knowing which locus leads to downregulation of *Prnp*. The human PrP^{C} screen was performed with three pooled siRNAs, which results in better replicate correlation and saves time and resources, which is advantageous in a whole genome screen (Ramo, Drewek et al. 2014). The ranking of the Net-FRET signal was as

well not the same in the murine and human PrP^C screens. The murine genes were ranked according to the descending Net-FRET signal of the mean of four siRNAs targeting the same gene. The human genes were ranked according to the descending mean Net-FRET signal of the technical duplicates targeted by the same pool of siRNAs against the same gene.

8 Outlook

8.1 Chaperone siRNA screens in murine cells

It would be interesting to perform double knockdown and triple knockdown screens to assess compensation of functional failure by one or two co-chaperones. For the PrP^{Sc} screen I plan to assess different ELISA substrates to bring the absorbance signal in a sufficiently high, but not oversaturated range. For proper assessment of PrP levels by Western blots upon transfection of cells with chaperone targeting siRNAs, at least three biological and technical replicates should be used. For a proof-of-concept, I had only used one replica per siRNA treatment. The effect of chaperones on PrP levels could be assessed as well by RNA-seq upon transfection of CAD5 cells with chaperone targeting siRNAs. RNA-seq data could then be confirmed by qRT-PCR, that I had established on the acoustic dispenser for 384-well format. RNA-seq is one method to test off-target effects but other deregulated genes could be indirectly affected by the siRNAs targeting the chaperone transcripts. If two additional siRNAs differing in the sequence from the ones used in the screen lead to the same modulation of PrP as observed in the RNAi screen, off-target effects can be excluded. Another method to confirm specificity and rule out off-target effects is using CRISPR-Cas9. Further it would be worth to investigate if the specific chaperones alter the levels of PrP^{C} alone or if they also alter the levels of other proteins that are associated with neurodegeneration, more specifically: Aβ and other amyloid inducing proteins. It would be highly interesting to overexpress chaperones downregulating PrP levels in cells and assess PrP^{Sc} levels later on. N2A PK1 which I had tested as an alternative cell line for hit validation showed reduced cell viability upon infection with RML6 prions. Toxicity of the crude brain homogenate could be reduced by pre-treating infectious brain homogenate for 30 min at 80°C followed by sonication. This method had been shown to reduce the toxicity of infectious brain homogenate on cell cultures (Solassol, Crozet et al. 2003). To increase the PrP^{Sc} signal in infected N2A cells, hit validation could be performed with a PrP overexpressing N2A cell line such as N2a#58 which showed stable and high PrP^{Sc} levels (Nishida, Harris et al. 2000). Non-carcinogenic cells such as primary neurons or neurons derived from induced pluripotent stem cells (iPSCs) would provide a more physiological system for hit validation than cancer cell lines.

8.2 Chaperone siRNA screens in human cells

Since only acute infection of murinized human SH-SY5Y cell lines was successful, a scrapie screen with these cells would not be feasible because residual inoculum in acute infection

masked potential PrP^{Sc} replication. In order to generate a murinized human cell line, either subcloning of already infected cells with selection of prion susceptible clones would be an option. Performing more sensitive PrP^{Sc} assays than Western blotting upon PK digestion would be another option. Another possibility could be to increase the time between passages during chronical infection to allow slow prion replication. Starting with a new cell line would bear the advantage to select a naturally high PrP expressing cell and match human amino acid polymorphism 129 and murine polymorphism 128 sites in advance with selected prion strains. Once a suitable cell line is generated, the PrP^{C} FRET and PrP^{Sc} ELISA screens could be performed with the genome wide siRNA library, that had already been used for the human PrP^{C} screen with U-251MG cells.

8.3 Comparison murine and human siRNA screens

Once established, it will be highly interesting to compare as well murine and human PrP^{Sc} screens. The comparison would be more meaningful if the screens would be performed in the same way, performing both murine and human screens with a neuroblastoma cell line and with a pooled siRNA library. It would be informative to screen different cell lines in both, murine and human screens and compare these to each other and gain knowledge about the actors of the prion protein replication machinery.

9 Material & Methods

9.1 Chemicals

All chemicals were purchased from Sigma-Aldrich unless stated otherwise. All DNA oligonucleotides were synthesized by Microsynth. The protein concentration was determined using the Pierce BCA Protein Assay Kit (ThermoFisher).

9.2 Cell lines

All cells were grown in T150 flasks, maintained in a cell incubator at 37°C in 95% humidity and 5% CO2 and routinely split 1:3 every 3-4 days.

SH-SY5Y: Originally derived from a metastatic bone tumor biopsy, SH-SY5Y (ATCC® CRL-2266™) cells are a subline of the parental line SK-N-SH (ATCC® HTB-11™). SK-N-SH were subcloned three times; first to SH-SY, then to SH-SY5, and finally to SH-SY5Y. SH-SY5Y were deposited to the ATCC® in 1970 by June L. Biedler (Biedler, Helson et al. 1973) (Biedler, Helson et al. 1973, Biedler, Roffler-Tarlov et al. 1978, Kovalevich and Langford 2013). SH-SY5Y neuroblastoma cell line was cultured in 50% MEM, 50% F-12 supplemented with 10% heat-inactivated fetal bovine serum (FBS) (ThermoFisher), 0.5% Glutamax, and 1% penicillin-streptomycin (all Gibco).

C3H/10T1/2 is a clonal myogenic cell line established and characterized by Reznikoff et al. (Reznikoff, Brankow et al. 1973). The tissue of origin is unknown because the cell line was derived from C3H whole mouse embryos (Pinney and Emerson 1989). C3H/10T1/2 were cultured at 37°C in DMEM with the addition of 10% FBS (ThermoFisher), 1% Glutamax, and 1% penicillin-streptomycin (all Gibco). The cells were a kind gift from the Laboratory of Translational Nutrition Biology, Institute of Food, Nutrition and Health, ETH Zurich.

The mouse cell line **CAD-2A2D5** (CAD5) was derived from Cath.a-differentiated cells and is highly prion-susceptible (Qi, Wang et al. 1997, Mahal, Baker et al. 2007). The mouse cell line **N2aPK1** is a highly prion susceptible subclone from N2aPD88. N2aPD88 is a less prion susceptible clone from N2a cells challenged with a 10^{-6} dilution of RML strain (Klohn, Stoltze et al. 2003). CAD5 and N2aPK1 cells were cultured at 37°C in Opti-MEM with the addition of 10% FBS (ThermoFisher), 1% Glutamax, and 1% penicillin-streptomycin (OFBS medium, all Gibco). The human embryonic kidney cell line **HEK293** was purchased by ATCC. The HEK293 *PRNP*-/- clone #F2 was generously provided by Mario Hermann.

The human glioblastoma cell line **U-251MG** was isolated from an astrocytoma tumor by explant technique and obtained from ATCC (Bigner, Bigner et al. 1981). The cells were cultivated in

Opti-MEM with the addition of 10% FBS (ThermoFisher), 1% Glutamax, and 1% penicillin-streptomycin, and 1% Non-Essential Amino Acids (all Gibco).

9.3 Generation of stable cell lines

The coding sequence of murine *Prnp* was amplified by PCR. Restriction sites for subsequent cloning into pcDNA3 (Addgene) were attached. The random sequence of 8 bp at the 5' end of the primer was attached to ensure efficient DNA cleavage by the restriction enzyme.

```
5′ AGG TAC CA TCTAGA GGATCC AGGCGACGTGGAAGAAAA 3′
Random        XbaI    BamHI   Primer

5′ AAG TCC TA CCATGG GAATTC TTGTAATCCAGAGGTTGATTATCG 3′
Random        NcoI    EcoRI   Primer
```

The PCR product was cloned into pcDNA3 (Addgene) at the BamHI and EcoRI restriction sites (pcDNA3-*Prnp*). Cells were stably transfected with pcDNA3-*Prnp* and Lipofectamine 2000 (ThermoFisher). Cellular clones were obtained by limited dilution and selection with G418 (Gibco).

9.4 siRNA libraries and control siRNAs

For the murine chaperone screens an arrayed murine siRNA library consisting of 376 siRNAs targeting 99 druggable chaperone transcripts was provided by the Novartis Institute for Biomedical Research. Each transcript was targeted by two up to five siRNAs. A second murine siRNA library containing 560 siRNAs targeting 140 non-druggable chaperone transcripts was purchased from ThermoFisher. Each transcript was targeted four siRNAs. The sequence of the control *Prnp*-siRNA (from ThermoFisher, siRNA ID # s72188) was: 5 '-CGUGAAAACAUGUACCGCUtt-3' The scrambled non-target siRNA (silencer select Negative Control No. 1 siRNA, catalog number 4390844) was purchased from ThermoFisher as well.
For the genome wide human PrP^C screen an arrayed silencer select siRNA library purchased from ThermoFisher was used. The library consisted of 64'752 siRNAs targeting 21'584 transcripts. Each transcript was targeted by three siRNAs. siRNAs targeting the same transcript were pooled from 186 source plates to 62 low density volume plates (1536-well plates). Three pooled *Prnp*-siRNAs and the same scrambled non-target siRNAs were used as controls (from ThermoFisher, siRNA ID # s11214, s11213, s11212). The siRNA samples were delivered

in Echo Qualified 384-Well Polypropylene Source Microplates (384PP) that were specifically used for siRNA printing on the LabCyte Echo acoustic liquid handling platform. siRNA samples were dispensed using the ”Cherry Pick” software, with sample picking lists and the “Tempo” scheduling software. siRNA controls were dispensed using the ”Plate Reformat” software and the ”Tempo” scheduling software.

9.5 Cell seeding and siRNA transfection

For the murine screens CAD5, CAD5 *Prnp*-/-, HyCAD or scHyCAD cells were harvested when TPP Tissue Culture (T150) flasks (Sigma) were 70% confluent. A cell suspension with 2800 cells/15 μl Opti-MEM reduced-serum medium (no phenol red, Gibco) plus 10% FBS (HyClone) was prepared. 15 μl of the cell suspension were dispensed into each well of 384-well tissue culture treated sterile ViewPlate microplates with white well walls and a clear bottom (Perkin Elmer). For forward transfection siRNAs and Lipofectamine® RNAiMAX Reagent (ThermoFisher) in Opti-MEM (Gibco) (final dilution 3x10-3) were added to intermediate plates. Plates with the transfection mix were centrifuged at 1300rpm for 1min and incubated for 20 minutes at room temperature. 5ul of transfection mix was dispensed into each well with the Janus robotic platform (Perkin Elmer) using the “Winprep” software. Plates were centrifuged at 750 rpm x 1 min and incubated at 37°C and 5% CO2. For reverse transfection the plates with printed siRNAs were frozen at -40°C. At the assay day the plates were thawed and Lipofectamine and 2800 CAD5 cells per well were added and incubated at 37°C and 5% CO2. The final siRNA concentration was 30nM.

For the human PrP^C screen U-251MG cells were harvested when TPP Tissue Culture (T150) flasks (Sigma) were 70% confluent. A cell suspension with 6000 cells/25 μl Opti-MEM reduced-serum medium (no phenol red, Gibco) plus 10% FBS (HyClone) was prepared. 25 μl of the cell suspension were dispensed into each well of white opaque 384-well OptiPlates (Perkin Elmer). siRNAs from three pooled source plates were printed into eight destination plates. Control siRNAs were dispensed from a separate plate. The total screen comprised 166 384-well plates. The plates containing the siRNAs were frozen. At the assay day they were thawed and Lipofectamine and U-251MG cells were added. The final siRNA concentration was 5nM.

9.6 Cell viability assay

In the murine screens 20 μl of Realtime-Glo (RT-Glo, Promega) in OFBS medium (1: 4000 dilution) were dispensed into each well 24 hrs after transfection. Plates were incubated at 37°C and 5% CO2 . 48 hours after adding RT-Glo, the plates were taken out from the incubator and

the RT-Glo luminescence was measured by the Envision Multilabel Reader (Perkin Elmer) at room temperature and 37°C. In the human screen the cell viability marker RT-Glo was added after 70 hrs of incubation (1:4 dilution). After 72 hrs the RT-Glo luminescence was measured with the Envision reader at 37°C. The RT-GloTM cell viability assay is a bioluminescent method, measuring the reducing potential of cells and thus their metabolism to identify the number of viable cells in culture. NanoLuc® luciferase and a cell-permeant pro-substrate are added to cells in culture. Viable cells reduce the pro-substrate, which leads to the generation of the substrate for NanoLuc luciferase. This substrate diffuses from the cells into the surrounding culture medium, where it is cleaved by the NanoLuc enzyme to produce a luminescent signal. The signal correlates with the number of viable cells.

9.7 PrP^C-HP-FRET assay

Immediately after reading the RT-Glo signal, PrP^C-HP-FRET was performed. The cell culture medium was aspirated with the Mircroplate ELx405 Washer (BioTek). Aspiration stopped 1mm above the well bottom, in order to avoid aspiration of cells. In the murine screen the cells were subsequently lysed by adding 50 μl/well of 1x standard lysis buffer (50 mM Tris-HCl pH 8, 150 mM NaCl, 0.5% Na deoxycholate, and 0.5% Triton X-100, stored at room temperature). The plate was shaken at 4°C for 20 min at 700 rpm. The FRET pair comprising the Europium donor (Eu-W1024 ITC chelate, AD0096, PerkinElmer) and the allophycocyanin acceptor (APC, AnaTagTM APC labeling kit from AnaSpec) fluorophores, was coupled to POM1 and POM19 anti-PrP antibodies (Polymenidou, Moos et al. 2008). POM1 binds alpha helix 1 of PrP, POM19 recognizes alpha helix 3 of PrP, respectively. The FRET antibody stock Eu-POM19 and APC-POM1 was diluted with 1x Lance buffer (LANCE® Detection Buffer for FRET,10x stock, diluted with dH2O for use) to 25 nM (concentration of POM19 antibody) and 50 nM (concentration of POM1 antibody). 5 μl/well of 25 nM Eu-POM19 and 5 μl/well of 50nM APC-POM1 were added separately to the lysed cells. The plates were shaken at 37°C for 1 h at 700 rpm and incubated over night at 4°C. The plate's clear bottom was sealed with white BackSeal-384 (Perkin Elmer) for the top read of time-resolved FRET. In the human screen, 10 μl of 1x standard lysis buffer were added per well for 2hrs at 4°C after aspiration of the cell culture medium. Europium-POM2 (final conc. 2.5nM) recognizing the octapeptides of PrP and APC-POM1 (final conc. 5nM) were added and FRET was measured after 4hrs incubation at 4°C. The donor Europium is excited at wavelength 340 nm and transfers energy to the acceptor APC if the distance between the FRET antibody pair measures less than 10 nm. APC then emits light at wavelength 665 nm. The FRET signal of PrP^C in each well was detected by the time-resolved EnVision Multilabel

Reader (Perkin Elmer).

9.8 Preparation of FRET antibody pairs

The monoclonal full-length POM1 as well as POM19 and POM2 antibodies were labelled in house with Allophycocyanin (APC, AnaTagTM Labeling Kit 72111, Anaspec) and Europium chelate (Eu-W1024 ITC chelate, AD0096, PerkinElmer) for HP-FRET assays. Europium chelate served as donor fluorophore. Aromatic isothiocyanate groups of the Europium chelate react with lysine residues and free N termini of POM19 and POM2 at alkaline pH. To remove compounds that could interfere with labelling (sulfhydryl groups, sodium azide, primary amines), POM19 and POM2 were diluted in 1ml 100mM sodium carbonate (Na_2CO_3), pH 9.16, loaded with a 24G syringe into dialysis cassettes with a cut-off of 10-20 kDa (Slide-A- Lyzer®, ThermoFisher), that were pre-incubated in H_2O for 2 min, and dialyzed. Dialysis was done under stirring in 5 L of 100 mM Na_2CO_3 at 4°C. The dialysis buffer was changed twice after 4-6 h of incubation and then incubated overnight. POM19 was concentrated by Amicon® Ultra 2mL centrifugal filters (Sigma) and the IgG concentration was adjusted upon measuring the protein concentration with NanoDrop Microvolume Spectrometrer (ThermoFisher) to a concentration of 5.2 mg/ml. Lyophilized Eu-W1024 ITC chelate (0.1 mg) was stored at - 20°C and immediately before use reconstituted in 20 μl distilled water which resulted in a concentration of 7 mM. A molar excess of 24x of Europium chelate over IgG was added into the POM19 solution on ice and incubated in 100 mM Na_2CO_3 overnight at 4°C shaking with 400 rpm. Purification of the labelled protein from non-reacted chelate was performed by size exclusion chromatography (Superdex 200 column, GE Healthcare). Elution from column was done with 50 mM Tris-HCl pH 7.8 + 0.9% sodium chloride. Sample fractions of 500 μl were collected. The superdex column was decontaminated with 10 mM phthalate buffer pH 4.1 containing 0.01% DTPA. Proteins in fractions were separated in a 12% Bis-Tris polyacrylamide gel (NuPAGE; Invitrogen) and stained with Coomassie blue (BioRad). Fractions with protein were pooled and concentrated with Amicon® Ultra 2mL centrifugal filters (Sigma). Labelling ratio and concentration of labelled proteins were assessed by an Eu standard solution (Perkin Elmer) and Nano drop measurement, respectively. Aliquots of antibodies were stored in liquid nitrogen. Allophycocyanin (APC, AnaTagTM Labeling Kit 72111, Anaspec) was coupled to POM1 antibody as acceptor fluorophore. Conjugation is established by a covalent bond between maleimide groups of APC and sulfhydryl groups on POM1. POM1 antibody (1.4 mg/mL) was concentrated with Amicon® Ultra 2mL centrifugal filters (Sigma), that were pre-washed with H_2O, in a Heraeus Multifuge 3SR Plus (DJB labcare) at 4000 x g in swinging buckets for 10 min at 4°C.

150 μl of POM1 were reduced with 20 μl dithiothreithol (DTT) per mL of IgG solution for 30 min without agitation at RT. Reduced POM1 was desalted on a desalting gravity column (APC, AnaTagTM Labeling Kit 72111, Anaspec). Fractions of 500 μl were collected and protein concentration was measured by NanoDrop Microvolume Spectrometrer (ThermoFisher). Fractions containing IgG were pooled and again concentrated with with Amicon® Ultra 2mL centrifugal filters. 1.33 mg POM1 were conjugated with 2 mg APC at RT for 1h with agitation, protected from light with aluminium foil. Excess of free thiols was blocked with DMSO and NEM for 30 min at room temperature. Aliquots of antibodies were stored at 4°C and protected from light.

9.9 FRET calculation

The distance-dependent energy transfer between the Eu- and APC-conjugated antibodies in the presence of PrP results in the FRET signal intensity. The net FRET signal is calculated from the raw FRET data. Net FRET signals are the number of APC counts depending on FRET events and calculated by using the following equation (eq.1).

$$\text{Net FRETsignal} = (\text{sample} - APC_{only})_{APC} - P \cdot (\text{sample} - \text{detection buffer})_{Eu} \quad (1)$$

The APC background fluorescence and detection buffer are subtracted from the raw FRET signal of each sample in APC and Eu channels. Spectral overlap compensation is measured by the proportionality factor P (eq.2)

$$P = \frac{(Eu_{only} - \text{detection buffer})_{APC}}{(Eu_{only} - \text{detection buffer})_{Eu}} \quad (2)$$

APC_{only} and Eu_{only} correspond to all reagents except cells and siRNA in the Eu and APC channel (Ballmer, Moos et al. 2017).

9.10 PrP^{Sc} Enzyme-linked immunosorbent assay (ELISA)

As in the PrP^{C} HP-FRET assay, the cell culture medium was aspirated after reading the RT-Glo luminescence with the Envision reader at 37°C. Cells were lysed with 50 μl 1x standard lysis buffer per well, containing 5 μg PK/mL (Roche) to digest PrP^{C}. The assay plate was sealed and shaken for 90 min at 37°C at 750 rpm. PK was inactivated by adding 8 μl/well of 15 mM PMSF (stored at -20°C) to reach a final concentration of 1.6 mM. The assay plate was sealed and shaken for 10 min at room temperature at 750 rpm. To disassemble PK-resistant PrP^{Sc} aggregates to monomers, 7 μl/well of denaturing buffer (sodium hydroxide buffer containing 0.5M NaOH, pH 14.0, stored at RT) were added to reach a final concentration of 47.9 mM. The assay plate was sealed and shaken for 10 min at RT at 750 rpm. To adjust the pH for

ELISA, 8 μl/well of neutralizing buffer (phosphate buffer containing 0.5M NaH_2PO_4, pH 4.0, stored at RT) were added to get a final concentration of 54.7 mM. The assay plate was sealed and shaken at RT for 10 min at 750 rpm. 50 μl of the sample solution were transferred to 384-well Spectraplates HB (Perkin Elmer). The ELISA plates were previously coated with 400 ng/ml POM1 in PBS at 4°C overnight. Plates were washed five times in PBS + 0.1% Tween-20 (0.1% PBS-T) and blocked with 80 μl per well of 5% SuperBlock (ThermoFisher) in 0.1% PBS-T for 2 hrs at RT. Blocking buffer was aspirated and samples and controls were added for 90 min at RT. 2-fold dilutions of $rmPrP_{23\text{-}230}$, starting at a dilution of 1.89 ng/ml in 1x standard lysis buffer were used as calibration curve. Biotinylated POM19 was used to detect PrP^C (200 ng/ml in 1% SuperBlock in 0.1% PBS-T). After washing 5 times with 0.1% PBS-T, biotinylated antibody was detected by adding 50 μl Streptavidin-HRP (1:1'000 in 1% SuperBlock in 0.1% PBS-T; BD Pharmingen). Plates were washed again 5 times in 0.1% PBS-T and 50 μl of the chromogenic HRP substrate 3,3', 5,5;-tetramethylbenzidine (TMB, Life Technologies) was added to each well. After ten minutes of incubation at RT, the chromogenic reaction was stopped by adding 50 μl of 0.5 M H2SO4. The absorbance was read at λ=450 nm on the EnVision Multilabel Reader (Perkin Elmer). The blank corresponded to wells filled with all ELISA reagents, but 1x standard lysis buffer instead of sample solution.

9.11 Screen quality control and data analysis

The raw screening data was analysed by collaborating bioinformaticians (Elke Schaper and Jéròme Dauvellier, Vital-IT lab University of Lausanne and Andra Chincisan, University Hosipital of Zurich) for the quality control reports, data normalization and hit selection.

9.11.1 Quality control

For quality control the strictly standardized mean difference (SSMD) defined for a moderately strong control was calculated for Net-FRET values of non-target siRNA and *Prnp* siRNA controls (Zhang 2007). The SSMD is the mean divided by the standard deviation of the difference between the controls treated with *Prnp* targeting siRNA and non-target siRNA (eq.3).

$$SSMD = \frac{mean_{Prnp} - mean_{non-target}}{\sqrt{STDEVP^2_{rnp2} + STDEV^2_{non-target}}} \quad (3)$$

SSMD levels below -2 indicate that the quality of a screen in the excellent range, for a screen with a moderate control. SSMD values between -2 and -1 indicate that the screen is in the good range, whereas SSMD values between -1 and -0.5 indicate the screen is in the inferior range

(Table 3). For a screen with a strong control SSMD levels below -3 indicate that the quality of a screen in the excellent range, SSMD values between -3 and -2 indicate that the screen is in the good range, SSMD values between -2 and -1 indicate the screen is in the inferior range, whereas SSMD higher than -1 indicate poor screen quality (Zhang 2011).

Quality Type	Moderate control	Strong control
Excellent	SSMD $\leq$ -2	SSMD $\leq$ -3
Good	-2 $<$ SSMD $\leq$ -1	-3 $<$ SSMD $\leq$ -2
Inferior	-1 SSMD $\leq$ -0.5	-2 SSMD $\leq$ -1
Poor	SSMD $>$ -0.5	SSMD $>$ -1

Table 3: SSMD based quality control criteria for moderate and strong controls (Zhang 2011).

The mean value over plates for odd and even rows and columns was compared to check for row or column effects on the plate. A gaussian fit model chosen by lowest Bayesian information criterion was applied to the Net-FRET sample values of each plate to process the data and take in account inter plate variability (Wit, van den Heuvel et al. 2012). Replicate correlation was calculated by robust linear regression applied to the raw Net-FRET signal of duplicates and to Gaussian process normalized net-FRET signal. A linear model was fit by robust regression using an M estimator. Compared to other estimators, M estimators are more robust to outliers, which is useful for biologically variable screen data from living cells (Wilcox 2012).

9.11.2 Data analysis

Hits were selected based on the best gaussian processed normalized sample signal versus non-target comparison at a p value threshold = 0.001. For comparison of murine and human PrP^C screens the murine genes were ranked according to the descending Net-FRET signal of the mean of four siRNAs targeting the same gene. The human genes were ranked according to the descending mean Net-FRET signal of the technical duplicates targeted by the same pool of siRNAs against the same gene. The code and the documentation of the customized High Throughput Screening Library software can be found here: http://elkeschaper.github.io, https://github.com/elkeschaper/hts

9.12 Brain homogenate preparation used for infection

20% RML6 brain homogenate (BH) was from CD1 mice, infected by intracerebral inoculation (i.c.) with Rocky Mountain Laboratory strain RML (RML; passage #6) (Mahal, Baker et al.

2007). 10% 22F BH was from prion strain 22A-infected Hsd;C57BL/6 (BL6) mice, passaged more than five times. 10% 22L BH was from prion strain 22L-infected Hsd;C57BL/6 (BL6) mice. 10% 87A BH was from prion strain 87A-infected Hsd;C57BL/6 (BL6) mice. 10% 79A BH was from prion strain 79A-infected Hsd;C57BL/6 (BL6) mice. 10% ME7 BH was from prion strain ME7-infected Hsd;C57BL/6 (BL6) mice. 10% mNS BH was from prion strain mNS-infected JC57BL/6 (BL6) mice. 10% 263K BH was from prion strain 263K-infected Syrian Hamster PrP transgenic (TgSHaPrP)mice. Non-infectious brain homogenate (NBH) controls are from the according mice without infection. Brains were removed at the stage of terminal disease (around 150 days after inoculation), washed two times in 70% Ethanol and four times in sterile phosphate buffer saline (PBS) and subsequently homogenized in 0.32M sucrose with the RiboLyser (Hybaid, Catalys). Supernatants were collected in 50 ml Falcon tubes and frozen at - 40°C.

9.13 Prion infection of cells

Acute infection $1.6 \cdot 10^5$ cells in 2 ml cell culture medium were seeded into 6-well plates (Corning Costar). After 3 hrs the cells were inoculated with 0.3 μg/mL infectious and non-infectious brain homogenate (NBH) diluted in 2 ml culture medium and incubated for 96h. After 96 hrs the cells were detached and washed four times with sterile PBS and lysed on ice with 100 μl 1x standard lysis buffer and assayed for PrP^{Sc} by PK-Westerns.

Chronical infection $2.5 \cdot 10^5$ cells in 10 ml cell culture medium were seeded into 10cm petri dishes (Corning Costar). After 3 hrs the cells were inoculated with 0.1 μg/mL infectious and non-infectious brain homogenate (NBH) diluted in 10 ml culture medium. The medium containing the inoculum was removed after 4 days and the cells were split 1 : 5 every 3 – 4 days. After splitting four consecutive slitting steps, the cells were washed two times with sterile PBS, lysed in 150 μl 1x standard lysis buffer and assayed for PrP^{Sc} by PK-Westerns.

9.14 Western blot analysis

Samples containing the same amount of total protein were digested with PK (20 μg protein per 20 μl, digested with 2 μg or 5 μg PK/ml) in 1x standard lysis buffer for 30 min at 37°C. PK digestion was stopped by adding 4x loading buffer (NuPAGE; Invitrogen) and boiling the samples at 95°C for 5 min. Proteins were separated in a 12% Bis-Tris polyacrylamide gel (NuPAGE; Invitrogen) and blotted onto a nitrocellulose membrane (iBlot® Transfer Stack, nitrocellulose, regular size; Invitrogen). Membranes were blocked with 5% SuperBlock (ThermoFisher) in 0.1% PBS-T (Sigma) and incubated with monoclonal mouse POM1 IgG primary

antibody (anti-PrP^C; 200 ng ml–1) in 1% SuperBlock (ThermoFisher). Horseradish peroxidase (HRP)–conjugated rabbit anti–mouse IgG (1 : 10,000; Zymed) was used as secondary antibody. The blots were developed with Luminata Crescendo Western HRP substrate (Sigma) using the LAS-3000 system (FujiFilm) and the contrast adjusted within the linear range by Photoshop (Adobe Photoshop CS6) (Zhu, Herrmann et al. 2016).

9.15 Immunoprecipitation

9.15.1 Preparation of dynabeads

Dynabeads Protein A for Immunoprecipitation (Invitrogen) were resuspended by vortexing. The supernatant was removed, while the tubes were on a magnetic rack. The dynabeads were washed twice with coating buffer (0.1% BSA albumin in PBS; essentially globulin-free, Sigma). Beats treated with and without POM1 IgG anti-PrP^C antibody (1.5 μg per 25 ul dynabeads) were incubated 2h at RT on a rotating wheel. Then the beads were washed three times with coating buffer.

9.15.2 Preparations of samples and IP

SH-SY5Y and HEK293 wt and PRNP-/- cells of both cell lines were lysed in Co-IP buffer (50 mM Tris-Cl, 1% Igepal (NP-40), 75 mM NaCl, pH 7.4) plus CompleteTM Mini Protease Inhibitor Cocktail (Roche). 2000 μg of protein were diluted in 1 ml of ice cold Co-IP buffer plus CompleteTM Mini Protease Inhibitor Cocktail (Roche), passed five times through a syringe and incubated for 30 min on a rotating wheel at 4°C. After centrifuging at 900 x g for 3 min, the supernatant was collected and transferred to new tubes. For pre-clearing, the samples were incubated dynabeads that had not been treated with POM1, resuspended in 0.5% BSA (Sigma) in PBS for one hour at room temperature on a rotating wheel. The supernatant was transferred to new tubes, dynabeads + POM1 or Mouse IgG isotype control (Abcam) were added and immunoprecipitation was carried out over night at 4°C. The supernatant was removed and the samples were washed twice in washing buffer (50 mM Tris-Cl, 0.5% Igepal, 150 mM NaCl, pH 7.4) and proteins eluted with 2x loading buffer (NuPAGE; Invitrogen) by boiling for 5 min at 95°C. Samples were immediately put on the magnetic rack for 12 min and the supernatant was used for western. The western was performed as described above with biotinylated POM2 IgG primary antibody (anti-PrP^C; 200 ng/ml) in 1% SuperBlock (ThermoFisher) and Avidin-HRP (1:000; BD-Pharmacon) in 1% SuperBlock (ThermoFisher).

9.16 Gradient centrifugation

900 μl of 10%, 20%, 30%, 40%, 50%, and 60% sucrose solutions were prepared and layered with decreasing concentration into 5pA tubes (ThermoFisher) suitable for the SS-52ST rotor of Sorvall Discovery M150 Micro-Ultracentrifuge (VBI Core Labs). Samples were diluted in 1x standard lysis buffer to a final concentration of 0.6 μg/μl and rotated for 20 min at 4°C on the rotation wheel to solubilize PrP^C. Then, the samples were centrifuged for 5 min at 4°C at 15'000 rpm to pellet down cell debris. 500 μl of the supernatant was added on top of the sucrose gradient. The samples were centrifuged for 1 hour at 4°C at 50'000 rpm with the Sorvall Discovery M150 Micro-Ultracentrifuge (VBI Core Labs). Fractions a 400 μl were collected into fresh 2ml screw cap tubes and precipitated with 1.8 ml MeOH at - 40°C, overnight. Samples were then centrifuged for 30 min at 4°C at 13'000 rpm. The MeOH was removed and samples completely dried by evaporation in the hood. Samples were re-suspended with 30 μl 2x loading buffer (NuPAGE; Invitrogen) and samples were boiled for 5 min at 95°C. The western was performed as described above.

9.17 POM1- POM2 Sandwich ELISA

ELISA with PRNP-/- candidate protein samples was performed in SpectraPlate-96 MB, Clear 96-well Microplate with Medium Protein Binding Affinity (Perkin Elmer) as described above, but with biotinylated POM2 antibody, instead of POM19. Unknown PrP^C concentrations were interpolated from the linear range of the calibration curve with rhPrP22-231. Each sample was compared with unpaired two tailed t test to the positive control.

9.18 Immunohistochemistry of cell monolayers

700 μl cells (750'000 cells/ml) were seeded into glass bottom μ-slide chamber slides (Ibidi) and incubated for 48 hrs. For staining of intracellular PrP the cells were washed two times with sterile PBS and fixed and permeabilized with ice-cold acetone for 5 min. Cells were washed again two times and blocked for one hour at room temperature with 10% goat serum (DAKO) and 5% bovine serum albumin (BSA) in PBS. Samples were incubated for one hour at room temperature with monoclonal mouse POM1 IgG primary antibody (anti-PrP^C; 1 μg /ml) in 1% SuperBlock (ThermoFisher). Alexa 488 conjugated goat anti–mouse IgG (1:1000; Sigma) in 1% SuperBlock (ThermoFisher) was used as secondary antibody and incubated for one hour at room temperature. After washing three times the nuclei were stained with DAPI (1:10'000; Sigma) in PBS for 5 min and samples washed again tree times with sterile PBS before being

imaged on a SP5 confocal microscope (Leica) using a 63 x oil immersed HCX PL APO Leica objective (NA 1.4, WD 0.1mm) at 3 x optical zoom. Laser intensities were kept constant across treatment groups during imaging.

9.19 Cell growth assessment

Quantification of the cell growth was assessed with the IncuCyte ZOOM live-cell analysis system (Essenbioscience). Cells were seeded into 384-well plates. Brightfield images were taken every 12 hrs. Data was analysed and visualized with the IncuCyte ZOOM Software using a confluency mask.

9.20 Real-time quantitative PCR

CAD5 cells transfected with different siRNAs were cultured in 6-well plates and harvested after 72 hrs at 70% confluency. RNA was extracted with the RNeasy Mini kit (QIAGEN). cDNA was generated according to the QuantiTect Reverse Transcription kit (QIAGEN) by eliminating genomic DNA in a first step followed by reverse transcription. All reactions were set up on ice to minimize the risk of RNA degradation. Primers for real-time quantitative PCR (qRT-PCR) were designed using the primer bank from Harvard: https://pga.mgh.harvard.edu/primerbank/index.html. To check the linear range of the qRT-PCR primers, each primer pair was tested with a standard curve consisting of five 1:10 dilutions of CAD5 wild type (wt) RNA starting at 100 ng RNA. Absolute mRNA expression was assessed by qRT-PCR. Technical triplicates of three biological replicates from different passages of CAD5 wt cells transfected with siRNAs targeting chaperones, *Prnp* and scrambled non-target siRNA were used. cDNA generated without reverse transcriptase and H_2O served as negative controls. The qPCR was performed in 96- and 384-well plates. The PCR reaction mix consisted of forward and reverse primer [final conc. 250nM], 1x SYBR green (Roche Diagnostics) and H_2O. The final cDNA concentration was 0.5ng/mL. The reagents were dispensed manually and by a LabCyte acoustic dispensing robot. The reaction was run on a ViiA7 Real-Time PCR System (Life Technologies). Eight different housekeeping genes (B2m, Eif2a, Gapd, Hmbs, Hprt, Ppib, Tbp, Utp6c) were tested. B2m, Gapdh, Hprt and Ppib were selected as reliable ones and used in every experiment as controls. All samples were normalized to Hprt. Absolute mRNA levels were calculated with the ViiA7 software, Microsoft Excel and GraphPad software.

9.21 Proteomics

The proteomic composition of the neuronal CAD5 cells was characterized by Pierre Goloubinoff and Bruno Fauvet. Herein 4142 proteins, representing 96.8% of the total mass of polypeptides, were quantified significantly above the back-ground noise (n=5 biological repeats; unpaired t-test using an initial p-value threshold of 0.01), out of 8403 protein identifications. The quantitative values as mass fractions and copy number per cubic micron were implemented into the chaperone hit characterization.

9.22 Statistical analysis

Statistical tests were computed by GraphPad Prism 5 (GraphPad) and Excel (Version 16.13.1). GraphPad Prism 5 and R Markdown were used for data visualization. Statistical significance between experimental groups was assessed using an unpaired t-test or two-way analysis of variance (ANOVA). p-values <0.05 were considered statistically significant. Results were presented as the mean of replicas $\pm$ SD unless stated otherwise.

10 Appendix

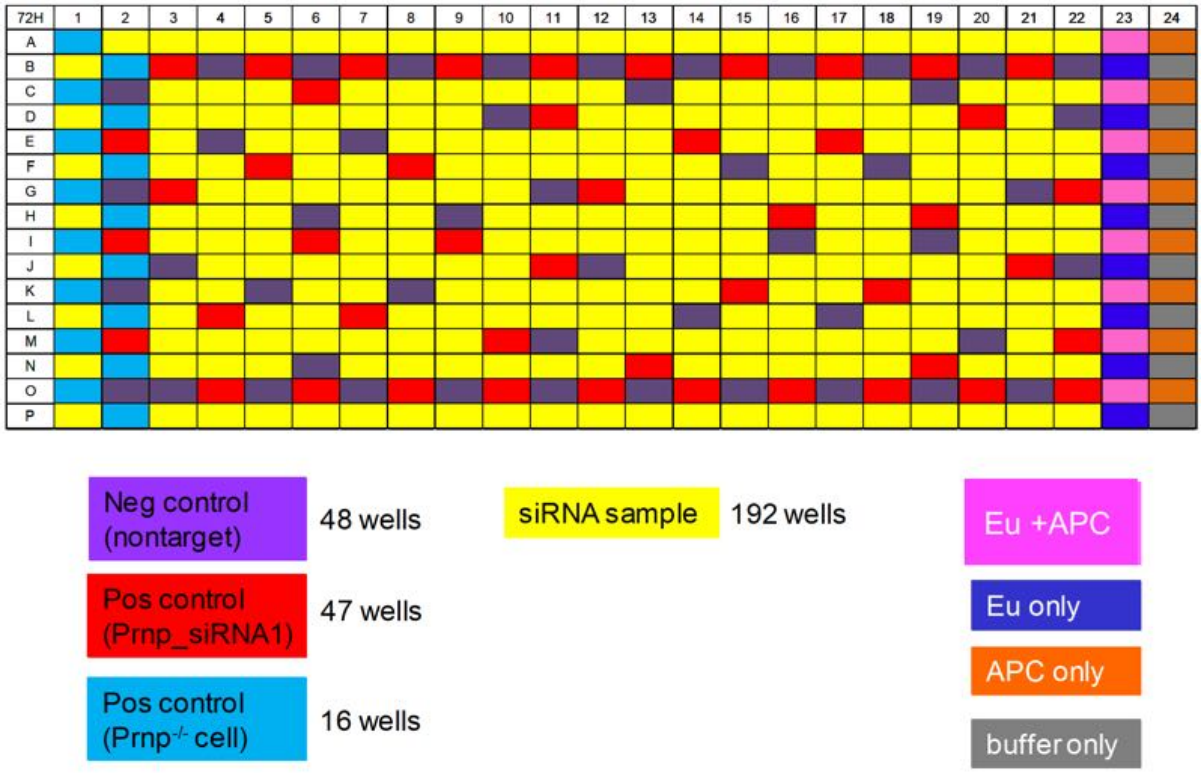

Figure 79: The randomized screen plate layout showed 192 samples (yellow), CAD5 Prnp-/- cells in the first two columns cells (blue). The control wells with non-target siRNA (purple) and with Prnp targeting siRNA (red) were evenly distributed over the plate. The last two columns contained the buffer controls with LANCE buffer (grey), Europium coupled to POM19 (dark blue), APC coupled to POM1 (orange) and a mixture of both detection antibodies (pink).

Figure 80: Cell viability quality control of the first PrP^C screen. In the first murine PrP^C screen each gene was targeted by two up to four different siRNAs in technical duplicates. Gene names were coloured according to the number of siRNAs targeting the same gene that led to modulation of PrP levels. Genes were targeted by four (yellow), three (dark orange) two siRNAs (bright orange) or one siRNA (blue). Each siRNA was assessed for cell viability and marked with blue if it passed the quality control and orange if it did no pass. The viability range was defined by the mean of non-target controls +/- 2 SD. Genes that were targeted by less than 4 siRNAs showed missing values in grey.

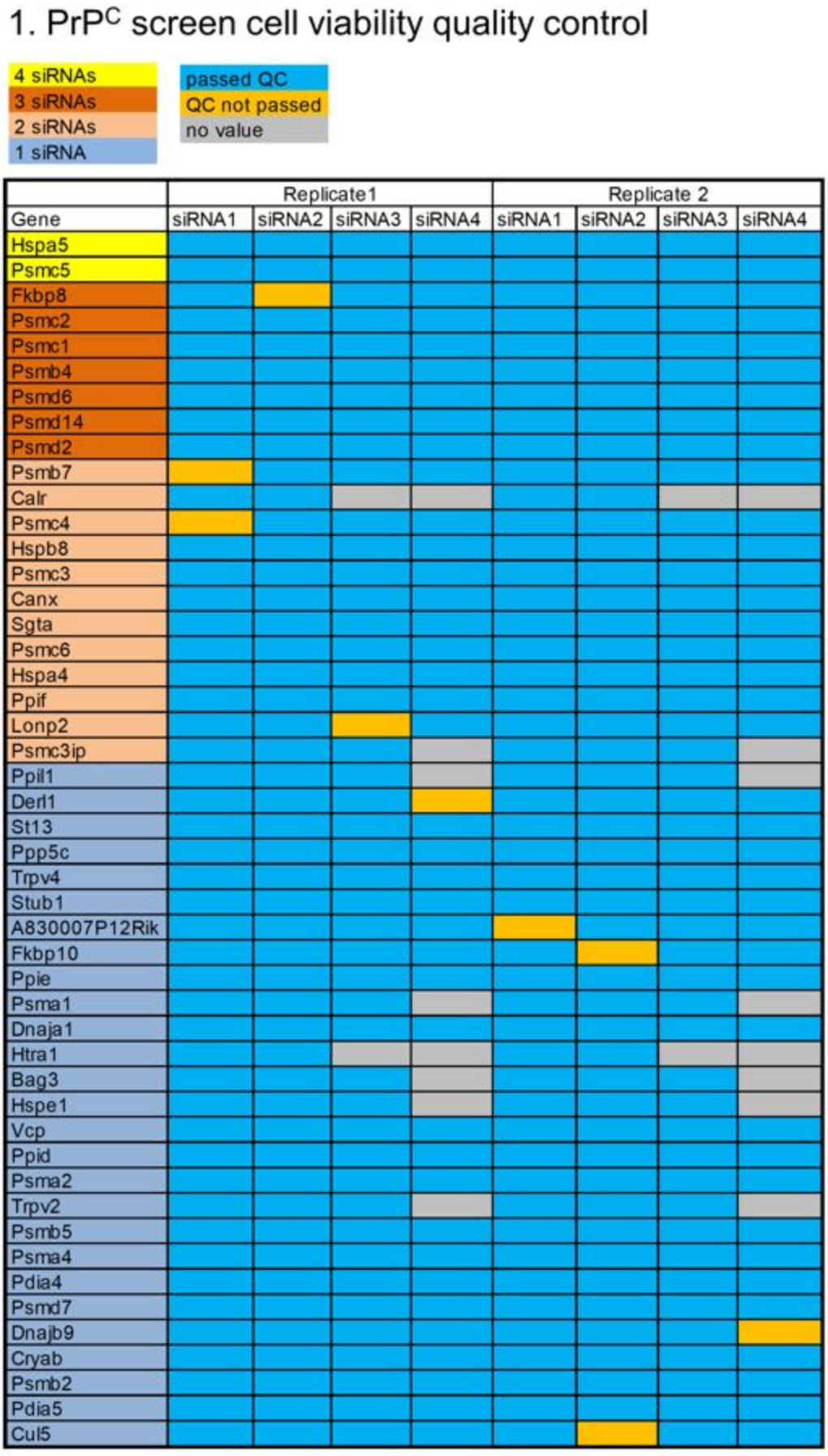

Figure 80: (Description on the previous page)

2. PrP^C screen cell viability quality control

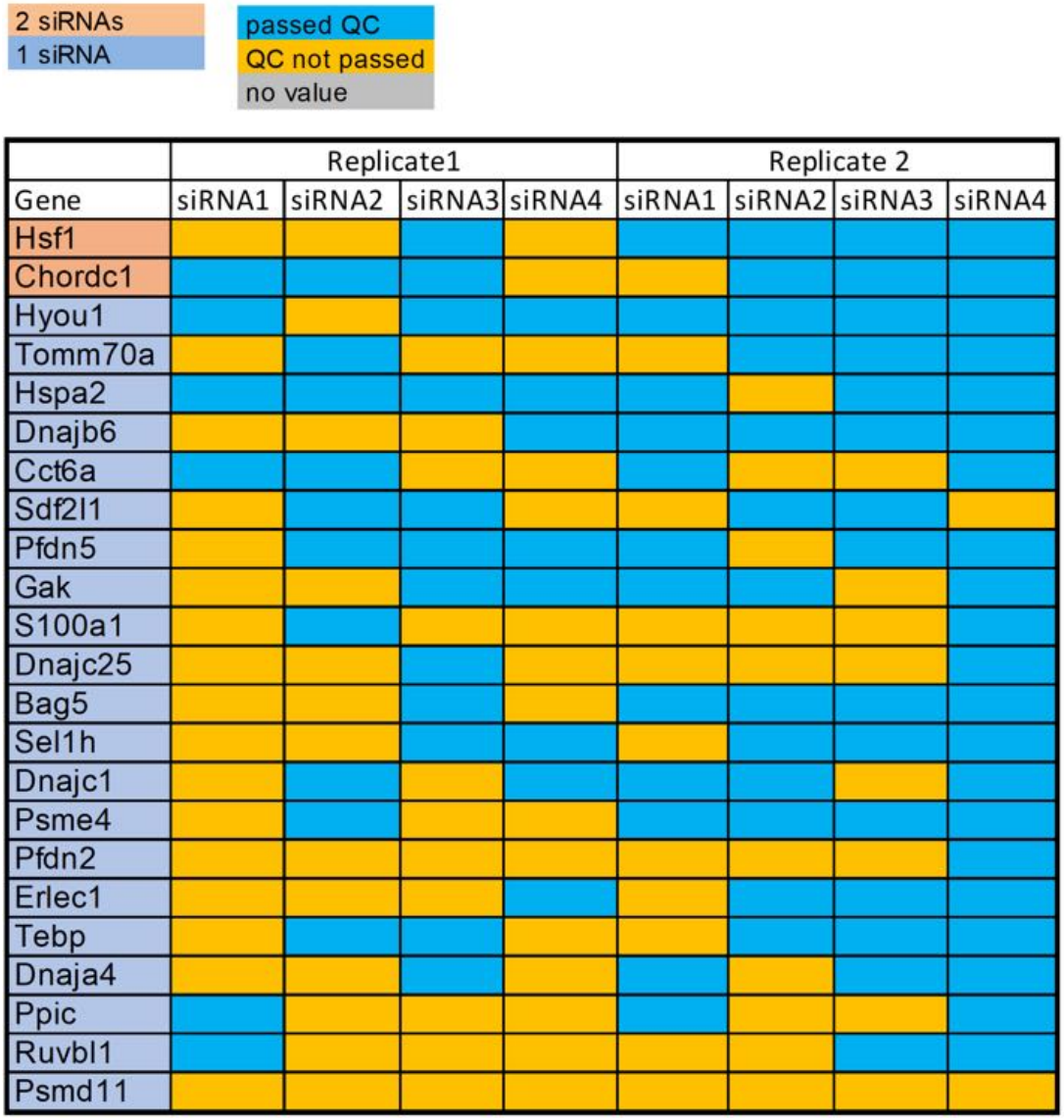

Figure 81: Cell viability quality control of the second PrP^C screen. In the second murine PrP^C screen each gene was targeted by four different siRNAs in technical duplicates. Gene names were coloured according to the number of siRNAs targeting the same gene that led to modulation of PrP levels. Genes were targeted by one (blue) or two siRNAs (bright orange). Each siRNA was assessed for cell viability and marked with blue if it passed the quality control and orange if it did no pass. The viability range was defined by the mean of non-target controls +/- 2 SD.

Figure 82: Summary of all chaperone hits from the first and second PrP^C screen. Gene names were coloured according to the number of siRNAs targeting the same gene that led to modulation of PrP levels. Genes were targeted by four (yellow), three (dark orange) or two siRNAs (bright orange). The number of siRNAs in duplicates, that passed (TRUE) or failed (FALSE) RT-Glo quality control were indicated in a column. The functions of each gene were indicated in the last column uniprot.org.

Functions of chaperone hits 1

Gene	Protein	Gene entrez	Pass RT-Glo QC	Function
Hspa5	Heat shock 70kDa protein 5	14828	TRUE	Probably plays a role in facilitating the assembly of multimeric protein complexes inside the endoplasmic reticulum. Involved in the correct folding of proteins and degradation of misfolded proteins via its interaction with DNAJC10, probably to facilitate the release of DNAJC10 from its substrate.
Psmc5	26S protease regulatory subunit 8	19184	TRUE	The 26S protease is involved in the ATP-dependent degradation of ubiquitinated proteins. The regulatory (or ATPase) complex confers ATP dependency and substrate specificity to the 26S complex.
Fkbp8	Peptidyl-prolyl cis-trans isomerase FKBP8	14232	1FALSE 3 TRUE	Constitutively inactive PPIase, which becomes active when bound to calmodulin and calcium. Seems to act as a chaperone for BCL2, targets it to the mitochondria and modulates its phosphorylation state. The BCL2/FKBP8/calmodulin/calcium complex probably interferes with the binding of BCL2 to its targets. The active form of FKBP8 may therefore play a role in the regulation of apoptosis.
Psmc2	26S protease regulatory subunit 7	19181	TRUE	The 26S protease is involved in the ATP-dependent degradation of ubiquitinated proteins. The regulatory (or ATPase) complex confers ATP dependency and substrate specificity to the 26S complex.
Psmc1	26S protease regulatory subunit 4	19179	TRUE	The 26S protease is involved in the ATP-dependent degradation of ubiquitinated proteins. The regulatory (or ATPase) complex confers ATP dependency and substrate specificity to the 26S complex.
Psmb4	Proteasome subunit beta type-4	19172	TRUE	The proteasome is a multicatalytic proteinase complex which is characterized by its ability to cleave peptides with Arg, Phe, Tyr, Leu, and Glu adjacent to the leaving group at neutral or slightly basic pH. The proteasome has an ATP-dependent proteolytic activity. Mediates the lipopolysaccharide-induced signal macrophage proteasome (By similarity). SMAD1/OAZ1/PSMB4 complex mediates the degradation of the CREBBP/EP300 repressor SNIP1.
Psmd6	26S proteasome non-ATPase regulatory subunit 6	66413	TRUE	Acts as a regulatory subunit of the 26S proteasome which is involved in the ATP-dependent degradation of ubiquitinated proteins.
Psmd14	26S proteasome non-ATPase regulatory subunit 14	59029	TRUE	Metalloprotease component of the 26S proteasome that specifically cleaves 'Lys-63'-linked polyubiquitin chains. The 26S proteasome is involved in the ATP-dependent degradation of ubiquitinated proteins. Plays a role in response to double-strand breaks (DSBs): acts as a regulator of non-homologous end joining (NHEJ) by cleaving 'Lys-63'-linked polyubiquitin, thereby promoting retention of JMJD2A/KDM4A on chromatin and restricting TP53BP1 accumulation. Also involved in homologous recombination repair by promoting RAD51 loading.
Psmd2	26S proteasome non-ATPase regulatory subunit 2	21762	TRUE	Acts as a regulatory subunit of the 26 proteasome which is involved in the ATP-dependent degradation of ubiquitinated proteins. Binds to the intracellular domain of tumor necrosis factor type 1 receptor. The binding domain of TRAP1 and TRAP2 resides outside the death domain of TNFR1.
Psmb7	Proteasome subunit beta type-7	19177	1 FALSE 3 TRUE	The proteasome is a multicatalytic proteinase complex which is characterized by its ability to cleave peptides with Arg, Phe, Tyr, Leu, and Glu adjacent to the leaving group at neutral or slightly basic pH. The proteasome has an ATP-dependent proteolytic activity. This unit is responsible of the trypsin-like activity.
Calr	Calreticulin	12317	TRUE	Calcium-binding chaperone that promotes folding, oligomeric assembly and quality control in the endoplasmic reticulum (ER) via the calreticulin/calnexin cycle. This lectin interacts transiently with almost all of the monoglucosylated glycoproteins that are synthesized in the ER. Interacts with the DNA-binding domain of NR3C1 and mediates its nuclear export. Involved in maternal gene expression regulation. May participate in oocyte maturation via the regulation of calcium homeostasis (By similarity).
Psmc4	26S protease regulatory subunit 6B	23998	1 FALSE 7 TRUE	The 26S protease is involved in the ATP-dependent degradation of ubiquitinated proteins. The regulatory (or ATPase) complex confers ATP dependency and substrate specificity to the 26S complex.
Hspb8	Heat shock protein beta-8	80888	TRUE	Displays temperature-dependent chaperone activity.
Psmc3	26S protease regulatory subunit 6A	19182	TRUE	The 26S protease is involved in the ATP-dependent degradation of ubiquitinated proteins. The regulatory (or ATPase) complex confers ATP dependency and substrate specificity to the 26S complex (By similarity).
Canx	Calnexin	12330	TRUE	Calcium-binding protein that interacts with newly synthesized glycoproteins in the endoplasmic reticulum. It may act in assisting protein assembly and/or in the retention within the ER of unassembled protein subunits. It seems to play a major role in the quality control apparatus of the ER by the retention of incorrectly folded proteins. Associated with partial T-cell antigen receptor complexes that escape the ER of immature thymocytes, it may function as a signaling complex regulating thymocyte maturation. Additionally it may play a role in receptor-mediated endocytosis at the synapse.
Sgta	Small glutamine-rich tetratricopeptide repeat-containing protein	52551	TRUE	Co-chaperone that binds directly to HSC70 and HSP70 and regulates their ATPase activity.
Psmc6	26S protease regulatory subunit 10B	67089	TRUE	The 26S protease is involved in the ATP-dependent degradation of ubiquitinated proteins. The regulatory (or ATPase) complex confers ATP dependency and substrate specificity to the 26S complex.
Hspa4	Heat shock 70 kDa protein 4	15525	TRUE	ATP binding, chaperone-mediated protein complex assembly, protein import into mitochondrial outer membrane
Ppif	Peptidyl-prolyl cis-trans isomerase F, mitochondrial	105675	TRUE	PPIase that catalyzes the cis-trans isomerization of proline imidic peptide bonds in oligopeptides and may therefore assist protein folding.
Lonp2	Lon protease homolog 2, peroxisomal	66887	1 FALSE 7 TRUE	ATP-dependent serine protease that mediates the selective degradation of misfolded and unassembled polypeptides in the peroxisomal matrix. Necessary for type 2 peroxisome targeting signal (PTS2)-containing protein processing and facilitates peroxisome matrix protein import (By similarity). May indirectly regulate peroxisomal fatty acid beta-oxidation through degradation of the self-processed forms of TYSND1.
Psmc3ip	Homologous-pairing protein 2 homolog	19183	TRUE	Plays an important role in meiotic recombination. Stimulates DMC1-mediated strand exchange required for pairing homologous chromosomes during meiosis. The complex PSMC3IP/MND1 binds DNA, stimulates the recombinase activity of DMC1 as well as DMC1 D-loop formation from double-strand DNA. This complex stabilizes presynaptic RAD51 and DMC1 filaments formed on single strand DNA to capture double-strand DNA. This complex stimulates both synaptic and presynaptic critical steps in RAD51 and DMC1-promoted homologous pairing. May inhibit HIV-1 viral protein TAT activity and modulate the activity of proteasomes through association with PSMC3. Acts as a tissue specific coactivator of hormone-dependent transcription mediated by nuclear receptors.
Hsf1	Heat shock factor protein 1	15499	3 FALSE 5 TRUE	Function as a stress-inducible and DNA-binding transcription factor that plays a central role in the transcriptional activation of the heat shock response (HSR), leading to the expression of a large class of molecular chaperones heat shock proteins (HSPs) that protect cells from cellular insults' damage. Plays a role in nuclear export of stress-induced HSP70 mRNA. Plays a role in the regulation of mitotic progression. Plays also a role as a negative regulator of non-homologous end joining (NHEJ) repair activity in a DNA damage-dependent manner. Involved in stress-induced cancer cell proliferation in a IER5-dependent manner.
Chordc1	Cysteine and histidine-rich domain-containing protein 1	66917	2 FALSE 6 TRUE	Regulates centrosome duplication, probably by inhibiting the kinase activity of ROCK2. Proposed to act as co-chaperone for HSP90. May play a role in the regulation of NOD1 via a HSP90 chaperone complex. In vitro, has intrinsic chaperone activity. This function may be achieved by inhibiting association of ROCK2 with NPM1.

Figure 82: (Description on the previous page)

Figure 83: Summary of all chaperone hits from the first and second PrP^C screen. Gene names were coloured according to their function. ER associated function (yellow), Proteasome (grey), Apoptosis (blue) and genes that led to upregulation of PrP were coloured in green.

Functions of chaperones reducing cell viability in PrP^{Sc} screen

Gene	Proein	Functions
Aip	Aryl hydrocarbon receptor interacting protein	Function is not well understood, it is known to interact with numerous other proteins, including one called the aryl hydrocarbon receptor. Cell proliferation, differentiation, cell survival. Tumor suppressor. Unfolded protein binding, protein maturation by protein foldingprotein targeting to mitochondrion.
Os9	Protein OS-9	Lectin which functions in endoplasmic reticulum (ER) quality control and ER-associated degradation (ERAD). May bind terminally misfolded non-glycosylated proteins as well as improperly folded glycoproteins, retain them in the ER, and possibly transfer them to the ubiquitination machinery and promote their degradation. Possible targets include TRPV4
Dnajb6	DnaJ homolog subfamily B member 6	Plays an indispensable role in the organization of KRT8/KRT18 filaments. Acts as an endogenous molecular chaperone for neuronal proteins including huntingtin. Suppresses aggregation and toxicity of polyglutamine-containing, aggregation-prone proteins. Has a stimulatory effect on the ATPase activity of HSP70 in a dose-dependent and time-dependent manner and hence acts as a co-chaperone of HSP70. Also reduces cellular toxicity and caspase-3 activity
Nsfl1c	NSFL1 cofactor p47	Reduces the ATPase activity of VCP. (VCP = TER ATPase is an ATPase enzyme present in all eukaryotes and archaebacteria. Its main function is to segregate protein molecules from large cellular structures such as protein assemblies, organelle membranes and chromatin, and thus facilitate the degradation of released polypeptides by the multi-subunit protease proteasome.) Necessary for the fragmentation of Golgi stacks during mitosis and for VCP-mediated reassembly of Golgi stacks after mitosis. May play a role in VCP-mediated formation of transitional endoplasmic reticulum (tER)
Dnajb11	DnaJ homolog subfamily B member 11	Serves as a co-chaperone for HSPA5. Binds directly to both unfolded proteins that are substrates for ERAD and nascent unfolded peptide chains, but dissociates from the HSPA5-unfolded protein complex before folding is completed. May help recruiting HSPA5 and other chaperones to the substrate. Stimulates HSPA5 ATPase activity

Figure 84: Summary of the function of the genes that reduced cell viability in the PrP^{Sc} screen.

Primer name	Gene	Accession #	Function	Sequence (5'→3')	Primer location (exon)	Amplicon length (bp)
Ppib fwd	Ppib	NM_011149.2	Secretory pathway	GGAGATGGCACAGGAGGAAA	3	73
Ppib rev				CCGTAGTGCTTCAGTTTGAAGTTCT	4	
Hmbs fwd	Hmbs	NM_013551.2	Heme synthesis, porphyrin metabolism	TCCCTGAAGGATGTGCCTA	7	73
Hmbs rev				AAGGGTTTTCCCGTTTGC	8	
Hprt1 fwd	Hprt	NM_013556.2	Purine synthesis	TCCTCCTCAGACCGCTTTT	1	90
Hprt1 rev				CCTGGTTCATCATCGCTAATC	2	
Eif2a fwd	Eif2a	NM_001005509.1	Protein translation	CAACGTGGCAGCCTTACA	2	74
Eif2a rev				TTTCATGTCATAAAGTTGTAGGTTAGG	3	
Utp6c fwd	Utp6	NM_144826.3	Rn18 s biogenesis	TTTCGGTTGAGTTTTTCAGGA	17	75
Utp6c rev				CCCTCAGGTTTACCATCTTGC	18	
B2m fwd	B2m	NM_009735	Histocompatibility	GGTCTTTCTGGTGCTTGTCTCA	1	103
B2m rev				GTTCGGCTTCCCATTCTCC	2	
Tbp fwd	Tbp	NM_008907	Protein peptidyl-prolyl isomerization	CAAACCCAGAATTGTTCTCCTT	7	131
Tbp rev				ATGTGGTCTTCCTGAATCCCT	8	
Gapdh fwd	Gapdh	NM_008084.2	Glicolysis and gluconeogenesis	TCCATGACAACTTTGGCATTG	4	72
Gapdh rev				CAGTCTTCTGGGTGGCAGTGA	5	

Figure 85: List of the housekeeping genes, their functions and according primers used for the qRT-PCR for hit validation.

11 References

Aguzzi, A. (2008). ”Unraveling prion strains with cell biology and organic chemistry.” Proc Natl Acad Sci U S A 105(1): 11-12.

Aguzzi, A., F. Baumann and J. Bremer (2008). ”The prion’s elusive reason for being.” Annu Rev Neurosci 31: 439-477.

Aguzzi, A. and A. M. Calella (2009). ”Prions: protein aggregation and infectious diseases.” Physiol Rev 89(4): 1105-1152.

Aguzzi, A., M. Heikenwalder and M. Polymenidou (2007). ”Mechanisms of disease - Insights into prion strains and neurotoxicity.” Nature Reviews Molecular Cell Biology 8(7): 552-561.

Aguzzi, A., A. K. K. Lakkaraju and K. Frontzek (2018). ”Toward Therapy of Human Prion Diseases.” Annu Rev Pharmacol Toxicol 58: 331-351.

Allen, K. D., R. D. Wegrzyn, T. A. Chernova, S. Muller, G. P. Newnam, P. A. Winslett, K. B. Wittich, K. D. Wilkinson and Y. O. Chernoff (2005). ”Hsp70 chaperones as modulators of prion life cycle: Novel effects of Ssa and Ssb on the Sacharomyces cerevisiae prion [PSI+].” Genetics 169(3): 1227-1242.

Alper, T. (1967). ”Does the agent of scrapie replicate without nucleic acid?” Nature 214(5090):764-6.

Ashe, K. H. and A. Aguzzi (2013). ”Prions, prionoids and pathogenic proteins in Alzheimer disease.” Prion 7(1): 55-59.

Auluck, P. K., H. Y. Chan, J. Q. Trojanowski, V. M. Lee and N. M. Bonini (2002). ”Chaperone suppression of alpha-synuclein toxicity in a Drosophila model for Parkinson’s disease.” Science 295(5556): 865-868.

Ballmer, B. A., R. Moos, P. Liberali, L. Pelkmans, S. Hornemann and A. Aguzzi (2017). ”Modifiers of prion protein biogenesis and recycling identified by a highly parallel endocytosis kinetics assay.” J Biol Chem 292(20): 8356-8368.

Barria, M. A., A. Mukherjee, D. Gonzalez-Romero, R. Morales and C. Soto (2009). ”De novo generation of infectious prions in vitro produces a new disease phenotype.” PLoS Pathog 5(5): e1000421.

Beat Hörnlimann, D. R., Hans Kretzschmar, Hans A. Kretzschmar, Walter de Gruyter (2007). Prions in Humans and Animals.

Biedler, J. L., L. Helson and B. A. Spengler (1973). ”Morphology and growth, tumorigenicity, and cytogenetics of human neuroblastoma cells in continuous culture.” Cancer Res 33(11): 2643-2652.

Biedler, J. L., S. Roffler-Tarlov, M. Schachner and L. S. Freedman (1978). ”Multiple neuro-

transmitter synthesis by human neuroblastoma cell lines and clones." Cancer Res 38(11 Pt 1): 3751-3757.

Bigner, D. D., S. H. Bigner, J. Ponten, B. Westermark, M. S. Mahaley, E. Ruoslahti, H. Herschman, L. F. Eng and C. J. Wikstrand (1981). "Heterogeneity of Genotypic and phenotypic characteristics of fifteen permanent cell lines derived from human gliomas." J Neuropathol Exp Neurol 40(3): 201-229.

Birmingham, A., L. M. Selfors, T. Forster, D. Wrobel, C. J. Kennedy, E. Shanks, J. Santoyo-Lopez, D. J. Dunican, A. Long, D. Kelleher, Q. Smith, R. L. Beijersbergen, P. Ghazal and C. E. Shamu (2009). "Statistical methods for analysis of high-throughput RNA interference screens." Nature Methods 6(8): 569-575.

Bolton, D. C., M. P. Mckinley and S. B. Prusiner (1982). "Identification of a Protein That Purifies with the Scrapie Prion." Science 218(4579): 1309-1311.

Borchelt, D. R., M. Scott, A. Taraboulos, N. Stahl and S. B. Prusiner (1990). "Scrapie and cellular prion proteins differ in their kinetics of synthesis and topology in cultured cells." J Cell Biol 110(3): 743-752.

Bosque, P. J. and S. B. Prusiner (2000). "Cultured cell sublines highly susceptible to prion infection." J Virol 74(9): 4377-4386.

Bosque, P. J., C. Ryou, G. Telling, D. Peretz, G. Legname, S. J. DeArmond and S. B. Prusiner (2002). "Prions in skeletal muscle." Proc Natl Acad Sci U S A 99(6): 3812-3817.

Bouhy, D., M. Juneja, I. Katona, A. Holmgren, B. Asselbergh, V. De Winter, T. Hochepied, S. Goossens, J. J. Haigh, C. Libert, C. Ceuterick-de Groote, J. Irobi, J. Weis and V. Timmerman (2018). "A knock-in/knock-out mouse model of HSPB8-associated distal hereditary motor neuropathy and myopathy reveals toxic gain-of-function of mutant Hspb8." Acta Neuropathologica 135(1): 131-148.

Bradley, R. (1990). "Bovine spongiform encephalopathy: the need for knowledge, balance, patience, and action." J Pathol 160(4): 283-285.

Brotherston, J. G., C. C. Renwick, J. T. Stamp, I. Zlotnik and I. H. Pattison (1968). "Spread and scrapie by contact to goats and sheep." J Comp Pathol 78(1): 9-17.

Brown, P., M. Preece, J. P. Brandel, T. Sato, L. McShane, I. Zerr, A. Fletcher, R. G. Will, M. Pocchiari, N. R. Cashman, J. H. d'Aignaux, L. Cervenakova, J. Fradkin, L. B. Schonberger and S. J. Collins (2000). "Iatrogenic Creutzfeldt-Jakob disease at the millennium." Neurology 55(8): 1075-1081.

Bruce, M. E. (1993). "Scrapie strain variation and mutation." Br Med Bull 49(4): 822-838.

Bruce, M. E. and A. G. Dickinson (1987). "Biological Evidence That Scrapie Agent Has an

Independent Genome." Journal of General Virology 68: 79-89.

Bueler, H., A. Aguzzi, A. Sailer, R. A. Greiner, P. Autenried, M. Aguet and C. Weissmann (1993). "Mice devoid of PrP are resistant to scrapie." Cell 73(7): 1339-1347.

Bueler, H., A. Raeber, A. Sailer, M. Fischer, A. Aguzzi and C. Weissmann (1994). "High prion and PrP^{Sc} levels but delayed onset of disease in scrapie-inoculated mice heterozygous for a disrupted PrP gene." Mol Med 1(1): 19-30.

Butler, D. A., M. R. Scott, J. M. Bockman, D. R. Borchelt, A. Taraboulos, K. K. Hsiao, D. T. Kingsbury and S. B. Prusiner (1988). "Scrapie-infected murine neuroblastoma cells produce protease-resistant prion proteins." J Virol 62(5): 1558-1564.

Cagampang, F. R., S. A. Whatley, A. L. Mitchell, J. F. Powell, I. C. Campbell and C. W. Coen (1999). "Circadian regulation of prion protein messenger RNA in the rat forebrain: a widespread and synchronous rhythm." Neuroscience 91(4): 1201-1204.

Cardinale, A., I. Filesi, V. Vetrugno, M. Pocchiari, M. S. Sy and S. Biocca (2005). "Trapping prion protein in the endoplasmic reticulum impairs PrP^{C} maturation and prevents PrP^{Sc} accumulation." J Biol Chem 280(1): 685-694.

Carra, S., M. Sivilotti, A. T. Chavez Zobel, H. Lambert and J. Landry (2005). "HspB8, a small heat shock protein mutated in human neuromuscular disorders, has in vivo chaperone activity in cultured cells." Hum Mol Genet 14(12): 1659-1669.

Carthew, R. W. and E. J. Sontheimer (2009). "Origins and Mechanisms of miRNAs and siRNAs." Cell 136(4): 642-655.

Caughey, B., R. E. Race, D. Ernst, M. J. Buchmeier and B. Chesebro (1989). "Prion protein biosynthesis in scrapie-infected and uninfected neuroblastoma cells." J Virol 63(1): 175-181.

Chakrabarti, O., A. Ashok and R. S. Hegde (2009). "Prion protein biosynthesis and its emerging role in neurodegeneration." Trends Biochem Sci 34(6): 287-295.

Chernoff, Y. O., S. L. Lindquist, B. Ono, S. G. Inge-Vechtomov and S. W. Liebman (1995). "Role of the chaperone protein Hsp104 in propagation of the yeast prion-like factor [psi+]." Science 268(5212): 880-884. Chesebro, B., R. Race, K. Wehrly, J. Nishio, M. Bloom, D. Lechner, S. Bergstrom, K. Robbins, L. Mayer, J. M. Keith and et al. (1985). "Identification of scrapie prion protein-specific mRNA in scrapie-infected and uninfected brain." Nature 315(6017): 331-333.

Chesebro, B., K. Wehrly, B. Caughey, J. Nishio, D. Ernst and R. Race (1993). "Foreign PrP expression and scrapie infection in tissue culture cell lines." Dev Biol Stand 80: 131-140.

Ciechanover, A., A. Orian and A. L. Schwartz (2000). "Ubiquitin-mediated proteolysis: biological regulation via destruction." Bioessays 22(5): 442-451.

Cox, B. (1994). "Cytoplasmic inheritance. Prion-like factors in yeast." Curr Biol 4(8): 744-748.

Creutzfeldt, H. G. (1920). ”A peculiar localised disease of the central nervous system (Preliminary announcement).” Zeitschrift Fur Die Gesamte Neurologie Und Psychiatrie 57: 1-18.

Cristofani, R., V. Crippa, G. Vezzoli, P. Rusmini, M. Galbiati, M. E. Cicardi, M. Meroni, V. Ferrari, B. Tedesco, M. Piccolella, E. Messi, S. Carra and A. Poletti (2018). ”The small heat shock protein B8 (HSPB8) efficiently removes aggregating species of dipeptides produced in C9ORF72-related neurodegenerative diseases.” Cell Stress Chaperones 23(1): 1-12.

Dana, H., G. M. Chalbatani, H. Mahmoodzadeh, R. Karimloo, O. Rezaiean, A. Moradzadeh, N. Mehmandoost, F. Moazzen, A. Mazraeh, V. Marmari, M. Ebrahimi, M. M. Rashno, S. J. Abadi and E. Gharagouzlo (2017). ”Molecular Mechanisms and Biological Functions of siRNA.” Int J Biomed Sci 13(2): 48-57.

Daude, N., M. Marella and J. Chabry (2003). ”Specific inhibition of pathological prion protein accumulation by small interfering RNAs.” J Cell Sci 116(Pt 13): 2775-2779.

Deleault, N. R., J. C. Geoghegan, K. Nishina, R. Kascsak, R. A. Williamson and S. Supattapone (2005). ”Protease-resistant prion protein amplification reconstituted with partially purified substrates and synthetic polyanions.” J Biol Chem 280(29): 26873-26879.

Dorsett, Y. and T. Tuschl (2004). ”siRNAs: applications in functional genomics and potential as therapeutics.” Nat Rev Drug Discov 3(4): 318-329.

Dunker, A. K., I. Silman, V. N. Uversky and J. L. Sussman (2008). ”Function and structure of inherently disordered proteins.” Curr Opin Struct Biol 18(6): 756-764.

Dupiereux, I., W. Zorzi, W. Rachidi, D. Zorzi, O. Pierard, B. Lhereux, E. Heinen and B. Elmoualij (2006). ”Study on the toxic mechanism of prion protein peptide 106-126 in neuronal and non neuronal cells.” J Neurosci Res 84(3): 637-646.

Eckhardt, V. (2015). Genome editing of the Prion Protein Gene, University of Zurich. Elleman, C. J. (1984). ”Attempts to establish the scrapie agent in cell lines.” Vet Res Commun 8(4): 309-316. Enari, M., E. Flechsig and C. Weissmann (2001). ”Scrapie prion protein accumulation by scrapie-infected neuroblastoma cells abrogated by exposure to a prion protein antibody.” Proc Natl Acad Sci U S A 98(16): 9295-9299.

Ferreiro, E., A. Eufrasio, C. Pereira, C. R. Oliveira and A. C. Rego (2007). ”Bcl-2 overexpression protects against amyloid-beta and prion toxicity in GT1-7 neural cells.” J Alzheimers Dis 12(3): 223-228. Finka, A., R. U. Mattoo and P. Goloubinoff (2016). ”Experimental Milestones in the Discovery of Molecular Chaperones as Polypeptide Unfolding Enzymes.” Annu Rev Biochem 85: 715-742.

Fire, A., S. Xu, M. K. Montgomery, S. A. Kostas, S. E. Driver and C. C. Mello (1998). ”Potent and specific genetic interference by double-stranded RNA in Caenorhabditis elegans.” Nature

391(6669): 806-811.

Fischer, M., T. Rulicke, A. Raeber, A. Sailer, M. Moser, B. Oesch, S. Brandner, A. Aguzzi and C. Weissmann (1996). "Prion protein (PrP) with amino-proximal deletions restoring susceptibility of PrP knockout mice to scrapie." EMBO J 15(6): 1255-1264.

Fons, R. D., B. A. Bogert and R. S. Hegde (2003). "Substrate-specific function of the translocon-associated protein complex during translocation across the ER membrane." J Cell Biol 160(4): 529-539.

Frydman, J., E. Nimmesgern, K. Ohtsuka and F. U. Hartl (1994). "Folding of nascent polypeptide chains in a high molecular mass assembly with molecular chaperones." Nature 370(6485): 111-117.

Gajdusek, D. C. and V. Zigas (1959). "Kuru; clinical, pathological and epidemiological study of an acute progressive degenerative disease of the central nervous system among natives of the Eastern Highlands of New Guinea." Am J Med 26(3): 442-469.

Gaudet, P., P. A. Michel, M. Zahn-Zabal, A. Britan, I. Cusin, M. Domagalski, P. D. Duek, A. Gateau, A. Gleizes, V. Hinard, V. Rech de Laval, J. Lin, F. Nikitin, M. Schaeffer, D. Teixeira, L. Lane and A. Bairoch (2017). "The neXtProt knowledgebase on human proteins: 2017 update." Nucleic Acids Res 45(D1): D177-D182.

Gibbs, C. J., Jr., D. C. Gajdusek, D. M. Asher, M. P. Alpers, E. Beck, P. M. Daniel and W. B. Matthews (1968). "Creutzfeldt-Jakob disease (spongiform encephalopathy): transmission to the chimpanzee." Science 161(3839): 388-389.

Glatzel, M., E. Abela, M. Maissen and A. Aguzzi (2003). "Extraneural pathologic prion protein in sporadic Creutzfeldt-Jakob disease." N Engl J Med 349(19): 1812-1820.

Glickman, M. H., D. M. Rubin, O. Coux, I. Wefes, G. Pfeifer, Z. Cjeka, W. Baumeister, V. A. Fried and D. Finley (1998). "A subcomplex of the proteasome regulatory particle required for ubiquitin-conjugate degradation and related to the COP9-signalosome and eIF3." Cell 94(5): 615-623.

Glover, J. R., A. S. Kowal, E. C. Schirmer, M. M. Patino, J. J. Liu and S. Lindquist (1997). "Self-seeded fibers formed by Sup35, the protein determinant of [PSI+], a heritable prion-like factor of S. cerevisiae." Cell 89(5): 811-819.

Goloubinoff, P. (2016). "Mechanisms of protein homeostasis in health, aging and disease." Swiss Med Wkly 146: w14306.

Greil, C. S., I. M. Vorberg, A. E. Ward, K. D. Meade-White, D. A. Harris and S. A. Priola (2008). "Acute cellular uptake of abnormal prion protein is cell type and scrapie-strain independent." Virology 379(2): 284-293.

Hadlow, W. J. (1959). ”Scrapie and Kuru.” Lancet 2(Sep5): 289-290. Haraguchi, T., S. Fisher, S. Olofsson, T. Endo, D. Groth, A. Tarentino, D. R. Borchelt, D. Teplow, L. Hood, A. Burlingame and et al. (1989). ”Asparagine-linked glycosylation of the scrapie and cellular prion proteins.” Arch Biochem Biophys 274(1): 1-13.

Hasier Eraña , J. C. (2016). ”The architecture of prions: how understanding would provide new therapeutic insights.” Swiss Medical Weekly Swiss Med Wkly. 2016;146:w14354.

Hebert, D. N. and M. Molinari (2007). ”In and out of the ER: protein folding, quality control, degradation, and related human diseases.” Physiol Rev 87(4): 1377-1408.

Hershko, A. and A. Ciechanover (1998). ”The ubiquitin system.” Annu Rev Biochem 67: 425-479.

Hinault, M. P., A. Ben-Zvi and P. Goloubinoff (2006). ”Chaperones and proteases: cellular fold-controlling factors of proteins in neurodegenerative diseases and aging.” J Mol Neurosci 30(3): 249-265.

Huang DW, Sherman BT, Lempicki RA. Systematic and integrative analysis of large gene lists using DAVID Bioinformatics Resources. Nature Protoc. 2009;4(1): 44-57.

Jakob, A. (1921). ”Über eigenartige Erkrankungen des Zentralnerven- systems mit bemerkenswertem anatomischem Befunde. (Spastische Pseudosklerose-Encephalomyelopathie mit dis- seminierten Degenerationsherden).” Z Neurol Psychiatr 1921;64: 147-228.

Jinek, M. and J. A. Doudna (2009). ”A three-dimensional view of the molecular machinery of RNA interference.” Nature 457(7228): 405-412.

Kang, S. C., D. R. Brown, M. Whiteman, R. L. Li, T. Pan, G. Perry, T. Wisniewski, M. S. Sy and B. S. Wong (2004). ”Prion protein is ubiquitinated after developing protease resistance in the brains of scrapie-infected mice.” Journal of Pathology 203(1): 603-608.

Kaufman, S. K., T. L. Thomas, K. Del Tredici, H. Braak and M. I. Diamond (2017). ”Characterization of tau prion seeding activity and strains from formaldehyde-fixed tissue.” Acta Neuropathol Commun 5(1): 41. Kim, S. J. and R. S. Hegde (2002). ”Cotranslational partitioning of nascent prion protein into multiple populations at the translocation channel.” Mol Biol Cell 13(11): 3775-3786.

Kim, S. J., D. Mitra, J. R. Salerno and R. S. Hegde (2002). ”Signal sequences control gating of the protein translocation channel in a substrate-specific manner.” Dev Cell 2(2): 207-217.

Kim, Y. C. and D. M. Smith (2014). ”The 26S Proteasomal ATPases: Structure, Function, Regulation, and Potential for Cancer Therapies.” Resistance to Proteasome Inhibitors in Cancer: Molecular Mechanisms and Strategies to Overcome Resistance 3: 347-364.

Kitamoto, T. and J. Tateishi (1994). ”Human prion diseases with variant prion protein.” Philos

Trans R Soc Lond B Biol Sci 343(1306): 391-398.

Klatzo, I., D. C. Gajdusek and V. Zigas (1959). ”Pathology of Kuru.” Lab Invest 8(4): 799-847.

Klohn, P. C., L. Stoltze, E. Flechsig, M. Enari and C. Weissmann (2003). ”A quantitative, highly sensitive cell-based infectivity assay for mouse scrapie prions.” Proc Natl Acad Sci U S A 100(20): 11666-11671.

Klucken, J., Y. Shin, E. Masliah, B. T. Hyman and P. J. McLean (2004). ”Hsp70 Reduces alpha-Synuclein Aggregation and Toxicity.” J Biol Chem 279(24): 25497-25502.

Knowles, T. P., C. A. Waudby, G. L. Devlin, S. I. Cohen, A. Aguzzi, M. Vendruscolo, E. M. Terentjev, M. E. Welland and C. M. Dobson (2009). ”An analytical solution to the kinetics of breakable filament assembly.” Science 326(5959): 1533-1537.

Kosir, R., J. Acimovic, M. Golicnik, M. Perse, G. Majdic, M. Fink and D. Rozman (2010). ”Determination of reference genes for circadian studies in different tissues and mouse strains.” BMC Mol Biol 11: 60.

Kovacs, G. G., G. Trabattoni, J. A. Hainfellner, J. W. Ironside, R. S. Knight and H. Budka (2002). ”Mutations of the prion protein gene phenotypic spectrum.” J Neurol 249(11): 1567-1582.

Kovalevich, J. and D. Langford (2013). ”Considerations for the use of SH-SY5Y neuroblastoma cells in neurobiology.” Methods Mol Biol 1078: 9-21.

Krejciova, Z., J. Alibhai, C. Zhao, R. Krencik, N. M. Rzechorzek, E. M. Ullian, J. Manson, J. W. Ironside, M. W. Head and S. Chandran (2017). ”Human stem cell-derived astrocytes replicate human prions in a *PRNP* genotype-dependent manner.” J Exp Med 214(12): 3481-3495.

Kurschner, C. and J. I. Morgan (1995). ”The cellular prion protein (PrP) selectively binds to Bcl-2 in the yeast two-hybrid system.” Brain Res Mol Brain Res 30(1): 165-168.

Ladogana, A., Q. Liu, Y. G. Xi and M. Pocchiari (1995). ”Proteinase-resistant protein in human neuroblastoma cells infected with brain material from Creutzfeldt-Jakob patient.” Lancet 345(8949): 594-595.

Lander, G. C., E. Estrin, M. E. Matyskiela, C. Bashore, E. Nogales and A. Martin (2012). ”Complete subunit architecture of the proteasome regulatory particle.” Nature 482(7384): 186-U175.

Langer, T., C. Lu, H. Echols, J. Flanagan, M. K. Hayer and F. U. Hartl (1992). ”Successive action of DnaK, DnaJ and GroEL along the pathway of chaperone-mediated protein folding.” Nature 356(6371): 683-689.

Leach, M. R. a. W., D.B. (2000-2013). ”Calnexin and Calreticulin, Molecular Chaperones of the Endoplasmic Reticulum.” Madame Curie Bioscience Database [Internet].

Leznicki, P. and S. High (2012). ”SGTA antagonizes BAG6-mediated protein triage.” Proc Natl

Acad Sci U S A 109(47): 19214-19219.

Li, B. (2016). "Establishment of An Automated Digital Prion Infectivity Cell Assay and PrP-HPFRET Based High-throughput siRNA Screening Platform."

Li, J. Y., E. Englund, J. L. Holton, D. Soulet, P. Hagell, A. J. Lees, T. Lashley, N. P. Quinn, S. Rehncrona, A. Bjorklund, H. Widner, T. Revesz, O. Lindvall and P. Brundin (2008). "Lewy bodies in grafted neurons in subjects with Parkinson's disease suggest host-to-graft disease propagation." Nat Med 14(5): 501-503.

Liebman, S. W. (2001). "Prions. The shape of a species barrier." Nature 410(6825): 161-162.

Liu, C. W. and A. D. Jacobson (2013). "Functions of the 19S complex in proteasomal degradation." Trends Biochem Sci 38(2): 103-110.

Locht, C., B. Chesebro, R. Race and J. M. Keith (1986). "Molecular cloning and complete sequence of prion protein cDNA from mouse brain infected with the scrapie agent." Proc Natl Acad Sci U S A 83(17): 6372-6376.

Luk, K. C., V. Kehm, J. Carroll, B. Zhang, P. O'Brien, J. Q. Trojanowski and V. M. Lee (2012). "Pathological alpha-synuclein transmission initiates Parkinson-like neurodegeneration in non-transgenic mice." Science 338(6109): 949-953.

Mabbott, N. A. and G. G. MacPherson (2006). "Prions and their lethal journey to the brain." Nat Rev Microbiol 4(3): 201-211.

Magrane, J., R. C. Smith, K. Walsh and H. W. Querfurth (2004). "Heat shock protein 70 participates in the neuroprotective response to intracellularly expressed beta-amyloid in neurons." J Neurosci 24(7): 1700-1706.

Mahal, S. P., C. A. Baker, C. A. Demczyk, E. W. Smith, C. Julius and C. Weissmann (2007). "Prion strain discrimination in cell culture: the cell panel assay." Proc Natl Acad Sci U S A 104(52): 20908-20913.

Mahal, S. P., C. A. Demczyk, E. W. Smith, Jr., P. C. Klohn and C. Weissmann (2008). "Assaying prions in cell culture: the standard scrapie cell assay (SSCA) and the scrapie cell assay in end point format (SCEPA)." Methods Mol Biol 459: 49-68.

Manson, J. C., A. R. Clarke, P. A. Mcbride, I. Mcconnell and J. Hope (1994). "Prp Gene Dosage Determines the Timing but Not the Final Intensity or Distribution of Lesions in Scrapie Pathology." Neurodegeneration 3(4): 331-340.

Marine, S., A. Bahl, M. Ferrer and E. Buehler (2012). "Common seed analysis to identify off-target effects in siRNA screens." J Biomol Screen 17(3): 370-378.

Martinez, T. and A. Pascual (2007). "Identification of genes differentially expressed in SH-SY5Y neuroblastoma cells exposed to the prion peptide 106-126." Eur J Neurosci 26(1): 51-59.

McCracken, A. A. and J. L. Brodsky (2003). ”Evolving questions and paradigm shifts in endoplasmic-reticulum-associated degradation (ERAD).” Bioessays 25(9): 868-877.

Medori, R., H. J. Tritschler, A. LeBlanc, F. Villare, V. Manetto, H. Y. Chen, R. Xue, S. Leal, P. Montagna, P. Cortelli and et al. (1992). ”Fatal familial insomnia, a prion disease with a mutation at codon 178 of the prion protein gene.” N Engl J Med 326(7): 444-449.

Merz, P. A., R. A. Somerville, H. M. Wisniewski, L. Manuelidis and E. E. Manuelidis (1983). ”Scrapie-associated fibrils in Creutzfeldt-Jakob disease.” Nature 306(5942): 474-476.

Meyer-Luehmann, M., J. Coomaraswamy, T. Bolmont, S. Kaeser, C. Schaefer, E. Kilger, A. Neuenschwander, D. Abramowski, P. Frey, A. L. Jaton, J. M. Vigouret, P. Paganetti, D. M. Walsh, P. M. Mathews, J. Ghiso, M. Staufenbiel, L. C. Walker and M. Jucker (2006). ”Exogenous induction of cerebral beta-amyloidogenesis is governed by agent and host.” Science 313(5794): 1781-1784.

Muchowski, P. J. (2002). ”Protein misfolding, amyloid formation, and neurodegeneration: a critical role for molecular chaperones?” Neuron 35(1): 9-12.

Muchowski, P. J. and J. L. Wacker (2005). ”Modulation of neurodegeneration by molecular chaperones.” Nat Rev Neurosci 6(1): 11-22.

Nakhro, K., J. M. Park, Y. J. Kim, B. R. Yoon, J. H. Yoo, H. Koo, B. O. Choi and K. W. Chung (2013). ”A novel Lys141Thr mutation in small heat shock protein 22 (HSPB8) gene in Charcot-Marie-Tooth disease type 2L.” Neuromuscul Disord 23(8): 656-663.

Nishida, N., D. A. Harris, D. Vilette, H. Laude, Y. Frobert, J. Grassi, D. Casanova, O. Milhavet and S. Lehmann (2000). ”Successful transmission of three mouse-adapted scrapie strains to murine neuroblastoma cell lines overexpressing wild-type mouse prion protein.” J Virol 74(1): 320-325.

Oesch, B., D. Westaway, M. Walchli, M. P. McKinley, S. B. Kent, R. Aebersold, R. A. Barry, P. Tempst, D. B. Teplow, L. E. Hood and et al. (1985). ”A cellular gene encodes scrapie PrP 27-30 protein.” Cell 40(4): 735-746.

Ohhashi, Y., M. Kihara, H. Naiki and Y. Goto (2005). ”Ultrasonication-induced amyloid fibril formation of beta2-microglobulin.” J Biol Chem 280(38): 32843-32848.

Owen, F., M. Poulter, J. Collinge and T. J. Crow (1990). ”Codon 129 changes in the prion protein gene in Caucasians.” Am J Hum Genet 46(6): 1215-1216.

Pan, K. M., M. Baldwin, J. Nguyen, M. Gasset, A. Serban, D. Groth, I. Mehlhorn, Z. Huang, R. J. Fletterick, F. E. Cohen and et al. (1993). ”Conversion of alpha-helices into beta-sheets features in the formation of the scrapie prion proteins.” Proc Natl Acad Sci U S A 90(23): 10962-10966.

Papageorgiou, A., J. Rapley, J. P. Mesirov, P. Tamayo and J. Avruch (2015). ”A genome-wide siRNA screen in mammalian cells for regulators of S6 phosphorylation.” PLoS One 10(3): e0116096.

Park, K. W., G. Eun Kim, R. Morales, F. Moda, I. Moreno-Gonzalez, L. Concha-Marambio, A. S. Lee, C. Hetz and C.

Soto (2017). ”The Endoplasmic Reticulum Chaperone GRP78/BiP Modulates Prion Propagation in vitro and in vivo.” Sci Rep 7: 44723.

Pattison IH, M. G. (1960). ”Further observations on the experimen- tal production of scrapie in goats and sheep.” J Comp Pathol 70: 182–193.

Peretz, D., M. R. Scott, D. Groth, R. A. Williamson, D. R. Burton, F. E. Cohen and S. B. Prusiner (2001).

”Strain-specified relative conformational stability of the scrapie prion protein.” Protein Sci 10(4): 854-863.

Pfeifer, A., S. Eigenbrod, S. Al-Khadra, A. Hofmann, G. Mitteregger, M. Moser, U. Bertsch and H. Kretzschmar (2006). ”Lentivector-mediated RNAi efficiently suppresses prion protein and prolongs survival of scrapie-infected mice.” J Clin Invest 116(12): 3204-3210.

Pinney, D. F. and C. P. Emerson, Jr. (1989). ”10T1/2 cells: an in vitro model for molecular genetic analysis of mesodermal determination and differentiation.” Environ Health Perspect 80: 221-227.

Polymenidou, M., R. Moos, M. Scott, C. Sigurdson, Y. Z. Shi, B. Yajima, I. Hafner-Bratkovic, R. Jerala, S. Hornemann, K. Wuthrich, A. Bellon, M. Vey, G. Garen, M. N. James, N. Kav and A. Aguzzi (2008). ”The POM monoclonals: a comprehensive set of antibodies to non-overlapping prion protein epitopes.” PLoS One 3(12): e3872.

Priya, S., S. K. Sharma and P. Goloubinoff (2013). ”Molecular chaperones as enzymes that catalytically unfold misfolded polypeptides.” FEBS Lett 587(13): 1981-1987.

Prusiner, S. B. (1998). ”Prions.” Proc Natl Acad Sci U S A 95(23): 13363-13383.

Prusiner, S. B., D. C. Bolton, D. F. Groth, K. A. Bowman, S. P. Cochran and M. P. Mckinley (1982). ”Further Purification and Characterization of Scrapie Prions.” Biochemistry 21(26): 6942-6950.

Prusiner, S. B., M. P. Mckinley, K. A. Bowman, D. C. Bolton, P. E. Bendheim, D. F. Groth and G. G. Glenner (1983). ”Scrapie Prions Aggregate to Form Amyloid-Like Birefringent Rods.” Cell 35(2): 349-358.

Prusiner, S. B. and M. R. Scott (1997). ”Genetics of prions.” Annu Rev Genet 31: 139-175.

Pulford, B., N. Reim, A. Bell, J. Veatch, G. Forster, H. Bender, C. Meyerett, S. Hafeman, B.

Michel, T. Johnson, A. C. Wyckoff, G. Miele, C. Julius, J. Kranich, A. Schenkel, S. Dow and M. D. Zabel (2010). ”Liposome-siRNA-peptide complexes cross the blood-brain barrier and significantly decrease PrP on neuronal cells and PrP in infected cell cultures.” PLoS One 5(6): e11085.

Pundir, S., M. J. Martin and C. O’Donovan (2017). ”UniProt Protein Knowledgebase.” Methods Mol Biol 1558: 41-55.

Qi, Y., J. K. Wang, M. McMillian and D. M. Chikaraishi (1997). ”Characterization of a CNS cell line, CAD, in which morphological differentiation is initiated by serum deprivation.” J Neurosci 17(4): 1217-1225. Race, R. (1991). ”The scrapie agent in vitro.” Curr Top Microbiol Immunol 172: 181-193.

Race, R. E., L. H. Fadness and B. Chesebro (1987). ”Characterization of scrapie infection in mouse neuroblastoma cells.” J Gen Virol 68 (Pt 5): 1391-1399.

Rambold, A. S., M. Miesbauer, D. Rapaport, T. Bartke, M. Baier, K. F. Winklhofer and J. Tatzelt (2006). ”Association of Bcl-2 with misfolded prion protein is linked to the toxic potential of cytosolic PrP.” Molecular Biology of the Cell 17(8): 3356-3368.

Ramo, P., A. Drewek, C. Arrieumerlou, N. Beerenwinkel, H. Ben-Tekaya, B. Cardel, A. Casanova, R. Conde-Alvarez, P. Cossart, G. Csucs, S. Eicher, M. Emmenlauer, U. Greber, W. D. Hardt, A. Helenius, C. Kasper, A. Kaufmann, S. Kreibich, A. Kuhbacher, P. Kunszt, S. H. Low, J. Mercer, D. Mudrak, S. Muntwiler, L. Pelkmans, J. Pizarro-Cerda, M. Podvinec, E. Pujadas, B. Rinn, V. Rouilly, F. Schmich, J. Siebourg-Polster, B. Snijder, M. Stebler, G. Studer, E. Szczurek, M. Truttmann, C. von Mering, A. Vonderheit, A. Yakimovich, P. Buhlmann and C. Dehio (2014). ”Simultaneous analysis of large-scale RNAi screens for pathogen entry.” BMC Genomics 15: 1162.

Rapoport, T. A. (2007). ”Protein translocation across the eukaryotic endoplasmic reticulum and bacterial plasma membranes.” Nature 450(7170): 663-669.

Reznikoff, C. A., D. W. Brankow and C. Heidelberger (1973). ”Establishment and characterization of a cloned line of C3H mouse embryo cells sensitive to postconfluence inhibition of division.” Cancer Res 33(12): 3231-3238.

Riek, R., S. Hornemann, G. Wider, M. Billeter, R. Glockshuber and K. Wuthrich (1996). ”NMR structure of the mouse prion protein domain PrP(121-231).” Nature 382(6587): 180-182.

Riesner, D. (2003). ”Biochemistry and structure of PrP(C) and PrP(Sc).” Br Med Bull 66: 21-33.

Rikhvanov, E. G., N. V. Romanova and Y. O. Chernoff (2007). ”Chaperone Effects on Prion and Nonprion Aggregates.” Prion 1(4): 217-222.

Ruiz-Riquelme, A., H. H. C. Lau, E. Stuart, A. N. Goczi, Z. L. Wang, G. Schmitt-Ulms and J.

C. Watts (2018). ”Prion-like propagation of beta-amyloid aggregates in the absence of APP overexpression.” Acta Neuropathologica Communications 6.

Sadlish, H., H. Rampelt, J. Shorter, R. D. Wegrzyn, C. Andreasson, S. Lindquist and B. Bukau (2008). ”Hsp110 chaperones regulate prion formation and propagation in S. cerevisiae by two discrete activities.” PLoS One 3(3): e1763.

Safar, J., P. P. Roller, D. C. Gajdusek and C. J. Gibbs, Jr. (1993). ”Thermal stability and conformational transitions of scrapie amyloid (prion) protein correlate with infectivity.” Protein Sci 2(12): 2206-2216.

Schatzl, H. M., L. Laszlo, D. M. Holtzman, J. Tatzelt, S. J. DeArmond, R. I. Weiner, W. C. Mobley and S. B. Prusiner (1997). ”A hypothalamic neuronal cell line persistently infected with scrapie prions exhibits apoptosis.” J Virol 71(11): 8821-8831.

Schiene-Fischer, C. (2015). ”Multidomain Peptidyl Prolyl cis/trans Isomerases.” Biochim Biophys Acta 1850(10): 2005-2016.

Sigurdson, C. J. (2008). ”A prion disease of cervids: chronic wasting disease.” Vet Res 39(4): 41.

Sigurdsson, B. (1954). ”RIDA, A Chronic Encephalitis of Sheep: With General Remarks on Infections Which Develop Slowly and Some of Their Special Characteristics.” British Veterinary Journal 110(9): 341-344.

Solassol, J., C. Crozet and S. Lehmann (2003). ”Prion propagation in cultured cells.” Br Med Bull 66: 87-97. Soti, C. and P. Csermely (2002). ”Chaperones and aging: role in neurodegeneration and in other civilizational diseases.” Neurochem Int 41(6): 383-389.

Soto, C. and N. Satani (2011). ”The intricate mechanisms of neurodegeneration in prion diseases.” Trends Mol Med 17(1): 14-24.

Sparkes, R. S., M. Simon, V. H. Cohn, R. E. Fournier, J. Lem, I. Klisak, C. Heinzmann, C. Blatt, M. Lucero, T. Mohandas and et al. (1986). ”Assignment of the human and mouse prion protein genes to homologous chromosomes.” Proc Natl Acad Sci U S A 83(19): 7358-7362.

Stahl, N., M. A. Baldwin, D. B. Teplow, L. Hood, B. W. Gibson, A. L. Burlingame and S. B. Prusiner (1993). ”Structural studies of the scrapie prion protein using mass spectrometry and amino acid sequencing.” Biochemistry 32(8): 1991-2002.

Steele, A. D., G. Hutter, W. S. Jackson, F. L. Heppner, A. W. Borkowski, O. D. King, G. J. Raymond, A. Aguzzi and S. Lindquist (2008). ”Heat shock factor 1 regulates lifespan as distinct from disease onset in prion disease.” Proceedings of the National Academy of Sciences of the United States of America 105(36): 13626-13631. Takeuchi, H., Y. Kobayashi, T. Yoshihara, J. Niwa, M. Doyu, K. Ohtsuka and G. Sobue (2002). ”Hsp70 and Hsp40 improve neurite

outgrowth and suppress intracytoplasmic aggregate formation in cultured neuronal cells expressing mutant SOD1." Brain Res 949(1-2): 11-22.

Tateishi, J. and T. Kitamoto (1995). "Inherited prion diseases and transmission to rodents." Brain Pathol 5(1): 53-59.

Taylor, D. R. and N. M. Hooper (2006). "The prion protein and lipid rafts." Mol Membr Biol 23(1): 89-99.

Uhlen, M., L. Fagerberg, B. M. Hallstrom, C. Lindskog, P. Oksvold, A. Mardinoglu, A. Sivertsson, C. Kampf, E. Sjostedt, A. Asplund, I. Olsson, K. Edlund, E. Lundberg, S. Navani, C. A. Szigyarto, J. Odeberg, D. Djureinovic, J. O. Takanen, S. Hober, T. Alm, P. H. Edqvist, H. Berling, H. Tegel, J. Mulder, J. Rockberg, P. Nilsson, J. M. Schwenk, M. Hamsten, K. von Feilitzen, M. Forsberg, L. Persson, F. Johansson, M. Zwahlen, G. von Heijne, J. Nielsen and F. Ponten (2015). "Proteomics. Tissue-based map of the human proteome." Science 347(6220): 1260419.

Vicario, M., S. D. Skaper and A. Negro (2014). "The small heat shock protein HspB8: role in nervous system physiology and pathology." CNS Neurol Disord Drug Targets 13(5): 885-895.

Vilette, D., O. Andreoletti, F. Archer, M. F. Madelaine, J. L. Vilotte, S. Lehmann and H. Laude (2001). "Ex vivo propagation of infectious sheep scrapie agent in heterologous epithelial cells expressing ovine prion protein." Proc Natl Acad Sci U S A 98(7): 4055-4059.

Vorberg, I., A. Raines and S. A. Priola (2004). "Acute formation of protease-resistant prion protein does not always lead to persistent scrapie infection in vitro." J Biol Chem 279(28): 29218-29225.

Wang, D., J. Baudys, Y. Ye, J. C. Rees, J. R. Barr, J. L. Pirkle and S. R. Kalb (2013). "Improved detection of botulinum neurotoxin serotype A by Endopep-MS through peptide substrate modification." Anal Biochem 432(2): 115-123.

White, M. D., M. Farmer, I. Mirabile, S. Brandner, J. Collinge and G. R. Mallucci (2008). "Single treatment with RNAi against prion protein rescues early neuronal dysfunction and prolongs survival in mice with prion disease." Proc Natl Acad Sci U S A 105(29): 10238-10243.

Wilcox, R. (2012). "Introduction to Robust Estimation and Hypothesis Testing, 3rd Edition." Introduction to Robust Estimation and Hypothesis Testing, 3rd Edition: 1-690.

Wilesmith, J. W., J. B. Ryan, W. D. Hueston and L. J. Hoinville (1992). "Bovine spongiform encephalopathy: epidemiological features 1985 to 1990." Vet Rec 130(5): 90-94.

Williams, E. S. and S. Young (1980). "Chronic wasting disease of captive mule deer: a spongiform encephalopathy." J Wildl Dis 16(1): 89-98.

Wit, E., E. van den Heuvel and J. W. Romeijn (2012). "All models are wrong...': an introduction

to model uncertainty." Statistica Neerlandica 66(3): 217-236.

Zabel, M. D. and C. Reid (2015). "A brief history of prions." Pathog Dis 73(9): ftv087. Zhang, X. D. (2007). "A pair of new statistical parameters for quality control in RNA interference high-throughput screening assays." Genomics 89(4): 552-561.

Zhang, X. (2011). Optimal High-Throughput Screening: Practical Experimental Design and Data Analysis for Genome-Scale RNAi Research. Cambridge: Cambridge University Press. doi:10.1017/CBO9780511973888.

Zhang, Z., Y. Zhang, F. Wang, X. Wang, Y. Xu, H. Yang, G. Yu, C. Yuan and J. Ma (2013). "De novo generation of infectious prions with bacterially expressed recombinant prion protein." FASEB J 27(12): 4768-4775.

Zhu, T., S. Hayat Khan, D. Zhao and L. Yang (2014). "Regulation of proteasomes in prion disease." Acta Biochim Biophys Sin (Shanghai) 46(7): 531-539.

12 Acknowledgements

I thank Adriano Aguzzi for providing me with equipment and scientific support to do experimental research on the exciting chaperone project.
I express many thanks to my PhD committee Stephan Neuhauss and Walter Schaffner for supporting me over three years with their time for discussions and participation in my PhD committee meetings. I would like to give a special thanks to Caihong Zhu, Bei Li and Karl Frontzek who broadened my horizon scientifically and personally and were fantastic office mates. I enjoyed spending time in and outside the lab with Isabella Gianella, Kristina Airich, Manuela Pfammatter, Claudia Scheckel, Uli Herrmann, and my office colleagues. I thank Daniel Heinzer, Merve Avar and Daniel Peace for sharing the data of the genome wide human PrP^C screen with me and for discussions.
Elke Schaper, Jérôme Dauvellier and Andra Chincisan did a great job in analysing the screen data. Rita Moos, Petra Schwarz and Irina Abakumova kindly taught me many techniques and supported me day and night with reagents, good advice and even cough sweets.
The following people have further – either personally or scientifically or both – enriched the time during my PhD (in arbitrary order): Assunta Senatore, Lakkaraju, Silvia Sorce, Francesca Daniela Franzoso, Orsolya Török, Clemence Tournaire, Pierre Gouloubinoff, Vijay Chandrasekar, Melanie Einsiedler, Flavio Vasella, Marie-Angela Wulf, Musa Hadzere, Gzim Aliu, Efrem Tesfay, Marco Losa, Manfredi Carta, Carmen Schiavi, Ahmet Varol, Regina Reimann, Paolo Dametto, Elisabeth Rushing, Meike Nau, Simone Hornemann, Katrin Frauenknecht, Daniel Kirschenbaum, Lisa Caflisch, Julie Domange, Rea Müller, Jingjing Guo, Yingjun Liu, Marianne König, Andreia Magalhaes, Rajlakshmi Marpakwar, Sabrina Meyer, Jacqueline Wiedler, Frank V. Girardi. There are many other people who were very helpful as well but I probably forgot to mention: please do not take it personally.
My PhD thesis was funded by Klinische Forschungsschwerpunkte (KFSP) Small RNAs from the University of Zurich.
I am grateful for being supported by my caring and loving family, my love and my dear friends and roommates who have been encouraging and inspiring all the time.

13 Curriculum Vitae

Personal

Surname	Eckhardt
Prename	Valeria
Date of birth	17th of August 1991
Place of origin	Ermatingen TG
Citizenship	Swiss

Education

08/2015 – 09/ 2018	PhD in Neuroscience in the lab of Prof. Adriano Aguzzi at the University Hospital Zurich. Thesis title: "Elucidating the role of chaperones in prion biosynthesis and replication by siRNA mediated screening".
01/2015 – 07/2015	Pre-PhD and Language stay in the US, Cambridge Proficiency CEFR C2
09/2013 – 12/2014	MSc in Neuroscience at University of Zurich. Master-thesis in the lab of Prof. Adriano Aguzzi "Genome Editing of the Prion Protein Gene with CRISPR-Cas9".
09/2009 – 09/2013	BSc in Biology at the University of Zurich, including 6 months research internship.
06/2009	Bilingual Matura (German and Italian) at Bündner Kantonsschule.

Work Experience

01/2017 - today	Forschung für Leben: Leading practical genetic engineering workshops
03/2017	Organization open days of the institute of neuropathology for BrainFair
09 - 12/2015	University of Zurich: Assistant in practical molecular genetics course for students of Biomedicine/Biology/Medicine organized by Prof. Michael Hengartner.
02/2015	Tec Day by Swiss Academy of Technical Science: Responsible for the module "day-to-day work in neuroscience" to foster STEM fields at high schools.

Memberships

01/2017 - today	Swiss Society of Neuroscience
08/2015 - today	reatch, research and technology in Switzerland

Awards

02/2018	Awarded for the best poster in the category "Neurodegenerative Diseases" by Swiss Society of Neuroscience and Synapsis Foundation
08/2016	Top 100 talented student from Europe at Roche Continents